Dedication

The volume 41(1,2) is dedicated in the memory of **Professor Dr. Md. Anwar Hossain** .

Professor Dr. Md. Anwar Hossain

(25 April 1943 - 27 May 2021)

For details, please see Issue-2, article 1, page 1-4.*

*A Legend of Computational Fluid Dynamics and an Eminent Mathematician: Professor Md. Anwar Hossain

ISSN 1606-3694 (Print)
2224-5111 (Online)

GANIT

JOURNAL OF
BANGLADESH MATHEMATICAL SOCIETY

Vol. 41 (1, 2) 2021

One Volume of **GANIT** *Journal of Bangladesh Mathematical Society* is published every year by
BANGLADESH MATHEMATICAL SOCIETY

ACKNOWLEDGEMENT

A generous contribution of the Ministry of Science and Information and Communication Technology
Government of the People's Republic of Bangladesh
towards the publication of
GANIT Journal of Bangladesh Mathematical Society
is gratefully acknowledged

- Publication Date (Volume 41 (1-2)) December 2021

- Price per volume including surface postage

Institution	:	Inland Tk.	400.00	Foreign	US $ 50.00
Individuals	:	Inland Tk.	200.00	Foreign	US $ 30.00

- Payment must accompany orders. Please add US $ 10.00 for air mail delivery to Burma, India, Nepal, Pakistan and Srilanka, and US $ 20.00 for air mail delivery to other parts of the world.

- **Address for all orders and enquiries**

  Secretary, Bangladesh Mathematical Society
  A F Mujibur Rahman Ganit Bhaban
  University of Dhaka
  Dhaka-1000, Bangladesh

- **Computer typesetting and printing**

  BCS Printing
  Rafin Plaza (2nd Floor)
  3/B Mirpur Road, Dhaka-1205
  Phone: 01710880728
  Email: bcsprinting123@gmail.com

GANIT
A Journal of Bangladesh Mathematical Society

Editorial Board: 2020-2021

AUTHOR GUIDELINES

- **GANIT** *Journal of Bangladesh Mathematical Society* features selected contributions in pure and applied mathematics. The emphasis will be on the original research papers, but from time to time GANIT will publish expository papers or survey articles. All contributions are to be rigorous in nature and mathematical in treatment and should be written in English.
- **Manuscripts** should be submitted in a soft-copy in MS-WORD in double space via email: ganit.bms@gmail.com to the Associate Editor.
    - All submissions to GANIT must be original, unpublished previously, and not submitted elsewhere and not under consideration for publication elsewhere.
    - Authors must ensure that contents of any submission are not held by the copyright of any other publication.
    - It is assumed that the submission is approved by all authors and the concerned authorities where the work was carried out.
    - It is the author's responsibility that any submission does not contain libelous or unlawful statements or in any way infringe the rights of others.
    - Copyrights for articles published in GANIT are retained by the authors, with first publication rights granted to GANIT as the work simultaneously licensed under a Creative Commons Attribution License that allows others to share the work with an acknowledgment of the work's authorship and initial publication in this journal.
- Authors are encouraged to provide a list of at least 3 (three) reviewers along with reviewer's Name, affiliation, email address.
- **Manuscripts** should be typed double spaced on one side of 8.5″ × 11″ inch or A4 size with one inch margin all around.
- All pages of the manuscript should be numbered. Page 1 should contain the article title, author and co-author names and affiliation(s). Any footnotes to the author(s) are to be placed at the bottom of page1; page 2 should have a proposed running head (in abbreviated form of the title) of less than 40 characters.
- An **abstract** summarizing the main points of the article should be written on page 3 of the manuscript in font size 9. The abstract should not exceed 250 words.
- **Mathematical expressions** should be avoided in the title and abstract as far as practicable.
- References should be avoided in abstract.
- Footnotes in the text should be avoided. If they are essential, they should be numbered consecutively by superscript and placed at the end of the paper, before the list of references.
- All mathematical expressions should be typewritten, if possible. Equations should be numbered serially or section-wise and indicated in the right margin.
- Use of **Greek letters** as superscripts and subscripts should be avoided. Levels of subscripts and superscripts should be clearly maintained.
- Complicated fractions in the text should be written using solidus (/) or negative exponents.
- $e^{(\ )}$ should be replaced by exp( ) where the expression in the parenthesis is complicated. Radical signs should also be replaced by fractional exponents as far as practicable.
- Clear distinction between upper and lower case letters, between 'oh' and 'zero', between 'el' and 'one', between 'kay' and 'kappa', 'bhee' and 'nu' etc. should be made.

- Authors are requested not to underline subheadings and mathematical symbols, as they will be automatically set in accordance with the style of the journal.
- **Diagrams** should be submitted as original line drawings on white drawing papers or tracing papers. Each diagram should be made on a separate sheet and numbered consecutively. **Lettering** and **data points** should be large enough so that when reduced to fit on the journal page they can be read with ease. **Legends** to diagrams should be typed on a separate sheet and attached at the end of the manuscript.
- **Tables** should be numbered consecutively, typed carefully on separate sheets in exact format desired and attached at the end of the manuscript. Table headings should be short but clearly descriptive.
- **References** should be listed in alphabetical order of surnames, at the end of the manuscript, as in the examples below:

  [1] Cronin, J., Bifurcation of periodic solutions. *J. Math. Anal. Appl*. **68** (1979), 130-151

  [2] Lee, E. B. and Markus, L. Optimal control for nonlinear processes, *Arch. Rat. Mach. Anal* **8** (1961), 36-58.

  [3] Timoshenko, S. and Goodier, J. N. *Theory of Elasticity*, McGraw-Hill Book Co., New York, 1970.
- **References** should be cited in the text by the serial number from the above list placed between square brackets as [1], [2], etc.
- **Galley proofs** may be sent to the author, if necessary. In that case they should be returned within 48 hours of receipt with correction marks. No new material may be inserted in the text at the time of proof reading.
- **More information can be found from** http://bdmathsociety.org/

G A N I T

ISSN 1606-3694 (Print)
2224-5111 (Online)

JOURNAL OF BANGLADESH MATHEMATICAL SOCIETY

Vol. 41 (1) 2021

C O N T E N T S

Vol. 41 (2) 2021

GANIT

Available online at https://ganitjournal.bdmathsociety.org/

GANIT: Journal of Bangladesh Mathematical Society

GANIT*J. Bangladesh Math. Soc.*41.1 (2021) 1–14
DOI:https://doi.org/10.3329/ganit.v41i1.55022

Galerkin Approximations for the Solution of Fredholm Volterra Integral Equation of Second Kind

Asma Akter Akhi[a], and Goutam Saha[a],*

[a]*Department of Mathematics, University of Dhaka, Dhaka-1000, Bangladesh.*

ABSTRACT

In this research, we have introduced Galerkin method for finding approximate solutions of Fredholm Volterra Integral Equation (FVIE) of 2nd kind, and this method shows the result in respect of the linear combinations of basis polynomials. Here, BF (product of Bernstein and Fibonacci polynomials), CH (product of Chebyshev and Hermite polynomials), CL (product of Chebyshev and Laguerre polynomials), FL (product of Fibonacci and Laguerre polynomials) and LLE (product of Legendre and Laguerre polynomials) polynomials are established and considered as basis function in Galerkin method. Also, we have tried to observe the behavior of all these approximate solutions finding from Galerkin method for different problems and then a comparison is shown using some standard error estimations. In addition, we observe the error graphs of numerical solutions in Galerkin method for different problems of FVIE of second kind.

Received: September 05, 2020 **Accepted:** January 04, 2021 **Published Online:** August 04, 2021

Keywords: Fredholm Volterra Integral Equation; BF, CH, CL, FL and LLE polynomials; Galerkin Method.

AMS Subject Classification 2020: 45A05; 65R20; 68W05

1. Introduction

Integral equation is a key mathematical perceptive in the area of mathematics, and it has vast applications in physics, biology, economics, signal processing, engineering and other fields of science. Many ordinary and partial differential equations associated with different initial and boundary values can be reduced to different integral equations. There are various types of integral equations, among them FIEs and VIEs are the main two classes of integral equations. Both of these have first and second kind, linear and nonlinear form.

Nomenclature	
BF	product of Bernstein and Fibonacci polynomials

* Corresponding author: Goutam Saha,*E-mail address:* gsahamath@du.ac.bd

CH	product of Chebyshev and Hermite polynomials
CL	product of Chebyshev and Laguerre polynomials
FL	product of Fibonacci and Laguerre polynomials
LLE	product of Legendre and Laguerre polynomials

Many analytical and numerical methods are developed to solve different types of FVIEs. Adomain Decomposition, Quadrature, Galerkin, Collocation, different version of Wavelet, successive substitutions methods are introduced and researched by many researchers. Maleknejad and Hadizadeh [1] suggested Adomain decomposition method for mixed nonlinear FVIE and they also discussed about the limitof it. Maleknejad and FadaeiYami [2] used Adomain decomposition method to solve the system of VFIEs. Hendi and Bakodah [3] compared approximate solution with the exact solution which is obtained from discrete Adomain decomposition method. They used FVIE in two dimensional space and reported that it's a method that can be used to solve nonlinear integral equations in two dimensional space. Hendi and Albugami [4] solved FVIE of second kind using Galerkin and Collocation method and they considered continuous kernel with respect to position and time. Moreover, Mustafa and Ghanim [5] discussed quadrature methods i.e, Trapezoidal rule, Weddle's rule and Richardson's extrapolation to solve linear VFIEs numerically. More recently, Molla and Saha [6]showed the approximate solution of FVIE of second kind using the methods used by Hendi and Albugami [4]. They have reported that the performance of different polynomials and collocation points are consistent for both these methods. Abdou et al. [7] established the general solution of VFIEs with discontinuous kernel in a Banach Space using separation of variables method.

In this research, Galerkin method is used to find the approximate solution of FVIE of 2nd kind where new set of polynomials (BF, CH, CL, FL, LLE polynomials) are used as basis functions. Here, BF refers to product of Bernstein and Fibonacci polynomials, CH refers to product of Chebyshev and Hermite polynomials, CL refers to product of Chebyshev and Laguerre polynomials, FL refers to product of Fibonacci and Laguerre polynomials, LLE refers to product of Legendre and Laguerre polynomials. As far our knowledge, BF, CH, CL, FL, LLE polynomials are not introduced before to find the approximate solutions of FVIE of second kind. In recent times, Molla and Saha [8] used LH polynomials as basis function in Galerkin method for finding approximate solution of FIE of 2nd kind within a very short description. A brief discussion about the performance of above mentioned polynomials for the solution of FVIE of 2nd kind is presented in this paper.

This article is designed as follows: In §2, brief introduction of five new set of polynomials (BF, CH, CL, FL, LLE) are given. After that, details formulation of Galerkin method in order to find approximate solutions of FVIE of 2nd kind is illustrated in §3. Then, numerical results of the Galerkin method using different polynomials are computed, consequent absolute errors are presented graphically and RMSE and MAE are calculated in §4. Finally, the study concludes with a brief conclusion in §5.

2. Introduction of Polynomials

Hermite, Chebyshev, Laguerre, Fibonacci and Legendre polynomials are the most widely used classical orthogonal polynomials in approximation theory and numerical analysis and they used often in order to find the approximate solutions of different kinds of integral equations. In this research, some special and new sets of polynomials are introduced, and they are obtained as a product of the well known polynomials.
Product of Bernstein and Fibonacci polynomials (BF):

$$BF_i(u) = B_i(u)F_i(u) \tag{2.1}$$

Here we use fourth degree Bernstein polynomials over the interval [0, 1] and first five BF polynomials are presented underneath:

$$\left.\begin{array}{c} BF_0(u) = 1 - 4u + 6u^2 - 4u^3 + u^4 \\ BF_1(u) = 4u^2 - 12u^3 + 12u^4 - 4u^5 \\ BF_2(u) = 6u^2 - 12u^3 + 12u^4 - 12u^5 + 6u^6 \\ BF_3(u) = 8u^4 - 8u^5 + 4u^6 - 4u^7 \\ BF_4(u) = u^4 + 3u^6 + u^8 \end{array}\right\} \tag{2.2}$$

Product of Chebyshev and Hermite polynomials (CH):

$$CH_i(u) = C_i(u)H_i(u) \tag{2.3}$$

Also, some of the CH polynomials are shown here:

$$\left.\begin{array}{c} CH_0(u) = 1 \\ CH_1(u) = 2u^2 \\ CH_2(u) = 2 - 8u^2 + 8u^4 \\ CH_3(u) = 36u^2 - 72u^4 + 32u^6 \\ CH_4(u) = 12 - 144u^2 + 496u^4 - 512u^6 + 128u^8 \end{array}\right\} \tag{2.4}$$

Product of Chebyshev and Laguerre polynomials (CL):

$$CL_i(u) = C_i(u)L_i(u) \tag{2.5}$$

Also, some of the CL polynomials are shown here:

$$\left.\begin{array}{c} CL_0(u) = 1 \\ CL_1(u) = u - u^2 \\ CL_2(u) = -1 + 2u + \dfrac{3u^2}{2} - 4u^3 + u^4 \\ CL_3(u) = -3u + 9u^2 - \dfrac{u^3}{2} - \dfrac{23u^4}{2} + 6u^5 - \dfrac{2u^6}{3} \\ CL_4(u) = 1 - 4u - 5u^2 + \dfrac{94u^3}{3} - \dfrac{383u^4}{24} - \dfrac{80u^5}{3} + \dfrac{71u^6}{3} - \dfrac{16u^7}{3} + \dfrac{u^8}{3} \end{array}\right\} \tag{2.6}$$

Product of Fibonacci and Laguerre polynomials (FL):

$$FL_i(u) = F_i(u)L_i(u) \tag{2.7}$$

Also, some of the FL polynomials are shown here:

$$\left.\begin{array}{c} FL_0(u) = 1 \\ FL_1(u) = u - u^2 \\ FL_2(u) = 1 - 2u + \dfrac{3u^2}{2} - 2u^3 + \dfrac{u^4}{2} \\ FL_3(u) = 2u - 6u^2 + 4u^3 - \dfrac{10u^4}{3} + \dfrac{3u^5}{2} - \dfrac{u^6}{6} \\ FL_4(u) = 1 - 4u + 6u^2 - \dfrac{38u^3}{3} + \dfrac{241u^4}{24} - 6u^5 + \dfrac{25u^6}{8} - \dfrac{2u^7}{3} + \dfrac{u^8}{24} \end{array}\right\} \tag{2.8}$$

Product of Laguerre and Legendre polynomials (LLE):

$$LLE_i(u) = L_i(u)LE_i(u) \tag{2.9}$$

Also, some of the LLE polynomials are shown here:

$$\left.\begin{aligned} LLE_0(u) &= 1 \\ LLE_1(u) &= u - u^2 \\ LLE_2(u) &= -\frac{1}{2} + u + \frac{5u^2}{4} - 3u^3 + \frac{3u^4}{4} \\ LLE_3(u) &= -\frac{3u}{2} + \frac{9u^2}{2} + \frac{u^3}{4} - \frac{29u^4}{4} + \frac{15u^5}{4} - \frac{5u^6}{12} \\ LLE_4(u) &= \frac{3}{8} - \frac{3u}{2} - \frac{21u^2}{8} + \frac{59u^3}{4} - \frac{439u^4}{64} - 15u^5 + \frac{415u^6}{32} - \frac{35u^7}{12} + \frac{35u^8}{192} \end{aligned}\right\} \quad (2.10)$$

3. Numerical Method

In Galerkin methods [9], solution is obtained in terms of basis functions. In order to find the approximate solution, next step is to determine the unknown parameters in trial solution. So Galerkin method gives a polynomial as an approximate solution at each points instead of values, and we can find values at any points within the defined domain. The details of the numerical formulation of FVIE of 2nd kind are presented in [6].

4. Results and Discussion

Galerkin method is used to obtain the approximate solution of linear FVIE of 2nd kind, and we tried to explore the performance of Galerkin method by using a set of new types of polynomials (BF, CH, CL, FL, LLE polynomials). Here, we use exact solution of the numerical problems in order to check the accuracy of our code and to examine the recital of different polynomials with regard to absolute errors. Numerical results and graphs are generated by using Wolfram Mathematica 9.

In the first section, we will investigate the approximate solutions of the problem using Galerkin method where we will use BF, CH, CL, FL, LLE polynomials as basis functions. Secondly, we will see the performance of basis functions by observing error graphs using n = 2, 3, 4, 5. Finally, we will calculate RMSE and MAE for the numerical solutions to observe the accuracy of Galerkin method for different basis functions. Here we consider two numerical examples to carry out the investigations and in both examples, domain of the problem is [0, 1].

Example 1: [6]

$$\phi(x) + \int e^{x+t}\phi(t)dt - \int e^{x+t}\phi(t)dt = e^{-x} - (x-1)e^{x}\,, \quad 0 \le x \le 1 \quad (4.1)$$

Exact solution of $\phi(x)$ *is* $\phi(x) = e^{-x}$.

Firstly, Galerkin solution for linear FVIE of second kind with n = 2, 3, 4, 5 are presented in Tables A1 to A4 with five special types of polynomials (BF, CH, CL, FL, LLE) called as basis functions. From Tables A1 to A4, it is evident that using BF, CH, CL, FL, LLE polynomials as basis function in Galerkin method in order to find numerical approximations of FVIEs of 2nd kind are possible, and it has shown that numerical approximations of all the polynomials are converging into the same direction. It is also examined that polynomial solutions in Galerkin method using BF, CH, CL, FL, LLE polynomials are different, but approximate solutions are approximately same for each of these polynomials with same degree. For example, in Table A5 we have shown five approximate polynomials solution using five different polynomials as basis function for n = 5 to verify the previous statement. It suggests that introducing these polynomials can be functional and these polynomials can be used to obtain approximate solutions in Galerkin method. And it is seen that there is an insignificant effect on the solution of FVIEs compared with the exact solution. In the second part, from Fig. 4.1, we have observed absolute error graphs of five new polynomials over the interval [0, 1] for n = 2, 3, 4, 5.

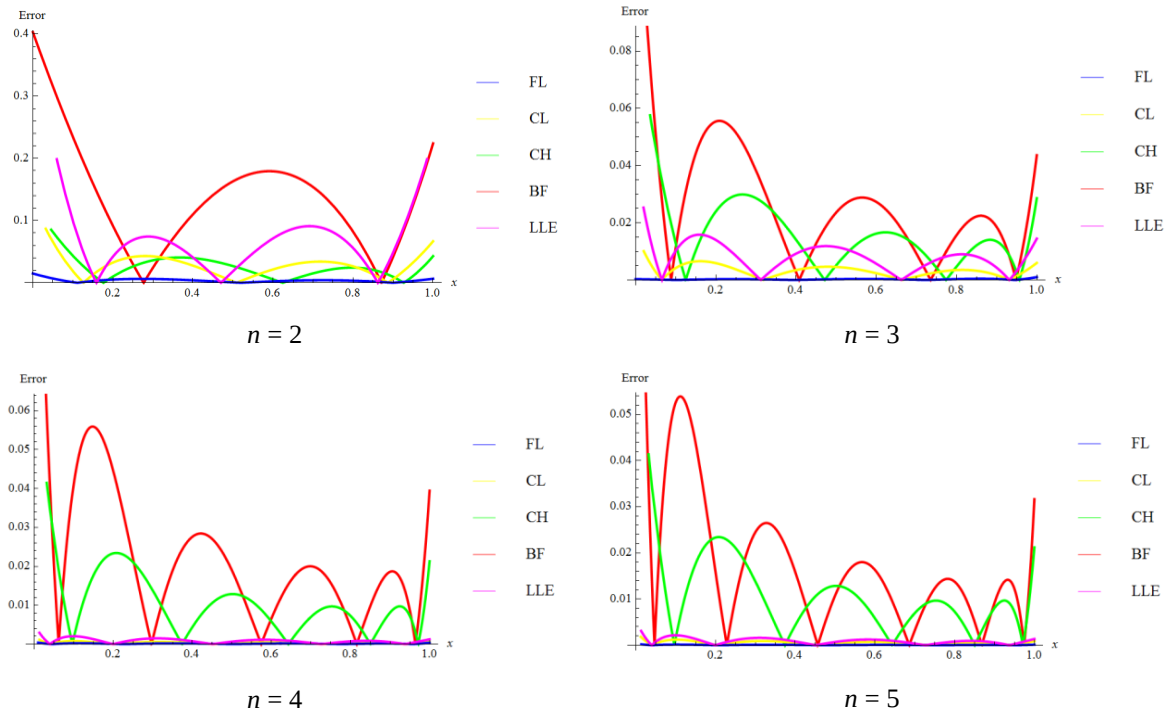

Fig. 4.1: Absolute error graph for Example 1

From this observation, we can claim that errors are decreasing as the values of n are increased. Hence, by increasing the values of n we can get desired accuracy using those basis polynomials. For this example, absolute errors are relatively high for BF and CH polynomials compared to the other polynomials. On the other hand, for FL polynomial absolute errors are significantly small for each values of n compared to the other polynomials.

Finally, we want to justify and understand our approximate solutions and error graphs more precisely and for this reason standard errors such as Mean Absolute Error (MAE) and Root Mean Square Error (RMSE) are observed for the approximate solutions. RMSE and MAE are given in Table 4.1 for different values of n with five different polynomials.

Table 4.1: RMSE and MAE results for Example 1

	n = 2		n = 3	
Polynomials	RMSE	MAE	RMSE	MAE
BF	0.1856936	0.1551874	0.0534938	0.0361026
CH	0.0472953	0.0346472	0.0321639	0.0227020
CL	0.0501415	0.0370874	0.0061832	0.00458443
FL	0.0059065	0.0044154	0.0003886	0.00029313
LLE	0.1513725	0.1066698	0.0152785	0.01132040
	n = 4		n = 5	
Polynomials	RMSE	MAE	RMSE	MAE
BF	0.0532509	0.0343142	0.0511507	0.0314623
CH	0.0242799	0.0159440	0.0242745	0.0159268
CL	0.0007080	0.0004955	0.0010927	0.0007841
FL	0.0002347	0.0001849	0.0001209	0.0000852
LLE	0.0018356	0.0012656	0.0019451	0.0013528

Above information shows that in all cases, both RMSEs and MAEs are decreased by increasing the values of n. It is again evident that FL polynomial gives the best accuracy of the approximate solution among the other polynomials for each values of n = 2, 3, 4, 5. Thus, for FL polynomial both errors are significantly small.

Example 2: [6]

$$\phi(x) + \int e^t \sin x\, \phi(t)dt - \int e^t \cos x\, \phi(t)dt = f(x)\,, \quad 0 \le x \le 1 \tag{4.2}$$

where

$$f(x) = e^x - \frac{1}{2}(e^{2x} - 1)\cos x + \frac{1}{2}(e^2 - 1)\sin x \tag{4.3}$$

Exact solution of $\phi(x)$ is $\phi(x) = e^x$

Similar procedures have also done for the above problem, and try to carry out our observation for this numerical example. Results are presented in Tables A6 to A9 with n = 2, 3, 4, 5. From Tables A6 to A9, It is again remarked that we can find numerical solution of FVIE of 2nd by using BF, CH, CL, FL, LLE polynomials as basis function in Galerkin method, and we have got significant result for each case. Secondly, we observe absolute error graphs for BF, CH, CL, FL, LLE polynomials in Galerkin method over the interval [0, 1] which are presented in Fig. 4.2.

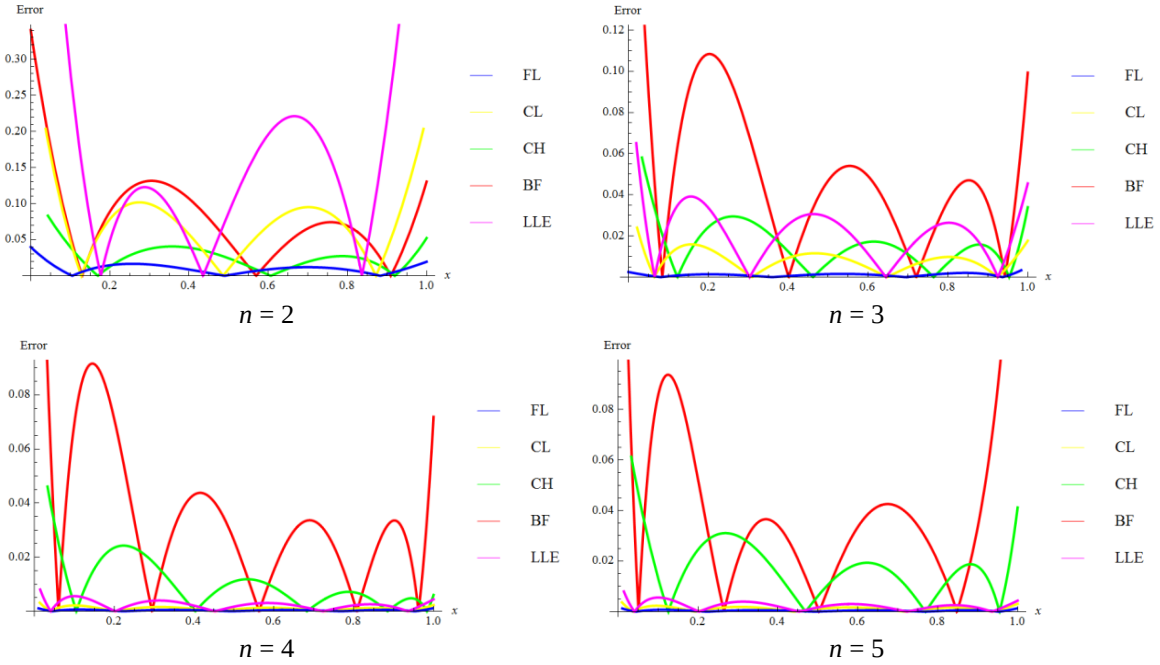

Fig.4.2: Absolute error graph for Example 2

We observe that errors reduce gradually as the values of n increase. For n = 4 & 5, absolute errors graphs are little high for BF and CH polynomials compared to the other polynomials. Similar findings are also observed for Example 1. It is observed that BF and CH polynomials exhibit higher functional values compare to other polynomials. This may play an important role to show higher absolute errors for these polynomials. According to the observation of the absolute error graphs, FL polynomial gives comparatively better results for each values of n in order to get approximate solutions of FVIEs of second kind in Galerkin method. In the last part, we have observed RMSE and MAE for each approximate solutions. RMSE and MAE are presented in Table 4.2 for n = 2, 3, 4 and 5.

Table 4.2: RMSE and MAE results for Example 2

	n = 2		n = 3	
Polynomials	RMSE	MAE	RMSE	MAE
BF	0.129489	0.0967744	0.1033868	0.0704576
CH	0.047037	0.0349461	0.0322473	0.0232427

CL	0.134701	0.1010860	0.0157194	0.0116686
FL	0.015932	0.0119732	0.0019901	0.0015194
LLE	0.399733	0.2743080	0.0401397	0.0298389
	n = 4		n = 5	
Polynomials	RMSE	MAE	RMSE	MAE
BF	0.0866670	0.056482	0.1027431	0.0695213
CH	0.0250143	0.014217	0.0342948	0.0253551
CL	0.0020563	0.001499	0.0022762	0.0017664
FL	0.0006835	0.000535	0.0008029	0.0006282
LLE	0.0052145	0.003625	0.0052129	0.0036167

Based on above information, in all cases both RMSEs and MAEs are decreased by increasing the values of n. So, same conclusion is also considerable for this problem.

Example 3:

$$\phi(x) + \int_0^1 e^{x-t}\phi(t)dt - \int_0^x (x-t)\,\phi(t)dt = f(x)\,, 0 \le x \le 1 \tag{4.4}$$

where

$$f(x) = e^x + x + 1 \tag{4.5}$$

Exact solution of $\phi(x)$is $\phi(x) = e^x$.

Accordingly, Tables A11 to A14 showed approximate solutions of linear FVIE of 2nd kind using Galerkin method for n=2,3,4,5 with BF, CH, CL, FL and LLE polynomials as basis functions. In Table A15, we show approximate polynomial solution for BF, CH, CL, FL, LLE polynomials (using as basis function in Galerkin method) with n=5, and each polynomial is a polynomial of degree 10. Then, we extent our observation by representing error graphs for BF, CH, CL, FL, LLE polynomials in Galerkin method over the interval [0, 1] and they are presented in Fig. 4.3.

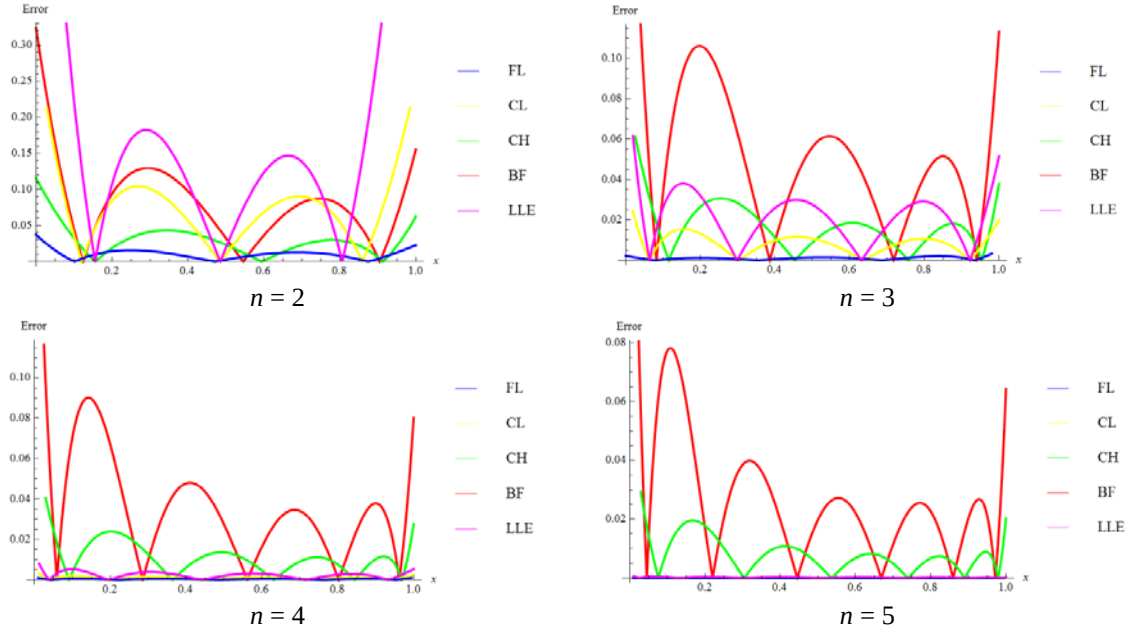

Fig.4.3: Absolute error graph for Example 3

We examine that absolute errors are decreasing significantly as the values of n increase. So, by increasing the values of n, it is possible to obtain desire accuracy of the problem. Finally, we have observed RMSE and MAE for each approximate solutions, and they are presented in Table 4.3 for n = 2, 3, 4 and 5.

Table 4.3: RMSE and MAE results for Example 3

	n = 2		n = 3	
Polynomials	RMSE	MAE	RMSE	MAE
BF	0.128485	0.0981224	0.1028080	0.0729980
CH	0.046646	0.0357625	0.0319543	0.0237026
CL	0.133949	0.1011620	0.0155413	0.0116668
FL	0.015758	0.0121843	0.0020232	0.0015067
LLE	0.394175	0.265560	0.0396560	0.0298728
	n = 4		n = 5	
Polynomials	RMSE	MAE	RMSE	MAE
BF	0.0861604	0.0578768	0.0748337	0.0482383
CH	0.0242705	0.0169154	0.0193992	0.0126937
CL	0.0020327	0.0014985	0.0001662	0.0001134
FL	0.0006825	0.0005388	0.0000536	0.0000413
LLE	0.0050217	0.0036309	0.0005045	0.0003298

According to the above information, in all cases both RMSEs and MAEs are decreased by increasing the values of n, and FL polynomial gives better result.

Conclusion

In this paper, new polynomials called BF, CH, CL, FL, LLE polynomials are introduced, and among them CH, CL, FL and LLE polynomials are polynomials of degree 2n. Then Linear FVIE of second kind is solved by Galerkin method where BF, CH, CL, FL, LLE polynomials are considered as basis function. Moreover, RMSE and MAE are calculated for each approximate solutions to examine the performance of basis functions in Galerkin method. And it is seen that in Galerkin method all approximate solutions are almost similar for different basis functions with same power. It is also seen that BF, FL, LLE and CL polynomials take less time than BF polynomials. Throughout this observation, we claim that it is possible to find approximate solutions of FVIE of 2nd kind by using BF, CH, CL, FL, LLE polynomials as basis function in Galerkin method. We have also examined that FL polynomial which is considered as basis function in Galerkin method gives us better result compared to the other basis functions (BF, CH, CL, LLE polynomials).

Conflict of Interest
The authors do not report any financial or personal connections with other persons or organizations, which might negatively affect the contents of this publication and/or claim authorship rights to this publication.

Publication Ethics
Submitted manuscripts must not have been previously published by or be under review by another print or online journal or source.

Funding
This research work is a self funded research.

References

[1] Maleknejad, K. & Hadizadeh, M. (1999). A new computational method for Volterra-Fredholm integral equation. Computers and Mathematics with Applications, 37, 1-8.

[2] Maleknejad, K. & FadaeiYami, M.R. (2006). A computational method for system of Volterra-Fredholm integral equations. Applied Mathematics and Computation, 183(1),589-595.

[3] Hendi, F.A. & Bakodah, H.O. (2012). Numerical solution of Fredholm-Volterra integral equation in two dimensional space by using discrete Adomain decomposition method. IJRRAS, 10(3), 466-471.

[4] Hendi, F.A. & Albugami, A.M. (2009). Numerical solution for Fredholm–Volterra integral equation of the second kind by using collocation and Galerkin methods. Journal of King Saud University (Science), 22, 37-40.doi: 10.1016/j. jksus. 2009. 12. 006

[5] Mustafa, M.M. & Ghanim, I.N. (2018). Numerical solution of linear Volterra-Fredholm integral equations using quadrature methods.

[6] Molla, H.U. & Saha, G. (2020). Numerical approximations of Fredholm-Volterra integral equation of second kind using Galerkin and Collocation methods. Suan Sunandha Science and Technology Journal, 7(2), 15-22.

[7] Abdou, M.A., Soliman, A.A. & Abdel-Aty, M.A. (2020). On a discussion of Volterra-Fredholm integral equation with discontinuous kernel. Journal of the Egyptian Mathematical Society, 28, 1-10.

[8] Molla, H.U. & Saha, G. (2018). Numerical approximation of Fredholm integral equation (FIE) of 2nd kind using Galerkin and collocation methods. GANIT: Journal of Bangladesh Mathematical Society, 38,11-25.doi:10.3329/ganit.v38i0.39782

[9] Lewis, P. E. & Ward, H. R. (1991). The finite element method: Principles and application. Addison-Wesley Publishing Company.

APPENDIX A:

Table A1: Numerical results for Example 1 (n = 2)

x	EXACT	BF	CH	CL	FL	LLE
0.0	1.000000	1.402747	0.872596	0.870121	1.014979	0.599279
0.1	0.904837	1.139234	0.861446	0.886132	0.905866	0.805545
0.2	0.818731	0.910140	0.828788	0.851282	0.813534	0.860804
0.3	0.740818	0.716518	0.776997	0.783340	0.734651	0.814721
0.4	0.670320	0.560129	0.710031	0.697982	0.666275	0.711115
0.5	0.606531	0.443447	0.633432	0.608796	0.605857	0.587965
0.6	0.548812	0.369653	0.554324	0.527277	0.551241	0.477405
0.7	0.496585	0.342642	0.481415	0.462832	0.500662	0.405729
0.8	0.449329	0.367015	0.424997	0.422777	0.452746	0.393385
0.9	0.406569	0.448087	0.396944	0.412337	0.406515	0.454980
1.0	0.367879	0.591881	0.410714	0.434648	0.361379	0.599279

Table A2: Numerical results for Example 1 (n = 3)

x	EXACT	BF	CH	CL	FL	LLE
0.0	1.000000	1.151427	0.909564	0.983350	1.000283	0.958811
0.1	0.904837	0.893436	0.892129	0.909014	0.904846	0.915063
0.2	0.818731	0.763348	0.842693	0.824616	0.818468	0.832715
0.3	0.740818	0.702516	0.769416	0.741811	0.740574	0.742461
0.4	0.670320	0.667598	0.684387	0.666867	0.670334	0.661109
0.5	0.606531	0.630116	0.601363	0.601975	0.606820	0.594997
0.6	0.548812	0.576096	0.532601	0.546445	0.549162	0.543118
0.7	0.496585	0.505819	0.484781	0.497807	0.496679	0.499986
0.8	0.449329	0.433663	0.454034	0.452799	0.449009	0.458221
0.9	0.406569	0.388805	0.420051	0.408261	0.406215	0.410863
1.0	0.367879	0.411482	0.339298	0.361912	0.368884	0.353421

Table A3: Numerical results for Example 1 (n = 4)

x	EXACT	BF	CH	CL	FL	LLE
0.0	1.000000	1.155063	0.929939	0.998042	0.999456	0.994885
0.1	0.904837	0.863940	0.906318	0.905615	0.905061	0.906862
0.2	0.818731	0.774149	0.842058	0.818743	0.818807	0.818722
0.3	0.740818	0.742091	0.754639	0.740257	0.740667	0.739346
0.4	0.670320	0.697897	0.665973	0.670017	0.670151	0.669564
0.5	0.606531	0.625539	0.593669	0.606764	0.606519	0.607169
0.6	0.548812	0.542236	0.542974	0.549244	0.548956	0.549918
0.7	0.496585	0.476581	0.503573	0.496725	0.496724	0.496899
0.8	0.449329	0.444874	0.456606	0.449053	0.449284	0.448609
0.9	0.406569	0.425150	0.398469	0.406342	0.406405	0.406042
1.0	0.367879	0.328439	0.389164	0.368410	0.368244	0.369117

Table A4: Numerical results for Example 1 (n = 5)

x	EXACT	BF	CH	CL	FL	LLE
0.0	1.000000	1.152473	0.929920	0.997018	1.000333	0.994609
0.1	0.904837	0.852263	0.906303	0.906036	0.904706	0.906984
0.2	0.818731	0.802881	0.842055	0.818795	0.818717	0.818717
0.3	0.740818	0.765297	0.756515	0.739939	0.740905	0.739239
0.4	0.670320	0.686192	0.665995	0.669803	0.670383	0.669510
0.5	0.606531	0.595780	0.593684	0.606879	0.606513	0.607225
0.6	0.548812	0.532499	0.542967	0.549516	0.548746	0.550011
0.7	0.496585	0.499803	0.503546	0.496832	0.496545	0.496924
0.8	0.449329	0.463076	0.456593	0.448883	0.449357	0.448541
0.9	0.406569	0.397390	0.398506	0.406191	0.406619	0.405995
1.0	0.367879	0.399509	0.389068	0.368743	0.367772	0.369225

Table A5: Approximate polynomial solutions for Example 1 (n = 5)

Polynomials	Approximate polynomial solutions ($\tilde{\varphi}(x)$)
BF	$1.15247345 - 5.7623672x + 38.190357x^2 - 123.676961x^3 + 191.28067x^4 - 136.574009x^5 + 38.150331x^6 - 9.717654x^7 + 7.637876x^8 - 0.33114693x^9 + 0.049938671x^{10}$
CH	$0.92992 - 2.4195x^2 + 5.8451x^4 - 6.9284x^6 + 2.9674x^8 - 0.0054445x^{10}$
CL	$0.99702 - 0.89614x - 0.372667x^2 + 2.79001x^3 - 4.6447x^4 + 3.31052x^5 - 0.47132x^6 - 0.55406x^7 + 0.240349x^8 - 0.031513x^9 + 0.00126052x^{10}$
FL	$1.000333 - 1.011737x + 0.60256x^2 - 0.550671x^3 + 0.800712x^4 - 0.890065x^5 + 0.640786x^6 - 0.292145x^7 + 0.0767605x^8 - 0.00912658x^9 + 0.000365063x^{10}$
LLE	$0.9946 - 0.8062x - 1.1962x^2 + 5.9365x^3 - 10.692x^4 + 9.587x^5 - 4.0378x^6 + 0.55248x^7 + 0.041717x^8 - 0.011685x^9 + 0.00046741x^{10}$

Table A6: Numerical results for Example 2 (n = 2)

x	EXACT	BF	CH	CL	FL	LLE
0.0	1.000000	1.340495	1.123314	1.330865	0.960178	1.994119
0.1	1.105171	1.160955	1.144839	1.153858	1.103909	1.387584
0.2	1.221403	1.132489	1.208674	1.142888	1.236002	1.172719
0.3	1.349859	1.218369	1.312602	1.250363	1.365524	1.228219
0.4	1.491825	1.384966	1.452928	1.434292	1.500473	1.447048
0.5	1.648721	1.601759	1.624478	1.658282	1.647782	1.736440
0.6	1.822119	1.841333	1.820598	1.891538	1.813315	2.017904
0.7	2.013753	2.079377	2.033160	2.108865	2.001874	2.227218
0.8	2.225541	2.294685	2.252554	2.290668	2.217189	2.314432
0.9	2.459603	2.469158	2.467693	2.422948	2.461928	2.243868
1.0	2.718282	2.587802	2.666012	2.497308	2.737691	1.994119

Table A7: Numerical results for Example 2 (n = 3)

x	EXACT	BF	CH	CL	FL	LLE
0.0	1.000000	1.287770	1.088912	1.041651	0.997498	1.106021
0.1	1.105171	1.075753	1.116687	1.094703	1.105588	1.079326
0.2	1.221403	1.113039	1.197124	1.207495	1.228030	1.187712
0.3	1.349859	1.279609	1.322029	1.348566	1.350633	1.348632
0.4	1.491825	1.491080	1.479356	1.501197	1.491285	1.517373
0.5	1.648721	1.695569	1.655607	1.659813	1.647235	1.677731
0.6	1.822119	1.871219	1.839203	1.826688	1.820821	1.833428
0.7	2.013753	2.024405	2.024819	2.008925	2.013859	2.000284
0.8	2.225541	2.188612	2.218677	2.215728	2.227315	2.199126
0.9	2.459603	2.420016	2.444802	2.455963	2.460987	2.449448
1.0	2.718282	2.817638	2.752245	2.736002	2.713251	2.763819

Table A8: Numerical results for Example 2 (n = 4)

x	EXACT	BF	CH	CL	FL	LLE
0.0	1.000000	1.250063	1.075603	1.005443	1.001539	1.014459
0.1	1.105171	1.035707	1.107548	1.103017	1.104544	1.099588
0.2	1.221403	1.150292	1.197907	1.221340	1.221217	1.221227
0.3	1.349859	1.353454	1.332069	1.351411	1.350290	1.353777
0.4	1.491825	1.534912	1.491309	1.492666	1.492259	1.493902
0.5	1.648721	1.674947	1.659734	1.648026	1.648696	1.647018
0.6	1.822119	1.806986	1.831007	1.820838	1.821687	1.819122
0.7	2.013753	1.980388	2.011856	2.013361	2.013400	2.012971
0.8	2.225541	2.221737	2.218509	2.226495	2.225741	2.227727
0.9	2.459603	2.493157	2.461356	2.460435	2.460091	2.461194
1.0	2.718282	2.646382	2.712265	2.715999	2.717108	2.713881

Table A9: Numerical results for Example 2 (n = 5)

x	EXACT	BF	CH	CL	FL	LLE
0.0	1.000000	1.254249	1.091654	1.005527	1.001895	1.014482
0.1	1.105171	1.019803	1.118548	1.102837	1.104430	1.099590
0.2	1.221403	1.168899	1.196909	1.221612	1.221193	1.221206
0.3	1.349859	1.370233	1.319937	1.351750	1.350369	1.353762
0.4	1.491825	1.525867	1.476966	1.492646	1.492329	1.493911
0.5	1.648721	1.650158	1.654892	1.647643	1.648683	1.647044
0.6	1.822119	1.788651	1.840925	1.820464	1.821612	1.819141
0.7	2.013753	1.972185	2.027304	2.013387	2.013346	2.012965
0.8	2.225541	2.205479	2.218559	2.226918	2.225780	2.227700
0.9	2.459603	2.492856	2.441719	2.460673	2.460170	2.461182
1.0	2.718282	2.906693	2.759489	2.715178	2.716914	2.713927

Table A10: Approximate polynomial solutions for Example 2 (n = 5)

Polynomials	Approximate polynomial solutions ($\tilde{\varphi}(x)$)
BF	$1.25424892 - 6.2712446x + 53.3211044x^2 - 164.4280359x^3 + 260.311097x^4 - 224.740958x^5 + 116.9850364x^6 - 49.6143677x^7 + 19.0062071x^8 - 3.27973169x^9 + 0.36333659x^{10}$
CH	$1.09165 + 2.70894x^2 - 1.95453x^4 + 0.367927x^6 + 0.641343x^8 - 0.095846x^{10}$
CL	$1.00552 + 0.79376x + 2.32544x^2 - 6.3448x^3 + 11.143x^4 - 9.2554x^5 + 3.25266x^6 - 0.050175x^7 - 0.182068x^8 + 0.0283702x^9 - 0.0011348x^{10}$
FL	$1.00182 + 0.94212x + 0.9369x^2 - 1.14966x^3 + 1.91422x^4 - 1.32656x^5 + 0.522955x^6 - 0.151293x^7 + 0.0293789x^8 - 0.00310813x^9 + 0.000124325x^{10}$
LLE	$1.014 + 0.4905x + 4.922x^2 - 15.74x^3 + 28.29x^4 - 26.0x^5 + 11.94x^6 - 2.361x^7 + 0.1566x^8 - 0.001385x^9 + 0.0000554x^{10}$

Table A11: Numerical results for Example 3 (n = 2)

x	EXACT	BF	CH	CL	FL	LLE
0.0	1.000000	1.324201	1.115579	1.308356	0.962619	1.925268
0.1	1.105171	1.149250	1.137576	1.140965	1.104778	1.326699
0.2	1.221403	1.127303	1.202765	1.136971	1.235658	1.114158
0.3	1.349859	1.220502	1.308749	1.248972	1.364328	1.168164
0.4	1.491825	1.394063	1.451533	1.435142	1.498791	1.383298
0.5	1.648721	1.616279	1.625519	1.659233	1.645981	1.668195
0.6	1.822119	1.858518	1.823518	1.890572	1.811768	1.945545
0.7	2.013753	2.095223	2.036734	2.104066	2.000953	2.152095
0.8	2.225541	2.303911	2.254778	2.280195	2.217269	2.238650
0.9	2.459603	2.465177	2.465661	2.405017	2.463385	2.170069
1.0	2.718282	2.562688	2.655796	2.470168	2.740901	1.925268

Table A12: Numerical results for Example 3 (n = 3)

x	EXACT	BF	CH	CL	FL	LLE
0.0	1.000000	1.278844	1.084872	1.039803	0.997773	1.101115
0.1	1.105171	1.071526	1.113146	1.094629	1.105565	1.079046
0.2	1.221403	1.115273	1.194925	1.208269	1.222673	1.189416
0.3	1.349859	1.287276	1.321589	1.349423	1.350513	1.350301
0.4	1.491825	1.501323	1.480482	1.501606	1.491237	1.517718
0.5	1.648721	1.704772	1.657481	1.659529	1.647277	1.676244
0.6	1.822119	1.876199	1.840591	1.825764	1.820935	1.830375
0.7	2.013753	2.023732	2.024562	2.007707	2.014001	1.996647
0.8	2.225541	2.184061	2.216542	2.214821	2.227411	2.196498
0.9	2.459603	2.422127	2.442752	2.456176	2.460938	2.449893
1.0	2.718282	2.831494	2.756182	2.738276	2.712925	2.769683

Table A13: Numerical results for Example 3 (n = 4)

x	EXACT	BF	CH	CL	FL	LLE
0.0	1.000000	1.244519	1.067028	1.005244	1.001463	1.013360
0.1	1.105171	1.034739	1.101384	1.103086	1.104569	1.099890
0.2	1.221403	1.154437	1.197524	1.221416	1.221248	1.221631
0.3	1.349859	1.359657	1.337214	1.351396	1.350291	1.353768
0.4	1.491825	1.539598	1.497925	1.492578	1.492232	1.493522
0.5	1.648721	1.676229	1.662302	1.647938	1.648659	1.646591
0.6	1.822119	1.805699	1.826778	1.820819	1.821668	1.818975
0.7	2.013753	1.979618	2.004689	2.013433	2.013414	2.013227
0.8	2.225541	2.224443	2.217937	2.226605	2.225781	2.228179
0.9	2.459603	2.497477	2.469875	2.460457	2.460113	2.461319
1.0	2.718282	2.638158	2.690828	2.715751	2.717015	2.712973

Table A14: Numerical results for Example 3 (n = 5)

x	EXACT	BF	CH	CL	FL	LLE
0.0	1.000000	1.217698	1.055374	1.000455	0.999877	1.001456
0.1	1.105171	1.027799	1.095602	1.105068	1.105212	1.104824
0.2	1.221403	1.204613	1.203637	1.221535	1.221371	1.221828
0.3	1.349859	1.388424	1.349121	1.349853	1.349835	1.349872
0.4	1.491825	1.511544	1.502509	1.491715	1.491848	1.491468
0.5	1.648721	1.628954	1.653403	1.648718	1.648752	1.648663
0.6	1.822119	1.800016	1.815297	1.822216	1.822114	1.822420
0.7	2.013753	2.025208	2.008863	2.013766	2.013719	2.013865
0.8	2.225541	2.248195	2.232277	2.225451	2.225534	2.225283
0.9	2.459603	2.439381	2.457459	2.459648	2.459643	2.459625
1.0	2.718282	2.782557	2.738509	2.718089	2.718188	2.718006

Table A15: Approximate polynomial solutions for Example 3 (n = 5)

Polynomials	Approximate polynomial solutions ($\tilde{\varphi}(x)$)
BF	$1.217698255 - 6.08849127x + 58.792735x^2 - 199.319805x^3 + 329.217429x^4 - 268.840521x^5 + 113.8964514x^6 - 47.3745451x^7 + 23.9235674x^8 - 2.98978067x^9 + 0.347819639x^{10}$
CH	$1.0553736 + 4.1374469x^2 - 11.703857x^4 + 24.242969x^6 - 23.550553x^8 + 8.557129x^{10}$
CL	$1.000454 + 0.974295x + 0.857404x^2 - 1.929012x^3 + 6.3477x^4 - 10.55566x^5 + 10.04022x^6 - 5.23671x^7 + 1.373203x^8 - 0.1602158x^9 + 0.00640863x^{10}$
FL	$0.999876 + 1.006006x + 0.42883x^2 + 0.52035x^3 - 0.861173x^4 + 1.306827x^5 - 1.093587x^6 + 0.542844x^7 - 0.1490253x^8 + 0.01795593x^9 - 0.000718237x^{10}$
LLE	$1.001456 + 0.918849x + 1.61144x^2 - 6.25213x^3 + 19.0753x^4 - 31.4524x^5 + 29.5633x^6 - 15.3024x^7 + 4.00281x^8 - 0.466882x^9 + 0.0186753x^{10}$

GANIT

Available online at https://ganitjournal.bdmathsociety.org/

GANIT: Journal of Bangladesh Mathematical Society

GANIT *J. Bangladesh Math. Soc.* 41.1 (2021) 15–25
DOI: https://doi.org/10.3329/ganit.v41i1.55023

Factorizing a Quadratic Expression with Reasoning

Anwar H. Joarder *

Department of CSE, Northern University of Business and Technology Khulna, Khulna 9100, Bangladesh.

ABSTRACT

It is not popularly realized that the factorization of a general quadratic expression basically requires solution to a hyperbola and a line. This fact is conspicuously pointed out and a few solutions to the problem are demonstrated that are scattered in the literature. In the high school level, the coefficients of a quadratic expression are mostly integers, and factorization is performed by the popular method of decomposition of the middle term. In this expository note, we have presented it in a simpler way that shows both insight and reasoning into the problem. Some other methods, namely, Linear Method, Average Method and Difference of two Squares Method are also discussed. Depending on the background, a reader may prefer a particular method to the others. The expository nature and artistry in presentation of the paper are expected to make the learning of the topic amusing and instructive.

Received: November 26, 2020 **Accepted:** March 18, 2021 **Published Online:** August 04, 2021

Keywords: Quadratic expression; polynomial of degree 2; factorization.

AMS Subject Classification 2020: 00-01; 00-02; 00A06

1. Introduction

Factorization of a quadratic expression or solving a quadratic equation pops up often in physics and engineering for calculating trajectories, and even in sports. If, while watching the Super Bowl, you want to estimate how far a pass thrown by a football quarterback travelled through the air, you solve a quadratic equation. A popular example of a quadratic equation appears at minimizing cost and maximizing profit in business.

The quadratic expression or its solution has a long history stretching as far back as the Old Babylonian Period around 2000–1600 B.C. See, for example, [1] and [2]. Over four millennia, many mathematicians have contributed to the topic. In particular, several books have surveyed the topic of the quadratic formula, such as Chapter 2 of [3], and mathematical history books such as [4], [5] and [1]. For a brief description see [6] and the references therein.

* Corresponding author: Anwar H. Joarder, *E-mail address:* ajstat@gmail.com

The general quadratic expression $q(x) = ax^2 + bx + c$ with leading coefficient $a \neq 0$ may be termed as a polynomial of degree 2 in the variable x or briefly a quadratic trinomial. The quantities a, b and c are coefficients of the quadratic expression. The quadratic expression with leading coefficient $a = 1$, i.e., $x^2 + bx + c$ is called a monic quadratic expression. Factorization of a quadratic expression appears at algebra at high school level and it is usually done by decomposing the middle term. But broad spectrum of students still feel a significant leap of insight. While factorization of the monic quadratic expression is relatively easier, its connection with the general quadratic expression is not usually spelled out to the students during factorization. See for example [7].

It is easy to check that $(y + j)(y + k) = y^2 + (j + k)y + jk$ which is a monic quadratic expression as the coefficient of y^2 is 1. We can write a standard monic quadratic expression as $y^2 + by + m.$ Then its factorization is a historic problem of determining j and k given the sum $j + k = b$ and the product $jk = m.$ While there are many solutions to the problem, the most popular is the decomposition of the middle term, i.e. given $b,$ we try to find j and k such that $jk = m.$ In case j and k are numbers, then $j + k = b$ and $jk = m$ are a line and a hyperbola whose precise graphical solution requires a computer. At the middle school level, j and k are usually integers, then $j + k = b$ and $jk = m$ are a dotted line and a dotted hyperbola.

It is not popularly realized that the factorization of a general quadratic expression basically requires solution to a line and a hyperbola. This fact is pointed out clearly for students of secondary or tertiary education and written at that level of simplicity. It is amazing that in some cases when the coefficients are integers, the dotted line and dotted hyperbola have a simple solution.

The paper is organized as follows. Section 2 shows the connection between a general quadratic expression and a monic quadratic expression while factorization. The solution to find two numbers given their sum and product, was known to the Babylonians. See, for example, [1], [3], [4], [8] and [18]. The method of Additive Decomposition of the Middle Term b is explained in Section 3 in an instructive way when the coefficients are integers. It is renamed as Factoring Method.

Two other methods namely, Linear Method and Average Method are also discussed in Sections 4 and 5 respectively. The average method is due to Babylonians but recently popularized by [6,9] providing a clear insight with much simplicity. The method of completing the square by al-Khawarizmi is discussed in Section 6 by characterizing it by the derivative of a quadratic expression and discriminant of the quadratic equation. Because of its importance, many authors have published on the issue with alternative representations. See for example, [10,11,12,13,14,15,16,17].

2. General and Monic Quadratic Expressions

The connection between the general quadratic expression and monic quadratic expression required during factorization is spelled out well in this section.

Theorem 2.1 Let

$$q(x) = ax^2 + bx + c,\ a \neq 0,\ c \neq 0,$$

(2.1)

be the quadratic expression. Also let the monic quadratic from $y^2 + by + m$ be factorized as

$$y^2 + by + m = (y + j)(y + k) = Q(y;\ j,\ k),$$

(2.2)

so that $j + k = b$

(2.3)

and $jk = m.$

(2.4)

Then $q(x)$ can be factorized by the following equivalent ways:

a. $q(x) = \frac{1}{a}\ (ax + j)(ax + k),$

(2.5a)

b. $q(x) = \frac{1}{a}\ Q(ax;\ j,k) = a\ Q\left(x;\ \frac{j}{a},\ \frac{k}{a}\right) = Q\left(\sqrt{a}x;\ \frac{j}{\sqrt{a}}, \frac{k}{\sqrt{a}}\right),$

(2.5b)

if $jk = ac.$

(2.6)

Proof. It is easy to check that $a \times q(x) = a^2x^2 + abx + ac,$ can be transformed to $y^2 + by + ac$ where $y = ax.$ By using (2.2), (2.3) and (2.4), we have 2.5(a). The part 2.5(b) follows from (2.5a).

It seems part 2.5(a) is the simplest. Note that j and k can be found by factorizing $y^2 + by + ac$ by (2.2) where a, b and c are available from the given quadratic expression $q(x).$ Then plugging them in (2.5a), we can get the factorized form of $q(x).$ Without any loss of generality, we assume that $a > 0.$ In case $a < 0,$ we may factorize $-q = -ax^2 - bx - c$ so that $-a,$ the coefficient of $x^2,$ is non-negative.

The solution to find numbers given their sum and product, was known to the Babylonians. See for example, [1,3,4,8,18].

3. Factoring Method (j and k are integers)

In Theorem 2.1, we have noticed that for factorization of a monic quadratic expression, $y^2 + by + m,$ we need (j,k) such that $j + k = b$ and $jk = m.$ Usually students stumble to find possible solution to (j,k) such that $j + k = b,$ and then look for (j,k) where $jk = m$ by trial and error, and the method is well known as Decomposition of the Middle Term. Since the set $\{(j,k) : j + k = b\}$ involves many solutions than that in $\{(j,k) : jk = m\},$ we recommend to decompose $jk = m$ first and look for (j,k) such that the dotted line $j + k = b$ is satisfied. In this section, we demonstrate a method that factorizes monic quadratic expression through a tabular representation of factoring $|m| = |jk|$ first and then $m = jk.$ Since $j + k = b,$ the larger one of (j,k) in absolute value has the same sign as that of $b.$ The method is renamed as Factoring Method for simplicity.

Case 1: Let (m,b) be in the first quadrant of m-b axes of co-ordinates, i.e., $m > 0$ and $b > 0.$ Obviously, $m = jk > 0$ implies that j and k are of the same sign. Then by virtue of $b = j + k > 0,$ we have $j > 0$ and $k > 0$ (first quadrant of j-k axes of co-ordinates)

Case 2: Let (m,b) be in the second quadrant of m-b axes of co-ordinates, i.e., $m < 0$ and $b > 0.$ Obviously, $m = jk < 0$ implies that j and k are of the opposite signs. Then by virtue of $b = j + k > 0,$

one possibility is to have $-k < j < 0,$ i.e., $j < 0$ and $k > 0$ (second quadrant of j-k axes of co-ordinates). Alternatively, by virtue of $b = j + k > 0,$ we have $-j < k < 0,$ i.e. $j > 0$ and $k < 0$ (fourth quadrant of j-k axes of co-ordinates).

Case 3: Let (m, b) be in the third quadrant of m-b axes of co-ordinates , i.e., $m < 0$ and $b < 0.$ Obviously, $m = jk < 0$ implies that j and k are of the opposite signs. Then by virtue of $b = j + k < 0,$ one possibility is to have $0 < j < -k,$ i.e., $j > 0$ and $k < 0$ (fourth quadrant j-k axes of co-ordinates). Alternatively by virtue of $b = j + k < 0,$ we have $0 < k < -j,$ i.e., $j < 0$ and $k > 0$ (second quadrant j-k axes of co-ordinates).

Case 4: Let (m, b) be in the fourth quadrant of m-b axes of co-ordinates, i.e., $m > 0$ and $b < 0.$ Obviously, $m = jk > 0$ implies that j and k are of the same sign. Then by virtue of $b = j + k < 0,$ and noting that the sign of b is the same as that of j and $k,$ we have $j < 0$ and $k < 0$ (third quadrant of j-k axes of co-ordinates).

The above rules may be summarized to two simple rules:

Rule I: If $m > 0,$ then both the signs of (j, k) are the same as that of $b.$
Rule II: If $m < 0,$ then the signs of (j, k) are different; the larger one of (j, k) in absolute value has the same sign as that of $b = j + k.$

Note that $Q1,$ $Q2,$ $Q3$ and $Q4$ in Table 3.1 denote axes of coordinates of j-k. Figure 3.1a contains the same information presented in a different style.

Table 3.1: Sign Table for (j, k)

(m, b)	(j, k)	Comment on Signs of (j, k)
$(+, +)$	$Q1: (+, +)$	The signs are the same as that of b
$(-, +)$	$Q2: (-, +),\ -k < j < 0$ / $Q4: (+, -),\ -j < k < 0$*	The signs are different. The larger one in absolute value has the same sign as that of b
$(-, -)$	$Q4: (+, -),\ 0 < j < -k$ / Q2: $(-, +),\ 0 < k < -j$*	
$(+, -)$	$Q3:\ (-, -)$	The signs are the same as that of b

*We have not considered the asterisk cases in the Factoring Method.

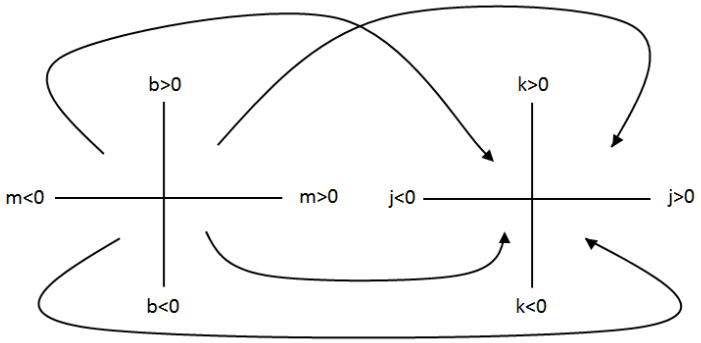

Figure 3.1a Sign table for (j, k)

Keep dividing $|m|=|jk|$ by possible divisors, say, $j=1,2,3,...,$ and then repeating it for $m=jk$ so that it is completely divisible. Stop at $|j|\leq|k|$. Then the solution (j,k) is obvious from their absolute values intuitively or by the above rules. An example is provided below to illustrate the idea.

Example 3.1 Factorize $q(x)=8x^2-2x-15.$

Solution: It is easy to check that $q(x)=\frac{1}{8}(8x^2\times 8-2x\times 8-15\times 8)$ can be transformed to

$\frac{1}{8}(y^2-2y-15\times 8)$ where $y=8x.$ We will factorize $y^2-2y-15\times 8$ first. By comparing it with $y^2+by+m,$ we have $m=jk=ac=8(-15)=-120$ and $b=-2.$ Obviously, $m=jk<0$ implies that j and k are of the opposite signs. Then by virtue of $b=j+k<0,$ one possibility is to have $0<j<-k,$ i.e., $j>0$ and $k<0.$ Another possibility not used here is $0<k<-j,$ i.e., $j<0$ and $k>0.$ You may check Case 3 and Rule II at the beginning of this section for general logic or Table 3.1 or Figure 3.1a.

Factoring $|jk|=120,$ and then $jk=-120$ by the above arguments or by eye inspection, we have the following table:

Table 3.2: Factoring Table

j	1	2	3	4	5	6	8	10
k	-120	-60	-40	-30	-24	-20	-15	-12

To satisfy $j+k=-2,$ we have $j=10,k=-12$ so that $y^2-2y-15\times 8=(y+10)(y-12)$ and finally by (2.5a), we have

$$q(x)=\frac{1}{8}(8x+10)(8x-12)=(4x+5)(2x-3).$$

4. Linear Method

In Section 2, we have mentioned that the process of factorization requires to solve a line $j+k=b$ and a hyperbola $jk=m.$ The Babylonian tablets clearly indicate that they had realized $j+k=2b$ and $jk=m$ as the perimeter and the area of a rectangle. These two equations are equivalent to two lines: $k+j=b$ and $k-j=t$ where t is defined in equation (4.1). Thus the problem of factorization boils down to equilibrium

point of two lines. Algebraically, it means, determining two numbers given their sum and difference. The method may be named as Linear Equilibrium Method or simply Linear Method.

The monic quadratic expression is given by $y^2 + by + m,$ (say). From Section 2, we have $k + j = b$ and $jk = m.$ Assuming $j \le k,$ by virtue of the identity $(k-j)^2 = (k+j)^2 - 4jk,$ another line $k - j = t$ can be determined where

$$t^2 = b^2 - 4m.$$
(4.1)

The solution to the lines $k + j = b$ and $k - j = t$ is
$$k = (b+t)/2 \text{ and } j = (b-t)/2.$$
(4.2)

To factorize $q(x) = 8x^2 - 2x - 15$ of Example 3.1, we have $k + j = -2$ and $jk = -120 < 0.$ Assuming $0 < k < -j,$ i.e., $k > 0$ and $j < 0,$ or, $k > 0$ and $-j > 0,$ it follows that $k + (-j) > 0.$ Then $(k-j)^2 = (k+j)^2 - 4jk = 484$ so that $k - j = 22.$ Solving $k + j = -2 (= b)$ and $k - j = 22 (= t),$ by equation (4.2), we have $k = [(-2) + 22]/2 = 10$ and $j = [(-2) - (22)]/2 = -12.$ Alternatively by assuming $0 < j < -k,$ i.e., $j > 0$ and $k < 0,$ we have $k = -12$ and $j = 10.$ Then the factorization is obvious by (2.5a).

5. Average Method

As mentioned earlier, Babylonians were interested in finding the dimensions j and k of a rectangle with a given area m and a given perimeter 2*b*. They solved it by a method what may be called the Average Method and is recently popularized by [6,9]. In general, let the average of the two numbers j and k be $b/2.$ Assume that the smaller number (j) is r units below the average and the larger one $(k \ge j)$ is r units above the average. That is, they are of the form: $j = (b/2) - r$ and $j = (b/2) + r,$ where $r (\ge 0)$ is yet to be determined. Then by equation (2.4) and (2.6), we have $jk = m = ac,$ and hence the following average equation:

$$\left(\frac{b}{2} - r\right)\left(\frac{b}{2} + r\right) = ac,$$
(5.1) or, $r^2 = (b/2)^2 - ac,$
(5.2)
or, $r = \sqrt{(b/2)^2 - ac},$
(5.3)
where $b^2 \ge 4ac.$

The beauty of this method is that r has a natural meaning. Moreover since a, b and c are known, r is easily determined. Also in Section 6, this method shows a new meaning of discriminant of a quadratic equation. Algebraically the Linear Method and the Average Method are equivalent but the clarity of natural meaning of r in the Average Method compared to t (see equation 4.2) in the Linear Method deserves appreciation.

To factorize $q(x) = 8x^2 - 2x - 15$ of Example 3.1, we see the average of j and k is $-2/2 = -1,$ and

they are of the form $j=-1-r$ and $k=-1+r$ so that by the average equation in (5.1), we have $(-1-r)(-1+r)=ac=-120,$ or, $r=11.$ Hence they are $j=-1-r=-12$ and $k=-1+r=10.$ Then the factorization is obvious by equation (2.5a).

Note that it follows from (5.2) that

$$2r=\sqrt{b^2-4ac}=k-j$$

(5.4)

Hence one may save time during factorization by utilizing the equation $2r=\sqrt{b^2-4ac}.$ In case $j+k=b$ is not an even number, it would be easier to assume average is $b/2=B$ so that the average equation (5.1) would be $(B-r)(B+r)=ac.$

6. Difference of Squares (DS) Method

In the year 825, about 2500 years after the Babylonian tablets were created, a general method similar to today's Quadratic Formula was authored by the Arab mathematician Muhammad ibn Musa al-Khwarizmi in a book titled *Hisab al-jabr w'al-muqabala.* His technique was completing the square and more general than those of the Babylonians. The word "al-jabr" in the title of his book led to our modern word "algebra". The word "algorithm" comes from al-Khwarizmi's name.The authors in [19,20,21] explore strategies for teaching the method of completing the square using a geometrical or conceptual approach. The method is characterized here in terms of the derivative of a quadratic form and the discriminant of a quadratic equation.

Theorem 6.1 Let $q(x)=ax^2+bx+c,\ a\neq 0$ be a quadratic expression, $q'(x)=2ax+b$ be its derivative and $d=b^2-4ac$ be the discriminant of the equation $q(x)=0.$ Then we have

$$q(x)=\frac{1}{4a}\Big(q'(x)+\sqrt{d}\Big)\Big(q'(x)-\sqrt{d}\Big).$$

(6.1)

Proof. Multiplying $q(x)=ax^2+bx+c$ by $4a,$ we have $4a\ q(x)=4a^2x^2+4abx+4ac.$ It can be expressed as $4a\ q(x)=(2ax+b)^2-(b^2-4ac)=\big(q'(x)\big)^2-\Big(\sqrt{d}\Big)^2$ which simplifies to (6.1).

The above is equivalent to the popular factorization by DS (Difference of Squares). Note that by (5.4), we have

$$\sqrt{d}=2r.$$

(6.2)

It exhibits an amazing connection between r and the discriminant d which is implicit in [6].

Example 6.1 Factorize $q(x)=7x^2-6x-13.$

Solution: Since $a=7,\ b=-6,\ c=-13,\ d=b^2-4ac=400,$ by using (6.1), we have

$$q(x)=\frac{1}{4\times 7}[(2\times 7x-6)^2-20^2]=(x+1)(7x-13).$$

Corollary 6.1 Let $q(x)=ax^2+bx+c,\ a\neq 0$ be a quadratic expression, $s=2ax+b$ and $2r$ be defined in the average equation in (5.1) or (5.4). Then we have the following:

$$q(x)=\frac{1}{4a}(s+2r)(s-2r).$$
(6.3)

The equation (6.3) can also be written as $q(x)=\frac{1}{a}\big((s/2)+r\big)\big((s/2)-r\big).$

An Algorithm for Factorization

An algorithm for factorization of a quadratic expression is discussed below with Example 6.1 in mind. It is suitable for any student not having exposed to derivative of a quadratic expression or discriminant of the quadratic equation.

STEP 1: Determining s

Determine the leading coefficient $a,$ the linear coefficient $b,$ the constant term c of the quadratic function $q(x)=ax^2+bx+c,\ a\neq 0$ and prepare the following table:

Table 6.1: Determination of s

$a=7$	$b=-6$	$c=-13$
$2x$	1	0

Then multiplying column wise and adding, we have $s=2ax+b=14x-6.$ Note that the second line of the table is always the same for any quadratic expression $q(x).$

STEP 2: Determining r

Since $b=-6$ and $ac=7(-13)=-91,$ from the average equation $\big((b/2)-r\big)\big((b/2)+r\big)=ac$ in (5.1), we have $(-3-r)(-3+r)=-91,$ or, $r=10.$

STEP 3: Factorized Form

From (6.3), we have

$$q(x)=\frac{1}{4a}(s+2r)(s-2r)=\frac{1}{4\times 7}(14x-6+20)(14x-6-20),$$
$$q(x)=(x+1)(7x-13).$$

Corollary 6.2 Let $q(x)=ax^2+bx+c,\ a\neq 0$ be a quadratic expression, $s=2ax+b$ and $2r$ be the defined in the average equation in (5.1) or (5.4). Then the solution to $q(x)=0$ can be determined by

$$s=\mp 2r.$$
(6.4)

To solve $7x^2-6x-13=0$ (see Example 6.1), we have $s=14x-6$ and $2r=20,$ so that $14x-6=\mp 20$ and finally we have $x=-1,$ or, $x=13/7.$

7. General Quadratic Equation

We mentioned in the introduction that the literature is extremely rich in solving a quadratic equation. Here we refer to [22] who has discussed a less known result of the roots of quadratic equation with amazing geometric meaning. See also two recent papers [23,24]. The following theorem provides a solution to the general quadratic equation in terms of the coefficients a, b and r.

Theorem 7.1 Let $ax^2 + bx + c = 0,\ a \neq 0$ be the quadratic equation. Then the roots of the equation are

$$x_1 = \frac{1}{a}(-b/2 - r), \text{ or, } x_2 = \frac{1}{a}(-b/2 + r), \tag{7.1}$$

where r can be obtained by the average equation in (5.1) or (5.4).

Proof. The solution to the general quadratic equation $ax^2 + bx + c = 0,$ with $a \neq 0$ follows from equation (2.5a) as $x_1 = -j/a,$ or, $x_2 = -k/a$ so that the sum and the product of the roots are $x_1 + x_2 = -(j+k)/a$ and $x_1 x_2 = jk/a^2$ respectively. By (2.3) and (2.6), we have $j + k = b$ and $jk = ac$ so that $x_1 + x_2 = -b/a$ and $x_1 x_2 = c/a.$ Assuming $x_1 \leq x_2,$ by virtue of the average equation in (5.1) or (5.4), and the identity $(x_2 - x_1)^2 = (x_2 + x_1)^2 - 4x_2 x_1,$ or, $(x_2 - x_1)^2 = (b^2 - 4ac)/a^2,$ we have $x_2 - x_1 = 2r/a.$ Then by (4.2), it follows that the solution to the general quadratic equation is given by (7.1).

Note that $b/2$ and $2r$ are the average and distance of the roots of $x^2 + bx + ac = 0.$

To solve $7x^2 - 6x - 13 = 0$ (see Example 6.1), we have $a = 7, b = -6, c = -13$ so that $2r = \sqrt{b^2 - 4ac} = 20$ and hence by equation (7.1), the roots are $x = -1,$ or, $x = 13/7.$

8. Conclusion

We have discussed, identified and named a few methods of factorization of a quadratic trinomial that have been developed over four millennia for making learning and teaching more effective. The rectangular method of the Babylonians is equivalent to solving the equilibrium point of a hyperbola and a line as mentioned in Section 1, and Average Method in Section 5. We recommend using the Factoring Method discussed in Section 3 for high school students as it tries to inculcate the reasoning of the problem. Readers motivated by algebra may like the Linear Method in Section 4 and the Average Method in Section 5. The method by al-Khwarizmi known as Difference of Squares is characterized in Section 6 by the derivative of a quadratic expression and the discriminant of the quadratic equation. Readers motivated by calculus may appreciate it though it has a mnemonic value for every reader. The choice of the method would certainly depend on the background of the reader.

Acknowledgement The author is grateful to the Editor, and also to Professor S.M. Shahidul Islam, Department of Mathematics, Hajee Mohammad Danesh Science and Technology University, Bangladesh for

comments on earlier versions of the manuscript.

References

[1] Katz, V.J. *A History of Mathematics*, 3rd ed. Pearson, MA, Boston, USA (2008).

[2] Robson, E. *Mathematics in Ancient Iraq: A Social History*. Princeton University Press, Princeton, NJ, USA (2008).

[3] Irving, R.S. *Beyond the Quadratic Formula*. The Mathematical Association of America, Washington, DC,
USA (2013).

[4] Burton, D.M. *History of Mathematics: An Introduction*, 7th ed. New York, NY: McGraw-Hill, New York,
USA (2010).

[5] Derbyshire, J. *Unknown Quantity: A Real and Imaginary History of* Algebra. Joseph Henry Press, Washington, DC, USA (2006).

[6] Loh, P.S. A simple proof of the quadratic formula. *arXiv:1910.06709v2* (2019).

[7] Steckroth, J. A transformational approach to slip-slide factoring. *Mathematics Teacher*, 109(3):228-234 (2015).

[8] Vi`ete, F. *Opera Mathematica*. Edited by Frans van Schooten. Reprinted Bonaventure and Abraham Elzevier, Leiden, The Netherlands.1646 (1579).

[9] Savage, J. Factoring quadratics. The *Mathematics Teacher*, 82:35-36 (1989).

[10] Autrey, M.A. and Austin, J.D. A novel way to factor quadratic polynomials. *The Mathematics Teacher*, 72(2):127-128 (1979).

[11] Baker, B. Developing a meaningful algorithm for factoring quadratic trinomials. *The Mathematics Teacher, 62*(8):629-631 (1969).

[12] Cabahug, J.A. The use of Bruner's Modes of representations in teaching factoring second-degree polynomials. *International Journal of Education*, 1(1):85-103 (2012).

[13] Dogbey, J., Gyening, J. and Kersaint, G. Factorising quadratic trinomials: An alternative approach. *Learning and Teaching Mathematics*, 2011(10):44-45 (2011).

[14] Erisman, R. J. Factoring trinomials. The *Mathematics Teacher*, 79:124-129 (1986).

[15] Hirsch, C.R. Finding factors physically. *The Mathematics Teacher*, 75(5):388-419 (1982).

[16] Kotsopoulos, D. Unravelling student challenges with quadratics: A cognitive approach. *Australian Mathematics Teacher*, 63(2):19-24 (2007).

[17] Moskol, A. An alternate method for factoring quadratic trinomials. *The Mathematics Teacher*, 72(9):676-

677 (1979).

[18] Gandz, S. The Origin and Development of the Quadratic Equations in Babylonian, Greek, and Early Arabic Algebra. *Osiris*, 3:405–557 (1937).

[19] Joarder, A.H. Factorising with geometric insights. *Australian Senior Mathematics Journal*, 29(1) :25-31 (2015).

[20] Maharaj, A. A geometrical introduction to the method of completing the square. *Learning and Teaching Mathematics*, 2005 (2):7-9 (2014).

[21] Samson, D. Completing the square: a conceptual approach. *Learning and Teaching Mathematics*, 2013 (14):8-11 (2013).

[22] Samson, D. A short quadratic diversion. *Learning and Teaching Mathematics*, 2018 (24):21-23 (2018).

[23] Makobe, M.L. Alternative quadratic formula. *Learning and Teaching Mathematics*, 2014 (17): 42 (2014).

[24] Man, Y.K. A simple approach deriving the quadratic formula. *Learning and Teaching Mathematics*, 2009 (7):34 (2009).

GANIT

Available online at https://ganitjournal.bdmathsociety.org/

GANIT: Journal of Bangladesh Mathematical Society

GANIT *J. Bangladesh Math. Soc.* 41.1 (2021) 26–40
DOI: https://doi.org/10.3329/ganit.v41i1.55024

Pricing Exotic Options Using Some Lattice Procedures

Sadia Anjum Jumana *[a] and A B M Shahadat Hossain †[b]

[a] *Department of Applied Mathematics, University of Dhaka, Dhaka-1000, Bangladesh.*
[b] *Department of Applied Mathematics, University of Dhaka, Dhaka-1000, Bangladesh.*

ABSTRACT

In this work, we discuss some very simple and extremely efficient lattice models, namely, Binomial tree model (**BTM**) and Trinomial tree model (**TTM**) for valuing some types of exotic barrier options in details. For both these models, we consider the concept of random walks in the simulation of the path which is followed by the underlying stock price. Our main objective is to estimate the value of barrier options by using **BTM** and **TTM** for different time steps and compare these with the exact values obtained by the benchmark Black-Scholes model (**BSM**). Moreover, we analyze the convergence of these lattice models for these exotic options. All the results have been shown numerically as well as graphically.

Received: November 26, 2020 **Accepted:** March 18, 2021 **Published Online:** August 04, 2021

Keywords: Binomial tree model (**BTM**); Trinomial tree model (**TTM**); Black-Scholes Model(**BSM**); Exotic options; Barrier Option.
AMS Subject Classifications 2020:

1 Introduction

In the last few decades, derivatives such as options became quite important part in the financial market. In otherwords, pricing options has become one of the vital phenomenons in finantial mathematics. Note that, trading options begun in the Chicago Board Options Exchange (CBOE) in 1973 and after that numerous other exchanges started trading options all around the world [1]. In 1973, Fischer Black and Myron Scholes established the first thoroughly acceptable model for pricing option [2]. After that Robert C. Merton expannded their version in various significant ways in the same year [3].

The binomial lattice model to approximate option premium came out of a discussion between W.F. Sharpe and M. Rubinstein at a conference. Their proposed model consists of the principle that, if an economy with three securities can only obtain two future states, one such security will be redundant. This inspection engendered to a two-state model. This was the birth of the binomial tree model (**BTM**) introduced first by J.C. Cox, S.A. Ross and M. Rubinstein in 1979 [5]. Then it became a very popular and useful for pricing options due to its simplicity.

On the other hand, Trinomial tree model (**TTM**) was developed by Boyle [4] and then it was modified by

*Sadia Anjum Jumana. *E-mail address:* sadiajumana@gmail.com
†A B M Shahadat Hossain. *E-mail address:* abmsh@du.ac.bd

Kamrad and Ritchen [14]. In **TTM** there exist three variation states for the underlying asset price at a specific time interval namely, up, down, and remain same. This concept is comparatively more practical than the **BTM** and it provides not only more accurate results but also faster.

Exotic options are established to fulfil the particular needs of the investors who are using the instruments to control financial risk. Inspite of referring exotic options as a class of options, they are rather considered as options with more convoluted properties than ordinary put and call options. Barrier options are most likely to be the oldest of all exotic options and have been traded in the US market ever since 1967 [7].

Pricing barrier options using lattice procedures (**BTM** and **TTM**) can be quite tricky. Although using a large number of time steps can generate precise outcomes for the standard options, the similar outcome might not occur in valuing barrier options. The problem arises in locating the barrier with corresponding adjacent branches of nodes in the lattice. In case of the barrier locates between the branches of the lattice, significant amount of errors might occur. We have found few papers about pricing barriers in the literature; Peter H. Ritchken discussed trinomial procedure for pricing and hedging most types of exotic barriers [15, 16]. On the other hand, lattice procedures have been considered by many researchers to price various options as they are easy to understand and very efficient [12–14].

The paper is structured as follows. In Section 2, we give some definitions regarding the options that we have worked on this paper along with their payoff diagr ams. Then we present a significant relationship between call and put option known as *Put-Call Parity*. After that, we briefly discuss three diffrent option pricing formulas namely, the **BSM, BTM** and **TTM** in section 3. In section 4, we provide some important numerical as well as graphical results about barrier option pricing using these models. Finally, we conclude how **BTM** and **TTM** fit against real market data in comparison with the **BSM** for pricing barriers in section 5.

2 Preleminaries

2.1 Some Definitions

Definition 1. (Option) *Option can be defined as a contract between two parties which provides the buyer (owner) of the option the right (but not an obligation) to buy or sell the underlying asset for the settled cost (strike price) on or before expiring time (maturity time) of the contract [1].*

There exist two fundamental types of options:

- Call option
- Put option

Definition 2. (Call Option) *A Call Option provides the holder (buyer) the right (but not the liability) to purchase the underlying asset by a fixed date for a fixed price.*

Definition 3. (Put Option) *A Put Option provides the holder the right (but not the liability) to sell the underlying asset by a fixed date for a fixed price.*

Definition 4. (European Option) *The type of option that provides the holder (buyer) of the option the right to implement the option only at the expiry date, is called European Option.*

Definition 5. (American Option) *An American option, in comparison with the European option, can be implementd at any time before the expiry date.*

2.2 Payoff Diagrams

In the following table we will discuss the payoff of the call (Long position) and the put (Long position) option [1].

Table 2.1: Payoff of European call and put Options

Option	Payoff Function	Payoff Diagram
Call	$(S_\tau - X)^+ = \begin{cases} S_\tau - X & S_\tau \geq X \\ 0 & S_\tau < X \end{cases}$	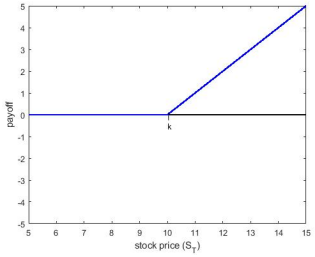
Put	$(X - S_\tau)^+ = \begin{cases} X - S_\tau & S_\tau \leq X \\ 0 & S_\tau > X \end{cases}$	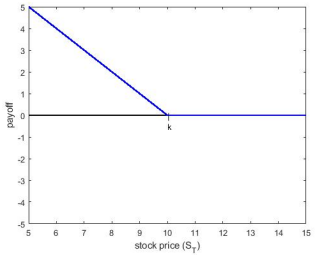

2.3 Barrier Options

Barrier options are regarded as one of the most fundamental kinds of path dependent exotic options. The exercise of the option depends on the underlying asset price crossing a definite barrier. Since the payoff is dependent on the path travelled by the asset price, it is called path dependent. However, the dependencey of the path is considered to be weak, since the only feature accounted is whether the barrier B has been activated or not [6]. These options are attractive as they are comperatively less costly than that of the corresponding standard options.

Definition 6. **(Barrier Option)** *The option for which the payoff depends on whether the price of the underlying asset hits a specific level during a specific time period, is called Barrier option [1].*

2.4 Types of Barrier Options

A barrier can be hit from above or from below. Depending on this characteristic a barrier option can be classified into two types [7].

1. **Knock-out Barrier Option:** This type of Barrier option begins it's life as a typical call or put option, but it becomes invalid if the spot price ever hits a specific predetermined knock-out barrier, even before the expiry date.
   Furthermore, depending on the position of the barrier with respect to the initial value of the underlying asset, the Knock-out barrier option can be classified in to two options.
   - **Down-and-out:** The option which comes to an end when the underlying asset price diminishes to a predetermined level.
   - **Up-and-out:** The option which comes to an end when the underlying asset price rises to a predetermined level.
2. **Knock-in Barrier Option:** This type of Barrier option begins its life inactive, and only becomes active when the underlying stock price hits the knock-in barrier, then it is regarded as a typical call or put option.
   The Knock-in barrier option can also be classified in to two options.

- **Down-and-in:** The option which becomes active when the underlying asset price decreases to a predetermined level.
- **Up-and-in:** The option which becomes active when the underlying asset price rises to a predetermined level.

In this paper we will only work with the **Down-and-Out Barrier Call Option** and **Down-and-Out Barrier Put Option** ,whose payoff functions and graphs are given below [8],

- **Down-and-Out Barrier Call**

$$(S_\tau - X)^+ \mathbb{1}_{\{\min\limits_{0\le t\le\tau} S_t > B\}} = \begin{cases} S_\tau - X & \text{if} \quad \min\limits_{0\le t\le\tau} S_t > X \\ 0 & \text{if} \quad \min\limits_{0\le t\le\tau} S_t \le X \end{cases}$$

Remark 7. *Here,* $\mathbb{1}$ *is the indicator function of a set (which set, is ususally specified as an index under the* 1*) - a function that is equal to* 1 *if the argument belongs to the set, and* 0 *if it doesn't.*

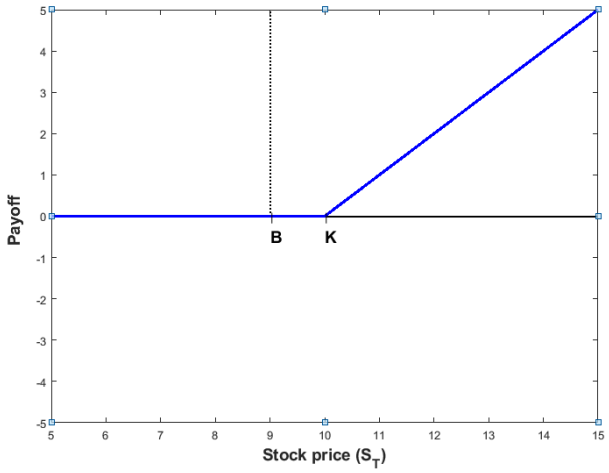

Figure 2.1: Payoff diagram of Down-and-Out Barrier Call Option

- **Down-and-Out Barrier Put**

$$(X - S_\tau)^+ \mathbb{1}_{\{\min\limits_{0\le t\le\tau} S_t > B\}} = \begin{cases} X - S_\tau & \text{if} \quad \min\limits_{0\le t\le\tau} S_t > X \\ 0 & \text{if} \quad \min\limits_{0\le t\le\tau} S_t \le X \end{cases}$$

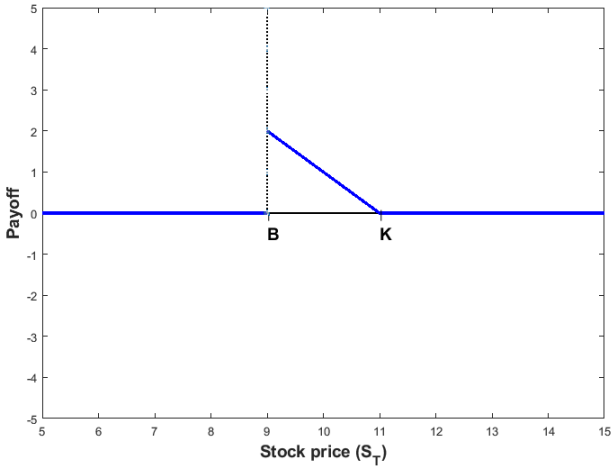

Figure 2.2: Payoff diagram of Down-and-Out Barrier Put Option

2.5 Put-Call Parity

The principle which explains the relation between the value of European call option (C_t) and European put option (P_t) with the same underlying asset (S_t), expiry date (τ), and strike price (X), is known as put-call parity [1]. Mathematically it is given by

$$P_t + S_t = C_t + Xe^{-r(\tau - t)} \tag{2.1}$$

This relation states that the simultaneous holding of a long European call along with a short European put of the same class will provide the identical result as holding one forward contract on the same underlying asset, with the same expiry, and a forward price same as the strike price of the option. In case of the prices of the call and put options conflict such that this relationship refrain holding, there exists an arbitrage opportunity. i.e. sophisticated traders get the opprtunity to receive a risk-free profit [9].

2.6 In-out Parity

In-out parity can be interpreted as the representation of the put-call parity for barrier option. The main concept here is almost identical as in put-call parity (2.1). It states that, if the value of the "in" option is added with the value of the "out" option, then it results in the value of the European option (for both call and put)[17].

$$C = C_{in} + C_{out} \tag{2.2}$$
$$P = P_{in} + P_{out} \tag{2.3}$$

3 Methodology

In this section, we will discuss the **BSM, BTM** and **TTM** option pricing models briefly that overviews the needs of this works. For details, readers are reffered [1].

3.1 Notations

Now we present some notations that are utilized in this paper as follows:

t	:	Any time	r	:	Risk-free interest rate
τ	:	Expiry date	σ	:	Volatility
S_t	:	Stock price at any time, t	u	:	Up movement
S_τ	:	Stock price at maturity, τ	d	:	Down movement
f	:	General option price	p_u	:	Probability to move up
C_0	:	Call option price	p_d	:	Probability to move down
P_0	:	Put option price	N	:	Number of steps
X	:	Strike price	B	:	Barrier of the stock price
μ	:	Drift			

3.2 The Black-Scholes Model

This model was presented by Fisher Black, Myron Sholes and Merton at the beginning of the 1970s for pricing European stock options. Since then it's been used as the standard model for pricing European options.[1]

Proposition 8. *Let, S be the asset price, which follows GBM process*

$$\frac{dS_t}{S_t} = \mu dt + \sigma dW_t \quad (W_t \text{ is Wiener process}) \tag{3.1}$$

and f be the value of the option, that follows the following PDE

$$\frac{\partial f}{\partial t} + \frac{1}{2}\sigma^2 S^2 \frac{\partial^2 f}{\partial S^2} + rS\frac{\partial f}{\partial S} - rf = 0 \tag{3.2}$$

Then the value of the call option is given by

$$C(S,t) = S\Phi(\delta_1) - Xe^{-r(\tau-t)}\Phi(\delta_2) \tag{3.3}$$

where

$$\delta_1 = \frac{\ln(S/X) + (r + \frac{1}{2}\sigma^2)(\tau - t)}{\sigma\sqrt{(\tau - t)}} \tag{3.4}$$

$$\delta_2 = \frac{\ln(S/X) + (r - \frac{1}{2}\sigma^2)(\tau - t)}{\sigma\sqrt{(\tau - t)}} = \delta_1 - \sigma\sqrt{(\tau - t)} \tag{3.5}$$

The parameter $\Phi(.)$ is called the cumulative probability distribution function corresponding to any standard normal random variable z,

$$\Phi(z) = \frac{1}{\sqrt{2\pi}}\int_{-\infty}^{z} e^{-\frac{1}{2}x^2} dx \tag{3.6}$$

Remark 9. *After obtaining the formula for valuing a European call option, we can apply the put–call parity (2.1) for establishing the value $P(S,t)$ of a European put option which is*

$$P(S,t) = Xe^{-r(\tau-t)}\Phi(-\delta_2) - S\Phi(-\delta_1) \tag{3.7}$$

Remark 10. *The first accepted scientific formula to price a Down-and-Out Barrier Call option was suggested by Merton [3] and shortly after Reiner and Rubinstein came up with the formulas for pricing all four kinds of Barrier call and put options [10]. From their inspection it was found that, the value of a barrier option depends on the parameters of the benchmark Black-Scholes model, along with the barrier level, B. According to them the value of a Down-and-In Barrier Call option is stated as below*

$$C_{down-in}(S,t) = \left(\frac{S}{B}\right)^{1-\frac{2r}{\sigma^2}} - C\left(\frac{B^2}{S}, \tau - t\right) \tag{3.8}$$

where, $C\left(\frac{B^2}{S}, \tau - t\right)$ is determined making use of the equation (3.3).

Having obtained that, the value of a Down-and-Out Call option can easily be calculated by utilizing the in-out parity (2.2)*, for* $B < X$, $B \leq S$ *and* $0 \leq t \leq \tau$.

$$\begin{aligned} C(S,t) &= C_{down-in}(S,t) + C_{down-out}(S,t) \\ C_{down-out}(S,t) &= C(s,t) - C_{down-in}(S,t) \\ &= C(s,t) - \left(\frac{S}{B}\right)^{1-\frac{2r}{\sigma^2}} - C\left(\frac{B^2}{S}, \tau - t\right) \end{aligned} \tag{3.9}$$

According to [11] the values of th barrier option can be obtained by using the formulas mentioned below.
Down-and-Out Call:

1. $X > B$:
$$C_{down-out}(S,t) = S(\Phi(\delta_1) - \beta(1 - \Phi(\delta_8))) - Xe^{-r(\tau-t)}(\Phi(\delta_2) - \alpha(1 - \Phi(\delta_7))).$$
2. $X < B$:
$$C_{down-out}(S,t) = S(\Phi(\delta_3) - \beta(1 - \Phi(\delta_6))) - Xe^{-r(\tau-t)}(\Phi(\delta_4) - \alpha(1 - \Phi(\delta_5))).$$

Down-and-Out Put:

1. $X > B$:
$$P_{down-out}(S,t) = -S(\Phi(\delta_3) - \Phi(\delta_1) - \beta(\Phi(\delta_8) - \Phi(\delta_6))) + Xe^{-r(\tau-t)}(\Phi(\delta_4) - \Phi(\delta_2) - \alpha(\Phi(\delta_7 - \Phi(\delta_5)))).$$
2. $X < B$:
$$P_{down-out}(S,t) = 0.$$

where, $\alpha = \left(\frac{B}{S}\right)^{-1+\frac{2r}{\sigma^2}}$, $\beta = \left(\frac{B}{S}\right)^{1+\frac{2r}{\sigma^2}}$.

$$\delta_3 = \frac{\ln(S/B) + (r + \frac{1}{2}\sigma^2)(\tau - t)}{\sigma\sqrt{(\tau - t)}} , \qquad \delta_4 = \frac{\ln(S/B) + (r - \frac{1}{2}\sigma^2)(\tau - t)}{\sigma\sqrt{(\tau - t)}}$$

$$\delta_5 = \frac{\ln(S/B) - (r - \frac{1}{2}\sigma^2)(\tau - t)}{\sigma\sqrt{(\tau - t)}} , \qquad \delta_6 = \frac{\ln(S/B) - (r + \frac{1}{2}\sigma^2)(\tau - t)}{\sigma\sqrt{(\tau - t)}}$$

$$\delta_7 = \frac{\ln(SX/B^2) - (r - \frac{1}{2}\sigma^2)(\tau - t)}{\sigma\sqrt{(\tau - t)}} , \qquad \delta_8 = \frac{\ln(SX/B^2) - (r + \frac{1}{2}\sigma^2)(\tau - t)}{\sigma\sqrt{(\tau - t)}}$$

3.3 Binomial Tree Model

A simple but convenient and quite popular procedure for valuing option requires constructing a binomial tree. It is basically a diagram based discrete time model demonstrating various possible paths accompanied by the asset prices throughout the life span of an option. It is considered that, the price of the stock follows a random walk. At every time step, there is a specific probability to move up by a definite percentage amount and a specific probability to move down by a definite percentage amount. As the number of steps of the tree increases, the time step gets smaller, and this model tends to the **BSM** [12].

Proposition 11. *Let,* S_n^m *and* f_n^m *be the n-th possible values of stock price and option price at time-step* $m\Delta t$ *respectively which have the following representations*

$$S_n^m = u^n d^{m-n} S_0^0 \qquad n = 0, 1, 2, ..., m, \tag{3.10}$$

and,

$$f_n^m = e^{-r\Delta t}[p f_{n+1}^{m+1} + (1 - p) f_n^{m+1}] \qquad n = 0, 1, 2, ..., m, \tag{3.11}$$

Then the current option price f_0 is given by

$$f_0 = e^{-r\tau}\mathbb{E}_p[f_\tau] = e^{-nr\Delta t}\sum_{h=0}^{n}\frac{n!}{h!(n-h)!}p^h(1-p)^{(n-h)}f_{u^h d^{(n-h)}} \tag{3.12}$$

where, $p = \frac{e^{r\Delta t}-d}{u-d}$,$u = e^{\sigma\sqrt{\Delta t}}$, $d = \frac{1}{u}$, $\quad u > 1$.

Remark 12. *The prices of european call and put option can be easily calculated by* (3.15) *with the following final conditions:*

$$f_n^N = \begin{cases} \max\{S_n^N - X, 0\} & \textit{for Call} \\ \max\{X - S_n^N, 0\} & \textit{for Put} \end{cases}$$

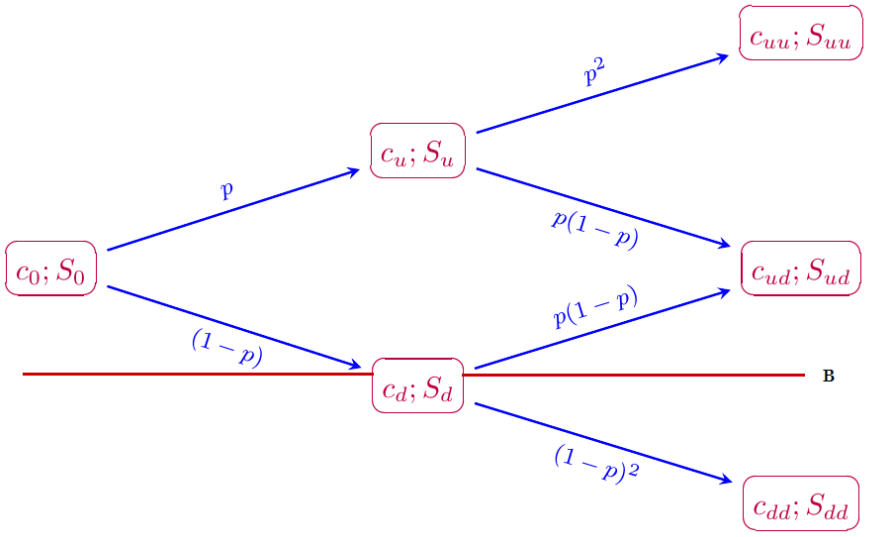

Figure 3.1: Two step Binomial tree of a Down-and-out Barrier Call option

Figure 3.1 represents a two step binomial tree for both the option price c and stock price S of a Down-and-out Barrier Call option. At each time step the prices may either go up by a factor $u > 1$ accompanied by probability p else go down by $d < 1$ accompanied by probability $(p-1)$. The option terminates when the underlying stock price falls to a predetermined level, B.

3.4 Trinomial Tree Model

The **BTM** has turned out to be considerably out of date and is of little practical use. Therefore, a more advanced model known as the **TTM** came into account. This model also provides discrete representation of stock price movement, analogous to **BTM**. This ameliorates the **BTM** by enabling the price of stock to shift up, down or remain same with specific probabilities [13].

Proposition 13. *Let, S_n^k and f_n^k be the n-th possible values of stock price and option price at time-step $k\Delta t$ respectively which have the following representations*

$$S_n^k = u^h d^l m^{n-h-l} S_0^0 \qquad n = 0, 1, 2, ..., k, \tag{3.13}$$

and,

$$f_n^k = e^{-r\Delta t}[p_u f_{n+1}^{k+1} + p_m f_n^{k+1} + p_d f_{n-1}^{k+1}] \qquad n = 0, 1, 2, ..., k, \tag{3.14}$$

Then the current option price f_0 is given by

$$f_0 = e^{-nr\Delta t} \sum_{h=0}^{n} \sum_{l=0}^{n-h} \frac{n!}{h!l!(n-h-l)!} p_u^h p_d^l p_m^{(n-h-l)} f_{u^h d^l m^{n-h-l}} \tag{3.15}$$

where, $u = e^{\lambda\sigma\sqrt{\Delta t}}, d = \frac{1}{u}, m = 1, u > 1$ and

$$\begin{cases} p_u = \dfrac{1}{2\lambda^2} + \dfrac{r - \frac{1}{2}\sigma^2}{2\lambda\sigma}\sqrt{\Delta t} \\ p_d = \dfrac{1}{2\lambda^2} - \dfrac{r - \frac{1}{2}\sigma^2}{2\lambda\sigma}\sqrt{\Delta t} \\ p_m = 1 - \dfrac{1}{\lambda^2} \end{cases}$$

are the risk neutral probabilities [14] [15].
Note that $\lambda < 1$ implies $p_m < 0$, which explains the condition $\lambda \geq 1$. In the case $\lambda = 1$, we have $p_m = 0$ and hence the trinomial tree reduces to a simple binomial tree. The Final conditions are given by Remark 12.

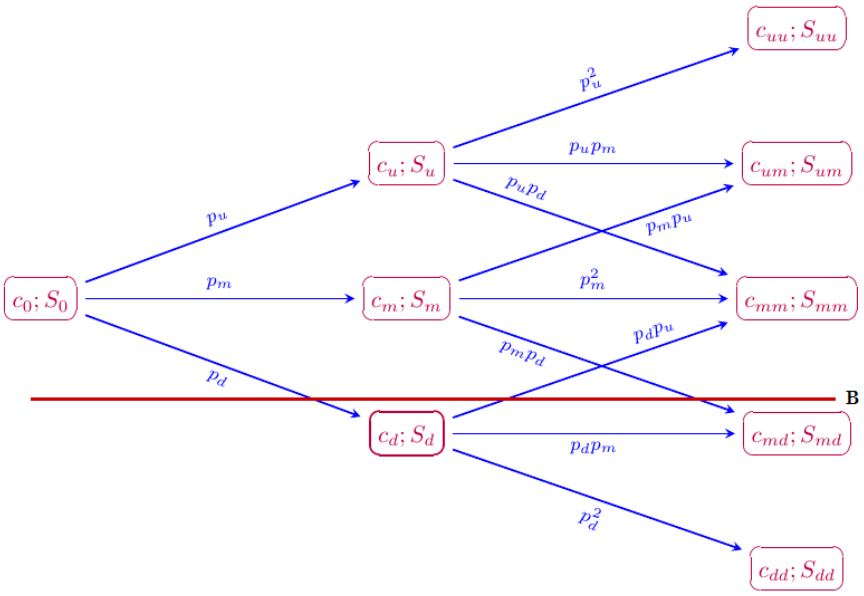

Figure 3.2: Two step trinomial tree of a Down-and-out Barrier Call option

Figure 3.2 represents a two step trinomial tree for both option price c and stock price S of a Down-and-out Barrier Call option. At each time step the prices changes by either a factor of $u > 1$ with probability p_u or m with probability p_m or $d < 1$ with probability p_d. The option terminates when the underlying stock price decreases to a predetermined level, B.

4 Results and Discussion

In this section, we approximate Down-and-Out Barrier Call and Put option prices by **BTM, TTM** and **BSM** with the following data set [16]

$$\{S_0 = \$95, B = \$90, X = \$100, \sigma = 0.25, r = 0.10, \tau = 1 \text{ yr}\}.$$

Table 4.1 and Table 4.2 show the values of the Down-and-Out Barrier Call and Put options using CRR **BTM** and Kamrad-Ritchken **TTM** for increasing number of steps.

Table 4.1: Barrier Call Option valuation using **BTM** and **TTM**

N	**BSM (Call)**	**BTM (Call)**	**TTM (Call)**	**Absolute Error(BTM)**	**Absolute Error(TTM)**
25		8.8406	6.0069	2.8438	0.0101
50		7.2372	5.9942	1.2404	2.6×10^{-3}
75		6.2981	5.9899	0.3013	6.9×10^{-3}
100		7.5028	5.9997	1.506	2.9×10^{-3}
125		6.9839	5.9985	0.9871	1.7×10^{-3}
150		6.5601	5.9976	0.5633	8×10^{-4}
175	5.9968	6.2087	5.9970	0.2119	2×10^{-4}
200		7.2299	5.9986	1.2331	1.8×10^{-3}
250		6.7074	5.9980	0.7106	1.2×10^{-3}
300		6.2903	5.9976	0.2935	8×10^{-4}
350		6.9599	5.9979	0.9631	1.1×10^{-3}
400		6.6501	5.9977	0.6533	9×10^{-4}
450		6.3819	5.9975	0.3851	7×10^{-4}
500		6.1456	5.9974	0.1488	6×10^{-4}

Table 4.2: Barrier Put Option valuation using **BTM** and **TTM**

N	**BSM (Put)**	**BTM (Put)**	**TTM (Put)**	**Absolute Error(BTM)**	**Absolute Error(TTM)**
25		0.1827	0.0322	0.1393	0.0112
50		0.0711	0.0334	0.0277	0.01
75		0.0570	0.0338	0.0136	9.6×10^{-3}
100		0.0948	0.0409	0.0514	2.5×10^{-3}
125		0.0703	0.0411	0.0269	2.3×10^{-3}
150		0.0612	0.0412	0.0178	2.2×10^{-3}
175	0.0434	0.0446	0.0412	1.2×10^{-3}	2.2×10^{-3}
200		0.0828	0.0424	0.0394	1×10^{-3}
250		0.0623	0.0425	0.0189	9×10^{-4}
300		0.0491	0.0425	5.7×10^{-3}	9×10^{-4}
350		0.0729	0.0429	0.0295	5×10^{-4}
400		0.0615	0.0429	0.0181	5×10^{-4}
450		0.0529	0.0430	0.0105	4×10^{-4}
500		0.0477	0.0430	4.3×10^{-3}	4×10^{-4}

It is clear from Table 4.1 that, call option valued by **BTM** oscillates towards the exact value obtained by **BSM** whereas, call option price obtained by **TTM** approximates the exact value correct upto two decimal places in only 50-th steps and as the step number rises, option value approaches to the exact value more accurately. Similar behaviour has been observed for barrier down and out put option in Table 4.2.
These behaviours are shown graphically in Figure 4.1– Figure 4.4.

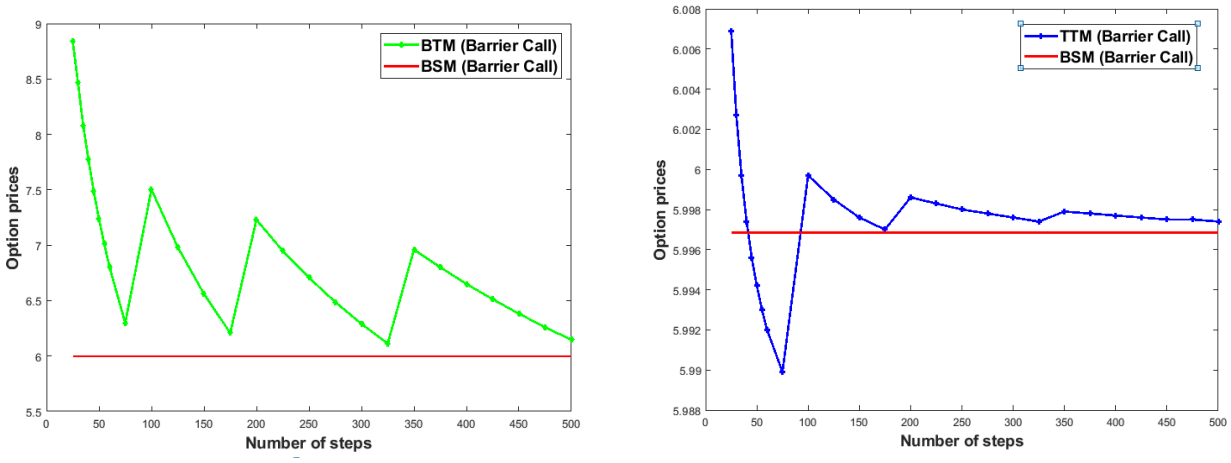

(a) Using BTM (b) Using TTM

Figure 4.1: Convergences for Barrier Call option prices obtained by **BTM** and **TTM**

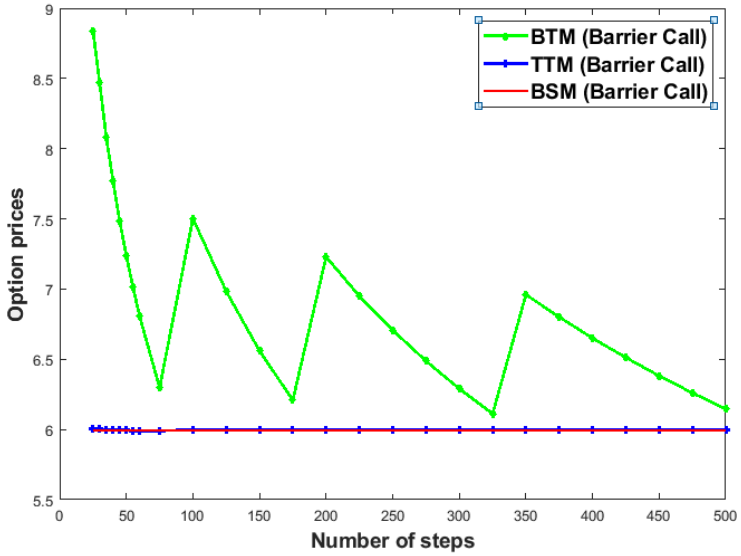

Figure 4.2: Comparison among Barrier Call option prices using different methods

From Figure 4.1 we observe that for a Down-and-Out Barrier Call option the values obtained by **BTM** oscillates towards the exact value obtained by **BSM**, whereas the values obtained by **TTM** initially oscillates and then converges towards the exact value.
While Figure 4.2 represents the comparison of the **BTM** and **TTM** values for Down-and-Out Barrier Call option. Clearly, it shows that the values obtained by **TTM** converges to the exact value more accurately than the values obtained by **BTM**.

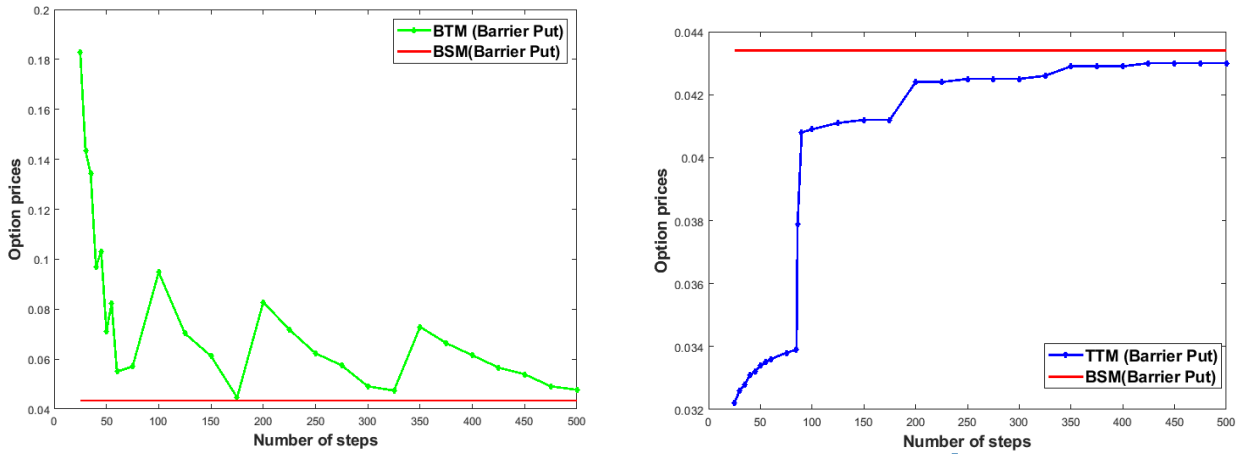

(a) Using BTM (b) Using TTM

Figure 4.3: Convergences for Barrier Put option prices obtained by **BTM** and **TTM**

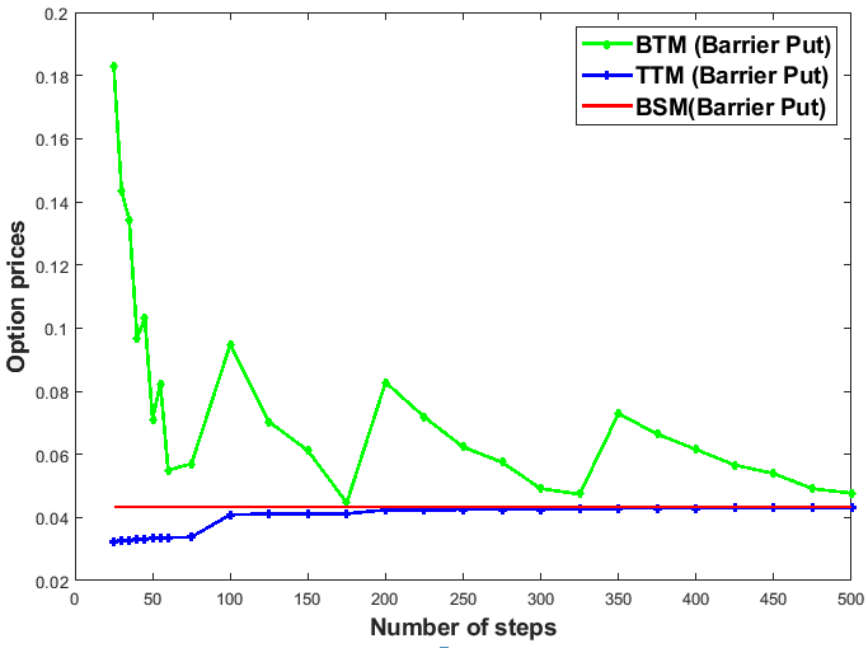

Figure 4.4: Comparison among Barrier Put option prices using different methods

From Figure 4.3 we observe that for a Down-and-Out Barrier Put option the the values obtained by **BTM** oscillates towards the exact value obtained by **BSM**, whereas the values obtained by **TTM** initially oscillates and then converges towards the exact value.
While Figure 4.4 represents the comparison of the **BTM** and **TTM** values for Down-and-Out Barrier Put option. Clearly, it shows that the values obtained by **TTM** converges to the exact value more accurately than the values obtained by **BTM**.

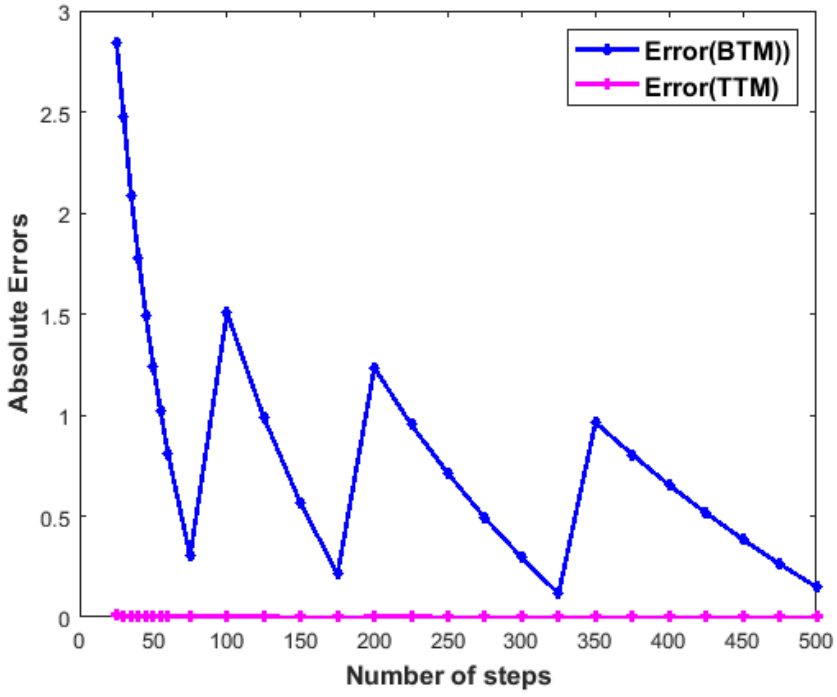

Figure 4.5: Comparison of Errors for different Barrier Call option prices

In Figure 4.5, we have shown the comparison of absolute errors for Down-and-Out Barrier Call option prices obtained by the **BTM** and **TTM** . It confirms that the **TTM** gives more accurate value than the **BTM** since the absolute errors of **TTM** tends to zero while the absolute errors of **BTM** is oscillating.

It is evident that both the lattice procedures **BTM** and **TTM** give very significant results against the data set mentioned at the beginning of this section. Our numerical results coincide with the results presented in [16]. In addition, we have shown the convergence of our results obtained by **BTM** and **TTM** with the **BSM** graphically (see Figure 4.1–Figure 4.5).

5 Conclusion

In this paper, we have got the opportunity to work on an exotic option, namely, Barrier option pricing. In particular, we approximate the Barrier option premium numerically using some lattice models such as **BTM** and **TTM**. For both these models we have got very significant results compare to that of **BSM**. We also found that **TTM** gives more accurate results than the **BTM**. Moreover, we can say that lattice models like **BTM** and **TTM** are satisfactorily flexible to price exotic options compare to other models such as Finite difference model, Monte carlo etc. We have generated some MATLAB coding to produce all our numerical and graphical results shown in this work (see Appendix). And finally, we can say that this study could be a useful guide line to evaluate other option price like Asian, Binary, Lookback etc.

References

[1] J. C. Hull., Options, Futures, and Other Derivatives. 8th ed.,Pearson Education Limited, 2012.

[2] F.Black and M.S.Scholes, The Pricing of Options and Corporate Liabilities, Journal of Political Economy, 81(3):637-654, May-June 1973.

[3] R.C.Merton, Theory of Rational Option Pricing, Bell Journal of Economics and Manage-ment Science, 4(1):141-183, Spring 1973.

[4] P. Boyle, Option valuation using a three jump process, Inter-national Options Journal,vol.3,pp.7–12,1986.

[5] Merima Nurkanovic, The Split tree for option pricing, May 2017.

[6] P. Wilmott, J. Dewynne, and S. Howison. Option pricing: mathematical models and computation, Oxford: Financial Press, 1995.

[7] Chriss, N, Black-Scholes and Beyond Option Pricing Models, McGraw-Hill, NewYork, 1997.

[8] Nicolas Privault, Stochastic Finance An Introduction with Market Examples, Chapman and Hall/CRC Financial Mathematics Series, 2014.

[9] Hans R. Stoll, The Relationship Between Put and Call Option Prices, The Journal of Finance, 1969.

[10] Reiner, E. and Rubinstein, M, Breaking down the barriers, Risk 4(8): 28–35, 1991.

[11] Dewynne, J., Howison, S. and Wilmott, P., The mathematics of financial derivatives: A student introduction, Press Syndicate of the University of Cambridge, Cambridge,UK,1995.

[12] Cox, J., Ross, S. and Rubinstein, M., Option pricing: A simplified approach, Journal of financial economics September, 1979.(1): 1–35.

[13] Paul Clifford, Yan Wang, Oleg Zaboronski, Kevin Zhang, Pricing Options Using Trinomial Trees, University of Warwick, 2008.

[14] Ritchken, P. and B. Kamrad, Multinomial Approximating Models for Options with k State Variables, Management Science, Volume 37, Issue 12, 1640-1652, 1991.

[15] Ritchken, P., On Pricing Barrier Options, The Journal of Derivatives, Vol. 3, No. 2, 19-28, 1995.

[16] Gonçalo Nuno Henriques Mendes, Valuation of Barrier Options Through Trinomial Trees, 2011.

[17] Wilmott, P. Paul Wilmott introduces quantitative finance, 2nd ed, John Wiley & Sons,London, UK.

APPENDIX : Matlab Code for pricing Down and Out Barrier Option

```
function [Price]=BarrierOptions(tree,bo,cp,ea,s0,k,r,sig,T,B,N,R)
del_t=(T)/N;
if (tree=='B') % for Binomial tree
niu=log(s0/B)/(sig*sqrt(del_t));
N0=fix(niu);
if(niu==N0)
lam=1;
else
lam=niu/N0;
end
else
lam=1; %for Binomial tree
end
u = exp(lam*sig*sqrt(del_t));
% probabilities
p_u = (1/(2*lam^2))+((r-0.5*(sig^2))*sqrt(del_t)/(2*lam*sig));
p_m = 1-1/lam^2;
p_d = (1/(2*lam^2))-((r-0.5*(sig^2))*sqrt(del_t)/(2*lam*sig));
%stock price at each node
for i=1:N+1
for j=N-i+2:N+i
s(j,i)=u^(N-j+1)*s0;
end
end
```

```
%payoff at maturity
switch bo
case {'do'} %for down_and_out barrier option
for j=1:2*N+1
if(s(j,N+1)<=B)
c(j,N+1)=R; %R is rebate
else
if(cp =='c') %for call option
c(j,N+1) = max(s(j,N+1)-k,0);
else
c(j,N+1) = max(k-s(j,N+1),0);
end
end
end
end
%payoffs at intermediate steps
switch bo
case {'do'}
i=N;
while i>0
for j=N-i+2:N+i
if(s(j,i)>B)
if (ea=='e') %for european option
c(j,i)=exp(-r*del_t)*(p_u*c(j-1,i+1)+p_m*c(j,i+1)+p_d*c(j+1,i+1));
else
if(cp =='c')
c(j,i)=max(exp(-r*del_t)*(p_u*c(j-1,i+1)+p_m*c(j,i+1)+p_d*c(j+1,i+1)),s(j,i)-k);
else
c(j,i)=max(k-s(j,i),exp(-r*del_t)*(p_u*c(j-1,i+1)+p_m*c(j,i+1)+p_d*c(j+1,i+1)));
end
end
else
c(j,i) = 0;
end
end
i=i-1;
end
end
Price = c(N+1,1)
```

GANIT

Available online at https://ganitjournal.bdmathsociety.org/

GANIT: Journal of Bangladesh Mathematical Society

GANIT *J. Bangladesh Math. Soc.* 41.1 (2021) 41–61
DOI: https://doi.org/10.3329/ganit.v41i1.55025

A mathematical analysis of the dynamics of chikungunya virus transmission

Saiful Islam *[a] and Chandra Nath Podder[b]

[a] [b] *Department of Mathematics, University of Dhaka, Dhaka 1000, Bangladesh*

ABSTRACT

In this paper, a deterministic model for the dynamics of chikungunya virus transmission is formulated and analyzed. It is shown that the model has a disease free equilibrium (DFE) and by using the basic reprodution number ($\Re_0$) local stability of DFE is proved when $\Re_0 < 1$. Also, the global stability of DFE is investigated by Lyapunov function and LaSalle Invariance Principle. We show that there exists a unique endemic equilibrium (EE) of the model which is locally asymptotically stable whenever $\Re_0 > 1$ and establish the global stability of the EE when $\Re_0 > 1$, by using Lyapunov function and LaSalle Invariance Principle for a special case. Numerical simulations and sensitivity analysis show that the destruction of breeding sites and reduction of average life spans of vector would be effective prevention to control the outbreak. Controlling of effective contact rates and reducing transmissions probabilities may reduce the disease prevalence.

Received: November 04, 2020 **Accepted:** March 01, 2021 **Published Online:** August 04, 2021

Keywords: Chikungunya; Epidemiological Model; Stability and numerical results; Treatment; Sensitivity Analysis.
AMS Subject Classifications 2020: 92D25, 35K61, 37N25, 34A34.

1 Intrduction

Chikungunya is an emerging mosqueto-borne viral disease caused by the chikungunya virus (CHIKV). It was first identified during an outbreak in southern Tanzania in 1952 [1, 2]. The term "chikungumya" comes from a word in the Makonde or Kimakonde language of southeast Tanzania and northern Mozambique and means "to become contorted" or "bend over" [1]. Chikungunya virus is transmitted to people by several species of mosquito of the genus *Aedes*, most common genus are *Aedes aegypti* and *Ades albopictus* [1, 3]. They mainly bite during daylight hour [3] and peaks of bitting activity is during early morning and late afternoon [1, 4]. A mosquito becomes infected after biting an infected human and an extrinsic incubation period is between two to four days [5, 6]. After the incubation period mosquitoes can transmit the virus. Mosquitoes remain inefectious for life time [7] and no vertical transmission is yet proved till today [8].
A human is infected after an effective bite of an infected mosquito, the intrinsic incubation period in the human host is usually 1 to 12 days [8, 9, 10] and during this period infected human unable to transmit the virus. After the incubation period most of the infected people develop symptoms. Common symptoms are: fever, severe

*Corresponding author. *E-mail address:* sislam@du.ac.bd

joint pain, headache, rash and some digestive symptoms: abdominal pain, nausea, vomiting or diarrhea may also occur [1, 3, 11]. Pain usually occurs in peripheral joints, such as wrists, ankles, joints of the hands and feet, in some of the larger joints: shoulders, elbows and knees, also may occur in muscles and ligaments [12, 13]. The joint pain may lasts a few days or a few weeks, but in some cases it may persist for a long time (several months, even years) following the acute infection [1, 14, 15] called subacute or chronic phase. After the viraemia period, during the period infected human is infectious, human recovers. But in some cases chikungunya viral antigen was found in a muscle biopsy of a person suffering a recurrent episode of disease three months after initial onset [16]. Additionally, viral antigen and viral RNA were found in macrophages in the synovial joint of a person experiencing a relapse of musculoskeletal disease 18 months after initial infection [17]. So, there is a possibility to transmit virus from human to mosquito after acute phase.

There is no specific preventive vaccine and antiviral medicine to treat the disease [1, 3, 18]. Supportive cares such as rest, drinking water, etc are suggested and symptomatic treatments including the use of nonsteroidal anti-inflammatory drugs such as naproxen, non-aspirin analgesics, such as, paracetamol (acetaminophen) are primarily directed to reduce fever and pain [18]. However, a vaccine exists but it is in an early-stage clinical trial and will not be commercially available in the near future [19].

Chikungunya re-emerges in many countries of Africa, Asia, Europe and America since the first outbreak in Tanzania. In Democratic Republic of the Congo, it was first isolated in 1958, after that it was isolated in 1960 [20]. But in 2000-2001, during an outbreak around 50,000 people became infected [1]. The first outbreak in Asia was in Bangkok, Thailand in 1958 [21]. Other outbreaks include India in 1960 and Srilanka in 1970 [22], Malaysia in 1998-1999 [23], Vietnam in 1975, Indonesia in 1982 [24], Italy in 2007 and France in 2010 [25]. In the last decade, the major outbreak was in Reunion Island in 2005, during this outbreak 2,666,000 people were infected while the total population was 770,000 and around 250 death cases were reported [26]. In India, outbreak was large in 2006-2007 and during this outbreak 1.39 million cases were reported officially in 2006 and 37,683 cases were reported by national authority in 2007 [1]. In American countries, from 2013-2014 around 1,118,763 suspected cases and 24,682 confirmed cases were reported by the Pan American Health Organization (PAHO) regional office [27]. In Bangladesh, the first outbreak of chikungunya was investigated in 2008 [28].

In the last century, compartmental mathematical models have been widely used for studying the epidemiological models, in particular vector borne infectious disease models [29, 30]. A several number of deterministic models have been proposed to study the chikungunya virus [5, 8, 9, 31] and the references therein. A simple deterministic model of the transmission of chikungunya virus between human and mosquitoes has developed by Yakob and Clements [31]. They have fitted the model with real data, estimated the type of basic reproduction number and analyzed the sensitivity of the parameters. Age structured deterministic model also proposed, analyzed theoritically and numerically [32]. Authors in [33], formulate a model that incorporate the dynamics of two circulating viral disease: dengue and chikungunya by considering variable population size and infection in sub-acute and chronic phase but not analyzed the model qualitatively. The spatio-temporal transmission of chikungunya is analysed in [34] and it is shown that the prevention of moving symptomatic individuals is not sufficient mechanisms to control the outbreak, since the presence of asymptomatic individuals spread the disease silently within the population. In [9], a temporal model is proposed to study the outbreak of chikungunya in several cities of Re'union island in 2005. In this model, the existence and the stability of the disease free equilibrium is investigated by using basic reproduction number but the dynamics of the endemic equilibrium are not considered.

In this research article, we develop a new deterministic model to study the transmission of chikungunya virus. In our model, we incorporate a class of infected individuals those are in subacute or chronic phase. Also we consider the treatment to the infected individuals in different classes. The paper is organized as follows: in section 2, the model is formulated and various properties including the boundedness and the positivity of the solutions are analyzed, also the existence and the stability of the equilibrium are investigated by using different techniques in section 3. Numerical simulations and sensitivity analysis are carried out in section 4. In section 5, discussion and conclusion of the study are drawn.

2 Model formulation

The human population is divided into the following six mutually-exclusive classes: susceptible (S_h), exposed (E_h), symptomatically infectious in acute phase (I_{s1}), infected in subacute phase (I_{s2}), asymptomatically infectious (I_a) and recovered (R_h). So, the total population at time t is $N_h(t) = S_h(t)+E_h(t)+I_a(t)+I_{s1}(t)+I_{s2}(t)+R_h(t)$. Similarly, the vector population is divided into the following three classes: susceptible (S_m), exposed

(E_m) and infectious (I_m). Therefore, the total matured mosquito population is $N_m(t) = S_m(t) + E_m(t) + I_m(t)$.

Assume that the requirement rate of human population is constant, π_1, and human population is born as susceptible, thus there is no vertical transmission. Also, suppose that the mosquito requirement rate is constant, π_2. A susceptible human is infected when bitten by an infectious mosquito and goes to the class (E_m). Suppose that the biting rate of each mosquito is b_m per day. Since the number of bites by mosquitoes equals to the total number of bites received by the humans so, we have

$$b_m N_m = b_h(N_h, N_m)N_h \tag{2.1}$$

where, b_h is the rate of bites received by humans. So that

$$N_m = \frac{b_h(N_h, N_m)N_h}{b_m} \tag{2.2}$$

Now, let β_1 be the probability that a bite from an infectious mosquito will lead a host infection. So that, $\beta_1 b_h$ is the effective contact rate between a susceptible human and infectious mosquito. Thus, the rate at which susceptible human acquire infection, after an effective contact with infectious mosquito, is λ_1 and given by

$$\lambda_1 = \frac{\beta_1 b_h(N_h, N_m)I_m}{N_m} \tag{2.3}$$

Thus, equation (2.2) and (2.3) gives

$$\lambda_1 = \frac{b_m \beta_1 I_m}{N_h} \tag{2.4}$$

This infection rate is called force of infection. After an intrinsic incubation period, the time elapsed by the virus from the moment of infection to the beginning of infectiousness, a portion p of populations in the class E_h moves to the asymptomatically infectious class I_a and the remaining portion $(1-p)$ enters into the symptomatically infectious class I_{s1}. After the viremic period, infectious humans of both class class I_a and I_{s1} are recovered and go forward to the class R_h. But some symptomatically infectious individuals go to the sub-acute or chronic phase I_{s2} and symptoms can persist for long time [14, 15]. Moreover, chikungunya virus antigen is found in a muscle biopsy of a person suffering of disease three months after initial onset [16]. So, there is a chance for susceptible mosquitoes to be infected from individuals in class I_{s2}. Let μ_1 be the natural mortality rate of human population.

A susceptible mosquito goes to the exposed class when it bites an infectious human in the class I_a and I_{s1}, also in class I_{s2} but the rate may be neglected. The effective contact rate between the susceptible mosquitoes and infectious hosts (I_a and I_{s1}) is $b_m\beta_{12}$, and between S_m and I_{s2} is $b_m b_{22}$, where β_{12} is the probability that a bite leads to infection of the mosquito from the classes I_a and I_{s1}, and β_{22} is that from I_{s2}. Hence, the rate at which mosquitoes acquire infection from both asymptomatically infectious and symptomatically infectious human is given by

$$\lambda_2 = \frac{b_m\beta_{12}(I_a + I_{s1}) + b_m\beta_{22}I_{s2}}{N_h} \tag{2.5}$$

Mosquitoes in the exposed class become infectious after an extrinsic incubation period, the period necessary for the virus to follow a cycle that brings it from the mosquito stomach to its salivary gland. The mortality rate for the classes S_m, E_m and I_m is μ_2. We also assume that there is no vertical transmission. Now, considering all of the above assumtions and using the law in[35], we can construct the following deterministic system of nonlinear

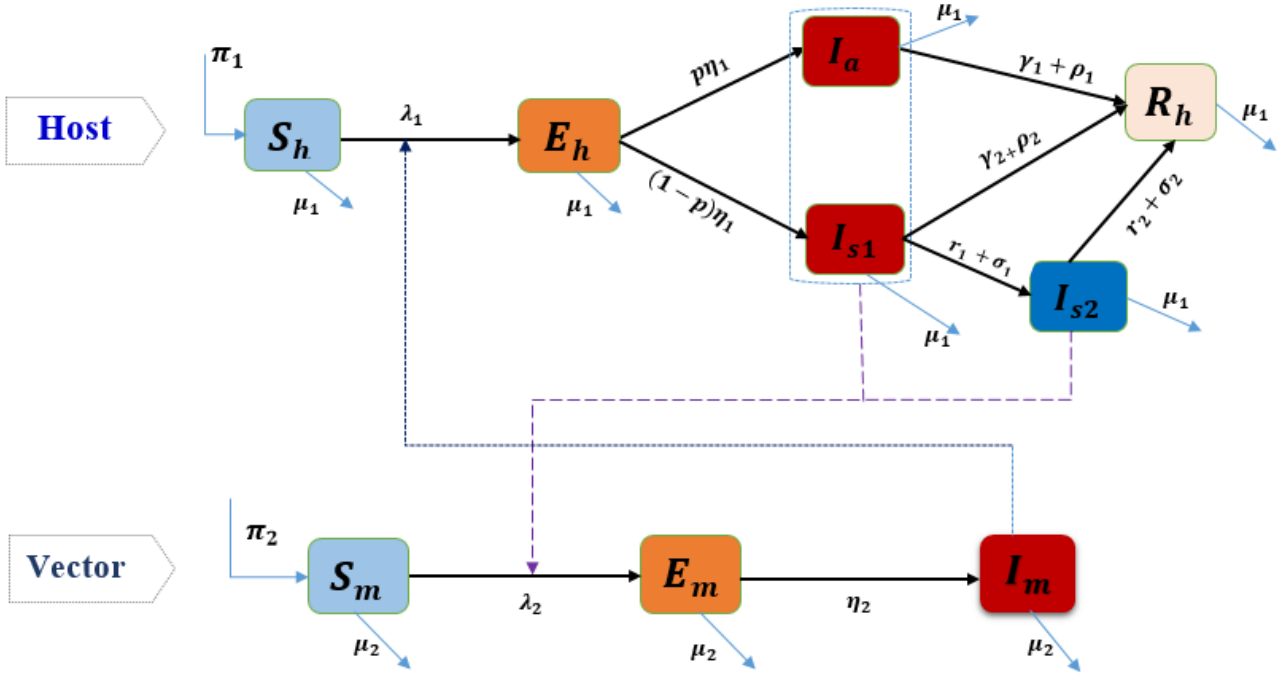

Figure 2.1: ***Schematic diagram for the chikungunya virus transmission.*** *The population of humans is divided into susceptible (S_h), exposed (E_h) to the disease, asymtomatically infectious (I_a), symptomatically infectious (I_{s_1}) in acute phase, infected in sub-acute phase (I_{s_2}) and recovered (R_h) from chikungunya. The mosquitoes population is divided into susceptible (S_m), exposed (E_m) and infectious (I_m). The black heavy arrows indicate the disease transition from one compartment to the other compartment and dashed arrows indicate the contacts between hosts and vector.*

differential equations to describe the transmission dynamics of chikungunya virus:

$$\begin{aligned}
\frac{dS_h}{dt} &= \pi_1 - \lambda_1 S_h - \mu_1 S_h \\
\frac{dE_h}{dt} &= \lambda_1 S_h - \eta_1 E_h - \mu_1 E_h \\
\frac{dI_a}{dt} &= p\eta_1 E_h - \gamma_1 I_a - \rho_1 I_a - \mu_1 I_a \\
\frac{dI_{s1}}{dt} &= (1-p)\eta_1 E_h - \gamma_2 I_{s1} - \rho_2 I_{s1} - r_1 I_{s1} - \sigma_1 I_{s1} - \mu_1 I_s \\
\frac{dI_{s2}}{dt} &= r_1 I_{s1} + \sigma_1 I_{s1} - r_2 I_{s2} - \sigma_2 I_{s2} - \mu_1 I_{s2} \\
\frac{dR_h}{dt} &= \gamma_1 I_a + \rho_1 I_a + \gamma_2 I_{s1} + \rho_2 I_{s1} + r_2 I_{s2} + \sigma_2 I_{s2} - \mu_1 R_h \\
\frac{dS_m}{dt} &= \pi_2 - \lambda_2 S_m - \mu_2 S_m \\
\frac{dE_m}{dt} &= \lambda_2 S_m - \eta_2 E_m - \mu_2 E_m \\
\frac{dI_m}{dt} &= \eta_2 E_m - \mu_2 I_m \\
S_h(0) = S_{h0}, E_h(0) &= E_{h0}, I_a(0) = I_{a0}, I_{s1}(0) = I_{s10}, I_{s2}(0) = I_{s20}, \\
R_h(0) = R_{h0}, S_m(0) &= S_{m0}, E_m(0) = E_{m0}, I_m(0) = I_{m0},
\end{aligned} \tag{2.6}$$

where, λ_1 and λ_2 are given in equation (2.4) and (2.5) respectively.

The schematic diagram of the model is depicted in Figure 2.1, and the description of the associated param-

eters of the model (2.6) is given in Table 2.1.

Table 2.1: The variables and parameters of the model (2.6) with description

Variables and Parameters	Description
S_h	Susceptible human population
E_h	Exposed human population
I_a	Asymptomatically infectious human population
I_{s1}	Symptomatically infectious human population in acute phase
I_{s2}	Infected humans population in sub-acute phase
R_h	Recovered human population
S_m	Susceptible mosquito population
E_m	Exposed mosquito population
I_m	Infectious mosquito population
π_1	Recruitment rate Human population
μ_1	Natural death rate of human population
π_2	Recruitment rate of mosquito population
μ_2	Natural mortality rate of mosquito population
β_1	Transmission probability per bite from I_m to S_h
β_{12}	Transmission probability per bite from both I_a and I_{s1} to S_m
β_{22}	Transmission probability per bite from I_{s2} to S_m
b_m	Daily mosquito biting rate
λ_1	Infection rate for human population
λ_2	Infection rate for mosquito population
η_1	Progression rate of exposed human population
η_2	Progression rate of exposed mosquito population
r_1	Progression rate from I_{s1} to I_{s2}
γ_1	Recovery rate of human population from the class I_a
γ_2	Recovery rate of human population from the class I_{s1}
r_2	Recovery rate of human population from the class I_{s2}
$\rho_1, \rho_2, \sigma_1, \sigma_2$	Treatment rate
p	Fraction of exposed human who do not develop symptoms
$1-p$	Fraction of exposed human who develop symptoms

3 Analysis of the model

3.1 Properties of the model

Here we prove some basic qualitative properties of solutions to the model (2.6), such as positivity and boundedness of the solutions. These properties can shown by the following lemma:

Lemma 1. *The region,* $\Omega = \{(S_h, E_h, I_a, I_{s1}, I_{s2}, R_h, S_m, E_m, I_m) : S_h + E_h + I_a + I_{s1} + I_{s2} + R_h \leq \frac{\pi_1}{\mu_1}, S_m + E_m + I_m \leq \frac{\pi_2}{\mu_2}\} \subset \mathbb{R}^9_+$, *is positively invariant and attracting for the basic model* (2.6).

Proof. The rate of change of the human population and mosquito population are obtained by adding the first six equations and last three equations of the model respectively (2.6) as follows

$$\frac{dN_h(t)}{dt} = \pi_1 - \mu_1 N_h(t)$$

$$\frac{dN_m(t)}{dt} = \pi_2 - \mu_2 N_m(t)$$

Thus, we see that $\frac{dN_h(t)}{dt} < 0$ if $N_h(t) > \pi_1/\mu_1$ and $\frac{dN_m(t)}{dt} < 0$ if $N_m(t) > \pi_2/\mu_2$. Also by using a standard comparison theorem [44], it can be shown that $N_h(t) = N_h(0)e^{-\mu_1 t} + (\pi_1/\mu_1)(1 - e^{-\mu_1 t})$ and $N_m(t) = N_m(0)e^{-\mu_2 t} + (\pi_2/\mu_2)(1 - e^{-\mu_2 t})$. In particular, $N_h(t) < \pi_1/\mu_1$ if $N_h(0) < \pi_1/\mu_1$ and $N_m(t) < \pi_2/\mu_2$ if $N_m(0) < \pi_2/\mu_2$ .Thus, Ω is positively invariant. Further, $N_h(t) > \pi_1/\mu_1$ and $N_m(t) > \pi_2/\mu_2$, then either the

solution enters Ω in finite time, or $N_h(t)$ approaches π_1/μ_1 and $N_m(t)$ approaches π_2/μ_2, and the variables $E_h(t), I_a(t), I_{s1}(t), I_{s2}(t), R_h(t), E_m(t)$ and $I_m(t)$ approach zero. Hence, Ω is attracting. Thus, the model (2.6) is well-posed in Ω epidemiologically and mathematically [30] and it is sufficient to study the dynamics of the model (2.6) in Ω. □

3.2 Equilibrium points and stability analysis

The model (2.6) may have two types of equilibrium, namely disease free equilibrium (*DFE*) and endemic equilibrium (*EE*). At any equilibrium, we set $\frac{dS_h}{dt} = 0, \frac{dE_h}{dt} = 0, \frac{dI_a}{dt} = 0, \frac{dI_{s1}}{dt} = 0, \frac{dI_{s2}}{dt} = 0, \frac{dR_h}{dt} = 0$, and obtain the following relations

$$\begin{aligned}
I_a &= \frac{p\eta_1}{k_5}E_h \\
I_{s1} &= \frac{(1-p)\eta_1}{k_7}E_h \\
I_{s2} &= \frac{\eta_1(1-p)k_1}{k_6k_7}E_h \\
R_h &= \frac{\eta_1(1-p)(k_1k_2k_5 + k_4k_5k_6) + \eta_1pk_3k_6k_7}{\mu_1k_5k_6k_7}E_h \\
S_h &= N_h - \frac{a}{k_5k_6k_7\mu_1}E_h \\
E_h &= \frac{\beta_1b_m\mu_1k_5k_6k_7I_mN_h}{k_5k_6k_7\mu_1(\mu_1+\eta_1)N_h + a\beta_1b_mI_m},
\end{aligned} \tag{3.1}$$

where, $k_1 = \sigma_1 + r_1$, $k_2 = \sigma_2 + r_2$, $k_3 = \gamma_1 + \rho_1$, $k_4 = \gamma_2 + \rho_2$, $k_5 = \gamma_1 + \rho_1 + \mu_1$, $k_6 = r_2 + \sigma_2 + \mu_1$,$k_7 = \gamma_2 + \rho_2 + \sigma_1 + r_1 + \mu_1$,
$a = k_5k_6k_7\mu_1 + k_5k_6\eta_1(1-p)(k_4+\mu_1) + k_1k_5\eta_1(1-p)(k_2+\mu_1+k_6k_7\eta_1p(k_3+\mu_1)$.

Also by setting $\frac{dS_m}{dt} = 0, \frac{dE_m}{dt} = 0, \frac{dI_m}{dt} = 0$, we have the following relations

$$\begin{aligned}
S_m &= \frac{\pi_2}{\lambda_2+\mu_2} \\
E_m &= \frac{\pi_2\lambda_2}{(\eta_2+\mu_2)(\lambda_2+\mu_2)} \\
I_m &= \frac{\pi_2\eta_2\lambda_2}{\mu_2(\eta_2+\mu_2)(\lambda_2+\mu_2)}
\end{aligned} \tag{3.2}$$

3.3 Stability of disease free equilibrium (*DFE*)

DFE of the model (2.6) is given by

$$\bar{E}_0 = (S_h^*, E_h^*, I_a^*, I_{s1}^*, I_{s2}^*, R_h^*, S_m^*, E_m^*, I_m^*) = \left(\frac{\pi_1}{\mu_1}, 0, 0, 0, 0, 0, \frac{\pi_2}{\mu_2}, 0, 0\right)$$

3.3.1 Local stability of *DFE*

We investigate the local stability of the *DFE* by using the next generation matrix of the system (2.6). Now, we calculate the basic reproduction number of the model (2.6) according to [49]. Consider the compartments

which are related to the infection to obtain the following subsystem

$$\begin{aligned}
\frac{dE_h}{dt} &= \lambda_1 S_h - \eta_1 E_h - \mu_1 E_h \\
\frac{dI_a}{dt} &= p\eta_1 E_h - \gamma_1 I_a - \rho_1 I_a - \mu_1 I_a \\
\frac{dI_{s1}}{dt} &= (1-p)\eta_1 E_h - \gamma_2 I_{s1} - \rho_2 I_{s1} - r_1 I_{s1} - \sigma_1 I_{s1} - \mu_1 I_{s1} \\
\frac{dI_{s2}}{dt} &= r_1 I_{s1} + \sigma_1 I_{s1} - r_2 I_{s2} - \sigma_2 I_{s2} - \mu_1 I_{s2} \\
\frac{dE_m}{dt} &= \lambda_2 S_m - \eta_2 E_m - \mu_2 E_m \\
\frac{dI_m}{dt} &= \eta_2 E_m - \mu_2 I_m.
\end{aligned} \tag{3.3}$$

From the subsystem (3.3), we find the following transmission matrix F (associated with new infection terms) and transition matrix V (considering transferred terms):

$$F = \begin{bmatrix} 0 & 0 & 0 & 0 & 0 & \frac{\beta_1 b_m S_h}{N_h} \\ 0 & 0 & 0 & 0 & 0 & 0 \\ 0 & 0 & 0 & 0 & 0 & 0 \\ 0 & 0 & 0 & 0 & 0 & 0 \\ 0 & \frac{\beta_{12} b_m S_m}{N_h} & \frac{\beta_{12} b_m S_m}{N_h} & \frac{\beta_{22} b_m S_m}{N_h} & 0 & 0 \\ 0 & 0 & 0 & 0 & 0 & 0 \end{bmatrix}$$

and

$$V = \begin{bmatrix} \eta_1 + \mu_1 & 0 & 0 & 0 & 0 & 0 \\ -p\eta_1 & k_5 & 0 & 0 & 0 & 0 \\ -(1-p)\eta_1 & 0 & k_7 & 0 & 0 & 0 \\ 0 & 0 & -k_1 & k_6 & 0 & 0 \\ 0 & 0 & 0 & 0 & \eta_2 + \mu_2 & 0 \\ 0 & 0 & 0 & 0 & -\eta_2 & \mu_2 \end{bmatrix},$$

where, $k_1 = r_1 + \sigma_1, k_5 = \gamma_1 + \rho_1 + \mu_1, k_6 = r_2 + \sigma_2 + \mu_1, k_7 = \gamma_2 + \rho_2 + r_1 + \sigma_1 + \mu_1$.
The basic reproduction number [49] is the spectral radius of the matrix FV^{-1}, that is, $\Re_0 = \rho(FV^{-1})$.

Now, the eigenvalues of FV^{-1} are
$0, 0, 0, 0, \frac{b_m\sqrt{\beta_1\eta_1\eta_2\{\beta_{12}k_5k_6(1-p)+\beta_{12}k_6k_7p+\beta_{22}k_1k_5(1-p)\}S_h^*S_m^*}}{\sqrt{k_5k_6k_7\mu_2(\mu_1+\eta_1)(\mu_2+\eta_2)N_h}}$ and $-\frac{b_m\sqrt{\beta_1\eta_1\eta_2\{\beta_{12}k_5k_6(1-p)+\beta_{12}k_6k_7p+\beta_{22}k_1k_5(1-p)\}S_h^*S_m^*}}{\sqrt{k_5k_6k_7\mu_2(\mu_1+\eta_1)(\mu_2+\eta_2)N_h}}$.
Therefore, it follows that the basic reproduction number of the model is

$$\Re_0 = \frac{b_m\sqrt{\beta_1\eta_1\eta_2\{\beta_{12}k_5k_6(1-p)+\beta_{12}k_6k_7p+\beta_{22}k_1k_5(1-p)\}S_m^*S_h^*}}{\sqrt{k_5k_6k_7\mu_2(\mu_1+\eta_1)(\mu_2+\eta_2)}N_h}$$

According to [49], we know that if $\Re_0 < 1$ then the *DFE* is locally asymptotically stable, that is the disease will not persist in the community; whereas if $\Re_0 > 1$, then it is unstable and the disease will be spread out. Thus we have the following result.

Theorem 1. *The DFE, $\bar{E}_0$, of the model (2.6) is locally asymptotically stable if $\Re_0 < 1$ and unstable if $\Re_0 > 1$.*

The basic reproduction number, $\Re_0$, is the average number of new cases produced by a single infected individual in a population that is totally susceptible. Thus, from the above Theorem (1), chikungunya will be eliminated from the community when $\Re_0 < 1$.

3.3.2 Global stability of *DFE*

Before to prove the global stability of *DFE*, we consider the region,

$$\Omega^* = \{(S_h, E_h, I_a, I_{s1}, I_{s2}, R_h, S_m, E_m, I_m) \in \Omega : S_h \le S_h^*, S_m \le S_m^*\}$$

and prove the following lemma:

Lemma 2. *The region Ω^* is positively invariant and attracting for the model (2.6).*

Proof. From the first equation of the model (2.6), where, $S_h^* = \pi_1/\mu_1$, it follows that

$$\begin{aligned}\frac{dS_h}{dt} &= \pi_1 - \lambda_1 S_h(t) - \mu_1 S_h(t)\\ &\leq \pi_1 - \mu_1 S_h(t)\\ &= \mu_1[\pi_1/\mu_1 - S_h(t)]\\ &= \mu_1[S_h^* - S_h(t)]\end{aligned}$$

Hence, we have

$$S_h(t) \leq S_h^* - [S_h^* - S_h(0)]e^{-\mu_1 t}$$

Thus, if $N_h(t) \leq \pi_1/\mu_1$ and $S_h(0) \leq \pi_1/\mu_1$, then it follows that either $S_h(t) \to S_h^*$ as $t \to \infty$, or after finite time $S_h(t) \leq S_h^*$, since $\frac{dS_h}{dt} < 0$ for $S_h(t) > S_h^*$.

Finally, it follows from the seventh equation of the model (2.6), where, $S_m^* = \pi_2/\mu_2$, it follows that

$$\begin{aligned}\frac{dS_m}{dt} &= \pi_2 - \lambda_2 S_m(t) - \mu_2 S_m(t)\\ &\leq \pi_2 - \mu_2 S_m(t)\\ &= \mu_2[\pi_2/\mu_2 - S_m(t)]\\ &= \mu_2[S_m^* - S_m(t)]\end{aligned}$$

Thus,

$$S_m(t) \leq S_m^* - [S_m^* - S_m(0)]e^{-\mu_2 t}$$

Hence, if $S_m(0) \leq \pi_2/\mu_2$, then either $S_m(t)$ approaches S_m^* asymptotically, or after some finite time $S_m(t) \leq S_m^*$, since $\frac{dS_m}{dt} < 0$, if $S_m(t) > S_m^*$. Therefore, the region Ω^* is positively invariant and attracts all solutions of the model (2.6) in $\mathbb{R}_+^9$. □

Now, we claim the following:

Theorem 2. *The DFE, $\bar{E}_0$, of the model (2.6) is globally asymptotically stable in the region Ω^* if $\Re_0 < 1$.*

Proof. We prove the theorem by using Lyapunov function [40, 45, 46] and LaSalle Invariance Principle [47]. Consider the following Lyapunov function

$$\mathcal{F} = f_1 E_h + f_2 I_a + f_3 I_{s1} + f_4 I_{s2} + f_5 E_m + f_6 I_m$$

where,

$$f_1 = \frac{\mu_2 N_h \Re_0}{b_m \beta_1 S_h^*}, f_2 = \frac{b_m \beta_{12} \eta_2 S_m^*}{k_5 N_h(\mu_2+\eta_2)\Re_0}, f_3 = \frac{b_m \eta_2 S_m^*(\beta_{12}k_6 + \beta_{22}k_1)}{k_6 k_7 N_h(\mu_2+\eta_2)\Re_0},$$
$$f_4 = \frac{b_m \eta_2 \beta_{22} S_m^*}{k_6 N_h(\mu_2+\eta_2)\Re_0}, f_5 = \frac{\eta_2}{\mu_2+\eta_2}, f_6 = 1$$

Now, the time derivative of the Lyapunov function is given by

$$\begin{aligned}\dot{\mathcal{F}} &= f_1\dot{E_h} + f_2\dot{I_a} + f_3\dot{I_{s1}} + f_4\dot{I_{s2}} + f_5\dot{E_m} + f_6\dot{I_m}\\ &= \frac{\mu_2 N_h \Re_0}{b_m \beta_1 S_h^*}[\lambda_1 S_h - \eta_1 E_h - \mu_1 E_h] + \frac{b_m \beta_{12}\eta_2 S_m^*}{k_5 N_h(\mu_2+\eta_2)\Re_0}[p\eta_1 E_h - k_5 I_a]\\ &+ \frac{b_m \eta_2 S_m^*(\beta_{12}k_6+\beta_{22}k_1)}{k_6 k_7 N_h(\mu_2+\eta_2)\Re_0}[(1-p)\eta_1 E_h - k_7 I_{s1}] + \frac{b_m \eta_2 \beta_{22} S_m^*}{k_6 N_h(\mu_2+\eta_2)\Re_0}[k_1 I_{s1} - k_6 I_{s2}]\\ &+ \frac{\eta_2}{\mu_2+\eta_2}[\lambda_2 S_m^* - \eta_2 E_m - \mu_2 E_m] + \eta_2 E_m - \mu_2 I_m\\ &= \frac{b_m \eta_2 \beta_{12} S_m^*}{N_h(\mu_2+\eta_2)\Re_0}(\Re_0 - 1)I_a + \frac{b_m \eta_2 \beta_{12} S_m^*}{N_h(\mu_2+\eta_2)\Re_0}(\Re_0 - 1)I_{s1}\\ &+ \frac{b_m \eta_2 \beta_{12} S_m^*}{N_h(\mu_2+\eta_2)\Re_0}(\Re_0 - 1)I_{s2} + \mu_2(\Re_0 - 1)I_m\end{aligned}$$

Thus, $\dot{\mathcal{F}} < 0$ if $\Re_0 < 1$ and $\dot{\mathcal{F}} = 0$ if and only if $I_a = I_{s1} = I_{s2} = I_m = 0$. It follows, from the LaSalle Invariance Principle [47] , that $E_h \to 0, I_a \to 0, I_{s1} \to 0, I_{s2} \to 0, E_m \to 0$ and $I_m \to 0$ as $t \to \infty$. That is, the disease will be eliminated. Now, from the first and seventh equations of the model with $E_h = I_a = I_{s1} = I_{s2} = R_h = E_m = I_m = 0$, it follows that $S_h \to S_h^*$ and $S_m \to S_m^*$ as $t \to \infty$.
Thus, $\lim_{t\to\infty}(S_h, E_h, I_a, I_{s1}, I_{s2}, R_h, S_m, E_m, I_m) = (S_h^*, 0, 0, 0, 0, 0, S_m^*, 0, 0) = \bar{E}_0$ for $\Re_0 \leq 1$. Therefore, the *DFE*, $\bar{E}_0$, is *GAS* in Ω^* if $\Re_0 \leq 1$. □

Epidemiological significance of the above theorem is that the chikungunya disease will be eliminated permanently from the community if we can reduce the threshold quantity ($\Re_0$) to less than one. The convergence of the total number of infected human population and mosquito population is shown in Figure 3.1 whenever the quantity $\Re_0 < 1$.

3.4 Stability of Endemic Equilibrium (*EE*)

3.4.1 Existence of Endemic Equilibrium

In this section, we find the condition for the existence of endemic equilibrium. Let the endemic equilibrium point of the model (2.6) be

$$\bar{E}_1 = (S_h^{**}, E_h^{**}, I_a^{**}, I_{s1}^{**}, I_{s2}^{**}, R_h^{**}, S_m^{**}, E_m^{**}, I_m^{**}),$$

and at the *EE*, the expressions in (3.1) and (3.2) become

$$\begin{aligned}
S_h^{**} &= \frac{\pi_1}{\lambda_1^{**} + \mu_1} \\
E_h^{**} &= \frac{\pi_1 \lambda_1^{**}}{(\lambda_1^{**} + \mu_1)(\eta_1 + \mu_1)} \\
I_a^{**} &= \frac{p\pi_1\eta_1\lambda_1^{**}}{k_5(\lambda_1^{**} + \mu_1)(\eta_1 + \mu_1)} \\
I_{s1}^{**} &= \frac{(1-p)\pi_1\eta_1\lambda_1^{**}}{k_7(\lambda_1^{**} + \mu_1)(\eta_1 + \mu_1)} \\
I_{s2}^{**} &= \frac{(1-p)\pi_1\eta_1\lambda_1^{**}k_1}{k_6k_7(\lambda_1^{**} + \mu_1)(\eta_1 + \mu_1)} \\
R_h^{**} &= \frac{\pi_1\eta_1\lambda_1^{**}[k_5(1-p)(k_1k_2 + k_4k_6) + pk_3k_6k_7]}{k_5k_6k_7\mu_1(\lambda_1^{**} + \mu_1)(\eta_1 + \mu_1)}
\end{aligned}$$

$$\begin{aligned}
S_m^{**} &= \frac{\pi_2}{\lambda_2^{**} + \mu_2} \\
E_m^{**} &= \frac{\pi_2 \lambda_2^{**}}{(\lambda_2^{**} + \mu_2)(\eta_2 + \mu_2)} \\
I_m^{**} &= \frac{\pi_2\eta_2\lambda_2^{**}}{\mu_2(\lambda_2^{**} + \mu_2)(\eta_2 + \mu_2)}
\end{aligned}$$

The forces of infection at the *EE* state are

$$\lambda_1^{**} = \frac{\beta_1 b_m I_m^{**}}{N_h^{**}}$$

and

$$\lambda_2^{**} = \frac{\beta_{12} b_m (I_a^{**} + I_{s1}^{**}) + b_m\beta_{22} I_{s2}^{**}}{N_h^{**}}$$

Now, substituting the expression of $I_a^{**}, I_{s1}^{**}, I_{s2}^{**}$ in the expression of λ_2^{**}, we have

$$\begin{aligned}
\lambda_2^{**} &= \frac{b_m\beta_{12}I_a^{**} + b_m\beta_{12}I_{s1}^{**} + b_m\beta_{22}I_{s2}^{**}}{N_h^{**}} \\
&= \frac{b_m\pi_1\eta_1\lambda_1^{**}[k_5(1-p)(k_1\beta_{22} + k_6\beta_{12}) + pk_6k_7\beta_{12}]}{k_5k_6k_7(\lambda_1^{**} + \mu_1)(\eta_1 + \mu_1)N_h^{**}}
\end{aligned}$$

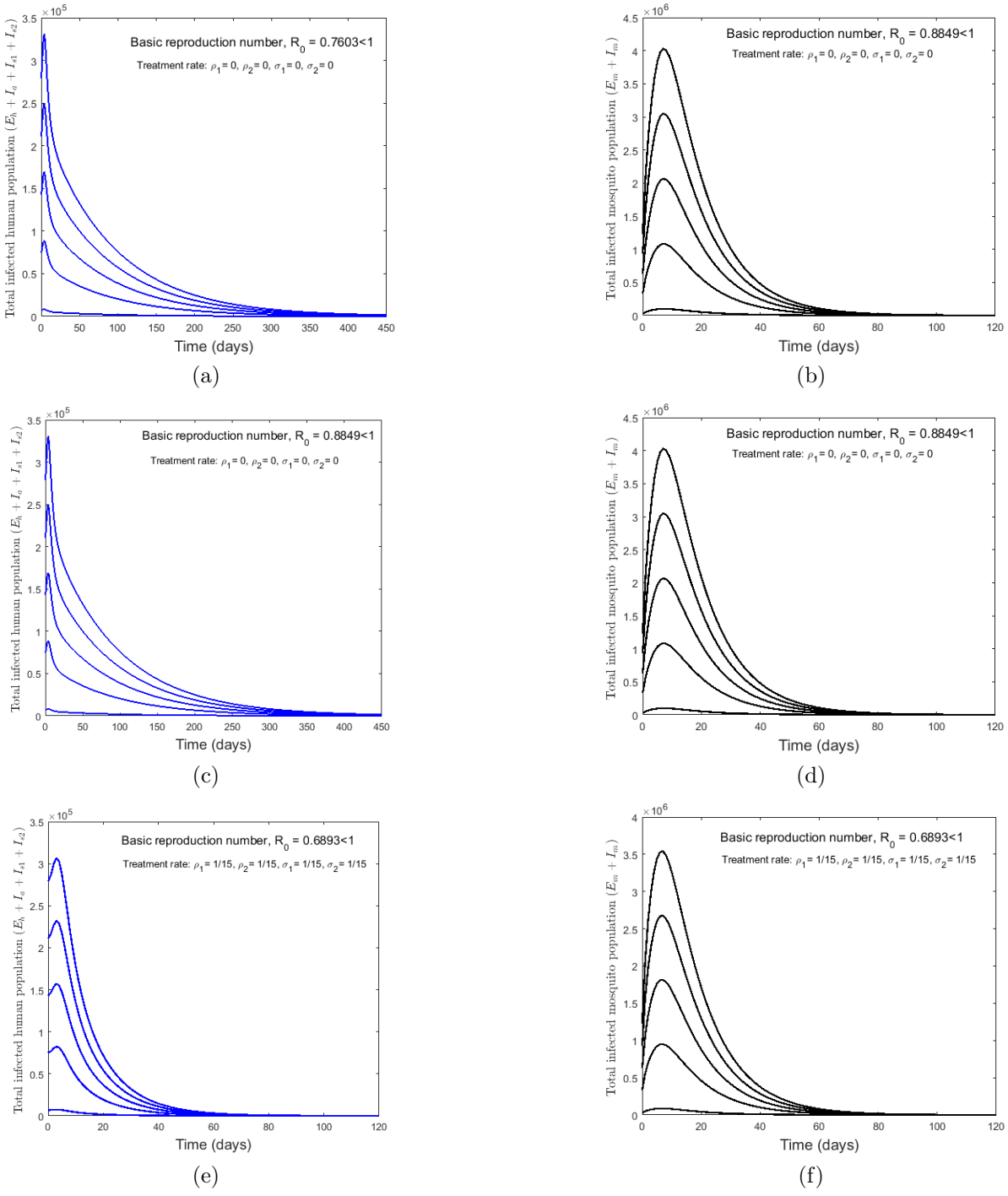

Figure 3.1: Simulations of the model (2.6) showing the total number of infected human population ($E_h + I_a + I_{s1} + I_{s2}$) as a function of time when $\Re_0 < 1$, using various initial conditions. Parameter values used as given in Table 4.2 with $\pi_1 = 1.2, \pi_2 = 3800$; (a) $\beta_{22} = 0$, without treatment; (c) $\beta_{22} = 0.005$, without treatment; (e) $\beta_{22} = 0.005$, with treatment. And (b), (d), (f) depict the corresponding total number of infected mosquito population ($E_m + I_m$).

Also, we have

$$\lambda_1^{**} = \frac{b_m \beta_1 I_m}{N_h^{**}}$$

$$= \frac{b_m^2 \pi_1 \pi_2 \eta_1 \eta_2 \beta_1 \lambda_1^{**}[k_5(1-p)(k_1\beta_{22} + k_6\beta_{12}) + pk_6k_7\beta_{12}]/[\mu_2(\mu_2+\eta_2)N_h^{**}]}{b_m \pi_1 \eta_1 \lambda_1^{**}[k_5(1-p)(k_1\beta_{22} + k_6\beta_{12}) + pk_6k_7\beta_{12}] + k_5k_6k_7\mu_2(\lambda_1^{**} + \mu_1)(\eta_1 + \mu_1)N_h^{**}}$$

From where, we find the following quadratic equation

$$c_1(\lambda_1^{**})^2 - c_2(\lambda_1^{**}) = 0,$$

where,

$$c_1 = \mu_2(\mu_2+\eta_2)N_h^{**}[\beta_{12}b_m k_6 k_7 \eta_1 p\pi_1 + \pi_1\eta_1 b_m k_5(1-p)(k_1\beta_{22}+k_6\beta_{12}) + k_5k_6\mu_2(\mu_1+\eta_1)N_h^{**}]$$

and

$$\begin{aligned} c_2 &= b_m^2\pi_1\pi_2\eta_1\eta_2\beta_1[k_5(1-p)(k_1\beta_{22}+k_6\beta_{12}) + pk_6k_7\beta_{12}] - k_5k_6k_7\mu_1\mu_2^2(\mu_1+\eta_1)(\mu_2+\eta_2)(N_h^{**})^2 \\ &= k_5k_6k_7\mu_1\mu_2^2(\mu_1+\eta_1)(\mu_2+\eta_2)(N_h^{**})^2 \\ &\quad\left[\frac{b_m^2\pi_1\pi_2\eta_1\eta_2\beta_1[k_5(1-p)(k_1\beta_{22}+k_6\beta_{12}) + pk_6k_7\beta_{12}]}{k_5k_6k_7\mu_1\mu_2^2(\mu_1+\eta_1)(\mu_2+\eta_2)(N_h^{**})^2} - 1\right] \\ &= k_5k_6k_7\mu_1\mu_2^2(\mu_1+\eta_1)(\mu_2+\eta_2)N_h^2(\Re_0^2-1) \end{aligned}$$

Therefore, the quadratic equation has a positive real root if $\Re_0^2 > 1$.

According to the above result, we claim the following:

Lemma 3. *The model (2.6) has a unique endemic equilibrium whenever $\Re_0 > 1$, and no positive equilibrium otherwise.*

3.4.2 Local Stability of *EE*

Using $N_h = N_h^{**}$, $N_m = N_m^{**}$ and the definition $S_h = N_h^{**} - E_h - I_a - I_{s1} - I_{s2} - R_h$ and $S_m = N_m^{**} - E_m - I_m$, we have the following reduced system

$$\begin{aligned} \frac{dE_h}{dt} &= \frac{b_m\beta_1 I_m}{N_h^{**}}(N_h^{**} - E_h - I_a - I_{s1} - I_{s2} - R_h) - \eta_1 E_h - \mu_1 E_h \\ \frac{dI_a}{dt} &= p\eta_1 E_h - k_5 I_a \\ \frac{dI_{s1}}{dt} &= (1-p)\eta_1 E_h - k_7 I_{s1} \\ \frac{dI_{s2}}{dt} &= k_1 I_{s1} - k_6 I_{s2} \\ \frac{dR_h}{dt} &= k_3 I_a + k_4 I_{s1} + k_2 I_{s2} - \mu_1 R_h \\ \frac{dE_m}{dt} &= \frac{b_m\beta_{12}I_a + b_m\beta_{12}I_{s1} + b_m\beta_{22}I_{s2}}{N_h^{**}}(N_m^{**} - E_m - I_m) - \eta_2 E_m - \mu_2 E_m \\ \frac{dI_m}{dt} &= \eta_2 E_m - \mu_2 I_m \end{aligned} \tag{3.4}$$

It is easy to show that the system (3.4) has a unique *EE* of the form $\bar{E}_1 = (E_h^{**}, I_a^{**}, I_{s1}^{**}, I_{s2}^{**}, R_h^{**}, E_m^{**}, I_m^{**})$. Now, we prove the local stability of *EE* following the method given in [42], which is based on using Krasnoselskii sub-linearity trick [48]. Assume that the reduced system has a solution of the form

$$\bar{Z}(t) = \bar{Z}_0 e^{-wt} \tag{3.5}$$

with $\bar{Z}_0 = (Z_1, Z_2, Z_3, Z_4, Z_5, Z_6, Z_7)$ and $w, Z_i \in \mathbb{C}(i = 1, 2, ..., 7)$, where, $\mathbb{C}$ denotes the set of complex numbers. Substituting a solution of the form (3.5) into the linearized system of (3.4) around the endemic equilibrium, we have the following system of linear equations

$$
\begin{aligned}
wZ_1 &= -\left(\frac{b_m\beta_1 I_m^{**}}{N_h^{**}} + \eta_1 + \mu_1\right) Z_1 - \frac{b_m\beta_1 I_m^{**}}{N_h^{**}} Z_2 - \frac{b_m\beta_1 I_m^{**}}{N_h^{**}} Z_3 - \frac{b_m\beta_1 I_m^{**}}{N_h^{**}} Z_4 \\
&\quad - \frac{b_m\beta_1 I_m^{**}}{N_h^{**}} Z_5 + \frac{b_m\beta_1 (N_h^{**} - N_h^{**} - I_{s1}^{**} - I_{s2}^{**} - R^{**})}{N_h^{**}} Z_7 \\
wZ_2 &= p\eta_1 Z_1 - k_5 Z_2 \\
wZ_3 &= (1-p)\eta_1 Z_1 - k_7 Z_3 \\
wZ_4 &= k_1 Z_3 - k_6 Z_4 \\
wZ_5 &= k_3 Z_2 + k_4 Z_3 + k_2 Z_4 - \mu_1 Z_5 \\
wZ_6 &= \frac{b_m\beta_{12}(N_m^{**} - E_m^{**} - I_m^{**})}{N_h^{**}} Z_2 + \frac{b_m\beta_{12}(N_m^{**} - E_m^{**} - I_m^{**})}{N_h^{**}} Z_3 \\
&\quad + \frac{b_m\beta_{22}(N_m^{**} - E_m^{**} - I_m^{**})}{N_h^{**}} Z_4 - \left(\frac{b_m\beta_{12} I_a^{**} + b_m\beta_{12} I_{s1}^{**} + b_m\beta_{22} I_{s2}^{**}}{N_h^{**}} + \eta_2 + \mu_2\right) Z_6 \\
&\quad - \frac{b_m\beta_{12} I_a^{**} + b_m\beta_{12} I_{s1}^{**} + b_m\beta_{22} I_{s2}^{**}}{N_h^{**}} Z_7 \\
wZ_7 &= \eta_2 Z_6 - \mu_2 Z_7
\end{aligned}
\tag{3.6}
$$

Solving the second, third and fourth equations for Z_2, Z_3, Z_4 in terms of Z_1 and substituting into the first equation, solving sixth equation for Z_7 substituting into the fifth equation and simplifying we obtain, the following equivalent system

$$
\begin{aligned}
&\left[1 + \frac{1}{\eta_1 + \mu_1}\left(w + \frac{b_m\beta_1 I_m^{**}}{N_h^{**}}\left[1 + \frac{p\eta_1}{w + k_5} + \frac{(1-p)\eta_1}{w + k_7} + \frac{k_1(1-p)\eta_1}{(w + k_6)(w + k_7)}\right]\right)\right] Z_1 \\
&= -\frac{b_m\beta_1 I_m^{**}}{N_h^{**}} Z_5 + \frac{b_m\beta_1 (N_h^{**} - N_h^{**} - I_{s1}^{**} - I_{s2}^{**} - R_h^{**})}{N_h^{**}} Z_7 \\
&\left(1 + \frac{w}{k_5}\right) Z_2 = \frac{p\eta_1}{k_5} Z_1 \\
&\left(1 + \frac{w}{k_7}\right) Z_3 = \frac{(1-p)\eta_1}{k_7} Z_1 \\
&\left(1 + \frac{w}{k_6}\right) Z_4 = \frac{k_1}{k_6} Z_3 \\
&\left(1 + \frac{w}{\mu_1}\right) Z_5 = \frac{k_3}{\mu_1} Z_2 + \frac{k_4}{\mu_1} Z_3 + \frac{k_2}{\mu_1} Z_4 \\
&Z_6 + \frac{1}{\eta_2 + \mu_2}\left(w + \frac{b_m\beta_{12} I_a^{**} + b_m\beta_{12} I_{s1}^{**} + b_m\beta_{22} I_{s2}^{**}}{N_h^{**}}\right) Z_6 \\
&+ \frac{1}{\eta_2 + \mu_2}\left(\frac{\eta_2}{w + \mu_2}\frac{b_m\beta_{12} I_a^{**} + b_m\beta_{12} I_{s1}^{**} + b_m\beta_{22} I_{s2}^{**}}{N_h^{**}}\right) Z_6 \\
&= \frac{b_m\beta_{12}(N_m^{**} - E_m^{**} - I_m^{**})}{N_h^{**}} Z_2 + \frac{b_m\beta_{12}(N_m^{**} - E_m^{**} - I_m^{**})}{N_h^{**}} Z_3 \\
&+ \frac{b_m\beta_{22}(N_m^{**} - E_m^{**} - I_m^{**})}{N_h^{**}} Z_4 \\
&\left(1 + \frac{w}{\mu_2}\right) Z_7 = \frac{\eta_2}{\mu_2} Z_6
\end{aligned}
\tag{3.7}
$$

Adding the first and fifth equation of the system (3.7), and moving all the negative terms to their respective left-hand side to give

$$\begin{aligned}
[1+F_1(w)]\,Z_1+[1+F_5(w)]Z_5 &= (M\bar{Z})_1+(M\bar{Z})_5\\
[1+F_2(w)]Z_2 &= (M\bar{Z})_2\\
[1+F_3(w)]Z_3 &= (M\bar{Z})_3\\
[1+F_4(w)]Z_4 &= (M\bar{Z})_4\\
[1+F_6(w)]Z_6 &= (M\bar{Z})_6\\
[1+F_7(w)]Z_7 &= (M\bar{Z})_7,
\end{aligned} \tag{3.8}$$

where,

$$\begin{aligned}
F_1(w) &= \frac{1}{\eta_1+\mu_1}\left(w+\frac{b_m\beta_1 I_m^{**}}{N_h^{**}}\left[1+\frac{p\eta_1}{w+k_5}+\frac{(1-p)\eta_1}{w+k_7}+\frac{k_1(1-p)\eta_1}{(w+k_6)(w+k_7)}\right]\right)\\
F_2(w) &= \frac{w}{k_5}\\
F_3(w) &= \frac{w}{k_7}\\
F_4(w) &= \frac{w}{k_6}\\
F_5(w) &= \frac{w}{\mu_1}+\frac{b_m\beta_1 I_m^{**}}{(\eta_1+\mu_1)N_h^{**}}\\
F_6(w) &= \frac{1}{\eta_2+\mu_2}\left(w+\frac{b_m\beta_{12}I_a^{**}+b_m\beta_{12}I_{s1}^{**}+b_m\beta_{22}I_{s2}^{**}}{N_h^{**}}\right)\\
&\quad+\frac{\eta_2}{(w+\mu_2)(\eta_2+\mu_2)}\frac{b_m\beta_{12}I_a^{**}+b_m\beta_{12}I_{s1}^{**}+b_m\beta_{22}I_{s2}^{**}}{N_h^{**}}\\
F_7(w) &= \frac{w}{\mu_2},
\end{aligned}$$

and M is the matrix

$$M=\begin{bmatrix}
0 & 0 & 0 & 0 & 0 & 0 & M_h\\
\frac{p\eta_1}{k_5} & 0 & 0 & 0 & 0 & 0 & 0\\
\frac{(1-p)\eta_1}{k_5} & 0 & 0 & 0 & 0 & 0 & 0\\
0 & 0 & \frac{k_1}{k_6} & 0 & 0 & 0 & 0\\
0 & \frac{k_3}{\mu_1} & \frac{k_4}{\mu_1} & \frac{k_2}{\mu_1} & 0 & 0 & 0\\
0 & M_m & M_m & M_m & 0 & 0 & 0\\
0 & 0 & 0 & 0 & 0 & \frac{n_2}{\mu_2} & 0
\end{bmatrix},$$

where, $M_h=\frac{b_m\beta_1(N_h^{**}-N_h^{**}-I_{s1}^{**}-I_{s2}^{**}-R_h^{**})}{N_h^{**}}$
and $M_m=\frac{b_m\beta_{12}(N_m^{**}-E_m^{**}-I_m^{**})}{N_h^{**}}$.

The notation $(M\bar{Z})_i$ $(i=1,2,...,7)$ denotes the ith coordinate of the vector $M(\bar{Z})$. Note that the matrix M has non-negative entries, and the equilibrium $\bar{E_1}$ satisfies $\bar{E_1}=M\bar{E_1}$. Moreover, since the coordinates of the equilibrium $\bar{E_1}$ are all positive, it follows then that if $\bar{Z}$ is a solution of (3.8), then it is possible to find a minimal positive real number s, such that

$$|\bar{Z}|\le s\bar{E_1},$$

where, $|\bar{Z}|=(|Z_1|,|Z_2|,...,|Z_7|)$ and $|.|$ is the norm in $\mathbb{C}$.

Now, our goal is to show that $Re(w)<0$. Assume the contrary (i.e., $Re(w)\ge 0$), we consider two cases: $w=0$ and $w\neq 0$. For the first case $(w=0)$, the system (3.8) is a homogeneous linear system in the variables $Z_i(i=1,2,...,7)$. The determinant of this system is given by

$$\begin{aligned}
\Delta &= \frac{\beta_1 b_m I_m^{**}(\lambda^{**}+\mu_2)[k_5k_6k_7(\mu_1+\eta_1)+\beta_1 b_m I_m^{**}\{k_6k_7(p\eta_1+k_5)+k_5\eta_1(1-p)(k_1+k_6)\}]}{k_5k_6k_7\mu_2(\mu_1+\eta_1)^2N_h^{**}}\\
&\quad+\frac{(\mu_1+\eta_1)N_h^{**}[k_5k_6k_7(\mu_1+\eta_1)+\beta_1 b_m I_m^{**}\{k_6k_7(p\eta_1+k_5)+k_5\eta_1(1-p)(k_1+k_6)\}]}{k_5k_6k_7\mu_2(\mu_1+\eta_1)^2N_h^{**}}>0
\end{aligned}$$

Thus, the system (3.8) has only trivial solution $\bar{Z} = 0$ for $w = 0$.

Now, we assume that $w \neq 0$ and $Re(w) > 0$. It is easy to see that in this case $|1+F_i(w)| > 1$ for $i = 1, 2, ..., 7$ and we define $F(w) = min\{|1 + F_i(w)|, i = 1, 2, ..., 7\}$, then $F(w) > 1$. Therefore, $\frac{s}{F(w)} < s$. Since s is the minimal positive real number such that $|\bar{Z}| \leq s\bar{E}_1$,so

$$|\bar{Z}| > \frac{s}{F(w)}\bar{E}_1.$$

Taking norms on both sides of (3.8) and using the fact that M is non-negative, we obtain the following inequality

$$F(w)\bar{Z} \leq M\bar{Z} \leq s(M\bar{E}_1) \leq s\bar{E}_1.$$

Thus, it follows that $\bar{Z} \leq \frac{s}{F(w)}\bar{E}_1$, which is a contradiction. Therefore, $Re(w) < 0$ and this proves that the EE, $\bar{E}_1$, is locally asymptotically stable for $\Re_0 > 1$.

3.4.3 Global Stability of *EE*

The global stability of EE of the model (2.6) is considered for a special case, where the ratio E_h^{**}/E_h equals to E_m^{**}/E_m. From the first six equations of the model (2.6), we see that

$$\begin{aligned} \frac{dS_h}{dt} + \frac{dE_h}{dt} + \frac{dI_a}{dt} + \frac{dI_{s1}}{dt} + \frac{dI_{s2}}{dt} + \frac{dR_h}{dt} &= \pi_1 - \mu_1 S_h - \mu_1 E_h - \mu_1 I_a - \mu_1 I_{s1} - \mu_1 I_{s2} - \mu_1 R_h \\ or, \frac{dN_h}{dt} &= \pi_1 - \mu_1 N_h, \end{aligned}$$

So, we have $N_h(t) \leq \frac{\pi_1}{\mu_1}$ for all $t \geq 0$. To prove the global stability, we consider $N_h^{**} = \frac{\pi_1}{\mu_1}$ for all $t > 0$. It is easy to see that the above assumptions have no effect on the basic reproduction number $\Re_0$ and the existence of unique EE for $\Re_0 > 1$. Now, we claim the following result.

Theorem 3. *The unique EE, $\bar{E}_1$, of the model (2.6), is globally asymptotically stable in Ω for a special case, $E_h^{**}/E_h = E_m^{**}/E_m$, whenever $\Re_0 > 1$.*

Proof. Consider the non-linear Lyapunov function

$$\begin{aligned} \mathcal{F} = &\left(S_h - S_h^{**} - S_h^{**} ln\frac{S_h}{S_h^{**}}\right) + \left(E_h - E_h^{**} - E_h^{**} ln\frac{E_h}{E_h^{**}}\right) \\ &+ \frac{b_m\beta_{12}S_m^{**}}{k_5N_h^{**}}\left(I_a - I_a^{**} - I_a^{**} ln\frac{I_a}{I_a^{**}}\right) + \frac{b_m\beta_{12}S_m^{**}}{k_7N_h^{**}}\left(I_{s1} - I_{s1}^{**} - I_{s1}^{**} ln\frac{I_{s1}}{I_{s1}^{**}}\right) \\ &+ \frac{b_m\beta_{22}k_1S_m^{**}}{k_6k_7N_h^{**}}\left(I_{s1} - I_{s1}^{**} - I_{s1}^{**} ln\frac{I_{s1}}{I_{s1}^{**}}\right) + \frac{b_m\beta_{22}S_m^{**}}{k_6N_h^{**}}\left(I_{s2} - I_{s2}^{**} - I_{s2}^{**} ln\frac{I_{s2}}{I_{s2}^{**}}\right) \\ &+ \left(S_m - S_m^{**} - S_m^{**} ln\frac{S_m}{S_m^{**}}\right) + \left(E_m - E_m^{**} - E_m^{**} ln\frac{E_m}{E_m^{**}}\right) \\ &+ \frac{b_m\beta_1S_h^{**}}{\mu_2N_h^{**}}\left(I_m - I_m^{**} - I_m^{**} ln\frac{I_m}{I_m^{**}}\right) \end{aligned}$$

and the Lyapunov derivative is given by

$$\begin{aligned} \dot{\mathcal{F}} = &\left(1 - \frac{S_h^{**}}{S_h}\right)\dot{S}_h + \left(1 - \frac{E_h^{**}}{E_h}\right)\dot{E}_m + \frac{b_m\beta_{12}S_m^{**}}{k_5N_h^{**}}\left(1 - \frac{I_a^{**}}{I_a}\right)\dot{I}_a \\ &+ \left(\frac{b_m\beta_{12}S_m^{**}}{k_7N_h^{**}} + \frac{b_m\beta_{22}k_1S_m^{**}}{k_6k_7N_h^{**}}\right)\left(1 - \frac{I_{s1}^{**}}{I_{s1}}\right)\dot{I}_{s1} \\ &+ \frac{b_m\beta_{22}S_m^{**}}{k_6N_h^{**}}\left(1 - \frac{I_{s2}^{**}}{I_{s2}}\right)\dot{I}_{s2} + \left(1 - \frac{S_m}{S_m^{**}}\right)\dot{S}_m \\ &+ \left(1 - \frac{E_m^{**}}{E_m}\right)\dot{E}_m + \frac{b_m\beta_1S_h^{**}}{\mu_2N_h^{**}}\left(1 - \frac{I_m^{**}}{I_m}\right)\dot{I}_m \end{aligned} \tag{3.9}$$

For further simplification, we use the following relations

$$\pi_1 = \frac{b_m\beta_1 S_h^{**} I_m^{**}}{N_h^{**} + \mu_1 S_h^{**}}$$
$$\pi_2 = \frac{b_m\beta_{12} S_m^{**} I_a^{**}}{N_h^{**}} + \frac{b_m\beta_{12} S_m^{**} I_{s1}^{**}}{N_h^{**}} + \frac{b_m\beta_{22} S_m^{**} I_{s2}^{**}}{N_h^{**}} + \mu_2 S_m^{**}$$
$$(\eta_1 + \mu_1) E_h^{**} = \frac{b_m\beta_1 S_h^{**} I_m^{**}}{N_h^{**}}$$
$$(\eta_2 + \mu_2) E_m^{**} = \frac{b_m\beta_{12} S_m^{**} I_a^{**}}{N_h^{**}} + \frac{b_m\beta_{12} S_m^{**} I_{s1}^{**}}{N_h^{**}} + \frac{b_m\beta_{22} S_m^{**} I_{s2}^{**}}{N_h^{**}}$$
$$\frac{p\eta_1}{k_5} = \frac{I_a^{**}}{E_h^{**}}$$
$$\frac{(1-p)\eta_1}{k_7} = \frac{I_{s1}^{**}}{E_h^{**}}$$
$$\frac{(1-p)\eta_1 k_1}{k_6 k_7} = \frac{I_{s2}^{**}}{E_h^{**}}$$
$$\frac{k_1}{k_6} = \frac{I_{s2}^{**}}{I_{s1}^{**}}$$
$$\frac{\eta_2}{\mu_2} = \frac{I_m^{**}}{E_m^{**}}$$

Now, from equation (3.9), we obtain the following simplified form

$$\begin{aligned}
\dot{\mathcal{F}} &= \frac{b_m\beta_1}{N_h^{**}}\left(3S_h^{**}I_m^{**} - \frac{(S_h^{**})^2}{S_h}I_m^{**} - S_h^{**}\frac{E_m}{E_m^{**}}\frac{(I_m^{**})^2}{I_m} - S_h^{**}I_m^{**}\frac{E_h}{E_h^{**}} - S_hI_m\frac{E_h^{**}}{E_h} + S_h^{**}I_m^{**}\frac{E_m}{E_m^{**}}\right)\\
&+ \frac{b_m\beta_{12}}{N_h^{**}}\left(3S_m^{**}I_a^{**} - \frac{(S_m^{**})^2}{S_m}I_a^{**} - S_m^{**}\frac{E_h}{E_h^{**}}\frac{(I_a^{**})^2}{I_a} - S_m^{**}I_a^{**}\frac{E_m}{E_m^{**}} - S_mI_a\frac{E_m^{**}}{E_m} + S_m^{**}I_a^{**}\frac{E_h}{E_h^{**}}\right)\\
&+ \frac{b_m\beta_{12}}{N_h^{**}}\left(3S_m^{**}I_{s1}^{**} - \frac{(S_m^{**})^2}{S_m}I_{s1}^{**} - S_m^{**}\frac{E_h}{E_h^{**}}\frac{(I_{s1}^{**})^2}{I_{s1}} - S_m^{**}I_{s1}^{**}\frac{E_m}{E_m^{**}} - S_mI_{s1}\frac{E_m^{**}}{E_m} + S_m^{**}I_{s1}^{**}\frac{E_h}{E_h^{**}}\right)\\
&+ \frac{b_m\beta_{22}}{N_h^{**}}\left(4S_m^{**}I_{s2}^{**} - S_m^{**}I_{s2}^{**}\frac{E_h}{E_h^{**}}\frac{I_{s1}^{**}}{I_{s2}} - \frac{(S_m^{**})^2}{S_m}I_{s2}^{**} - S_m^{**}\frac{I_{s1}}{I_{s1}^{**}}\frac{(I_{s2}^{**})^2}{I_{s2}} - S_m^{**}I_{s2}^{**}\frac{E_m}{E_m^{**}} - S_mI_{s2}\frac{E_m^{**}}{E_m}\right)\\
&+ \frac{b_m\beta_{22}}{N_h^{**}}S_m^{**}I_{s2}^{**}\frac{E_h}{E_h^{**}} + \mu_1 S_h^{**}\left(2 - \frac{S_h^{**}}{S_h} - \frac{S_h}{S_h^{**}}\right) + \mu_2 S_m^{**}\left(2 - \frac{S_m^{**}}{S_m} - \frac{S_m}{S_m^{**}}\right)\\
&= \frac{b_m\beta_1 S_h^{**}I_m^{**}}{N_h^{**}}\left(3 - \frac{S_h^{**}}{S_h} - \frac{E_m}{E_m^{**}}\frac{I_m^{**}}{I_m} - \frac{S_h}{S_h^{**}}\frac{I_m}{I_m^{**}}\frac{E_m^{**}}{E_m}\right)\\
&+ \frac{b_m\beta_{12}S_m^{**}I_a^{**}}{N_h^{**}}\left(3 - \frac{S_m^{**}}{S_m} - \frac{E_h}{E_h^{**}}\frac{I_a^{**}}{I_a} - \frac{S_m}{S_m^{**}}\frac{I_a}{I_a^{**}}\frac{E_h^{**}}{E_h}\right)\\
&+ \frac{b_m\beta_{12}S_m^{**}I_{s1}^{**}}{N_h^{**}}\left(3 - \frac{S_m^{**}}{S_m} - \frac{E_h}{E_h^{**}}\frac{I_{s1}^{**}}{I_{s1}} - \frac{S_m}{S_m^{**}}\frac{I_{s1}}{I_{s1}^{**}}\frac{E_h^{**}}{E_h}\right)\\
&+ \frac{b_m\beta_{22}S_m^{**}I_{s2}^{**}}{N_h^{**}}\left(4 - \frac{S_m^{**}}{S_m} - \frac{E_h}{E_h^{**}}\frac{I_{s1}^{**}}{I_{s1}} - \frac{I_{s1}}{I_{s1}^{**}}\frac{I_{s2}}{I_{s2}^{**}} - \frac{S_m}{S_m^{**}}\frac{I_{s2}}{I_{s2}^{**}}\frac{E_h^{**}}{E_h}\right)\\
&+ \mu_1 S_h^{**}\left(2 - \frac{S_h^{**}}{S_h} - \frac{S_h}{S_h^{**}}\right) + \mu_2 S_m^{**}\left(2 - \frac{S_m^{**}}{S_m} - \frac{S_m}{S_m^{**}}\right)
\end{aligned}$$

Since the geometric mean does not exceed the arithmetic mean, it follows that

$$2 - \frac{S_h^{**}}{S_h} - \frac{S_h}{S_h^{**}} \le 0,\ 2 - \frac{S_m^{**}}{S_m} - \frac{S_m}{S_m^{**}} \le 0\ 3 - \frac{S_h^{**}}{S_h} - \frac{E_m}{E_m^{**}}\frac{I_m^{**}}{I_m} - \frac{S_h}{S_h^{**}}\frac{I_m}{I_m^{**}}\frac{E_m^{**}}{E_m} \le 0$$
$$3 - \frac{S_m^{**}}{S_m} - \frac{E_h}{E_h^{**}}\frac{I_a^{**}}{I_a} - \frac{S_m}{S_m^{**}}\frac{I_a}{I_a^{**}}\frac{E_h^{**}}{E_h} \le 0\ 3 - \frac{S_m^{**}}{S_m} - \frac{E_h}{E_h^{**}}\frac{I_{s1}^{**}}{I_{s1}} - \frac{S_m}{S_m^{**}}\frac{I_{s1}}{I_{s1}^{**}}\frac{E_h^{**}}{E_h} \le 0$$
$$4 - \frac{S_m^{**}}{S_m} - \frac{E_h}{E_h^{**}}\frac{I_{s1}^{**}}{I_{s1}} - \frac{I_{s1}}{I_{s1}^{**}}\frac{I_{s2}}{I_{s2}^{**}} - \frac{S_m}{S_m^{**}}\frac{I_{s2}}{I_{s2}^{**}}\frac{E_h^{**}}{E_h} \le 0$$

Therefore, we have $\dot{\mathcal{F}} \leq 0$ for $\Re_0 > 1$. Thus, by the lyapunov function $\mathcal{F}$, and the LaSalle Invariance Principle [47], every solution to the equations in the model (2.6) approaches $\bar{E_1}$ as $t \to \infty$ for $\Re_0 > 1$. □

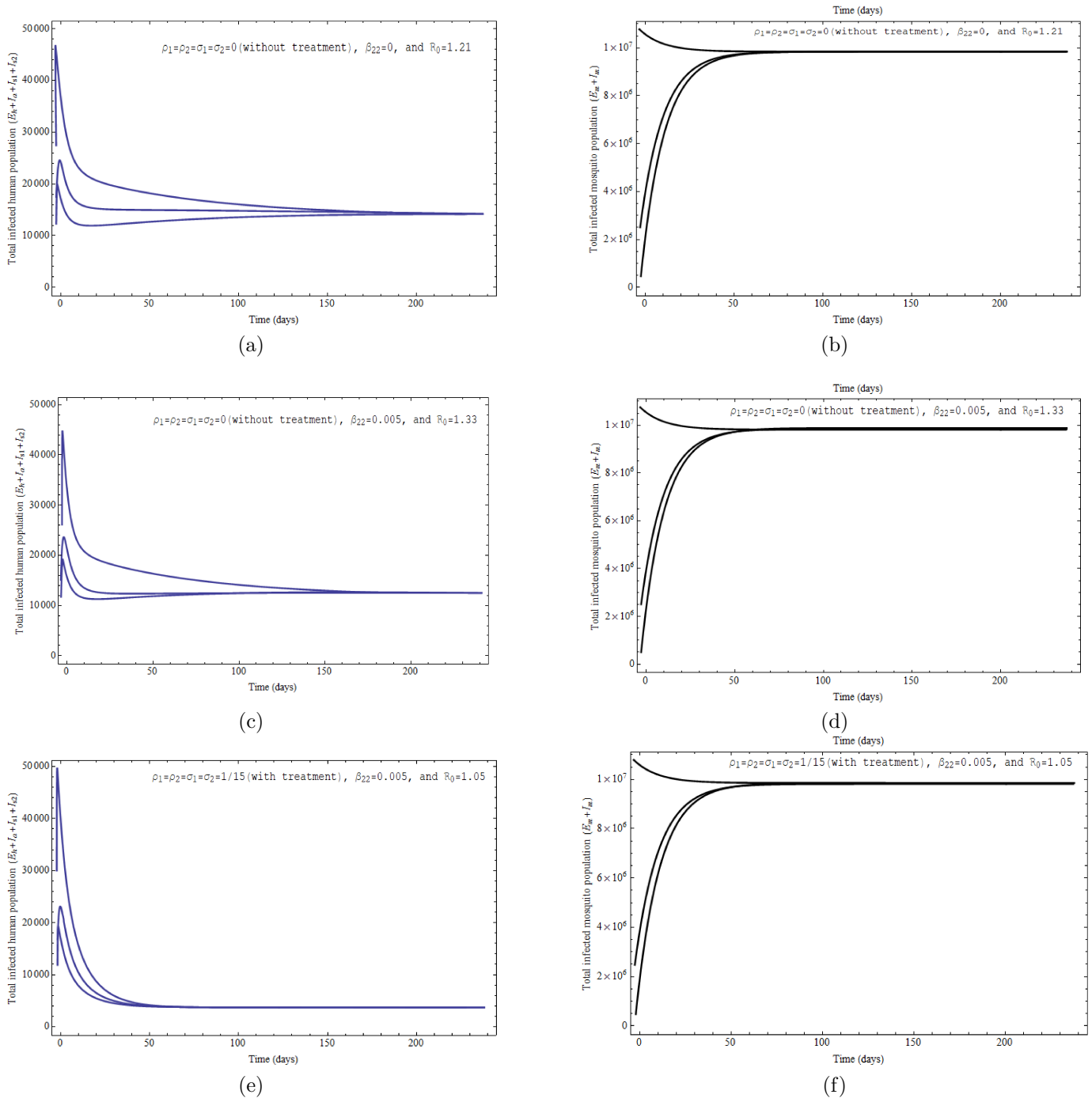

Figure 3.2: Simulations of the model (2.6) showing the total number of infected human population ($E_h + I_a + I_{s1} + I_{s2}$) as a function of time when $\Re_0 > 1$, using various initial conditions. Parameter values used as given in Table 4.2 with $\pi_1 = 332.5; \pi_2 = 75500; b_m = 0.6; p = 0.15; \beta_{12} = 0.35;$ (a) $\beta_{22} = 0$, without treatment, and $\Re_0 = 1.21;$ (c) $\beta_{22} = 0.005$, without treatment, and $\Re_0 = 1.33;$ (e) $\beta_{22} = 0.005$, with treatment, and $\Re_0 = 1.05$. And (b), (d), (f) depict the corresponding total number infected mosquito population ($E_m + I_m$).

4 Numerical simulations

Simulations of the model (2.6) presented in Figure 3.1 and Figure 3.2 show that the DFE and EE are stable for different parameter values with the threshold quantity $\Re_0 < 1$ and when $\Re_0 > 1$ respectively. Therefore, if the disease burden reduces $\Re_0$ to less one then the infected population will be eliminated and in contrast, when $\Re_0 > 1$ the disease will persist in the population. So, some measure should be taken to alleviate or eliminate the disease. Now, we investigate the effect of treatment of different population class and also analyse the sensitivity of the decease burden to the various parameters in the following two subsections.

4.1 Efficacy of treatment

Medicine of chikungunya is not available commercially. An experimental vaccine in an early stage of clinical trial. But we are interested to analyze effectiveness of treatment of the infected individuals by determining the impact of treatments on the threshold number $\Re_0$. Figure 4.1 depicts the profile of $\Re_0$ as a function of treatment rates ρ_1, ρ_2, σ_1, and σ_2. When $\beta_{22} = 0$, Figure 4.1(a) shows that the treatment of symptomatically infected individuals and asymptomatically infected individuals reduces the quantity $\Re_0$ to less than unity but the treatment in class I_{s1} is more effective and that of has no impact to infected individuals in sub acute phase. If the infected individuals at subacute phase are considered as infectious, Figure 4.1(b) reveals that the treatment of individuals in this class has a significant impact to reduce the disease burden.

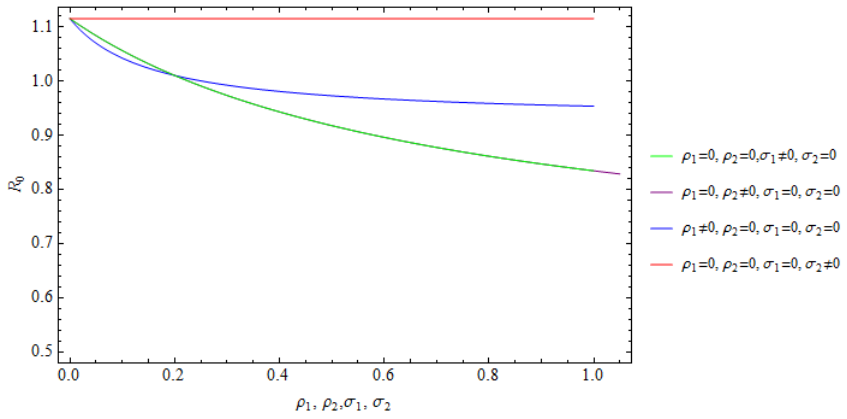

(a)

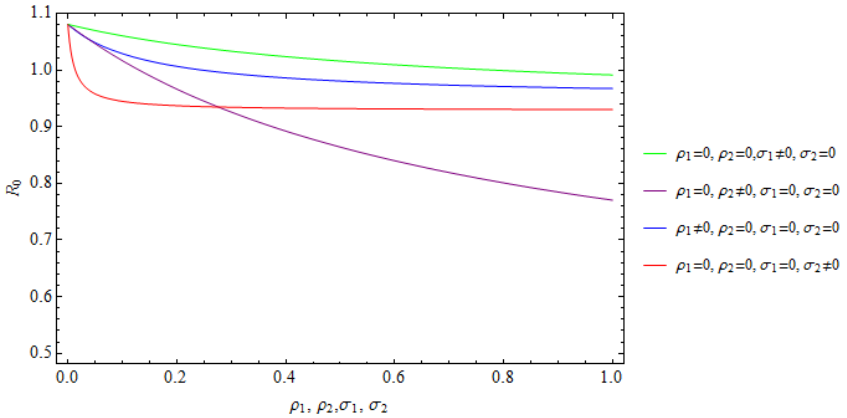

(b)

Figure 4.1: Reproduction number $\Re_0$ as a function of treatment rates ρ_1 or ρ_2 or σ_1 or σ_2. Parameter values used as given in Table 4.2 with (a) $\pi_1 = 2.2, \pi_2 = 15000, \beta_{22} = 0$, and (b) $\pi_1 = 1.8, \pi_2 = 8500, \beta_{22} = 0.005$.

4.2 Sensitivity Analysis

Sensitivity analysis is performed on the parameters of a model to determine which of the parameters play vital role in the dynamics of the model [36]. We calculate the sensitivity indices of the basic reproduction number ($\Re_0$) to the parameters in the model (2.6), to determine which of the parameter have high impact on $\Re_0$, and consequently to the disease transmission. We follow the approach as in [37]. The normalized sensitivity indices of $\Re_0$ on parameter P_i is given by

$$I_{P_i}^{\Re_0} = \frac{\partial \Re_0}{\partial P_i}\frac{P_i}{\Re_0}.$$

Sensitivity indices of $\Re_0$ are calculated at the parameter values as in Table 4.2 and the results are presented in Table 4.1, where second column corresponds to the case when $\rho_1 = 0, \rho_2 = 0, \sigma_1 = 0, \sigma_2 = 0$, and the third column for $\rho_1 = 1/15, \rho_2 = 1/15, \sigma_1 = 1/15, \sigma_2 = 1/15$.
In general, when one of the parameters with positive sign increases (or decreases) while the other parameters are constant, the value of $\Re_0$ increases (or decreases). For example, increasing β_1 by 10% increases $0.5 \times 10\%$ of $\Re_0$. Table 4.1 shows that the most important cruicial parameters are mosquito mortality rate (μ_2), mosquito biting rate (b_m). Other important parameters are disease transmission probability rate from infectious mosquito to susceptible human (β_1), human recruitment rate (π_1), mosquito recruitment rate (π_2), human mortality rate (μ_1), disease transmission probability rate from infectious human to susceptible mosquito (β_{12}) and (β_{22}), and recovery rates (γ_2, γ_1 and r_2).

Table 4.1: Sensitivity indices of $\Re_0$ to parameters for the model (2.6), evaluated at the parameter values given in Table 4.2.

Parameter	Sensitivity Indices without Treatment ($\rho_1 = \rho_2 = \sigma_1 = \sigma_2 = 0$)	Sensitivity Indices with Treatment ($\rho_1 = \rho_2 = \sigma_1 = \sigma_2 = 1/15$)
π_1	-0.5	-0.5
π_2	0.5	0.5
μ_1	0.49942	0.49988
μ_2	-1.06667	-1.06667
b_m	1.00002	1.00002
p	0.0706	0.08623
η_1	0.00006	0.00006
η_2	0.06667	0.06667
β_1	0.5	0.5
β_{12}	0.36905	0.46907
β_{22}	0.13095	0.03093
γ_1	-0.11351	-0.08699
γ_2	-0.19322	-0.150963
r_1	-0.06227	-0.12589
r_2	-0.13049	-0.00442
ρ_1	...	-0.04059
ρ_2	...	-0.03522
σ_1	...	-0.02937
σ_2	...	-0.02649

5 Conclusion

In this research, a new deterministic model for the dynamics of chikungunya virus transmission is formulated and analyzed rigorously. It has been shown that the model is mathematically and epidemiologically well-posed and it has a locally-asymptotically stable disease free equilibrium (DFE) when the basic reproduction number $\Re_0$, which is derived by next generation matrix method, is less than unity. The DFE is also globally-asymptotically stable, which is established by Lyapunov function and LaSalle Invariance Principle whenever $\Re_0 < 1$. Also, when $\Re_0 > 1$, there exists a unique endemic equilibrium (EE) of the model. Local stability of the EE is shown by sublinearity trick when $\Re_0 > 1$ and the global stability of EE is proved by using nonlinear Lyapunov function and LaSalle Invariance Principle for a special case whenever the threshold, $\Re_0$ is greater

Table 4.2: Value of the parameters of the model (2.6) for simulation. Most of the parameter values are obtained from entomologists researches on *Aedes sp.* and chikungunya.

Parameters	Base Line Value	Range	Reference
π_1	1.2	$Variable$	—
π_2	1800	$Variable$	—
$1/\mu_1$	70×365		[43]
$1/\mu_2$	13	$[7, 42]$	[9, 38]
b_m	0.4	$[0.1, 1]$	[9, 38]
β_1	0.35	$[0.001, 0.8]$	[9, 38, 6]
β_{12}	0.35	$[0.005, 0.9]$	[9, 38, 6]
β_{22}	0.005		[6]
$1/\eta_1$	3	$[1, 12]$	[9, 10]
$1/\eta_2$	2	$[2, 4]$	[5]
$1/\gamma_1$	7	$[3, 7]$	[41]
$1/\gamma_2$	0.5×7	$0.5/\gamma_1$	[10]
$1/r_1$	0.5×7	$0.5/\gamma_1$	[10]
$1/r_2$	90	$[14, 280]$	[10]
$\rho_1, \rho_2, \sigma_1, \sigma_2$	1/15		[19]
p	0.1	$[0.03, 0.28]$	[39]

than unity. Numerical simulations of the model for different parameter values and initial conditions verify these mathematical analysis for both the cases $\Re_0 < 1$ and $\Re_0 > 1$. Further, simulation of the model has been suggested that the treatment of symptomatically infected individuals and asymptomatically infected individuals can reduce the disease burden but the treatment of infected individuals in acute phase is more effective and that of has no impact of infected individuals in sub acute phase when they are not infectious. Also the sensitivity analysis has been revealed that the most effective parameters are mosquito mortality rate and average biting rate . So, the reduction of average life spans of mosquito and prevention against the effective contact with infectious mosquitoes would be effective control strategy. So, during the outbreak of the disease, insects repellents can be used to prevent the mosquito bites. Also the mosquito bed nets, which are available in market, can protect from mosquito biting. Transmission probability rates are also important parameters, reducing the value of these parameters can curtail the disease burden. Human and mosquito recruitment rates have great significance on controlling the disease so destruction of breeding sites of mosquito may be better prevention to the disease.

References

[1] World Health Organization: Chikungunya, (2017). [http://www.who.int/mediacentre/factsheets/fs327/en/]

[2] Lumsden, W. H. R., An epidemic of virus disease in Southern province, Tanganyika territory in 1952–1953, II General description and epidemiology, Transactions of the Royal Society of Tropical Medicine and Hygiene 49(1): 23 (1955).

[3] Centers for Disease Control and Prevention: Chikungunya Virus, (2017).

[4] Novak, R., The asian tiger mosquito, Aedes albopictus, Wing Beats, 3 (5): 1 (1992).

[5] Dumont, Y. and Chiroleu, F., Vector control for the Chikungunya disease, Mathematical Biosciences and Engineering, 7 (2): 313–345 (2010).

[6] Massad, E., Ma, S., Burattini, M. N., Tun, Y., Coutinho, F. A. B. and Ang, L. W., The risk of chikungunya fever in a dengue-endemic area, Journal of Travel Medicine, 15 (3): 147–155 (2008).

[7] Ruiz-Moreno, D., Vargas I. S., Olson, K. E., Harrington, L. C., Modeling Dynamic Introduction of Chikungunya Virus in the United States, PLoS Negl Trop Dis, 6(11): e1918 (2012).

[8] Moulay, D., Aziz-Alaoui, M. A., Cadivel, M., The chikungunya disease: Modeling, vector and transmission global dynamics, Mathematical Biosciences, 229: 50–63 (2011).

[9] Dumont, Y., Chiroleu, F. and Domerg, C., On a temporal model for the Chikungunya disease: modeling, theory and numerics, Mathematical Biosciences, 213 (1): 80–91 (2008).

[10] Pineda, C., Muñoz-Louis, R., Caballero-Uribe, C.V. and Viasus, D., Chikungunya in the region of the Americas. A challenge for rheumatologists and health care systems, Clin Rheumatol 35: 2381–2385 (2016).

[11] powers, A. M. and Logue, C. H., Changing patterns of chikungunya virus: re-emergence of a zoonotic arbovirus, J. Gen. Virol, 88 (9): 2363–77 (2007).

[12] Thiberville, S. D., Moyen, N., Dupuis-Maguiraga, L., Nougairede, A., Gould, E. A., Roques, P. and de LamballerieS, X., Chikungunya fever: Epidemiology, clinical syndrome, pathogenesis and therapy, Antiviral Research, 99 (3): 345–370 (2013).

[13] Burt, F. J., Rolph, M. S., Rulli, N. E., Mahaligam, S. and Heise, M. T., Chikungunya: a re-emerging virus, The Lancet, 379 (9816): 662–671 (2012).

[14] Schilte, C., Staikowsky, F., Couderc, T., Madec, Y., Carpentier, F., Kassab,... Michault, A., Chikungunya virus-associated long-term arthralgia: a 36-month prospective longitudinal study, PLoS neglected tropical diseases, 7 (3): e2137 (2013).

[15] Moro, M. L., Grilli, E., Corvetta, A., Silvi, G., Angelini, R., Mascella, F.,... Macini, P., Long-term chikungunya infection clinical manifestations after an outbreak in Italy: a prognostic cohort study, The Journal of infection, 65 (2): 165–72 (2012).

[16] Ozden, S., Huerre, M., Riviere, J. P., Coffey, L. L., Afonso, P. V., Mouly, V.,... Ceccaldi, P. E., Human muscle satellite cells as targets of Chikungunya virus infection, PLoS ONE, 2 (6): e527 (2007).

[17] Hoarau, J. J., Jaffar-Bandjee, M. C., Krejbich Trotot P., Das, T., Li-Pat-Yuen, G., Dassa, B.,... Gasque, P., Persistent chronic inflammation and infection by Chikungunya arthritogenic alphavirus in spite of a robust host immune response, Journal of Immunology, 184 (10): 5914–27 (2010).

[18] Caglioti, C., Lalle, F., Castilletti, C., Carletti, F., Capobianchi, M. R., Bordi, L., Chikungunya virus infection: an overview, The new microbiologica 36 (3): 211–27 (2013).

[19] Chang, L., Dowd, K. A., Mendoza, F. H., Saunders, J. G., Sitar, S., Plummer, S. H.,... VRC 311 Study Team, Safety and tolerability of chikungunya virus-like particle vaccine in healthy adults: a phase 1 dose-escalation trial, The Lancet 384 (9959): 2046–2052 (2014).

[20] Pastorino, B., Muyembe-Tamfum, J. J., Bessaud, M., Tock, F., Tolou, H. and Durand, J. P., Epidemic resurgence of chikungunya virus in Democratic Republic of the Congo: identification of a new central African strain, J Med Virol. 74: 277–82 (2004).

[21] Leo, Y. S., Chow, A. L., Tan, L. K., Lye, D. C., Lin, L., Ng, L. C., Chikungunya outbreak, Singapore, 2008, Emerg Infect Dis. 15: 836–7 (2009).

[22] Muniaraj, M., Fading chikungunya fever from India: beginning of the end of another episode?, Indian J. Med. Res. 139 (3): 468–70 (2014).

[23] Siddique, A. B., Sam, I. C., Wong, P. R., Math Rahim, N. Z., Hooi, P.S. and Roslan, N., Reemergence of endemic chikungunya, Malaysia, Emerg Infect Dis. 13: 147–9 (2007).

[24] Mackenzie, J. S., Chua, K. B., Daniels, P. W., Eaton, B. T., Field, H. E., Hall, R. A., ... Williamsm, D. T., Emerging viral diseases of Southeast Asia and the Western Pacific, Emerg. Infect. Dis. 7: 497 (2001).

[25] Rezza, G., Nicoletti, L., Angelini, R., Romi, R., Finarelli, A. C., Panning, M.,... CHIKV study group, Infection with chikungunya virus in Italy: an outbreak in a temperate region. Lancet 307: 1840–1846 (2007).

[26] Renault, P., Balleydier, E., D'Ortenzio, E., Baville, M., Filleul, L., Epidemiology of chikungunya infection on Reunion Island, Mayotte, and neighboring countries, Med Mal Infect. 42: 93–101 (2012).

[27] Pan-American Health Organization (PAHO): Number of cumulative cases 2013–2014. [www.paho.org]

[28] icddr,b, First identified outbreak of chikungunya in Bangladesh, Health Sci Bull 7(1) (2008).

[29] Diekman, O., Heesterbeck, J. A. P., Mathematical epidemiology of infectious diseases Wiley Series in Mathematical and Computational Biology, Wiley, New York (2000).

[30] Hethcote, H. W., The mathematics of infectious diseases, SIAM Rev. 42: 599 (2000).

[31] Yakob, L., Clements, A. C. A., A Mathematical Model of Chikungynya Dynamics and Control: The major Epidemic on Re'union Island. PLoS ONE 8 (3): e57448 (2013).

[32] Agusto, F. B., Easley, S., Freeman, K., Thomas, M., Mathematical Model of Three Age-Structured Transmission Dynamics of Chikungunya Virus, Computational and Mathematical Methods in Medicine 2016, e4320514 (2016).

[33] Báez-Hernández, N., Casas-Martínez, M., Danis-Lozano, R., Velasco-Hernández, J. X., A mathematical model for Dengue and Chikungunya in Mexico, Creative Commons (2017).

[34] Dommar, C. J., Lowe, R., Robinson, M., Rodó, X., An agent-based model driven by tropical rainfall to understand the spatio-temporal heterogeneity of a chikungunya outbreak, Acta Tropica 129: 61–73 (2014).

[35] Wilson, E. B., Worcester, J., The law of mass action in epidemiology, Proc. Natl. Acad. Sci. U. S. A. 31(1):24–31 (1945).

[36] Alam, M. S., Kamrujjaman, M., Islam, M. S., Parameter sensitivity and qualitative analysis of dynamics of ovarian tumor growth model with treatment strategy, Journal Of Applied Mathematics And Physics, 8(6): 941-955 (2020).

[37] Chitnis, N., Hyman, J. M., Cushing, J. M., Determining Important Parameters in the Spread of Malaria Through the Sensitivity Analysis of a Mathematical Model, Bull. Math. Biol. 127 (70): 1272–1296 (2008) .

[38] Manore, C. A., Hickmann, K. S., Xu, S., Wearing, H. J., Hyman, J. M., Comparing dengue and chikungunya emergence and endemic transmission in A. aegypti and A. albopictus, Journal of Theoretical Biology 356 (7): 174–191 (2014).

[39] Staples, J. E., Hills, S. L., Powers, A. M., Chikungunya, Centers for Disease Control and Prevention (CDC) (2014).

[40] Sharomi, O., Podder, C. N., Gumel, A. B., Elbasha, E. H., Watmough, J., Role of incidence function in vaccine-induced backward bifurcation in some HIV models, Mathematical Biosciences 210 (2): 436-463 (2007).

[41] Lahariya, C., Pradhan, S. K., Emergence of chikungunya virus in Indian subcontinent after 32 years: a review, Journal of Vector Borne Diseases 43(4): 151–160 (2006).

[42] Hethcote, H. W., Thieme, H. R., Stability of the endemic equilibrium in epidemic models with subpopulations, Math. Biosci. 75: 205 (1985).

[43] Chitnis, N., Hyman, J. M., Cushing, J. M., Determining important parameters in the spread of malaria through the sensitivity analysis of a mathematical model, Bulletin of Mathematical Biology 70 (5): 1272–1296 (2008).

[44] Lakshmikantham, V., Leela, S., Martynyuk, A. A., Stability Analysis of Nonlinear Systems, Marcel Dekker, New York, USA (1989).

[45] Sharomi, O., Podder, C. N., Gumel, A., Song, B., Mathematical analysis of the transmission dynamics of HIV/TB coinfection in the presence of treatment, Mathematical Biosciences and Engineering 5 (1): 145 (2008).

[46] Kamrujjaman, M., Shahriar Mahmud, M., Islam, M. S. Dynamics of a diffusive vaccination model with therapeutic impact and non-linear incidence in epidemiology, Journal of Biological Dynamics, 1-29 (2020).

[47] LaSalle, J. P., The stability of dynamical system, Regional Conference Series in Applied Mathematics, SIAM, Philadelphia (1976).

[48] Thieme, H. R. Capasso, V., Grosso, E., Paveri-Fontana (Eds.), S. L., Local Stability in Epidemic Models for Heterogenous Populations, Lecture Notes in Biomathematics, Springer 57: 185-189 (1985).

[49] Driessche, P. V. D., Watmough, J., Reproduction numbers and sub threshold endemic equilibria for compartmental models of disease transmission, Mathematical Biosciences 180: 29–48 (2002).

GANIT

Available online at https://ganitjournal.bdmathsociety.org/

GANIT: Journal of Bangladesh Mathematical Society

GANIT *J. Bangladesh Math. Soc.* 41.1 (2021) 62–77
DOI: https://doi.org/10.3329/ganit.v41i1.55027

Arterial pharmacokinetics in a patient-specific atherosclerotic artery-a simulation study

Sayantan Biswas[a], Sarifuddin[b], and Prashanta Kumar Mandal *[c]

[a,c] *Department of Mathematics, Visva Bharati University, Santiniketan-731 235, West Bengal, India*
[b] *Department of Mathematics, Berhampore College, Berhampore-742 101, West Bengal, India*

ABSTRACT

Of concern in the paper is a numerical study of endovascular drug delivery in a patient-specific atherosclerotic artery through a mathematical model in which the luminal flow is governed by an incompressible viscous Newtonian fluid, and the transport of luminal as well as tissue concentration is modeled as an unsteady convection-diffusion process. An image processing technique has been successfully adopted to detect the edges of the computational domain extracted from an asymmetric (about the centerline of the artery) patient-specific atherosclerotic artery. Considering each pixel as a control volume, the Marker and Cell (MAC) method has been leveraged to get a quantitative insight of the model considered by exploiting physiologically realistic initial, boundary as well as interface conditions. Simulated results reveal that the number as well as the length of separation zone does increase with increasing Re, and the near-wall velocity contour might be important for estimating the near-wall residence time for the pool of drug molecules available for tissue uptake. Results also show that the more the tissue porosity and interface roughness do not necessarily imply the more the effectiveness of delivery, even though they enhance the averaged concentration in the tissue domains, and also the area under concentration diminishes with increasing Peclet number. Thus, the tissue porosity, the Peclet number and various geometrical shapes (interface roughness) play a pivotal role in the dispersion and the effectiveness of drug delivery.

Received: June 21, 2021 **Accepted:** July 20, 2021 **Published Online:** August 04, 2021

Keywords: Patient-specific asymmetric atherosclerotic artery; Endovascular delivery; Image processing; Marker and Cell Method; Flow separation; Tissue content
AMS Subject Classifications 2020: 35Q35, 92B05, 92C45.

1 Introduction

Constriction in an artery occurs due to the accumulation of low-density lipoprotein (LDL) and other macromolecules and/or the proliferation of smooth muscle cells (SMCs) present in *tunica media* along the inner lining of the arterial wall. The formation of such constriction or plaque (stenosis) starts blocking the artery and reduces the normal flow of blood, medically termed as 'atherosclerosis'[1]. The study of disturbances arising out of atherosclerotic flow together with its control is a much-researched topic for the last few decades, however,

*Corresponding author. *E-mail address:* prashantakumar.mandal@visva-bharati.ac.in

the convection as well as diffusion-driven transport of drug in a patient-specific atherosclerotic artery has been paid less attention, perhaps due to its inherent complexity in the geometry. During intravenous delivery into an atherosclerotic artery, clinicians are interested to analyze how the luminal drug is dispersed with the flowing blood and its subsequent uptake into the arterial tissue, and also the tissue content for the better efficacy of the delivery.

A large volume of work on the transport of luminal concentration (solute) in the presence of an absorbing wall (lumen-wall interface) has already been carried out, both theoretically and/or numerically, in various domains of interest [2, 3, 4, 5, 6, 7, 8, 9]. Taylor [2] and Aris [3] studied the solute dispersion in steady flow through a circular tube. Gill and Sankarasubramanian [4] carried out the exact analysis of an unsteady convection-diffusion process. In their study, a fully developed steady laminar flow and the dispersion of an injected solute in each time without interphase mass transfer across boundaries were analyzed. A more rigorous generalization was derived by taking the key attributes of solute transfer in the presence of an absorbing boundary [5]. The effect of wall absorption on shear dispersion in plane and pipe flows was successfully studied by Smith [6]. Purnama [7] considered the dispersion of solute between a moving region and adjoining immobile medium. Dash et al. [8] explored the effect of yield stress on solute dispersion in Casson fluid flow. The study of Sarkar and Jayaraman [9], taking annular and axisymmetric oscillatory flow consecutively into account, was based on irreversible boundary reaction on the dispersion of solute. **Nagarani et al. [10]** analyzed the dispersion process in a tube in the presence of a catheter. The investigation on the mass transport contemplated a steady Poiseuille flow through a circular tube considering reversible and irreversible reactive boundary condition [11]. In the presence of reversible and irreversible wall reaction in an annular tube with an oscillatory flow, Mazumder and Paul [12] analyzed the longitudinal dispersion following Aris's method of moments. Rana and Murthy [13, 14] analytically determined the transport coefficients with the help of Gill's generalized dispersion model and discussed the effect of yield stress, wall reaction, Womersley parameter and flow pulsatility on the dispersion of solute in a tube and in two-phase flow respectively. Three layers of fluid having non-Newtonian Casson model in the middle layer were considered to investigate the effect of yield stress, the thickness of the layer and wall reaction on solute transport using the Aris-Barton method of moments by Debnath et al. [15].

In all the studies cited above, studies on the solute transport were restricted only in the luminal region. It is surprising to know that the transport of solute in the lumen as well as in the tissue is not well documented so far. Few studies have considered the transport of solute followed by its absorption at the lumen-tissue interface in an idealized (non-realistic and smooth having no surface roughness) wall [16, 17]. In a theoretical study, Griffiths et al.[16] made an attempt to optimize the mass transport in a thin porous tube. Since the therapeutic domain is an atherosclerotic artery, Das et al. [17] successfully simulated the dispersion of solute in an idealized stenotic artery. They showed that the dispersion of solute in the lumen and the tissue is directly related to the yield stress, the wall absorption parameter and the severity of the stenosis. It is well established that the uptake of solute from the luminal side depends on the near-wall velocity gradient. Some studies showed the alteration of flow characteristics in presence of surface irregularities by disregarding the solute transport in the tissue [18, 19, 20, 21, 22, 23, 24]. These studies, though less flexible, are still of relevance to establish the effects of roughness on solute transport. Studies related to drug delivery in various geometries have been successfully carried out in the recent past [25, 26, 27].

Relatively very little is known about the drug transport in the vicinity of a realistic atherosclerotic artery. An issue of central interest in the present study is the consideration of irregular lumen-tissue interfaces which promote multi-directional drug uptake from the luminal side as opposed to the smooth interface. In this work, a longitudinal image of an asymmetric patient-specific atherosclerotic arterial segment obtained from intravascular ultrasound (IVUS) is taken into consideration [28]. An image processing technique was successfully applied to obtain the outlines of the computational domain [29]. For a quantitative insight of this coupled fluid-drug transport model considering the continuity of flux and concentration as the lumen-tissue interface, the well-known Marker and Cell method is leveraged [30] where each pixel of the longitudinal image is considered as a control volume. It may be recorded that this asymmetric geometry consisting varying irregularities at the upper and lower interfaces contributes much to the varying uptake of drug therein. Our study differs considerably from the studies cited above by taking additional consideration of an unsteady drug transport in tissue domains having varying lumen-tissue interface roughness in the upper and lower domains. The transport of drug molecules with the streaming blood in the lumen after injected at the luminal inlet and its subsequent uptake at the irregular lumen-tissue interface followed by diffusion in the tissue is relevant in the study of arterial pharmacokinetics. The objective of the present computational study is to investigate the convective and diffusive transport of drug in an irregular asymmetric patient-specific atherosclerotic artery and to estimate various physiological factors like velocity, wall shear stress, pressure drop, streamlines, concentration in their respective irregular domains as

well as the effectiveness of delivery. The novelty of the present study lies in the inclusion of a patient-specific asymmetric atherosclerotic artery with varying irregularities at the lumen-tissue interfaces and the dispersion of the drug molecules in the lumen and tissue in general, and the choice of solute administration at the luminal inlet for three different geometrical models which more closely resembles the physiological situation relevant to intravenous drug delivery. The possible implications of the results are discussed.

2 Formulation of the Problem

2.1 Geometry Reconstruction

The three different models of an atherosclerotic vessel shown in Fig. 1 (a-c) have been examined. The 'Original' shape considered here is the patient-specific asymmetric model (Fig 1(c)) [28]. The 'Toy' model considered is a much simpler smooth version of the original shape (Fig. 1(a)). Finally, by gradually adding interface roughness to the toy model, a new stenosis model, termed as 'Smooth' model, is obtained which exhibits the same general form as the original model with few surface roughness elements are present (Fig. 1(b)). The computational domain for the original model was constructed from a single, patient-specific asymmetric arterial vessel obtained from König and Klauss [28]. In this case, intravascular ultrasound (IVUS) imaging was performed to obtain a longitudinal cross-section of the vessel followed by virtual histology on the derived image to identify the outlines of the computational domain. An image segmentation technique was leveraged to automatically identify different outlines of the image [29]. IVUS is a tomographic imaging tool that allows visualization of atherosclerosis, its length and area, plaque compositions and coronary remodeling. The motivation of selecting this image is simply due to its availability and it allows us to define boundary and interface conditions straightforwardly. **We limited our formulation in a two-dimensional geometry of an asymmetric patient-specific atherosclerotic artery due to its availability in the literature [28].**

2.2 Governing Equations

Although blood, being a suspension of enumerable corpuscles, behaves like a non-Newtonian fluid while flowing through smaller vessels, but in larger arteries, the rheology of the streaming blood may be treated as Newtonian [31]. In our study, the luminal blood flow is treated as unsteady and two-dimensional which is characterized by Newtonian model. The dimensionless governing equations representing the trasport of momentum (eqns. 1,2) and conservation of mass (eqn. 3) for viscous incompressible fluid in Cartesian coordinates system (x, y) may be written in the conservative form as

$$\frac{\partial u}{\partial t} + \frac{\partial (\mathbf{uv})}{\partial y} + \frac{\partial u^2}{\partial x} = -\frac{1}{\rho}\frac{\partial p}{\partial x} - \frac{1}{Re}\left(\frac{\partial^2 u}{\partial x^2} + \frac{\partial^2 u}{\partial y^2}\right), \tag{2.1}$$

$$\frac{\partial v}{\partial t} + \frac{\partial v^2}{\partial y} + \frac{\partial (\mathbf{uv})}{\partial x} = -\frac{1}{\rho}\frac{\partial p}{\partial y} - \frac{1}{Re}\left(\frac{\partial^2 v}{\partial x^2} + \frac{\partial^2 v}{\partial y^2}\right), \tag{2.2}$$

$$\frac{\partial u}{\partial x} + \frac{\partial v}{\partial y} = 0, \tag{2.3}$$

where x and y are the dimensionless coordinates, scaled with respect to the proximal diameter d of the artery with the x axis placed along the centreline of the asymmetric artery, u and v are the axial and the transverse components of dimensionless velocity scaled with the centreline velocity U_0 respectively. Here, ρ represents the density of flowing blood and μ, the viscosity coefficient. The dimensionless time (t), the pressure (p) may be defined as

$$t = \frac{U_0 t^*}{d}, p = \frac{p^* d}{\mu U_0}.$$

Here, $Re(= \frac{\rho U_o d}{\mu})$ stands for the Reynolds number.

The respective convection-diffusion equations representing the transport of drug in the domains considered, namely, the lumen, the upper tissue and the lower tissue, may be written in dimensionless forms as

$$\frac{\partial c_l}{\partial t} + u\frac{\partial c_l}{\partial x} + v\frac{\partial c_l}{\partial y} = \frac{1}{Pe_l}\left(\frac{\partial^2 c_l}{\partial x^2} + \frac{\partial^2 c_l}{\partial y^2}\right), \tag{2.4}$$

$$\frac{\partial c_{tu}}{\partial t} + V_{filt}\frac{\partial c_{tu}}{\partial y} + = \frac{1}{Pe_{tu}}\left(\frac{\partial^2 c_{tu}}{\partial x^2} + \frac{\partial^2 c_{tu}}{\partial y^2}\right), \tag{2.5}$$

$$\frac{\partial c_{tl}}{\partial t} + V_{filt}\frac{\partial c_{tl}}{\partial y} + = \frac{1}{Pe_{tl}}\left(\frac{\partial^2 c_{tl}}{\partial x^2} + \frac{\partial^2 c_{tl}}{\partial y^2}\right), \tag{2.6}$$

where the volume-averaged concentrations of free drug in the lumen(c_l), in the upper tissue(c_{tu}) and in the lower tissue(c_{tl}) are scaled with respect to the inlet concentration c_0. Here, $V_{filt}(= \frac{v_{filt}}{U_o})$ represents the dimnesionless tranmural filtration velocity in the upper and lower tissue regions and $Pe_l(= \frac{U_0 d}{D_l})$,$Pe_{tu}(= \frac{U_0 d}{D_{tu}})$, $Pe_{tl}(= \frac{U_0 d}{D_{tl}})$ stand for the Peclet number for the lumen, the upper tissue and the lower tissue respectively, with the diffusion coefficients D_l in the lumen, D_{tu} in the upper tissue, D_{tl} in the lower tissue.

2.3 Initial, Boundary and lumen-tissue Interface Conditions

An asymmetric velocity profile at the inlet(Γ_i) may be taken as

$$u = \frac{(y - R_u)(y - R_l)}{(R_m - R_u)(R_m - R_l)},\ v = 0 \ \text{ on } \ \Gamma_i, \tag{2.7}$$

where R_i $(i = u, l)$ be the proximal lumen radii (upper and lower) of the arterial segment and $R_m(= \frac{R_u + R_l}{2})$ is the mean radius at the luminal inlet.
At the downstream (Γ_o), the flow is left free which is mathematically represented by

$$\frac{\partial u}{\partial x} = 0 = \frac{\partial v}{\partial x} \text{ on } \Gamma_o. \tag{2.8}$$

At the lumen-tissue interfaces (Γ_i^u, Γ_i^l), the usual no-slip condition of velocity-vector is given by

$$u = 0 = v \ \text{ on } \Gamma_i^u, \Gamma_i^l. \tag{2.9}$$

At the proximal(Γ_p^u, Γ_p^l) and distal (Γ_d^u, Γ_d^l) boundaries of the tissue domains, the no flux conditions for free drug are as follows:

$$\frac{\partial c_{tu}}{\partial x} = 0 \text{ on } \Gamma_p^u, \Gamma_d^u, \tag{2.10}$$

$$\frac{\partial c_{tl}}{\partial x} = 0 \text{ on } \Gamma_p^l, \Gamma_d^l. \tag{2.11}$$

At the perivascular end(Γ_u, Γ_l), a perfectly sink condition may be written mathematically as [16]

$$c_{tu} = 0 \text{ on } \Gamma_u, \tag{2.12}$$

$$c_{tl} = 0 \text{ on } \Gamma_l. \tag{2.13}$$

At the lumen-tissue interfaces (Γ_i^u, Γ_i^l), the continuity of drug concentrations and fluxes are assumed whose mathematical representations are as [16]

$$c_{tu} = c_l \text{ and } \frac{\partial c_l}{\partial \mathbf{n}} = \alpha_1 \frac{\partial c_{tu}}{\partial \mathbf{n}} \text{ on } \Gamma_i^u, \tag{2.14}$$

$$c_{tl} = c_l \text{ and } \frac{\partial c_l}{\partial \mathbf{n}} = \alpha_2 \frac{\partial c_{tl}}{\partial \mathbf{n}} \text{ on } \Gamma_i^l, \tag{2.15}$$

where $\mathbf{n}$ is the transmural unit normal vector, $\alpha_1 = \phi\frac{D_{tu}}{D_l}$ and $\alpha_2 = \phi\frac{D_{tl}}{D_l}$; ϕ designates the porosity of the tissue medium. Due to nonavailability of data, equal porosity and equal diffusivity for both the tissue regions have been assumed, and hence we assume, in the sequel, $\alpha_1 = \alpha_2 = \alpha$. Initially, it is assumed that there is no drug inside the domains (lumen and tissue), except the dimensionless concentration of injected drug at the luminal inlet is constant (unity). Therefore,

$$c_l = 1 \text{ at } x = 0,\ \forall t \text{ and } c_l = c_{tu} = c_{tl} = 0, \text{ elsewhere, at } t = 0 \tag{2.16}$$

3 Method of Solution

3.1 The MAC Methodology

The governing equations along with the physiologically realistic conditions are solved numerically by a finite-difference method in staggered grids. The computational geometry is comprised of 71,876 pixels encompassing the patient-specific atherosclerotic vessel where each pixel is considered as a control volume (Fig. 2). Concerning the second order spatial accuracy of the boundary conditions, some fictitious grid points outside the domain have been taken into consideration. Here, we set $x_i = i\delta x, y_j = j\delta y$ and $t_k = k\delta t$ in which k refers to the time direction, δt, the time increment. Here, δx and δy are the dimensions of the pixels. The discretized versions of the governing equations are not given here, for the sake of brevity, however, the interested readers may be referred to [32]. The discretized equation for calculating pressure-field as obtained from the discretized momentum and continuity equations is solved by Successive-over-Relaxation(SOR) method ehere the value of over-relaxation parameter is 1.2. Using the principle of conservation of mass, we calculate the divergence of the velocity-field at each cell and check for its prescribed tolerance. If the divergence does not satisfy the tolerance limit, then the pressure and velocity components are corrected. The discretized versions of the governing equations are not given here, for the sake of brevity, however, the interested readers may be referred to [32]. The computational code has successfully been programmed in FORTRAN language.

3.2 Pressure and velocity correction

To reduce the computational cost for each cycle, we limit the number of iterations in the S.O.R scheme to 10 to get pressure-field. So the velocity-field obtained using this inaccurate pressure-field will not, in general, satisfy the continuity equation which prompts us to correct the pressure as well as velocity-field. If the cell-divergence is found to be greater than the prescribed tolerance value (10^{-8}) at any cell in an absolute sense, the pressure and, subsequently, the velocity components are immediately corrected at each cell using the formulae below:

$$p^k_{i,j} = p^*_{i,j} + \omega\delta p_{i,j},$$

where $\delta p_{i,j} = \frac{-Div^*_{i,j}}{2\delta t\left(\frac{1}{\delta x^2}+\frac{1}{\delta y^2}\right)}$, $p^*_{i,j}$ is the obtained pressure from the Poisson equation using limited iterations, $\omega(\leq 0.5)$ represents the relaxation parameter for S.O.R. scheme and $Div^*_{i,j}$ stands for derived divergence of the velocity-field at $(i,j)^{\text{th}}$ cell.

$$\begin{aligned} u^{k+1}_{i,j} &= u^*_{i,j} + \frac{\delta t\delta p_{i,j}}{\delta x}, \\ u^{k+1}_{i-1,j} &= u^*_{i-1,j} - \frac{\delta t\delta p_{i,j}}{\delta x}, \\ v^{k+1}_{i,j} &= v^*_{i,j} + \frac{\delta t\delta p_{i,j}}{\delta y}, \\ u^{k+1}_{i,j-1} &= u^*_{i,j-1} - \frac{\delta t\delta p_{i,j}}{\delta y}, \end{aligned}$$

where $u^*_{i,j}, u^*_{i-1,j}, v^*_{i,j}, v^*_{i,j-1}$ stand for the updated velocity-field.

3.3 Numerical Stability: Time-Stepping Procedure

Welch et al.[33] suggested the stability criterion by imposing restriction on time step (δt_1) involving Reynolds number as

$$\delta t_1 \leq \text{Min}\left(\frac{Re}{2}\frac{\delta x^2\delta y^2}{\delta x^2+\delta y^2}\right)_{i,j} \tag{3.1}$$

This condition for stability is related to viscous effect which can be applied directly in order to select an appropriate time step [34].

Another approach for stability criterion is that no fluid particles should cross more than one cell boundary in a given interval of time (δt_2) (Markham and Proctor [35]), which may be written mathematically as

$$\delta t_2 \leq \text{Min}\left(\frac{\delta x}{|u|}, \frac{\delta y}{|v|}\right)_{i,j} \tag{3.2}$$

Courant-Friedrichs-Lewy (CFL) stability criteria [38] based on various diffusivities of the drug and dimension of the control volume provide the time step (δt_3).

Finally, the variable time step (δt) to be applied at a given point in the calculation will be

$$\delta t = d_1 \text{Min}\left(\delta t_1, \delta t_2, \delta t_3\right), \tag{3.3}$$

where the reason for this extra factor d_1, $(0 < d_1 \leq 1)$ is to reduce the computational cost [35].

4 Numerical Results and Discussion

The computational domain is considered of non-dimensional length of 8.5 in which extra non-stenotic lengths at the upstream and downstream are added in a bid to justify the boundary conditions assumed at the proximal and distal end of the arterial segment. The computational domain is comprised of 71,876 pixels encompassing a patient-specific asymmetric atherosclerotic vessel where each pixel is considered as a control volume. Steady states have been achieved when the divergence of the velocity-field was less than 10^{-8} and a reduction of 5.0×10^{-7} in the solute transport residual. For simulation purposes, the following plausible baseline values have been made use of [4, 18, 36, 37]:
$Re = 300, Pe_l = 1000, Pe_{tu} = 10000, Pe_{tl} = 10000, \alpha = 0.1, V_{filt} = \mathcal{O}(10^{-6})$

4.1 Model Validation

Direct validation of our model with ones available in the literature is almost impossible as, to the authors' knowledge, not a single article is available in the literature which accounts for the mass and momentum transport in the domains considered, however, a sincere attempt is made in Figure 3 to qualitatively compare the variation of normalized pressure drop with Reynolds number. The pressure drop is computed across the patient-specific irregular stenosis, and one can easily verify from Fig. 3 that the obtained result does significantly differ from those of [18, 22] who studied the model in cylindrical coordinates system with different plaque geometry, but a similar trend is observed that the predicted pressure drop decreases with increasing Reynolds number. The distinction among these findings is certainly due to the length, the severity and the different irregularities of atherosclerotic plaque considered herein.

4.2 Velocity Contour, Wall Shear Stress and Streamlines

The effect of Reynolds number on the vorticity contours of the flow characteristics in an asymmetric patient-specific atherosclerotic vessel can be recorded from the results of Figure 4. The velocity profiles at the throats are significantly distorted as shown in these patterns. These distortions span downstream with increasing Re. The velocity contours have some interesting features to note that the magnitude of the velocity in the vicinity of the plaque is negative indicating the existence of flow separation regions at those sites and the area of the regions having negative velocity does increase with increasing Re. The correct prediction of the near-wall velocity contour might be important for estimating near-wall residence time for the pool of drug molecules available for tissue uptake. Thus the flow velocity (specifically near the wall) contributes much to the uptake of drug from the luminal side.

The wall shear stress plays a significant role in the genesis and progression of atherosclerosis. The variations of the wall shear stress along the asymmetric as well as irregular vessel for the upper and lower walls for different Re are portrayed in Figure 5(a-b) respectively. The multiple peak values of the wall shear stress occur at the multiple throats of the stenosis and the maximum value is noted where the arterial narrowing is maximum, and also, this peak value increases with increasing Re. It may also be noted that the number, as well as the length of recirculation/ separation region, do increase with increasing Re which may have a pivotal role for the aggravation of the disease (cf. Figs. 6). It is also interesting to note that the number as well as the length of separation zone increases in the upper wall as compared to the lower wall due to more interface irregularities present in the upper interface. Hence, proper importance should be given to the interface irregularities in the context of the atherosclerotic lesion. The elevated wall shear stress is responsible for endothelial damage and activates cellular proliferation mechanism too, and the complex separation regions are responsible for the aggregation sites of macromolecules as opined by Asakura and Karino [39]. The results of Figure 6(a-c) showing patterns of streamlines for an irregular atherosclerotic plaque for different Re clearly indicate that the streamlines are less perturbed for $Re = 100$, however, with an increase of Re, the formation of several complex recirculation regions

is observed due to an increase fluid inertia which is responsible for the establishment of an adverse pressure gradient. This adverse pressure gradient does reverse the flow. The figure also highlights that the streamlines at the lower wall are less perturbed as compared to the upper wall for a particular Re which is due to less surface roughness present in the lower wall. This, however, at least describes quantitatively what happens for flows in blood vessels when the inertia is important. Thus, based on the patterns of the streamlines, one may conclude that the irregularity of the inner lining of the vessel wall affects the streamlines significantly and hence proper importance should be given to the irregular stenosis model in the context of atherosclerotic lesion.

4.3 Effect of diffusivity (Peclet number), tissue porosity (α) and interface roughness on drug dispersion

Figure 7(a-c) exhibits the distributions of local drug concentrations in the axial direction of the atherosclerotic artery at three distinct transluminal positions, namely, $y = 0.2$ for lumen, $y = 1.15$ for upper tissue and $y = -1.15$ for lower tissue, while Figure 8(a-c) displays the spatiotemporal patterns of drug concentration for the whole domain (lumen as well as tissue). Figure 7a shows that the value of the luminal concentration for different luminal Peclet numbers (Pe_l) starts from one due to all-time constant value ($c_l = 1$, eq. 2.16) at the inlet, and thereafter increases followed by a gradual decline at the downstream. Figures 7(b-c) gives an idea on how the local concentration is perturbed for different tissue Peclet numbers (Pe_{tu}, Pe_{tl}). This figure establishes the fact that the drug concentration reduces significantly with the increasing Peclet number. One interesting feature may be noted that the concentration profiles reveal asymmetric distribution between regions distal and proximal to the plaque due to the convective nature of drug transport as well as varying thickness and roughness of the domains. Simulations predicted that recirculation regions create pockets of stagnant drug-laden blood that allow more drug accumulation at lumen-tissue interfaces, and eventually more uptake of drug from the luminal side into the arterial tissue [32]. All these findings are in conformity with the spatiotemporal patterns of drug concentration as depicted in Figure 8(a-c). Here too, the concentration of drug diminishes, more specifically, the area under concentration (AUC) diminishes with increasing Peclet number, and the penetration of drug into the tissue domains is more from the sites of recirculation regions and the more the thickness of the domains, the less the concentration at a particular instant of time.

Temporal variations of averaged concentration of drug for different values of Peclet number and tissue porosity for the upper and lower tissue regions are sketched in Figure 9(a-b) respectively. It is found that the averaged concentration increases from zero, thereafter reaches a steady state with the advancement of time. It is worthwhile to note that the averaged tissue concentration reaches its quasi-steady state more quickly for lesser Peclet number (i.e. for higher diffusivity). As anticipated, the averaged concentration decreases with the increase of Peclet number. Moreover, as the porosity in the tissue α $(= \phi \frac{D_{tu}}{D_l} = \phi \frac{D_{tl}}{D_l})$ increases from 0.05 to 0.1, the averaged concentration of drug in both the tissue domains increases which may be justified in the sense that with the increase of porosity in the tissue, the diffusive flux of luminal concentration into the tissue domain increases, which in turn, diminishes the luminal concentration (cf. Fig. 11(a-c)) and enhances the averaged concentration in the arterial tissue. The averaged concentrations of drug for three different geometrical models (Toy model having no interface roughness, smooth model having few interface roughness and original model having much roughness; cf. Sec. 2.1, Fig. 1(a-c)) for the upper and lower tissue regions are depicted in Figure 10(a-b). The three models differ from each other in terms of interface roughness, and eventually, the length of the interface of the domains changes as the more the roughness present at the interface, the more the lumen-tissue interface length. The curves from both figures are analogous in nature. It is to be noted that the concentration is all-time lower for the toy model, as compared to the smooth and original model for both the tissue domains. This observation makes sense that the smaller interface roughness (interface length) for the toy model gives rise to lesser absorption of drug in the tissue and hence, it may be concluded that the more the interface roughness, the more the absorption of drug, and finally, the more the averaged concentration in the tissue.

4.4 Effect of diffusivity (Peclet number), tissue porosity (α) and interface roughness on the effectiveness of delivery

Following Saltzman [40], the effectiveness of delivery in the target tissue is defined as the ratio of the averaged concentration and maximum concentration. He also opined that the higher value of this ratio implies good effectiveness. Figure 12(a-b) depicts the influence of the Peclet number (diffusivity) and the tissue porosity (α) on the effectiveness of endovascular drug delivery for upper and lower therapeutic domains over time respectively.

As anticipated, the effectiveness of delivery diminishes with increasing Peclet number, which is in tune with the averaged concentration for various Peclet numbers (cf. Fig. 9), but a reverse trend is observed in case of varying porosity. Although the averaged concentration increases with increasing tissue porosity in the upper and lower tissue regions, the effectiveness of delivery decreases. Figure 13(a-b) exhibits the effect of geometrical shape, i.e., interface roughness or interface length on the effectiveness of endovascular drug delivery. Simulated results show that the effectiveness of drug delivery diminishes with increasing interface roughness as opposed to the averaged concentration in both the tissue domains (cf. Fig 10). This observation may be justified in the sense that with the increase of tissue porosity and the interface roughness, the averaged concentration in the tissue domains does increase, but the higher porosity and roughness implying higher tissue uptake of the injected drug give much higher maximum concentration in the tissue, and eventually, the ratio (effectiveness) decreases.

5 Conclusion and future direction

Endovascular delivery through a patient-specific atherosclerotic arterial segment has been considered in the present study. The drug which is transported with the luminal flow and its subsequent uptake into the porous tissue regions clearly resemble intravenous delivery in a realistic situation. **Image processing technique has been successfully used to determine the boundary of the domain of study.** The luminal fluid is modeled as an incompressible Newtonian fluid governed by Navier-Stokes equations. The transport of drug in the lumen and tissue domains are modeled as an unsteady advection-diffusion process. Considering each pixel as a control volume, the Marker and Cell (MAC) method has been leveraged to get a quantitative insight of the model considered by exploiting physiologically realistic initial, boundary as well as interface conditions. Simulated results predict that the number as well as the length of separation zones increases with **increasing** Re **and** the near-wall velocity contour plays a pivotal role for estimating the residence times for the pool of drug molecules available for tissue uptake. One interesting phenomenon may be noted that although the tissue porosity and the interface roughness do enhance the averaged concentration of drug in both the tissue domains, it may not enhance the effectiveness of delivery. Hence, the porosity as well as the interface roughness of the asymmetric therapeutic domains play a pivotal role in the dispersion and the effectiveness of drug delivery.

To model endovascular drug delivery in a complex physiological system is an uphill task, still a sincere attempt is made to study such a problem in a tractable form by making a lot of assumptions. Our model did not consider the rheological effects on dispersion. The consideration of the retention of drug in the therapeutic domains together with its endocytosis (internalization) in the heterogeneous compositions of the plaque may be taken into account in our future endeavor. We intend to revisit these topics mentioned in this section as part of our future research.

Acknowledgement

The authors gratefully acknowledge the research fellowship received from Special Assistance Programme (SAP-III) [Grant No. F.510/3/DRS-III/ 2015 (SAP-I)] sponsored by the University Grants Commission, New Delhi, India.

Conflicts of interest

The authors declare that they have no known competing interest.

References

[1] Ross, R. (1993). Atherosclerosis: a defense mechanism gone awry. The American Journal of Pathology, 143(4), 987–1002.

[2] Taylor, G. I.(1953). Dispersion of a soluble matter in solvent flowing slowly through a tube. Proceedings of the Royal Society of London. Series A. Mathematical and Physical Sciences, 219(1137), 186–203.

[3] Aris, R. (1956). On the dispersion of a solute in a fluid flowing through a tube. Proceedings of the Royal Society of London. Series A. Mathematical and Physical Sciences, 235(1200), 67–77.

[4] Gill, W. N. and Sankarasubramanian, R. (1970). Exact analysis of unsteady convective diffusion. Proceedings of the Royal Society of London. A. Mathematical and Physical Sciences, 316(1526), 341–350.

[5] Sankarasubramanian, R. and Gill, W.N. (1973). Unsteady convective diffusion with inter-phase mass transfer. Proceedings of the Royal Society of London. A. Mathematical and Physical Sciences, 333(1592), 115–132.

[6] Smith, R. (1983). Effect of boundary absorption upon longitudinal dispersion in shear flows. Journal of Fluid Mechanics, 134, 161–177.

[7] Purnama, A. (1988). Boundary retention effects upon contaminant dispersion in parallel flows. Journal of Fluid Mechanics, 195, 393–412.

[8] Dash, R.K., Jayaraman, G. and Mehta, K.N. (2000). Shear augmented dispersion of a solute in a Casson fluid flowing in a conduit. Annals of Biomedical Engineering, 28(4), 373-385.

[9] Sarkar, A. and Jayaraman, G. (2002). The effect of wall absorption on dispersion in annular flows. Acta Mechanica 158, 105-119.

[10] Nagarani, P., Sarojamma, G. and Jayaraman, G. (2006). Exact analysis of unsteady convective diffusion in Casson fluid flow in an annulus–Application to catheterized artery. Acta Mechanica, 187(1-4), 189–202.

[11] Ng, C.O., Rudraiah, N.(2008). Convective diffusion in steady flow through a tube with a retentive and absorptive wall. Physics of Fluids, 20, 073604.

[12] Mazumder, B.S. and Paul, S. (2012). Dispersion of reactive species with reversible and irreversible wall reactions. Heat and Mass Transfer, 48(6), 933-944.

[13] Rana, J., Murthy, P. (2016). Solute dispersion in pulsatile casson fluid flow in a tube with wall absorption. Journal of Fluid Mechanics 793, 877–914.

[14] Rana, J., Murthy, P. (2017). Unsteady solute dispersion in small blood vessels using a two-phase Casson model. Proceedings of the Royal Society A: Mathematical, Physical and Engineering Sciences 473(2204), 20170427.

[15] Debnath, S., Saha, A.K., Mazumder, B., Roy, A.K. (2017). Dispersion phenomena of reactive solute in a pulsatile flow of three-layer liquids. Physics of Fluids 29(9), 097107.

[16] Griffiths, I.M.,Howell, P.D., Shipley, R.J. (2013). Control and optimization of solute transport in a thin porous tube. Physics of Fluids, 25, 033101.

[17] Das, P., Sarifuddin, M. and Mandal, P. K. (2020). Solute dispersion in Casson fluid flow through a stenosed artery with absorptive wall. Zeitschrift Angewandte Mathematik und Physik, 71(3), p.100.

[18] Back, L.H., Cho, Y.I., Crawford, D.W. and Cuffel, R.F. (1984). Effect of mild atherosclerosis on flow resistance in a coronary artery casting of man. ASME Journal of Biomechanical Engineering 106, 48–53.

[19] Johnston, P.R. and Kilpatrick, D. (1991). Mathematical modelling of flow through an irregular arterial stenosis. Journal of Biomechanics, 24(11),1069-1077.

[20] Andersson, H.I., Halden, R. and Glomsaker, T. (2000) Effects of surface irregularities on flow resistance in differently shaped arterial stenoses. Journal of Biomechanics, 33(10), 1257-1262.

[21] Yakhot, A., Grinberg, L. and Nikitin, N. (2005). Modeling rough stenoses by an immersed-boundary method. Journal of Biomechanics, 38(5), 1115-1127.

[22] Sarifuddin, Chakravarty, S., Mandal, P.K. and Andersson, H.I. (2009). Mass transfer to blood flowing through arterial stenosis. Zeitschrift für Angewandte Mathematik und Physik, 60(2), 299-323.

[23] Sarifuddin, Chakravarty, S. and Mandal, P.K. (2013). Physiological flow of shear-thinning viscoelastic fluid past an irregular arterial constriction. Korea-Australia Rheology Journal, 25(3),163-174.

[24] Sarifuddin, Chakravarty, S. and Mandal, P.K. (2014). Numerical simulation of Casson fluid flow through differently shaped arterial stenoses. Zeitschrift für angewandte Mathematik und Physik, 65(4), 767-782.

[25] Ne'mati, S.M.A., Ghassemi, M. and Shahidian, A. (2017). Numerical Investigation of Drug Delivery to Cancerous Solid Tumors by Magnetic Nanoparticles Using External Magnet. Transport in Porous Media, 119, 461–480.

[26] Spiridonova, T.I., Tverdokhlebov, S.I. and Anissimov, Y.G. (2019). Investigation of the size distribution for diffusion-controlled drug release from drug delivery systems of various geometries. Journal of Pharmaceutical Sciences, 108(8), 2690–2697.

[27] Kashkooli, F. M.,Soltani, M., Rezaeian, M., Meaney, C., Hamedi, M. H., Kohandel, M. (2020). Effect of vascular normalization on drug delivery to different stages of tumor progression: In-silico analysis. Journal of Drug Delivery Science and Technology, 60, 101989.

[28] König, A. and Klauss, V. (2007). Virtual histology. Heart, 93(8), 977-982.

[29] Mandal, P.K., Sarifuddin and Kolachalama, V.B.(2016). Computational model of drug-coated balloon delivery in a patient-specific arterial vessel with heterogeneous tissue composition. Cardiovascular Engineering and Technology, 7(4), 406-419.

[30] Harlow, F.H. and Welch, J.E. (1965). Numerical calculation of time-dependent viscous incompressible flow of fluid with free surface. The Physics of Fluids, 8(12), 2182-2189.

[31] Taylor,M. G. (1959). The influence of the anomalous viscosity of blood upon its oscillatory flow. Physics in Medicine and Biology, 3(3),273-290.

[32] Mandal, A. P., Sarifuddin and Mandal, P. K. (2015). An unsteady analysis of arterial drug transport from half-embedded drug-eluting stent. Applied Mathematics and Computation, 266, 968-981.

[33] Welch, J. E., Harlow, F. H., Shannon, J. P. and Daly, B. J. (1966). The MAC method, Los Alamos Scientifc Lab. Report LA 3425.

[34] Hirt, C. W. (1968). Heuristic stability theory for finite difference equations, Journal of Computational Physics, 2, 339-355.

[35] Markham, G. and Proctor, M. V. (1983). Modifications to the two-dimensional incompressible fluid flow code zuni to provide enhanced performance. CEGB Report TPRD= L, vol. 63, p. M82.

[36] Huang, Z. J. and Tarbell, J. M. (1997). Numerical simulation of mass transfer in porous media of blood vessel walls. American Journal of Physiology-Heart and Circulatory Physiology, 273(1), H464-H477

[37] Creel, C. J., Lovich, M. A. and Edelman, E. R. (2000). Arterial paclitaxel distribution and deposition. Circulation Research, 86(8), 879-884.

[38] Strikwerda, J.C. (2004). Finite Difference Schemes and Partial Differential Equations, vol. 88. SIAM, Philadelphia.

[39] Asakura, T., and Karino, T. (1990). Flow patterns and spatial distribution of atherosclerotic lesions in human coronary arteries. Circulation Research, 66(4), 1045-1066.

[40] Saltzman, W. M. (2001). Drug delivery: engineering principles for drug therapy. Oxford University Press.

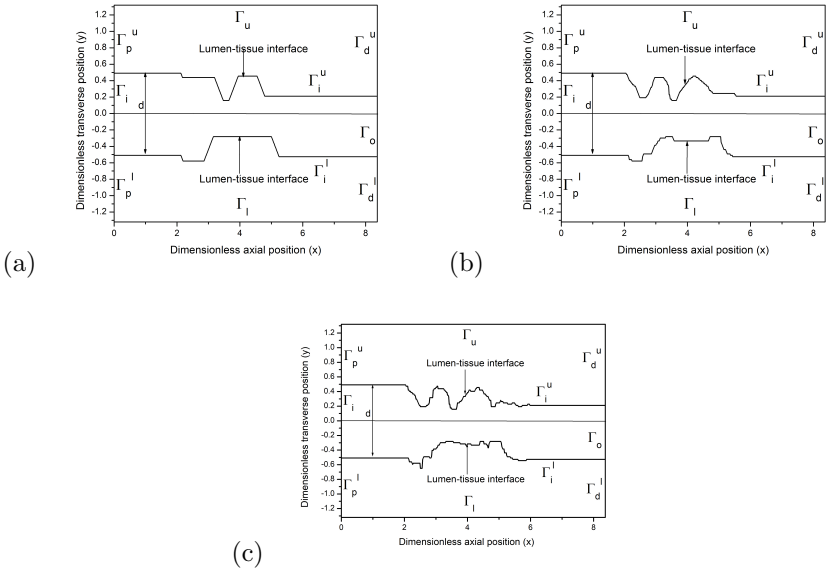

Figure 1: Computational domain, (a) Toy model, (b) Smooth model, (c) Original model, outline of the geometry derived from an IVUS image of a patient-specific atherosclerotic artery [28].

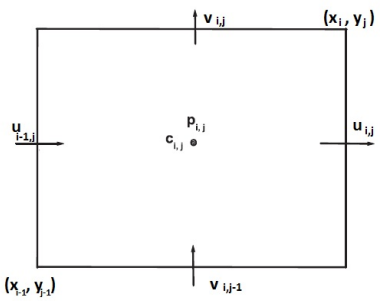

Figure 2: A typical MAC cell

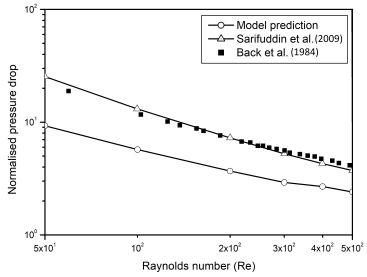

Figure 3: Comparison of normalized pressure drop across an irregular stenosis.

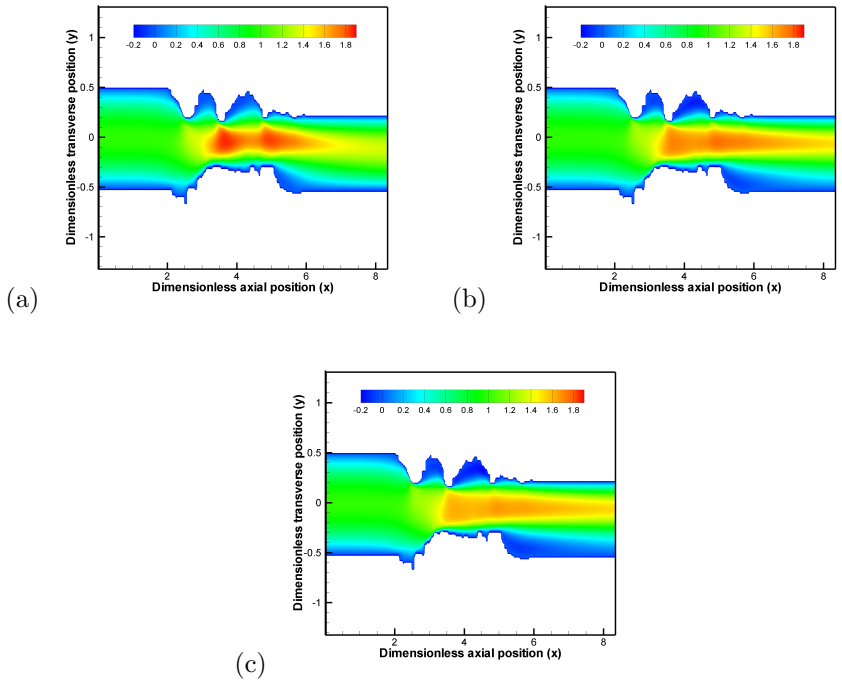

Figure 4: Longitudinal velocity contour, (a)$Re = 100$, (b)$Re = 300$, (c) $Re = 500$.

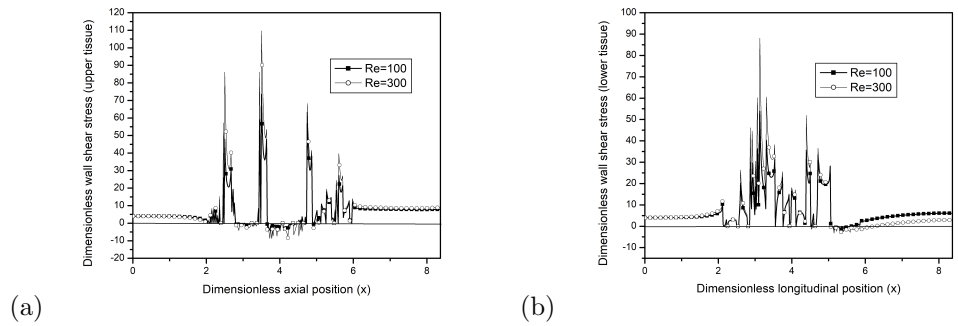

Figure 5: Variation of the wall shear stress along asymetrical atherosclerotic stenosis, (a) upper tissue, (b) lower tissue.

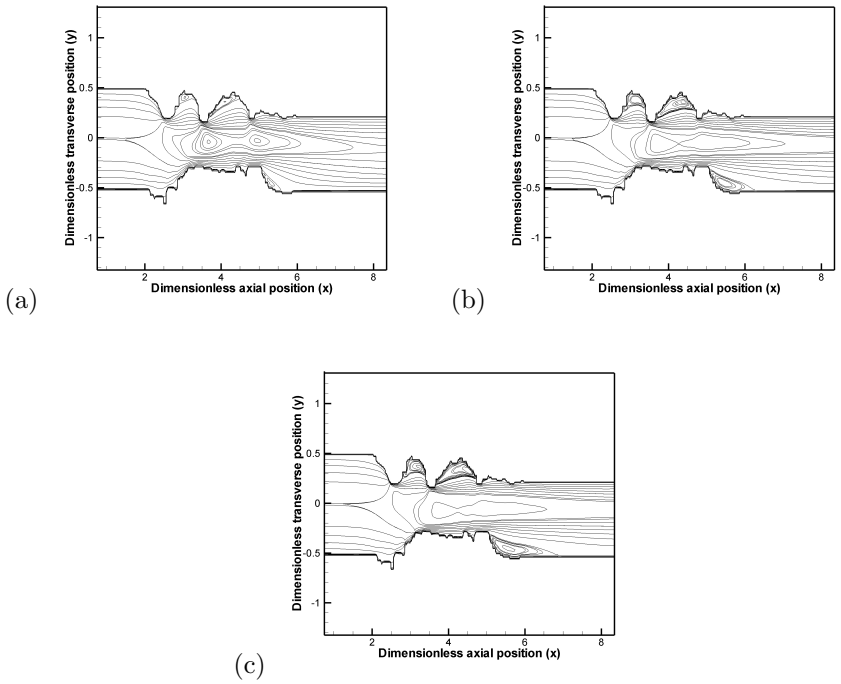

Figure 6: Variation of streamlines,(a)$Re = 100$, (b)$Re = 300$, (c)$Re = 500$.

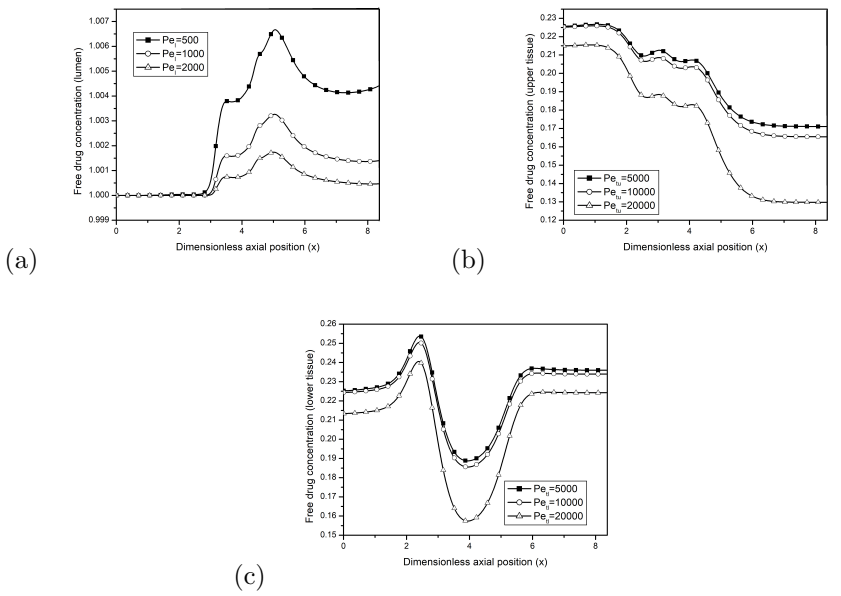

Figure 7: Axial variation of the local concentration of drug for different Peclet numbers, (a) lumen at $y = -0.2$, (b) upper tissue at $y = 1.15$, (c) lower tissue at $y = -1.15$.

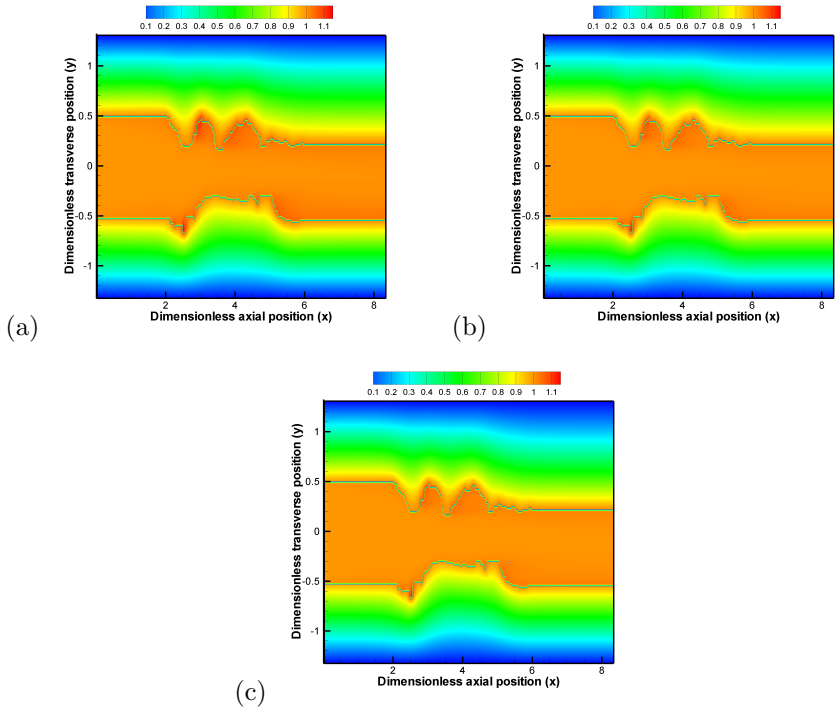

Figure 8: Spatiotemporal variation of drug concentration for different Peclet numbers ($Pe_{tu} = Pe_{tl} = 10 \times Pe_l$), (a) $Pe_l = 500$, (b)$Pe_l = 1000$, (c) $Pe_l = 2000$.

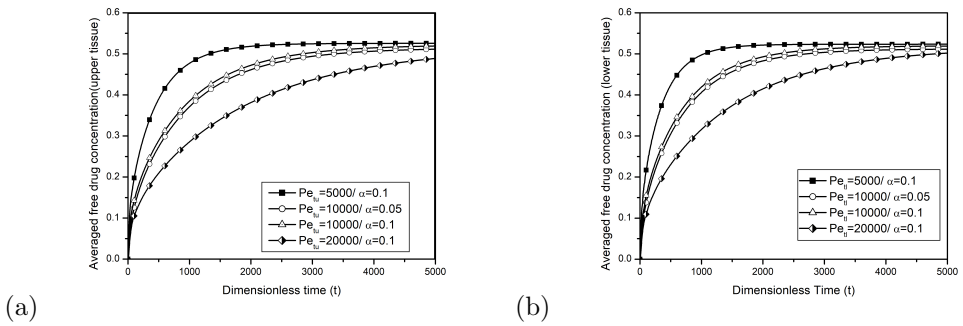

Figure 9: Temporal variation of dimensionless averaged concentration for different Peclet numbers and porosities, (a) upper tissue, (b) lower tissue.

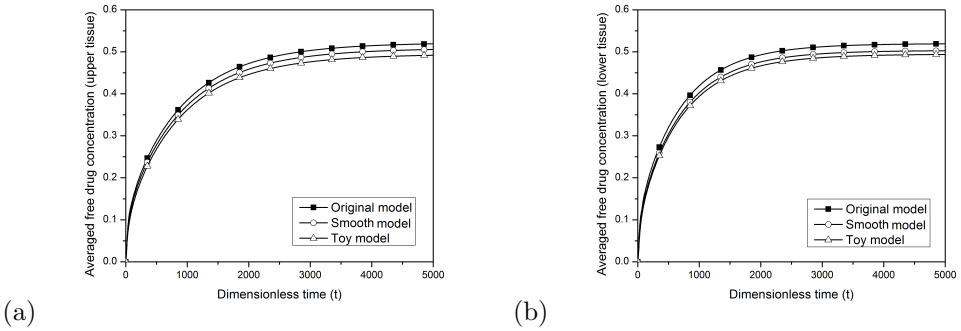

(a) (b)

Figure 10: Temporal variation of dimensionless averaged concentration for various geometrical models ($Pe_l = 1000, Pe_{tu} = Pe_{tl} = 10000, Re = 300, \alpha = 0.1$), (a) upper tissue, (b) lower tissue.

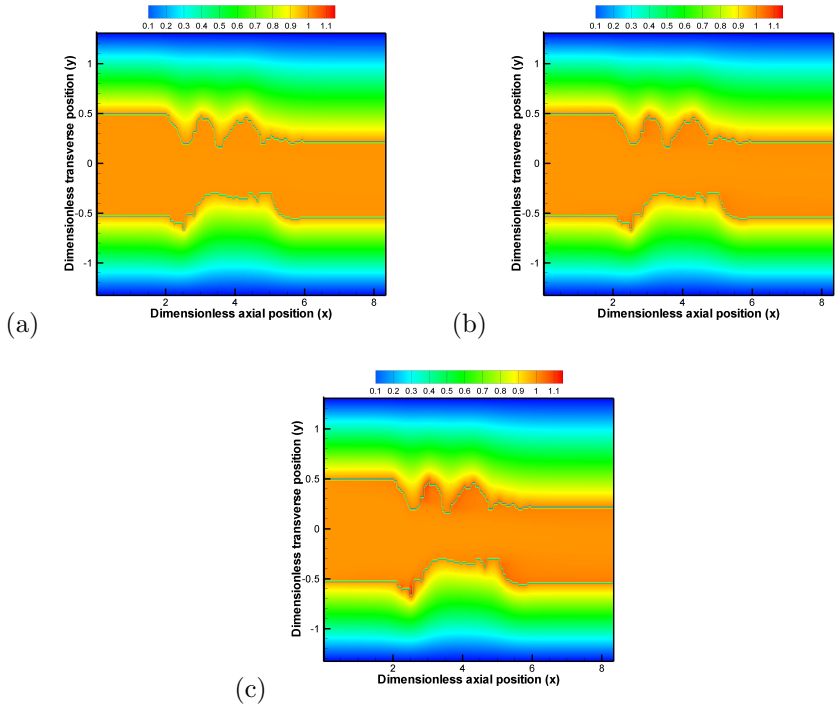

(a) (b) (c)

Figure 11: Spatiotemporal variation of drug concentration for different porosities ($Pe_l = 1000, Pe_{tu} = Pe_{tl} = 10000$), (a) $\alpha = 0.01$, (b) $\alpha = 0.05$, (c) $\alpha = 0.1$.

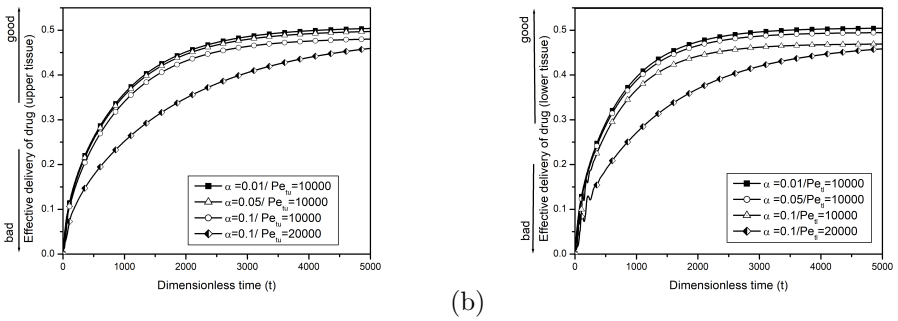

(a) (b)

Figure 12: Influence of Peclet number and porosity on the effectiveness of delivery, (a) upper tissue, (b) lower tissue.

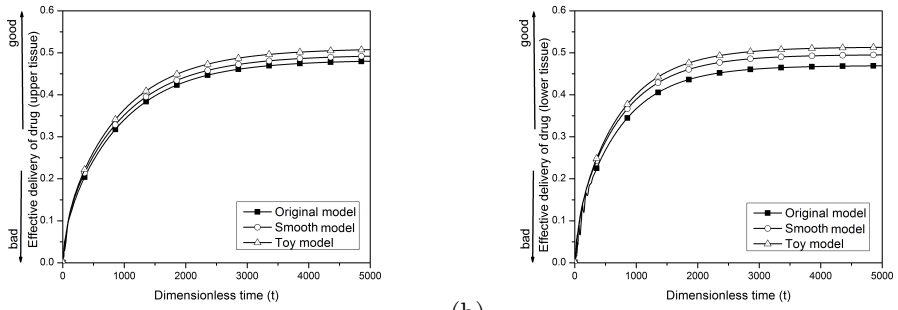

(a) (b)

Figure 13: Influence of surface roughness on the effectiveness of delivery ($Pe_l = 1000, Pe_{tu} = Pe_{tl} = 10000, Re = 300, \alpha = 0.1$), (a) upper tissue, (b) lower tissue.

Vol. 41 (2) 2021

GANIT

Available online at https://www.banglajol.info/index.php/GANIT/index

GANIT: Journal of Bangladesh Mathematical Society

GANIT *J. Bangladesh Math. Soc.* 41.2 (2021) 01–04

DOI: https://doi.org/10.3329/ganit.v41i1.55021

A Legend of Computational Fluid Dynamics and an Eminent Mathematician: Professor Md. Anwar Hossain

M. Kamrujjaman*[a], M. Mamun Molla[b], M. H. Kabir[c], M. H. A. Biswas[d], and M. A. H. Khan[e]

[a]*Department of Mathematics, University of Dhaka, Dhaka-1000, Bangladesh*
[b]*Department of Mathematics & Physics, North South University, Dhaka-1229, Bangladesh*
[c]*Department of Mathematics, Jahangirnagar University, Dhaka-1342, Bangladesh*
[d]*Mathematics Discipline, Khulna University, Khulna-9208, Bangladesh*
[e]*Department of Mathematics, Bangladesh University of Engineering & Technology, Dhaka-1000, Bangladesh*

OBITUARY

Professor Md. Anwar Hossain (25 April 1943 - 27 May 2021) was a Bangladeshi mathematician and a legend of computational fluid dynamics. He was a professor of mathematics at the University of Dhaka, a Fellow of the Bangladesh Academy of Sciences. He was also a Senior Associate of the Abdus Salam International Center for Theoretical Physics (ICTP), Italy.

Received: September 22, 2021 **Accepted:** December 09, 2021 **Published Online:** January 07, 2022

1 Early Life and Education

Dr. Md. Anwar Hossain was born on 25 April 1943 in Chandpur, Bangladesh. His father is Md. Delwar Hossain, a railway engineer, and his mother is Nurunnahar Chowdhury. His grandfather is Bohorot Ali Khan, and his great grandfather, Omar Khan was a Jaminder in Chandpur, Comilla. Dr. Hossain lost his mother to cholera when he was only three months. Professor Hossain spent his early school years in Laksham and studied in Laksham A. Malek Institution, where he passed the Matriculation in 1960. He had a bright and curious mind and excelled at school. After that, he got admitted to Barishal B. M. College. Due to his uncle's job, he came to Dhaka and was admitted to Jagannath College, where he completed H.S.C in 1964.

Professor Md. Anwar Hossain received his B.Sc. from Jagannath College, Bangladesh in 1966, M.Sc. in Applied Mathematics from the University of Dhaka (DU) in 1969, M.Sc. in Pure Mathematics in 1971. He achieved his Ph.D. on "Infinite horizontal rolls under the effect of vertical and horizontal temperature gradients" under the supervision of Professor S. M. A. Haque in 1978 as a research fellow of Bose Center.

*Corresponding author: M. Kamrujjaman, *E-mail address:* kamrujjaman@du.ac.bd

(a)

(b)

Figure 1: Professor Anwar Hossain was born and grew up here archive-heritage, Chandpur, Bangladesh.

(a)

(b)

Figure 2: Professor Anwar Hossain's family and his great grandfather Jaminder niche in Chandpur, Comilla; another heritage.

2 Academic Career

Soon after the completion of his Ph.D. study, Dr. Md. Anwar Hossain joined the Department of Mathematics, Dhaka University (DU) as a Lecturer in 1978 and was promoted to Assistant Professor in 1983, Associate Professor in 1989, and a full professor in 1993. Dr. Hossain worked as a Visiting Professor of the Department of Mathematics, COMSATS Institute of Information Technology Islamabad from 2005 to 2007, Foreign Professor from 2007 to 2009. He served as an Assistant Professor at Al-Fathah University, Tripoly, Libya from 1986 to 1989. Dr. Hossain became University Grant Commission (UGC) Professor of DU from 2015 to 2017 for his distinguished contributions to physical sciences. He was a Fellow of the Bangladesh Academy of Sciences, Senior Associate, Abdus Salam International Centre for Theoretical Physics, Trieste, Italy; Honorary Fellow, Australian Institute of High Energetic Materials, Australia since October 2011.

Professor Anwar Hossain was the founder Associate Editor of the GANIT: *Journal of Bangladesh Mathematical Society*. He had tremendous efforts in promoting mathematics education in Bangladesh. He played a pivotal role to initiate National Undergraduate Mathematics Olympiad in Bangladesh. He was the Co-Convener of the olympiad committee until his death. Professor Hossain was also the President of the Bangladesh Mathematical Society from 2012 to 2013. He was always active in organizing international conferences, workshops, research schools, etc. in different corners of Bangladesh. Professor Hossain was an amicable, kind-hearted, good soul in every sense of the term.

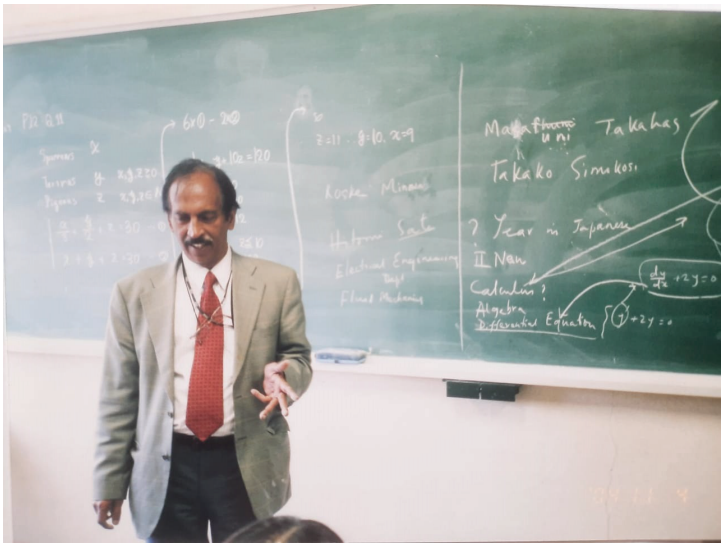

Figure 3: Professor Anwar Hossain.

Professor Hossain had a remarkable attempt to initiate a thesis group in the MSc program of the department of mathematics, DU, in 1981. He has supervised numerous undergraduate final year students, twenty Masters of Science students, and ten doctoral students and worked as a potential mentor for his students. Several of his graduates are now working as full professors in various academic institutions or as scientists in research institutions worldwide, e.g. Dr. Rowshan Ara Begum (University of Durban, South Africa), Dr. Md. Zulfiker Hafiz (IIT, DU), Dr. Bidyut Baran Saha (Kyushu University, Japan), Dr. K C Amanul Alam (East West University), Dr. Sushanta Kumar Das (Kettering University, USA), Dr. Abdul Alim (BUET), Dr. Zafor Iqbal Khan (BUET), Dr. Sarder Firoz Ahmed (Khulna University), Dr. Tahmina Akhter (Yorkville University, Canada), Dr. Akhtar Hossain (East West University), Dr. Manosh Chandra Paul (University of Glasgow, UK), Dr. Sreebash Chandra Paul (Ahsanullah University of Sci. & Tech.), Dr. Suvash Chandra Saha (University of Technology, Australia), Dr. Md. Mamun Molla (North South University), Dr. Asma Selim (Digital animation maker, BD), Dr. Shiddartha Bhowmik (Jagannath University), Dr. Md. Kamrujjaman (DU), Dr. Litan Kumar Saha (DU), and Dr. Nepal Chandra Roy (DU). Moreover, Professor Hossain was the Ph.D. supervisor of Professor Mostafa Kamal Chowdhury (BUET) and Dr. Sharmina Hussain (BRAC University).

3 Publications

Professor Md. Anwar Hossain published more than 200 articles in top-notch peer-reviewed journals, such as Elsevier's journal, Springer's journals, Taylor & Francis's journal, Emerald's journals, Wiley & Son's journals, ASME's journals, etc. The total citations in the Research gate of his papers are 5056 with an RG score of 40.19 and h-index 37. The citations in Scopus are 3854, with an h-index of 32.

4 Awards

Professor Hossain received numerous awards for his outstanding contributions to his research area. He was awarded Ibrahim Gold Medal (1985-86) for distinguished research works by the University of Dhaka, Dean's Award for the year 1999-2001 by the Faculty of Science, University of Dhaka, an award for contribution in physical Science for the year 2002 by the Physical Society of Bangladesh and University Grant Commission (UGC) Research and innovation in Physical Sciences award for 2002.

Figure 4: Memorandum and many achievements of Professor Hossain.

5 Death

Professor Md. Anwar Hossain breathed his last at the age of 78 on 27 May 2021 at his residence in Dhaka. His demise is undoubtedly an irreparable loss to the mathematics community. He is survived by his wife, Mrs. Rowshan Akhtar, and his only son, Mr. Iftekhar Anwar (Upal). He was buried at the Azimpur Koborsthan in Dhaka. Professor Md. Anwar Hossain will be remembered forever as an outstanding mathematician and researcher.

Figure 5: Azimpur Koborsthan (graveyard) where Professor Hossain is sleeping forever.

Acknowledgments

The authors acknowledged to Iftekhar Anwar, Son of Professor Hossain for sharing the archive photos.

References

[1] Bidyut Baran Saha (2021). Obituary Professor Dr. Md. Anwar Hossain, Thermal Science and Engineering Progress, 25, 100996.

GANIT

Available online at https://ganitjournal.bdmathsociety.org/

GANIT: Journal of Bangladesh Mathematical Society

GANIT *J. Bangladesh Math. Soc.* 41.2 (2021) 05–17
DOI: https://doi.org/10.3329/ganit.v41i2.55026

Profit Optimization of Soap Industry by using Benders' Decomposition Method

Sanjida Aktar *, and Mohammed Forhad Uddin

Department of Mathematics, Bangladesh University of Engineering and Technology, Dhaka 1000, Bangladesh

ABSTRACT

In this paper, a large-scale linear programming problem including several parameters such as labor cost, raw material cost, machine and other cost have been formulated. Then the formulated problem has been solved by using Benders' Decomposition Method. The formulated large model is divided into master and small sub problem. In order to validate and calibrate the model, real data from a soap industry named Mega Sornali Soap and Cosmetics Industry have been collected. Soap industry is one of the most feasible business options owing to the straightforward manufacturing process involved starting a soap and detergent manufacturing business in Bangladesh. These models are solved by using AMPL. To find out the significant parameters of the model, the sensitivity analysis of different cost parameters such as labor cost, raw material cost and machine cost have been be considered. From the sensitivity analysis, the decision makers of the factory would able to find out the ranges of cost coefficients and all the resources. As a result, the company could able to see how any change can affect the profit or loss of the factory. From the numerical results, the most profitable product of the company is found to be Sornali Soap and Mega Extra Powder. On the contrary, Mega SornaliSobiMarka Soap and Mega Washing Powder are not more profitable. Further, raw material cost is the most significant sensitive cost. If the raw material cost can be decreased the profit could also beincreased. Finally, the result of the optimal solution has been represented in tabular and graphs.

Received: June 12, 2021 **Accepted:** November 06, 2021 **Published Online:** January 07, 2022

Keywords: Benders' Decomposition Method, Soap Industry, Linear Program, Profit Optimization

AMS Subject Classification 2020: 90C05, 90C08

1. Introduction

Linear programming is a method to achieve the best outcome such as maximum profit or lowest cost in a mathematical model of any business organizations. Decomposition technique is one of the most commonly used techniques for solving Linear Programming Problem (LPP). If the number of decision variables and constraints are very large then it would be very difficult to solve manually. Benders' Decomposition Method

* Corresponding author: Sanjida Aktar, *E-mail address:* mssanjidaaktar24@gmail.com

(BDM) is a solution method for solving certain large-scale optimization problems that have special block structure.

In literature, [1] introduced a decomposition algorithm for linear programming. [2] Explained a method of decomposition for integer programs. [3] reported the partitioning procedures for solving mixed variables programming problems.[4] presented an integer programming algorithm for vehicle routing problem involving capacity and distance restrictions. They derived exact solutions for problems involving up to sixty cities. [5] Established decomposition-based pricing model for solving a large-scale MILP for an integrated fishery. They described how a fishery manager can schedule fishing trawlers to determine when and where they should go and return their caught fish to the factory. The authors of [6] presented technique for solving large nonconvex water resources management models using generalized BDM. Then [7] developed a decomposition algorithm for the design of a no simultaneous capacitated evacuation tree network. Vendor-Bayer coordination and supply chain optimization with deterministic demand function was analyzed by [8].

A mixed-integer programming techniques for decomposing IMRT fluency maps using rectangular apertures had explained by [9]. They studied the problem of minimizing the number of rectangles (and their associated intensities) necessary to decompose such a matrix. They proposed an integer programming-based methodology for providing lower and upper bounds on the optimal solution and demonstrate the efficacy of their approach on clinical data. In [10], the authors implemented the Dantzig-Fulkerson-Johnson algorithm for large travelling salesman problems. An algorithm is described for solving large-scale instances of the Symmetric Travelling Salesman Problem (STSP) to optimality. [11] Showed a Benders' decomposition algorithm for the single allocation hub location problem under congestion. The single allocation hub location problem under congestion is addressed in this article. Then a very efficient and effective generalized Benders decomposition algorithm is deployed, enabling the solution of large-scale instances in reasonable time. An approach for the locomotive and car assignment problem using Benders' Decomposition illustrated in [12]. One of the problems faced by rail transportation companies is to optimize the utilization of the available stock of locomotives and cars. They described a decomposition method for the simultaneous assignment of locomotives and cars in the context of passenger transportation.

This paper proposes an optimal formulation optimization model for Soap industry. To formulate a linear programming model that would suggest a viable product-mix to ensure optimum profit for company. This study minimizes the production cost and find out various types of effects of parameters in production period. In addition, find out the significant constraints of the company regarding cost and resources. The formulated model soles by BD method using Mathematical Programming Language (AMPL). The solution of the problem discusses briefly and carries out the optimal product for the industry.

The paper is structured as follows: in Section 2, the adaptation of the BD model for the Soap industry formulation is described and a Linear programming problem is developed, aiming at the maximization of profit. In Section 3, an effect of the model with solution and findings is worked out. Finally, Section 4 concludes the paper, highlighting the main results and introducing some research challenges for the future.

2. Formulation of the problem

In this section, it will be developed a mathematical model from this data which will be resulting into a large LPP and by applying the solving procedure of LPP and by applying the solving procedure of LPP in its production planning. It will be tried to identify its desired production rate and to answer some questions that may arise when thinking about the profit. It will be showed the impact of LPP in business planning. To understand the effect of several parameters and the profit, we propose a mathematical model that can predict the significant parameters.

A standard form of a Linear Program is:

Maximize $z = c^T x$

Subject to Constraints: $Ax \leq b$

$x \geq 0,$

Where $c \in \mathbb{R}^n$, $b \in \mathbb{R}^m$ are given vectors and $A \in \mathbb{R}^{m \times n}$ is a matrix.

The following table show the decision variables and their descriptions.

Table 2.1: List of the parameters involved in the model

Parameters	Description
X_1	The unit of Mega SornaliSobiMarka Soap (250g).
X_2	The unit of SornaliBati Soap (175g).
X_3	The unit of Sornali Soap 2015 (500g).
X_4	The unit of Sornali Soap (250g).
X_5	The unit of Mega Sornali Full Marka Soap (250g).
X_6	The unit of Mega Washing Powder (25g).
X_7	The unit of Mega Washing Powder (200g).
X_8	The unit of Mega Washing Powder (500g).
X_9	The unit of Mega Extra Powder (200g).
X_{10}	The unit of Mega Extra Powder (500g).

General mathematical form of our proposed problem as the following:

$$Maximize, Z = \sum_{n=1}^{10} C_n X_n$$

Subject to constraints,

$$\sum_{n=1}^{10} B_n^1 X_n \le b_1$$

$$\sum_{n=1}^{10} B_n^2 X_n \le b_2$$

$$\sum_{n=1}^{10} B_n^3 X_n \le b_3$$

$$0 \le X_n \le \alpha_i$$

Where b1, b2 and b3 are available labour cost, machine and other cost and raw material cost. α_i are lower and upper bound of different products.

To solve the above problem real-life data has been collected from a company named Mega Sornali Soap and Cosmetics Industries Ltd. It was established in 2015. This company produces five types of soap, three types of lemon powder and two types of mega extra powder.
In Table 2.2, presents the different types of per unit raw materials cost. Table 2.3, shows per unit raw materials cost to produce Lemon Detergent Powder. Table 2.4, display per unit raw materials cost to produce Extra Detergent Powder.

Table 2.2: Different types of raw materials cost

No.	Name	Cost (TK)/Kg
01.	Silicate	14
02.	Palm Oil	76
03.	Palm Pati	80
04.	Rice Pati	54
05.	Palm Stearing	80.50
06.	Soybean	48.50
07.	Caustic Soda	32
08.	S.L.S.(Foam Powder)	290
09.	Perfumed	1000
10.	Colour	1000

Table 2.3: Raw Materials to produce Lemon Detergent Powder

No.	Name	Cost (TK)/Kg
01.	Dolomite	5
02.	Global Salt	12
03.	Calcium Carbonet	15
04.	Soda	32
05.	Lapsa (Foam)	125
06.	Colour	4000
07.	Perfume	1000

Table 2.4: Raw materials to produce Extra Detergent Powder

No.	Name	Cost(TK)/Kg
01.	Limestone	7
02.	Soda	32
03.	Calcium Carbonet	15
04.	Global Salt	12
05.	Lapsa	125
06.	Sky White	300
07.	S. Perkel	55
08.	Perfume	1000

Table 2.5: Selling Price of Soap

No.	Name	Quantity(g)	Selling Prices Per piece (TK)
01.	Mega Sornali Sobi Marka Soap	250	11.66
02.	SornaliBati Soap	175	6.50
03.	Sornali 2015	500	20
04.	Sornali Soap	250	10.41
05.	Mega Sornali Full Marka	250	8.33

Table 2.6: Selling Price of Lemon Powder

No.	Name	Quantity(g)	Selling Prices Per piece (TK)
01.	Mega Washing Powder	25	2.5
02.	Mega Washing Powder	200	6.86
03.	Mega Washing Powder	500	14

Table 2.7: Selling Price of Mega Extra Powder

No.	Name	Quantity(g)	Selling Prices Per piece

			(TK)
01.	Mega Extra Powder	200	10.32
02.	Mega Extra Powder	500	20

Table 2.8: Price of machine

No.	Name	Price
01.	Mixer Machine	210000
02.	Sipter Machine	100000
03.	Packing Machine (Mini)	150000
04.	Packing Machine (250g, 500g)	300000

Table 2.9: Salary Structure

Post	Salary monthly (TK)
Mechanical Engineer	15000
Manager	10000
Electrician	8000
Fueling	9500
Sweeper	5000
Machine Operator	5000

Table 2.10: Some brands of foreign material

Country	Brand
Bhutan	Limestone, Dolomite
India	Lapsa
Taiwan	Foam Powder

Table 2.11: Other cost

Purpose	Cost (TK)
Oil	2250
Tools	3000
Electric Motor (5 pieces)	9000
Total	14250

In Table 2.5, represents the selling price of various companies of per unit soap. Table 2.6, defines the selling price of different types of Lemon Powder. Table 2.7, denotes the selling price of different types of Mega Extra Powder. Table 2.8, describes various types of machine price. Table 2.9, represents the salary of various employers. Table 2.10, denotes the some brands of foreign material. Finally, Table 2.11; ensure other cost to produce different types of soap. The following Table 2.12 shows the information of different soaps and their raw materials cost, labor cost and machine and other cost that has obtained the previous primary data described in Table 2.11.

Table 2.12: Product wise cost and profit

Variable	Labor cost B^1_n	Machine and other cost B^2_n	Raw material cost B^3_n	Profit for each variable
X_1	0.236	0.054	8.644	2.725
X_2	0.295	0.068	3.447	2.69
X_3	0.295	0.065	11.991	7.649
X_4	0.268	0.055	6.818	3.269
X_5	0.322	0.067	5.278	2.663
X_6	0.163	0.029	2.0	0.308
X_7	0.271	0.062	3.81	2.717
X_8	0.295	0.075	7.5	6.13
X_9	0.236	0.06	6.4	3.62
X_{10}	0.3	0.1	13.33	6.26

According to the above data the LPP problem for the Mega Sornali Soap and Cosmetics Industries Ltd is formulated as follows.

The objective function of the LPP model is:
Maximize,

$$Z = 2.725X_1 + 2.69X_2 + 7.649X_3 + 3.269X_4 + 2.663X_5 + 0.308X_6 + 2.717X_7 + 6.13X_8 + 3.62X_9 + 6.26X_{10}$$

Subject to:

$$0.236X_1 + 0.295X_2 + 0.295X_3 + 0.268X_4 + 0.322X_5 + 0.163X_6 + 0.271X_7 + 0.295X_8 + 0.236X_9 + 0.3X_{10} \leq 60000 \quad (2.1)$$

$$0.054X_1 + 0.068X_2 + 0.065X_3 + 0.055X_4 + 0.067X_5 + 0.029X_6 + 0.062X_7 + 0.075X_8 + 0.06X_9 + 0.1X_{10} \leq 850000 \quad (2.2)$$

$$8.644X_1 + 3.447X_2 + 11.991X_3 + 6.818X_4 + 5.278X_5 + 2.0X_6 + 3.81X_7 + 7.5X_8 + 6.4X_9 + 13.33X_{10} \leq 1000000 \quad (2.3)$$

$$0 \leq X_1 \leq 25000 \quad (2.4)$$

$$0 \leq X_2 \leq 20000 \quad (2.5)$$

$$0 \leq X_3 \leq 20000 \quad (2.6)$$

$$0 \leq X_4 \leq 22000 \quad (2.7)$$

$$0 \leq X_5 \leq 18000 \quad (2.8)$$

$$0 \leq X_6 \leq 35000 \quad (2.9)$$

$$0 \le X_7 \le 21000 \tag{2.10}$$

$$0 \le X_8 \le 20000 \tag{2.11}$$

$$0 \le X_9 \le 25000 \tag{2.12}$$

$$0 \le X_{10} \le 20000 \tag{2.13}$$

Where, the objective function is to maximize the total profit where the coefficients are the profit of each product, equation (2.1) describes the labour cost where the coefficients are the labor cost required for each product. Equation (2.2) illustrates the machine cost where the coefficients are the cost of machine required for each product. Equation (2.3) represents other cost that includes tax, interest, electricity bill, fix cost etc. and the coefficients are the cost required for product production. In this study raw material cost are included with other cost that associate to the company to produce above ten products. Equations (2.4) to (2.13) are lower bound and upper bound of different products. These are the boundary constraints that illustrate the limit of the production amount of ten soaps.

2.1 Optimal solution by Bender Decomposition

In this subsection master problem is expressed. The master problems of Bender Decomposition method are as follows:

Master Problem: Maximize, $\mathrm{M} = 2.725X_1 + 2.69X_2 + 7.649X_3 + 3.269X_4 + 2.663X_5$

Subject to:

$$0 \le X_1 \le 25000 \tag{2.1.1}$$

$$0 \le X_2 \le 20000 \tag{2.1.2}$$

$$0 \le X_3 \le 20000 \tag{2.1.3}$$

$$0 \le X_4 \le 22000 \tag{2.1.4}$$

$$0 \le X_5 \le 18000 \tag{2.1.5}$$

a. Primal sub-problem

In this subsection primal sub-problem is generated. The primal sub-problem of Bender Decomposition method are as follows

Maximize, $P = 0.308X_6 + 2.717X_7 + 6.13X_8 + 3.62X_9 + 6.26X_{10}$

Subject to:

$$\begin{aligned} &0.163X_6 + 0.271X_7 + 0.295X_8 + 0.236X_9 + 0.3X_{10} \\ &\le 60000 - 0.236X_1 - 0.295X_2 - 0.295X_3 - 0.268X_4 + 0.322X_5 \end{aligned} \tag{2.2.1}$$

$$\begin{aligned} &0.029X_6 + 0.062X_7 + 0.075X_8 + 0.06X_9 + 0.1X_{10} \\ &\le 850000 - 0.054X_1 - 0.068X_2 - 0.065X_3 - 0.055X_4 - 0.067X_5 \end{aligned} \tag{2.2.2}$$

$$2.0X_6 + 3.81X_7 + 7.5X_8 + 6.4X_9 + 13.33X_{10} \leq 1000000 - 8.644X_1 - 3.447X_2 - 11.991X_3 - 6.818X_4 - 5.278X_5 \quad (2.2.3)$$

$$0 \leq X_6 \leq 35000 \quad (2.2.4)$$

$$0 \leq X_7 \leq 21000 \quad (2.2.3)$$

$$0 \leq X_8 \leq 20000 \quad (2.2.4)$$

$$0 \leq X_9 \leq 25000 \quad (2.2.5)$$

$$0 \leq X_{10} \leq 20000 \quad (2.2.6)$$

2.3 Dual sub-problem

Considering the data and above formation the dual problem can be derived as follows:

$$\begin{aligned}
&Minimize,\ D = \lambda_1(60000 - 0.236X_1 - 0.295X_2 - 0.295X_3 - 0.268X_4 + 0.322X_5) \\
&+\lambda_2(850000 - 0.054X_1 - 0.068X_2 - 0.065X_3 - 0.055X_4 - 0.067X_5) \\
&+\lambda_3(1000000 - 8.644X_1 - 3.447X_2 - 11.991X_3 - 6.818X_4 - 5.278X_5) \\
&+35000\lambda_4 + 21000\lambda_5 + 20000\lambda_6 + 25000\lambda_7 + 20000\lambda_8 \\
&= \lambda_1(60000 - 0.236*25000 - 0.295*20000 - 0.295*20000 - 0.268*22000 - 0.322*18000) \\
&+\lambda_2(850000 - 0.054*25000 - 0.068*20000 - 0.06520000 - 0.055*22000 - 0.067*18000) \\
&+\lambda_3(1000000 - 8.644*25000 - 3.447*20000 - 11.991*20000 - 6.818*22000 - 5.278*18000) \\
&+ 35000\lambda_4 + 21000\lambda_5 + 20000\lambda_6 + 25000\lambda_7 + 20000\lambda_8 \\
&= 30600\lambda_1 + 843600\lambda_2 + 9230660\lambda_3 + 35000\lambda_4 + 21000\lambda_5 + 20000\lambda_6 + 25000\lambda_7 + 20000\lambda_8
\end{aligned}$$

Subject to:

$$0.163\lambda_1 + 0.029\lambda_2 + 2.06\lambda_3 + \lambda_4 \geq 0.308 \quad (2.3.1)$$

$$0.271\lambda_1 + 0.062\lambda_2 + 3.81\lambda_3 + \lambda_5 \geq 2.717 \quad (2.3.2)$$

$$0.295\lambda_1 + 0.075\lambda_2 + 7.5\lambda_3 + \lambda_6 \geq 6.13 \quad (2.3.3)$$

$$0.236\lambda_1 + 0.06\lambda_2 + 6.49\lambda_3 + \lambda_7 \geq 3.62 \quad (2.3.4)$$

$$\text{All } \lambda_i \geq 0 \quad (2.3.5)$$

3. Solution and results discussion

The formulated LPP has been solving using AMPL. The program consists of three parts: model file, data file and run file. After developing a model file, it must arrange a data file according to the model file. Both the model and related data file must be called in command file with proper codes. Then to obtain the output of the problem it must call command in AMPL. Then the solution can be found by run file using solver CPLEX.

After solving the LP formulated in previous section the maximum profit is obtained: 623195.5866 and the following Table 3.1 shows the values of the estimated parameters.

Table 3.1: Estimated values of the parameters

Parameter	Values
X_1	0.00
X_2	20000
X_3	20000
X_4	22000
X_5	18000
X_6	0.00
X_7	21000
X_8	20000
X_9	25000
X_{10}	4218.3

The formulated Master problem, Primal problem, and Duet problem are solved in several iterations. The estimated values of the parameters and shown in Table 3.2 as follows:

Table 3.2: Solution of the BD Method with iteration

Iteration number	Master solution	Primal solution	Dual solution
01.	X_1=25000, X_2=20000, X_3=20000, X_4=22000, X_5=18000, Master value: 394667.	X_6=35000, X_7=21000, X_8=20000, X_9=25000, X_{10}=20000; Primal value: 406137	$\lambda_1 = 20.8667, \lambda_2=\lambda_3=\lambda_4=\lambda_5=\lambda_6=\lambda_7=\lambda_8=0$; Dual value 638520
02.	X_1=0, X_2=16000, X_3=20000, X_4=22000; Master value: 354757	X_5=18000, X_6=0, X_7=21000, X_8=20000, X_9=25000, X_{10}=11000; Primal value 386951	λ_1=14.327, λ_2=6.27,$\lambda_3=\lambda_4=\lambda_5=\lambda_6=\lambda_7=\lambda_8$=0; Dual value 563806.2
03.	X_1=0, X_2=20000, X_3=20000; Master value: 306075.265	X_4=22000, X_5=18000, X_6=0, X_7=21000, X_8=20000, X_9=25000, X_{10}=4218.3; Primal value 306075.558	λ_1=14.003, λ_2=0,$\lambda_3=\lambda_4=\lambda_5=\lambda_6=\lambda_7=\lambda_8$=0; Dual value 553891.8

Table 3.2 describes the estimated parameters after iteration-3 of the Master problem, primal and Dual problems. The results of Table 3.2 demonstrate that the solutions are almost identical; this means that the optimal solution is achieved**.**

The following Table 3.3 describes the comparison of the optimal results are obtained by the main problem and by BD method.

Table 3.3: Comparison of solution of main problem and BDM problem

Solution of main problem	**Solution of BDM**

X_1=0, X_2 = 20000, X_3 =20000, X_4 = 22000, X_5 = 18000, X_6 = 0, X_7 = 21000, X_8 = 20000, X_9 = 25000, X_{10} = 4218.3; objective z = 623195.5866	X_1=0, X_2 = 20000, X_3 =20000, X_4 = 22000, X_5 = 18000, X_6 = 0, X_7 = 21000, X_8 = 20000, X_9 = 25000, X_{10} = 4218.1; objective z = 623194.859

In the following Fig. 1.1 and Fig 1.2, show that relation among selling price, profit, and cost of numerous parameters. Fig1.1 shows that profit has negative influence with selling price. Fig 1.2 describes that labor and machine cost is very low in compare to raw materials cost.

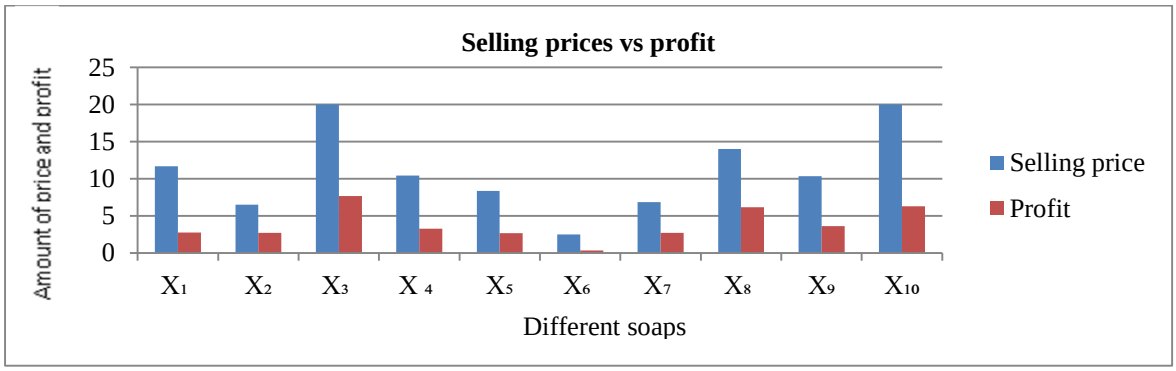

Fig 1.1: Selling price and profit

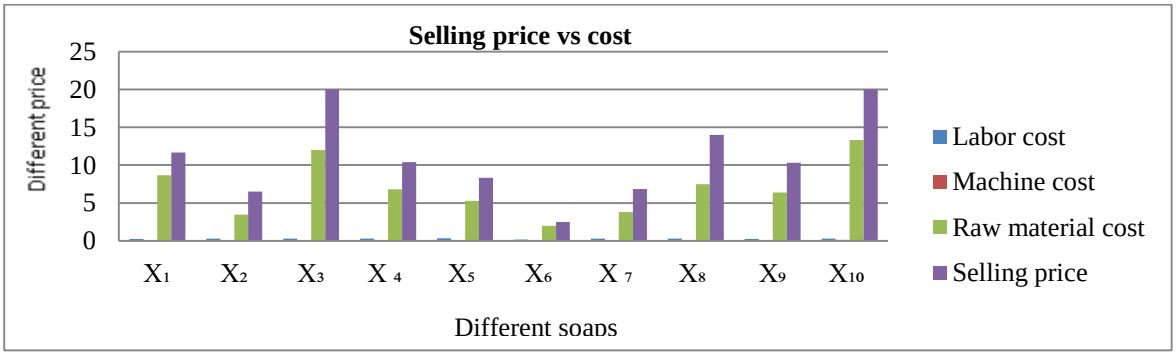

Fig 1.2: Selling price and cost

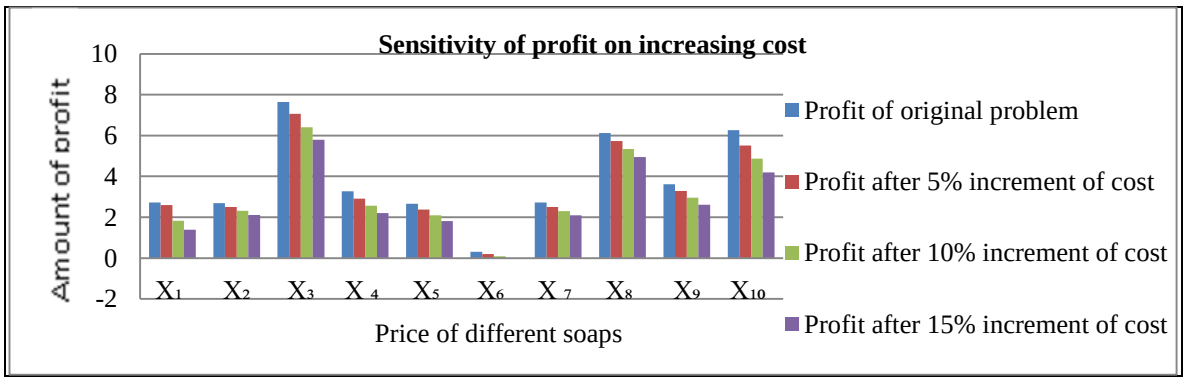

Fig1.3: Decreasing of profit by increasing cost parameters

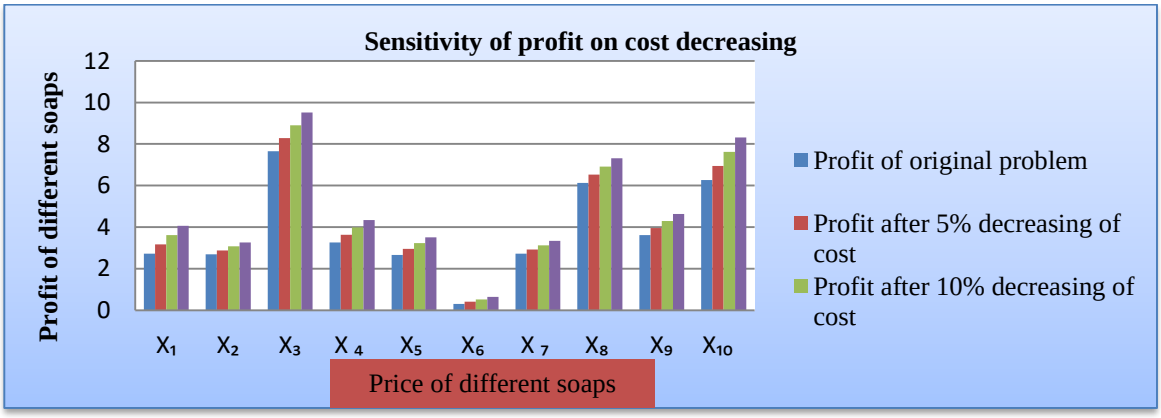

Fig 1.4: Increasing of profit by decreasing cost parameters

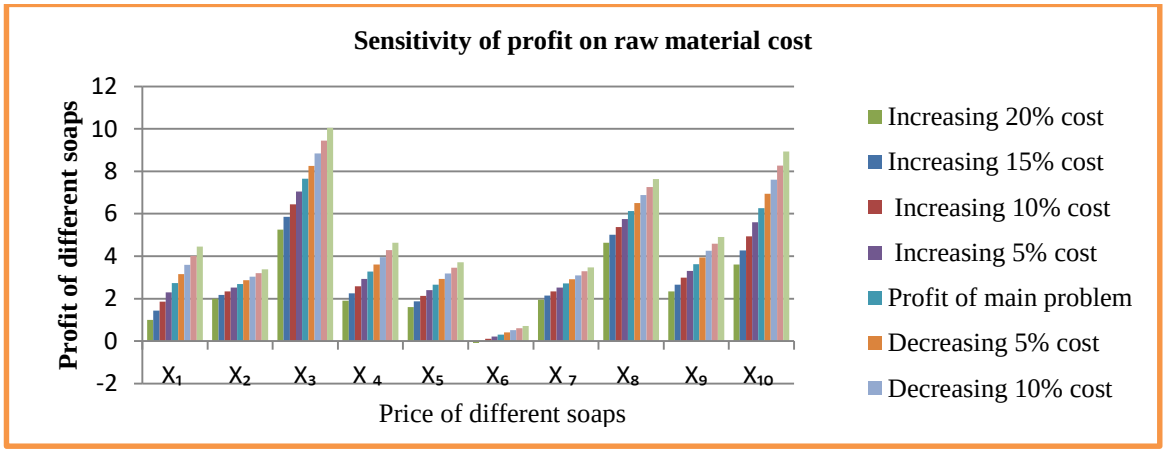

Fig 1.5: Profit analysis on raw material cost

In the Fig 1.3 and Fig 1.4 illustrate that all the cost parameters have significant effect of the profit. They demonstrate that how profit change if the cost parameters decrease. Further, if cost parameters decrease, then profit increase. From the Fig 1.5, it is shown that how profit changes if raw material cost changes. From the above Fig 1.5, if raw material cost increases profit decreases. Again, if the raw material cost decreases profit increases.Fig1.5 depicts the effects of raw materials cost on profit. Raw materials cost has significant influence on profit.

For the considered problem, the objective function is of maximization type and the objective function value gives the maximum profit. Here, the objective function value is 623195.5866. That means the maximum profit of the company is Tk 623195. From the result it is found that, 20000 unit of SornaliBati Soap, 20000 unit of Sornali Soap (2015), 22000 unit of Sornali Soap, 18000 unit of Mega Sornali Full Marka Soap, 0 unit of Mega Washing Powder (25g), 21000 unit of Mega Washing Powder (200g), 20000 unit of Mega Washing Powder (500g), 25000 unit of Mega Extra Washing Powder (200g), 4218 unit of Mega Extra Washing Powder (500g) are produced.

It is noticed from the result that, the production of product type one and six are zero. They are not so profitable. So, the company can stop to produce these two types of products. It is also noticed that production types three and ten are more profitable than other types of production. From sensitivity analysis, it has been found that if cost parameters increase by 5%, 10% and 15%, profit decrease. If cost parameters are decreased by 5%, 10%, 15% profit increase. It is also clear that labor cost and machine cost have not much effect on profit in the soap industry because labor cost and machine cost are very low in compare to other costs. Further, raw material

cost is very much effective on profit. From the sensitivity analysis, it is also clear that if raw material cost can be reduced profit will be increased. It is shown that a small change can affect the profit a lot.

So, if the government can reduce tax and vat on raw materials of soap industry that is imported from abroad, this sector will become more profitable for the businessmen. If these raw materials can be produced in our country, soap industry will be more profitable in future than before. This sector can increase our GDP. It will also be able to contribute a lot to our economy. From this data, the company can easily get a clear idea about their profit, production rate and selling procedures. The main aim of any company is to maximize their gain with minimum resources. In the case of this company, they can get best profit with minimum cost. Dual variable that is shadow prices help the company to assume their profit. Now it can be said that, if the company uses mathematical modelling technique and plans about its production according to the optimal solution, obtained by computer programming, they will get an accurate idea about the cost, production rate and profit.

4. Conclusion

In this paper it is shown that the maximization of profit of Mega Sorsnali Soap and Cosmetic Industries Ltd. BDM is used to maximize profit. After obtaining the optimal result sensitivity analysis is also used to see the changes of optimal result after changing cost parameters.

Here ten types of production from the selected company have been taken into consideration. Labor cost, machine cost and raw material cost have also been taken into consideration. Then using this data an LPP is formulated. In this LPP, objective function is to maximize profit. Labor cost, machine cost, raw material cost and other cost are considered as subject to constraints. Maximum production rate that the company gave us are also taken into consideration as subject to constraints. After that this LPP is solved in AMPL. Then this problem is solved by BDM. Both solutions gave the same result. After that sensitivity analysis is discussed. Sensitivity analysis helps the company to improve their business policy. In the sensitivity analysis, we have increased cost parameters by 5%, 10% and 15%. Then we have found that profits decrease. Similarly, we have decreased cost parameters by same percentage. In this case, it is found that profits increase. Both cases are shown in the Fig 1.3 and Fig 1.4. We know that labor cost is very low in our country. We have taken machine cost also very low. But raw material cost is very high. In the Fig1.5 it is shown that if the raw material cost can be reduced this sector becomes more profitable. Like this company, applying of mathematical programming can help the owners of business organization to take correct decisions. This can identify the future production patterns and outlook resulting in the establishment of new production units, while thinking for maximizing profit and minimizing the cost of the company.

When we want to collect data the industry owners did not want to disclose their real data. In this study, we have collected data from a single industry. Future study can be done by collecting data from more industries to get better result. In future some other cost parameters such as transportation cost can be included. In this paper, there is no discussion on shadow price. In future, anyone can work on it. In future this model can be used in other industries.

References

[1] Dantzig, G. B. and Wolfe, P., The Decomposition Algorithm for Linear Programming, *Econometrica*, 29(4): 767-778 (1961).

[2] Sweeny, D. J. and Murphy, R. A., A Method of Decomposition for Integer Programs, *Operation Research*, 27(6): 1128-1141 (1979).

[3] Benders, J. F., Partitioning Procedures for Solving Mixed-variables Programming Problems, *Numerische Mathematics*, 4(1): 238–252 (1962).

[4] Laporte, G., Nobert, Y. and Desrochers, M., Optimal Routing with Capacity and Distance Restrictions, *Operations Research*, 33: 1050–1073 (1985).

[5] Cai, X., McKinney, D. C., Lasdon, L. S. and Watkins, Jr. D.W., Solving Large Non Convex Water Resources Management Models Using Generalized Benders Decomposition, *Operations Research*, 49(2): 235–245 (2001).

[6] Andreas, A. K. and Smith, J. C., Decomposition Algorithms for The Design of ANonsimultaneous

Capacitated Evacuation Tree Network, networks, 53(2): 91–103 (2009).

[7] Uddin, M. F., Mondal, M. and Kazi, A. H., Vendor-Bayer coordination and supplychain optimization with Deterministic Demand Function, *Yugoslav Journal of Operation Research*, 26: 361-379 (2016).

[8] Taskin, Z. C., Smith, J. C. and Romeijn, H. E., Mixed-integer programming techniques for decomposing IMRT fluence maps using rectangular apertures, Technical report, Department of Industrial and Systems Engineering, University of Florida, Gainesville, FL, 2009.

[9] Applegate, D., Bixby, R., Chavatal, V. and Cook W., Implementing the Dantzig-Fulkerson-Johnson algorithm for large traveling salesman problems, *Mathematical Programming*, 97(1-2): 91-153 (2003).

[10] De Camargo, R.S., de Miranda, Jr. G. and Ferreira, R.P. M., A hybrid outer approximation/benders decomposition algorithm for the single allocation hub location problem under congestion, *Operations Research Letters*, 39(5): 329-337 (2011).

[11] Cordeau, J. F., Soumis F. and Desrosiers, J., A Benders' decomposition approaches for the locomotive and car assignment problem, *Transportation Science*, 34(2): 133-149 (2000).

[12] Akter, S, Linear Programming Problem Formulation and Solution using Benders Decomposition Method, M.Sc. Thesis, Bangladesh University of Engineering and Technology, (February 26, 2020).

GANIT

Available online at https://ganitjournal.bdmathsociety.org/

GANIT: Journal of Bangladesh Mathematical Society

GANIT *J. Bangladesh Math. Soc.* 41.2 (2021) 18–33
DOI: https://doi.org/10.3329/ganit.v41i2.57574

Performance Analysis of a Direct Absorption Solar Collector using Different Nanofluids: Effect of Physical Parameters

Salma Parvin*[a] , Abrar Islam[b] , and Afroza Nahar[c]

[a] *Department of Mathematics, Bangladesh University of Engineering and Technology, Dhaka 1000, Bangladesh*
[b] *Department of Chemical and Materials Engineering, University of Alberta, 9211 116 Street NW, Edmonton T6G 1H9, Alberta, Canada*
[c] *Department of Computer Science, American International University – Bangladesh, Dhaka 1229, Bangladesh*

ABSTRACT

Nanofluids have been used in direct absorption solar collectors (DASC) to enhance their performance, wherein contribution of entropy generation plays a decisive role. Among other factors, entropy generation is influenced including physical structure of the system and operation conditions. In this article, heat transfer and efficiency of a nanofluid based DASC considering the entropy generation has been performed for various physical alterations and operating conditions. Working nanofluids are chosen to Cu-water nanofluid, Al2O3-waternanofluid, TiO2-waternanofluid and water is chosen as base fluid. Solar irradiation value for the current analysis is considered 225W/m2 from the annual average solar irradiance range (215 W/m² in the north-west to 235 W/m² in the south-west per day) in Bangladesh according to UNDP report. Governing equations consisting of Navier–Stokes and energy equations are solved by Penalty finite element method with Galerkins weighted residual approach. Impact of parameters nanoparticle concentration and thickness of flow on isotherms, average output temperature, the average Nusselt number, collector efficiency, average entropy generation and Bejan number are discussed for all considered fluids. Results reveal that DASC system exhibits efficacy in heat transfer using 2% Cu nanoparticles under 225W/m2 irradiance, 0.015 kg/s mass flow rate and 0.015 m flow thickness. The outcomes will be supportive in designing DASC to attain improved heat transfer performance considering entropy generation.

Received: August 18, 2021 **Accepted:** November 11, 2021 **Published Online:** January 07, 2022

Keywords: DASC; nanofluid; solar irradiation heat transfer performance; flow depth; entropy.

AMS Subject Classification 2020: 76M10; 80M10; 80A19

1. Introduction

Energy demand is growing day by day, but fossil fuels are limited. Renewable energy sources, especially solar energy is considered as reliable source with very little ecological impact. The hourly incident solar flux

* Corresponding author: Salma Parvin, *E-mail address:* salpar@math.buet.ac.bd

on the earth's surface is greater than the global annual energy consumption [1]. However, the challenge is to efficiently harvest and convert the solar energy into the useful form. Solar collectors convert the solar energy into heat and flat-plate or evacuated-tube solar collectors are the commonly used devices in this regard. Recently, a new type of collector namely direct absorption solar collector (DASC) [2] have been developed that offer enhanced thermal efficiency.

However, the main drawback with DASC collectors is the poor absorption properties of conventional fluids used in these collectors. To solve this problem, researchers tried the use of nanofluids in DASC because of their improved thermal properties over the conventional fluids [3]. Heat transfer enhancement in solar devices is one of the key issues of energy saving and compact designs. An attempt had been made by Verma and Kundan [4] to experimentally investigate the variation in collector efficiency using nanofluids in a DASC. Parvin et al. [5] investigated the influence of Reynolds number and solid volume fraction of nanofluid in heat transfer through a nanofluid based direct absorption solar collector. Tyagi et al. [6] theoretically investigated the efficiency of a nanofluid-based direct absorption solar collector and compared it to the typical flat plate collector. Otanicar et al. [7] reported on the experimental results on solar collectors based on nanofluids where they demonstrated efficiency improvements of up to 5% in solar thermal collectors by utilizing nanofluids. Mahian et al. [8] made a review of the applications of nanofluids in solar energy. Two-phase (non-homogeneous) nanofluid approach towards the convection heat transfer within a wavy direct absorber solar collector is reported by Alsabery et al. [9].

All thermofluidic processes involve irreversibilities and therefore incur an efficiency loss. In practice, the extent of these irreversibilities can be measured by the entropy generation rate. In designing practical systems, it is desirable to minimize the rate of entropy generation to maximize the available energy. Bejan[10,11] studied on entropy generation minimization in order to minimize the irreversibility associated with convective heat transfer process. Mixed convection and entropy generation of Cu–water nanofluid in a cavity was numerically studied by Khorasanizadeh et al. [12]. They showed the influence of Reynolds number in enhancing heat transfer and minimizing entropy generation. Mohseni-Languri et al. [13] performed experimental study on energy and exergy of a solar thermal air collector. The rate of entropy generation increases as the irreversibility distribution ratio increase. Moreover, for given values of the irreversibility distribution ratio, the entropy generation rate is determined by the heat transfer irreversibility and/or fluid friction irreversibility.

Shahi et al. [14] investigated the entropy generation induced by natural convection heat transfer in a square cavity containing Cu-water nanofluid and a protruding heat source. Results showed that the Nusselt number increased and the entropy generation reduced as the nanoparticle volume fraction was increased. In addition, it was shown that the heat transfer performance could be maximized, and the entropy generation minimized by positioning the heat source on the lower cavity wall. Esmaeilpour and Abdollahzadeh [15] examined the natural convection heat transfer behavior and entropy generation rate in a Cu-water nanofluid-filled cavity comprising two vertical wavy surfaces with different temperatures and two horizontal flat surfaces with thermal insulation. The results showed that the mean Nusselt number and entropy generation rate both decreased as the volume fraction of nanoparticles increased. It was also shown that the mean Nusselt number and rate of entropy generation both increased with an increasing Grashof number but decreased with an increasing surface amplitude.

Cho et al. [16] investigated the natural convection heat transfer performance and entropy generation rate in a water-based nanofluid-filled cavity bounded by a left wavy-wall with a constant heat flux, a right wavy-wall with a constant low temperature, and flat upper and lower walls with adiabatic conditions. Results showed that the mean Nusselt number increased and the entropy generation rate decreased as the volume fraction of nanoparticles increased. Also, it was shown that the mean Nusselt number could be maximized and the entropy generation minimized by carefully controlling the geometry parameters of the two wavy surfaces.

It may be mentioned here that, several researchers like Karami et al. [17], Tahereh et al. [18] and Goel et al. [19] focused mainly on first-law efficiency of the nanofluid based direct absorption solar collector without

considering entropy generation. Parvin et al. [20], Parvin and Alim [21] incorporated entropy production and irreversibility issue in analyzing the performance as functions of solar irradiance and mass flow rate.

Recently, Kumar et al. [22] reported that gold nanoparticles (Au-NPs) seeded plasmonic nanofluids (PNFs) have shown promising results in overall performance enhancement of direct absorption solar collector (DASC) due to localized surface plasmon resonance (LSPR) effect. On the other hand, to achieve high-efficiency photo-thermal conversion Guo et al. [23] introduced optical fiber as interior light source in a DASC to boost photo-thermal conversion performance of MWCNT-H2O nanofluids. Authors reported an accomplishment of 64.5% photo-conversion efficiency for 0.010 wt% MWCNT and the optical fiber location of 15 mm.

Based on the above literature, it can be concluded that though entropy generation has been considered by few researchers in evaluating nanofluid-based DASC collector efficiency, effect of physical changes with operating conditions is not focused that much. Hence, there is a need to evaluate the effect of physical diversities and operating conditions on the performance of DASCs. In this regard, an attempt has been made to numerically simulate fluid flow, heat transfer and entropy generation behaviors through a direct-absorption solar collector with the variation of thickness of flow (D) and solid volume fraction (ϕ) of nanoparticles for various nanofluids and water under the solar irradiation value 225W/m2 taken from the annual average solar irradiance range in Bangladesh [24]. Results are presented in terms of isotherm distribution, average output temperature, mean Nusselt number, collector efficiency, rate of entropy generation, and Bejan number.

2. Problem formulation

a. Geometric modeling

Fig. 1 shows the geometry of the direct absorption solar collector filled with nanofluid. The fluid is enclosed within the space between the glass cover and the insulated bottom surface of the DASC. Two-dimensional heat transfer analysis is considered for the nanofluid in the DASC with computational domain of surface area, length and height of A, L and D respectively in which direct sunlight is incident on a thin glass cover and the incident solar flux pass through it. The ratios of dimensions of the collector are chosen according to the experimental setup of Verma and Kundan [4]. Four different fluids; Cu-water nanofluid, Al2O3-waternanofluid, TiO_2-waternanofluid and water are utilized as the heat transfer medium. The inlet temperature and velocity of the fluid are T_{in} and U_{in} respectively. The bottom wall is insulated, i.e., no heat flux can pass through it. This assumption is based on the case when the bottom surface is highly insulating. In order to model the heat transfer characteristics, the top surface is assumed to be exposed to the ambient atmosphere that loses heat through convection.

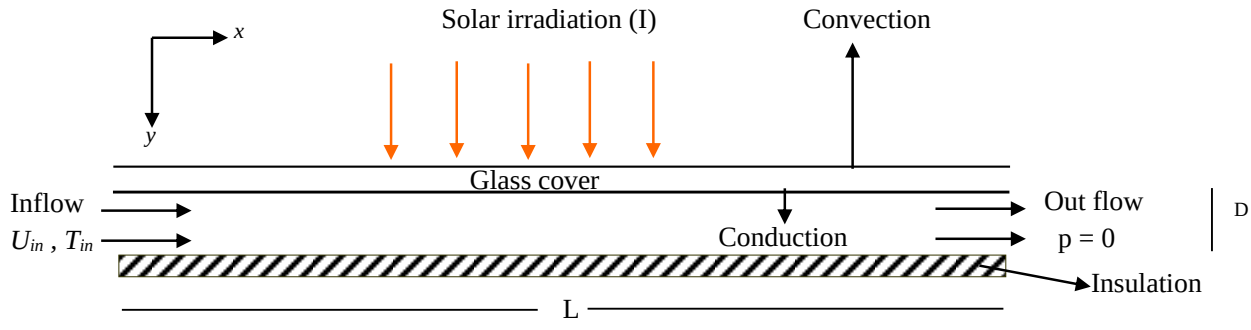

Fig. 1. Geometry of the computational domain of the DASC

b. Thermo-physical properties

In the present study, a comparative heat transfer performance analysis of a DASC system has been performed for base fluid water and, nanofluids Cu-water, Al2O3-water and TiO2.Table 1 gives the thermo-physical properties of water and the nanoparticles [25].

Table 1: Thermo physical properties of fluid and nanoparticles at 300K

Physical Properties	Fluid phase (Water)	Cu Copper	Al_2O_3 Alumina	TiO_2 Titania
C_p(J/kgK)	4179	385	765	686.2
ρ (kg/m^3)	997.1	8933	3970	4250
k (W/mK)	0.613	400	40	8.9538
β (/K)	21×10^{-5}	5.1×10^{-5}	2.4×10^{-5}	2.4×10^{-5}

c. Mathematical modeling

The nanofluid flow is assumed to be laminar and incompressible. Water and nanoparticles are taken in thermal equilibrium and no slip occurs between them. Boussinesq approximation is used for the density variation of the nanofluid. Only steady state case is considered. The governing equations for the flow throughout a direct absorption solar collector in terms of the Navier-Stokes and energy equations are given as:

Continuity equation:

$$\frac{\partial u}{\partial x}+\frac{\partial v}{\partial y}=0 \tag{1}$$

x-momentum equation:

$$\rho_{nf}\left(u\frac{\partial u}{\partial x}+v\frac{\partial u}{\partial y}\right)=-\frac{\partial p}{\partial x}+\mu_{nf}\left(\frac{\partial^2 u}{\partial x^2}+\frac{\partial^2 u}{\partial y^2}\right) \tag{2}$$

y-momentum equation:

$$\rho_{nf}\left(u\frac{\partial v}{\partial x}+v\frac{\partial v}{\partial y}\right)=-\frac{\partial p}{\partial y}+\mu_{nf}\left(\frac{\partial^2 v}{\partial x^2}+\frac{\partial^2 v}{\partial y^2}\right) \tag{3}$$

Energy equation:

$$u\frac{\partial T}{\partial x}+v\frac{\partial T}{\partial y}=\alpha_{nf}\left(\frac{\partial^2 T}{\partial x^2}+\frac{\partial^2 T}{\partial y^2}\right)-\left(\frac{1}{\rho C_p}\right)_{nf}\frac{\partial q_r}{\partial y} \tag{4}$$

The energy equation is coupled to the Radiative Transport Equation (RTE)[5]through the divergence of the radiative flux $\frac{\partial q_r}{\partial y}=\int_{\lambda}K_{e\lambda}\tau I_{\lambda}d\lambda$.

Also, $\rho_{nf}=(1-\phi)\rho_f+\phi\rho_s$ is the density,

$(\rho C_p)_{nf}=(1-\phi)(\rho C_p)_f+\phi(\rho C_p)_s$ is the heat capacitance,

$\alpha_{nf} = k_{nf} \big/ \left(\rho C_p\right)_{nf}$ is the thermal diffusivity,

In the current study, the viscosity of the nanofluid is considered by the Pak and Cho correlation [26]. This correlation is given as

$$\mu_{nf} = \mu_f \left(1 + 39.11\phi + 533.9\phi^2\right) \tag{5}$$

and the thermal conductivity of Maxwell Garnett (MG) model [27] is

$$k_{nf} = k_f \frac{k_s + 2k_f - 2\phi\left(k_f - k_s\right)}{k_s + 2k_f + \phi\left(k_f - k_s\right)} \tag{6}$$

The boundary conditions are:

at all solid boundaries: $u = v = 0$

at the top surface: inward heat flux per unit area $k_{nf} \dfrac{\partial T}{\partial Y} = q = h_{conv}\left(T_{col} - T_{amb}\right)$

at the left inlet: $T = T_{in}$ $u = U_{in}$

at the outlet boundary: convective boundary condition $p = 0$

at the bottom surface: $\dfrac{\partial T}{\partial y} = 0$

d. Average Nusselt number

The average Nusselt number (Nu) is expected to depend on several factors such as thermal conductivity, heat capacitance, viscosity, flow structure of nanofluids, volume fraction, dimensions and fractal distributions of nanoparticles. The form of local heat transfer rate at the top surface is:

$$\overline{Nu} = -\frac{k_{nf}}{k_f}\frac{\partial T}{\partial y} \tag{7}$$

By integrating the local Nusselt number over the top heated surface, the average heat transfer rate along the top surface of the collector can be written as:

$$Nu = \int_0^L \overline{Nu}\ dx \tag{8}$$

e. Entropy generation

The average entropy generation, S for the entire computational domain is as follows:

$$S = \frac{1}{\overline{V}} \int S_{gen}\, d\overline{V} = S_{gen,h,m} + S_{gen,v,m} \tag{9}$$

where $\overline{V}$ is the volume occupied by the nanofluid and $S_{gen,h,m}$ and $S_{gen,v,m}$ are the average entropy generation for heat transfer and viscous effect respectively [5].

The Bejan number Be, defined as the ratio between the entropy generation due to heat transfer by the total entropy generation, is expressed as:

$$Be = \frac{S_{gen,h,m}}{S} \tag{10}$$

It is known that the heat transfer irreversibility is dominant when Be approaches to 1. When Be becomes much smaller than 1/2 the irreversibility due to the viscous effects dominates the processes and if Be = 1/2 the entropy generation due to the viscous effects and the heat transfer effects are equal [14].

f. Collector efficiency

A measure of a collector performance is the collector efficiency (η) defined as the ratio of the useful energy gain to the incident solar energy which can be written as:

$$\eta = \frac{\text{useful gain}}{\text{available energy}} = \frac{mC_p\left(T_{out} - T_{in}\right)}{AI} \tag{11}$$

where m is the mass flow rate of the fluid flowing through the collector; C_p is the specific heat at constant pressure and T_{in} and T_{out} are the inlet and outlet fluid temperatures, respectively.

3. Methodology

Penalty finite element method (FEM) [28] is used to solve the nonlinear governing equations along with boundary conditions for the considered problem. Due to mass conservation the continuity equation of has been used as a constraint to find the pressure distribution. Eqs. (1) - (4) are solved by the finite element method, where the pressure p is eliminated by a constraint. For large values of this constraint, the equation of continuity is automatically satisfied. Then the velocity components (u, v) and temperature (T) are expanded by means of a basis set. The Galerkin's finite element technique yields the subsequent nonlinear residual equations. The integrals in these equations are evaluated employing three points Gaussian quadrature method. The non-linear residual equations are solved using Newton–Raphson method to determine the coefficients of the expansions. The convergence of solutions is assumed once the relative error for every variable between successive iterations is recorded below the convergence criterion $\left|\psi^{n+1} - \psi^{n}\right| \le 10^{-4}$, where n is the number of iteration and ψ is any function of u, v and T.

a. Discretization

In the FEM, mesh generation is the procedure to subdivide a domain into a set of sub-domains, named finite elements, control volume, etc. The discrete locations are defined by the numerical grid, at which the variables are to be calculated. It is principally a discrete representation of the computational domain on which the problem is to be solved. Fig. 2 displays the finite element mesh of the present physical domain. Physics controlled mesh is created for the model where free triangular element with unstructured grid is used for discretization.

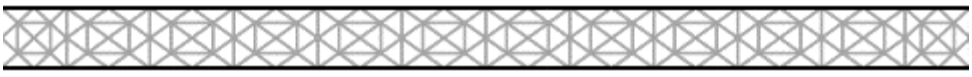

Fig. 2. Discretization of the computational domain

b. Grid independent test

A wide-ranging mesh testing process is carried out to guarantee a grid-independent solution at I = 225 W/m^2, m = 0.15kg/s, D = 0.015m and ϕ = 2% in a DASC. In the present work, five different non-uniform grid systems with the following number of elements within the resolution field: 48, 192, 768, 1616 and 3072 are examined. The numerical method is performed for the values of average Nusselt number for water-Cu nanofluid as well as base for the abovementioned elements to develop a perceptive of the grid fineness as shown in Table 2 and Fig. 3. The scale of the average Nusselt numbers for nanofluid and base fluid for 1616 elements shows a little difference with the results obtained for the more elements. Hence, the non-uniform grid system of 1616 elements are chosen for the whole numerical computation.

Table 2: Grid sensitivity test at I= 225 W/m^2, m= 0.15kg/s, D =0.015m and ϕ = 2%

Nodes (elements)	407 (48)	1434 (192)	5360 (768)	9484 (1616)	20700 (3072)
Nu(nanofluid)	2.40051	2.89143	3.30279	3.582503	3.609242
Nu(base fluid)	1.30253	1.61958	1.93253	2.13084	2.15753
Time (s)	126.265	312.594	398.157	481.328	929.377

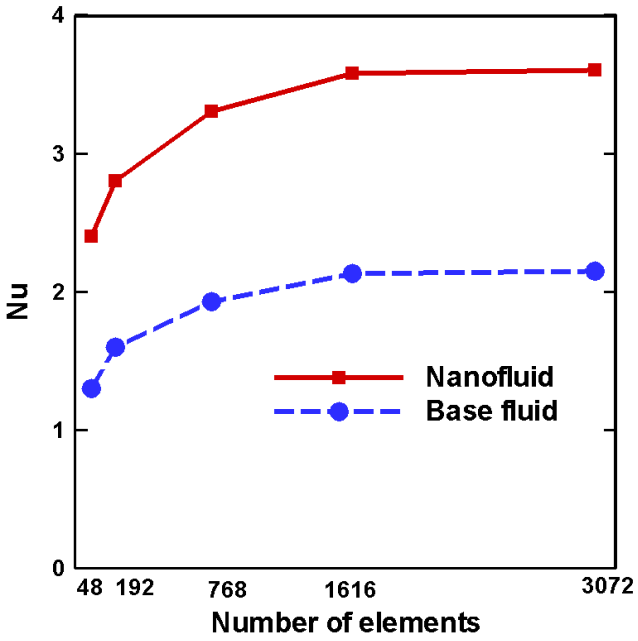

Fig. 3. Grid independence analysis

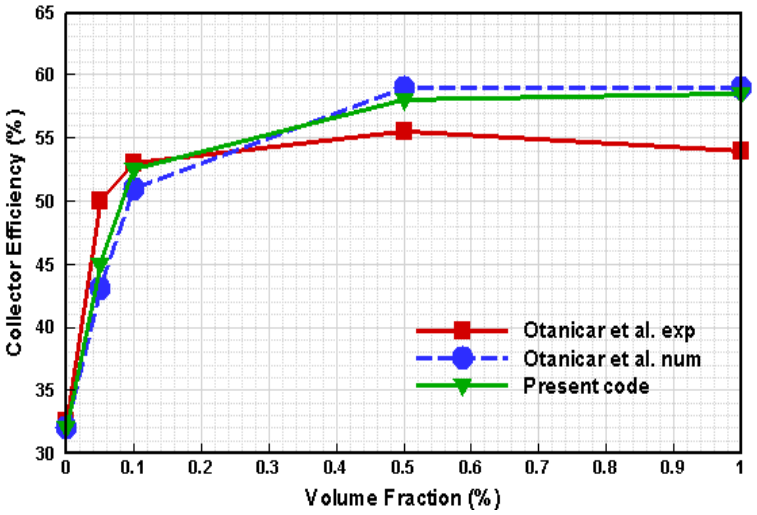

Fig. 4. Comparison of collector efficiency between present code and Otanicar et al. [7] at I = 1000 W/m^2

c. Validation

The present numerical procedure is validated with the graphical representation of Otanicar et al. [7] for collector efficiency (%) versus volume fraction (%) of water/graphite nanofluid of 30 nm spherical graphite nanoparticles. The validation was carried out in a direct absorption solar thermal collector at irradiation level I = 1000 W/m^{2}and mass flow rate=42 ml/h, respectively, which are used in [7] for modelling and experiment. Fig. 4 exhibits very good agreement of the numerical results obtained in present work with those reported by Otanicar et al. [7] for the above stated condition.

4. Results and Discussion

Numerical simulation has been carried out to display the outcomes in terms of isotherms, average temperatures at the outlet, average Nusselt number, percentage of collector efficiency, mean entropy generation and Bejan number for different values of parameters flow thickness and solid volume fraction for a DASC filled with various nanofluids. The considered values of flow thickness are D = 0.012, 0.015, 0.018, 0.02 m and solid volume fraction are ϕ = 0%, 1%, 2%, 3% and 4%. Three different nanofluids; Cu-water, Al_2O_3-water and TiO_2-water are used in addition to the base fluid water. Irradiation I = 225 W/m^2 and mass flow rate m = 0.015 kg/s are found to me most effective in transferring heat and have been chosen for this simulation.

a. Effect of solid volume fraction

Fig. 5 (a) - (d) stands for the effect of solid volume fraction ϕ on the thermal fields. The values of ϕ varies from 0% to 3%. Isotherms are almost like the active parts for water-copper nanofluid. The temperature distributions show that due to escalating values of ϕ, the maximum temperature in the domain rises which results an enhancement in the overall heat transfer. This effect can be accredited to the dominance of the thermal conductivity property. It is worth noting that as the values of ϕ increase, the rate of increment is notable up to the solid volume fraction 2%.

The average outlet temperature, average Nusselt number and collector efficiency for various ϕ are exhibited in Fig. 6 (a)-(c). Different nanofluids and pure water are tested. Parabolic profiles are seen for ϕ versus the average outlet temperature, average heat transfer rate and collector efficiency for all nanofluids. Like profiles are observed in all three figures. Output temperature, heat transfer rate and collector efficiency rise for raising the values of ϕ from 0% to 2% then these values increase at a very slow rate and become

independent of ϕ for ϕ > 3%.This occurs due to the fact that for higher concentration of nanoparticles, sedimentation in the fluid starts and movement of the fluid becomes slower which reduces the heat transport process and consequently the efficiency of the collector.

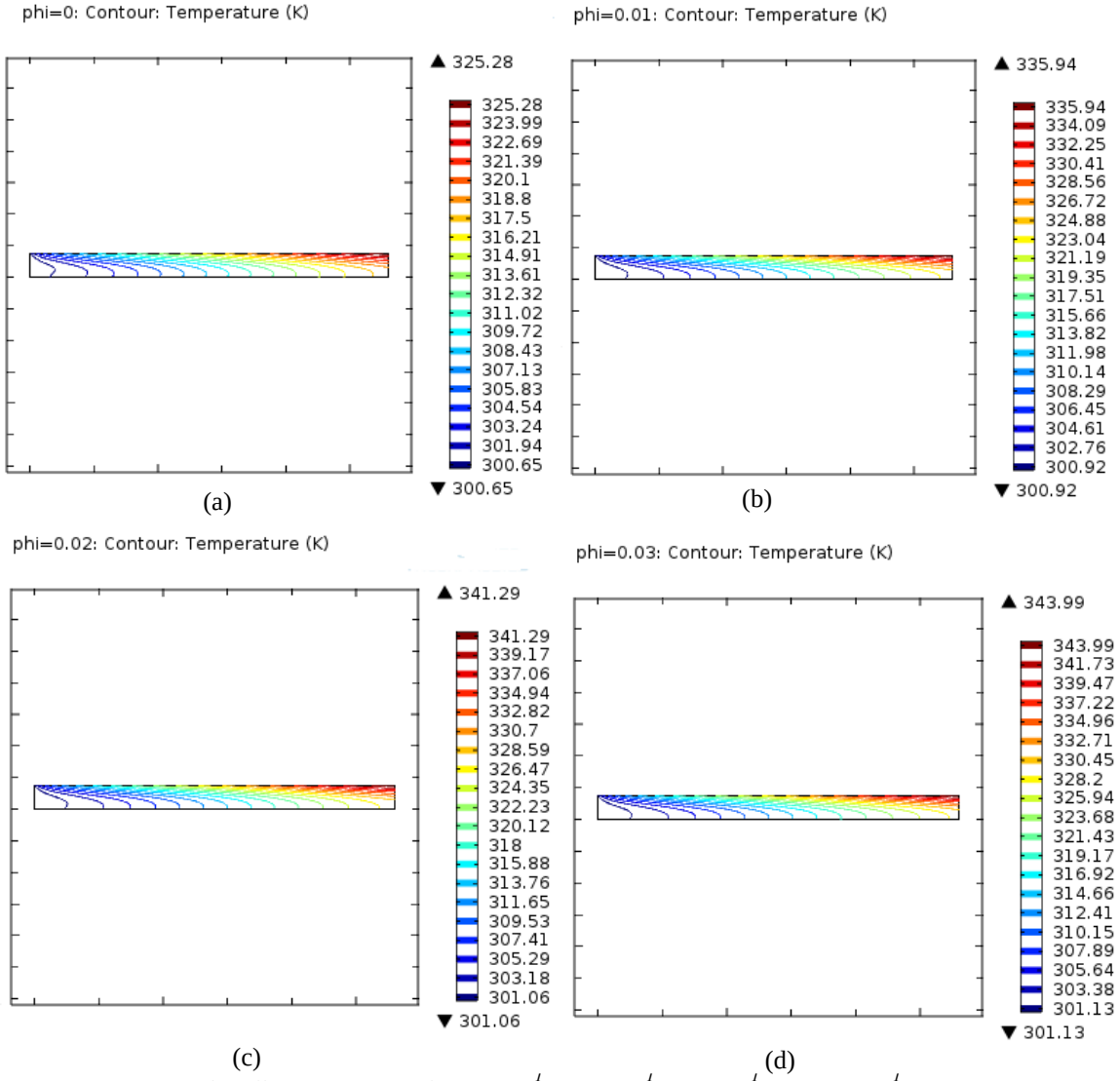

Fig. 5. Isothermal contours for different solid volume fraction (a) ϕ = 0%, (b) ϕ = 1%, (c) ϕ = 2%, and (d) ϕ = 3% with I = 225 (W/m^2), m = 0.015 (kg/s) and D = 0.015(m) for Cu-water nanofluid.

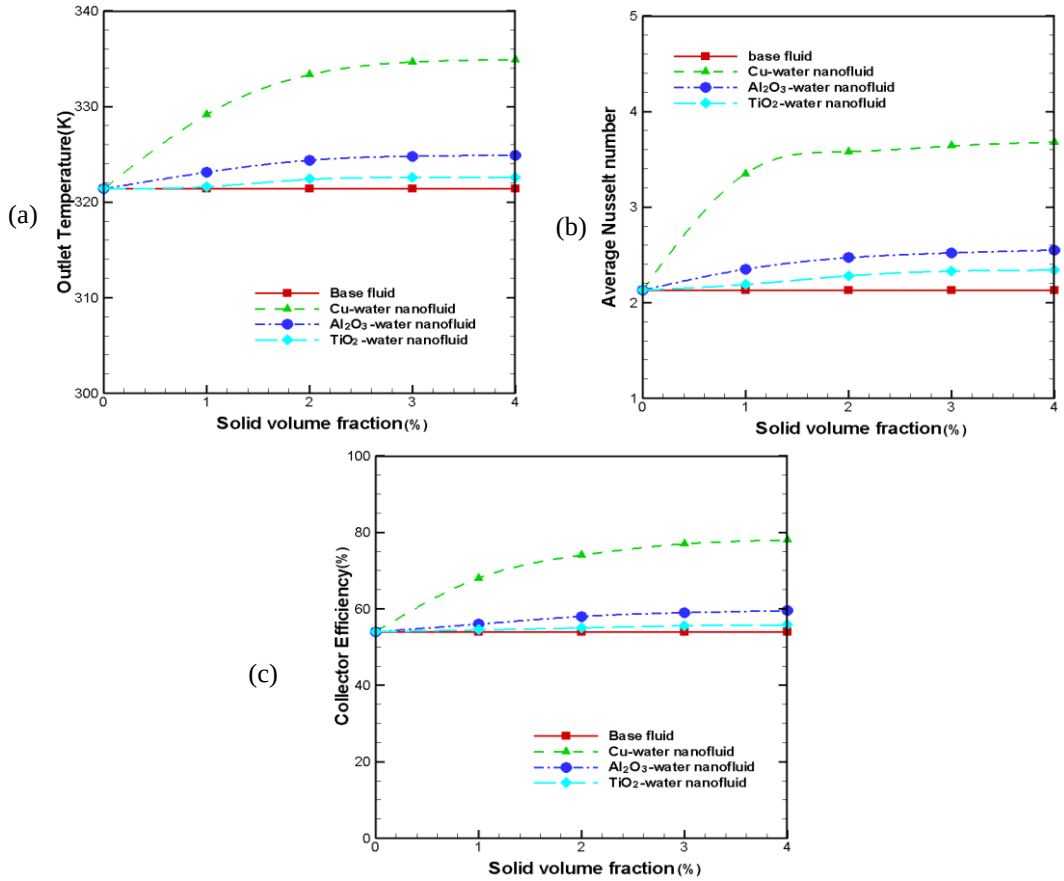

Fig. 6. Effect of solid volume fraction on (a) average output temperature, (b) Average Nusselt number and (c) collector efficiency with I = 225 (W/m^2), m = 0.015 (kg/s) and D = 0.015(m) for different nanofluid as well as base fluid.

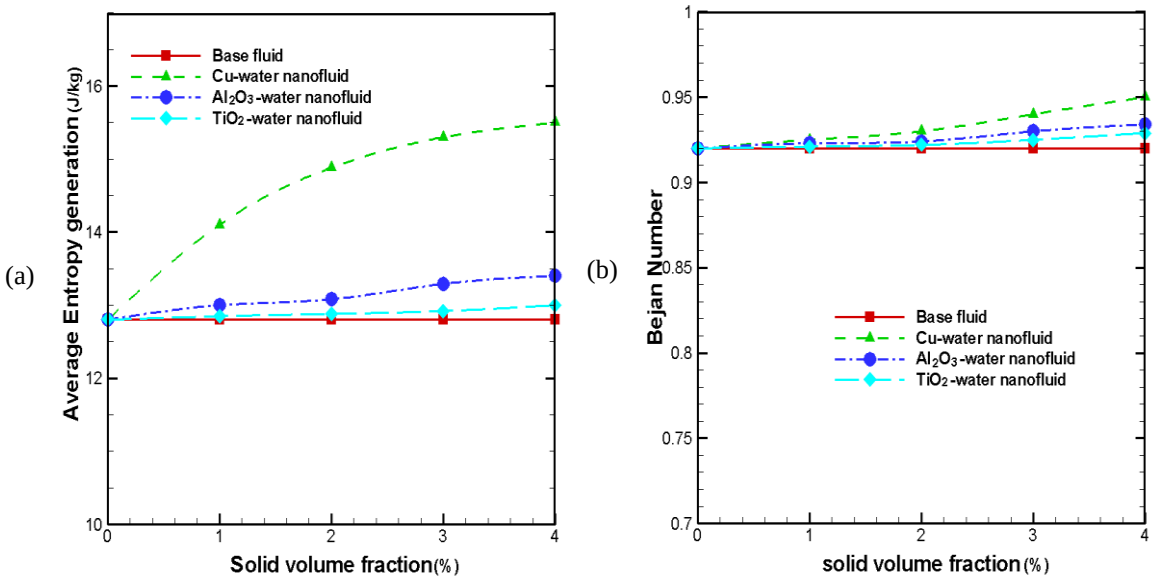

Fig. 7. Effect of solid volume fraction on (a) average entropy generation and (b) Bejan number with I = 225 (W/m^2), m = 0.015 (kg/s) and D = 0.015(m) for different nanofluid as well as base fluid.

Fig 7 (a)-(b) depicts the effects of nanoparticle concentration on entropy generation and Bejan number for various nanofluid and base fluid. The entropy generation rises as the nanoparticle concentration rises. Entropy production has the similar effect as the heat transfer for growing values of solid volume fraction. From the Bejan number versus ϕ picture, it is clearly seen that entropy generation occurs due to the dominant heat transfer effect and this effect becomes larger corresponding to upper ϕ values.

b. Effect of flow thickness

The influence of depth of fluid in a DASC for four different values; D = (0.012, 0.015, 0.018, 0.02) [m] on isothermal contours are exposed in Fig. 8 (a)-(d). From the figure, it is observed that larger flow thickness cannot always raise the temperature. For the calculated values, flow depth of 0.015 [m] is found to give the maximum temperature. Fluid mass becomes greater with escalating the flow depth. That is larger amount of fluid also collects the same amount of heat and transmits though the larger domain. Thus, maximum temperature falls after a certain depth of flow.

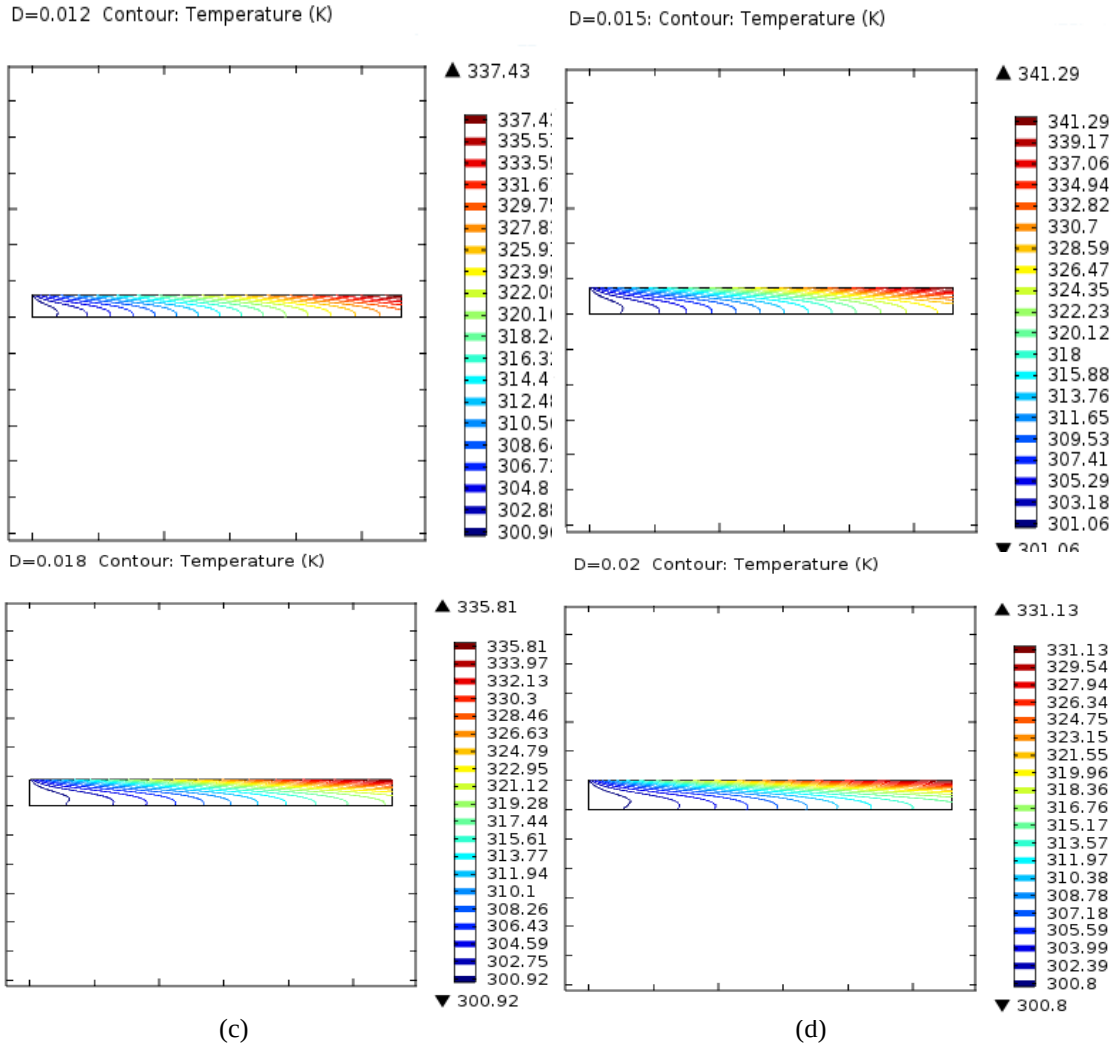

Fig. 8. Isothermal contours for different flow thickness (a) D = 0.012(m), (b) D = 0.015(m), (c) D = 0.018(m), and (d) D = 0.02(m), with ϕ = 2%, m = 0.015 (kg/s) and I = 225 (W/m^2) for Cu-water nanofluid.

Fig. 9 (a)-(c) demonstrates how the distance between the upper and lower surface affects the average

temperature of the outlet, average heat transfer rate and collector efficiency for various nanofluid and base fluid. The 2% concentration is preferred for the nanofluids. The average outlet temperature, average heat transfer rate and collector efficiency for all nanofluid and base fluid slightly increase as the value of D increase from 0.012[m] to 0.015[m]and after that they devalues monotonically with deeper flow. The reason behind this is the deeper flow correspond to larger fluid mass cannot transport more amount of heat from the upper surface. Therefore, collector efficiency cannot be enhanced by choosing greater flow thickness. Similar phenomena are observed for all the considered fluids. However, the Cu-water nanofluid is found to be most effective in enhancing the performance of the collector.

The effects of flow thickness on entropy generation and Bejan number for various nanofluid and water are plotted in Fig 10 (a)-(b). The entropy generation rises by the deepness of the flow. The enhancement of entropy production becomes slower for higher depth of flow. Although the heat transfer reduces for higher collector depth, but entropy production grows because viscosity plays a part here in escalation the entropy generation which is also explained from the Bejan number profile. The Bejan number profile shows the falling trend with larger flow depth. The entropy generation because of viscous term increasing but still heat transfer entropy is leading since the values of Bejan number is much higher than 0.5.

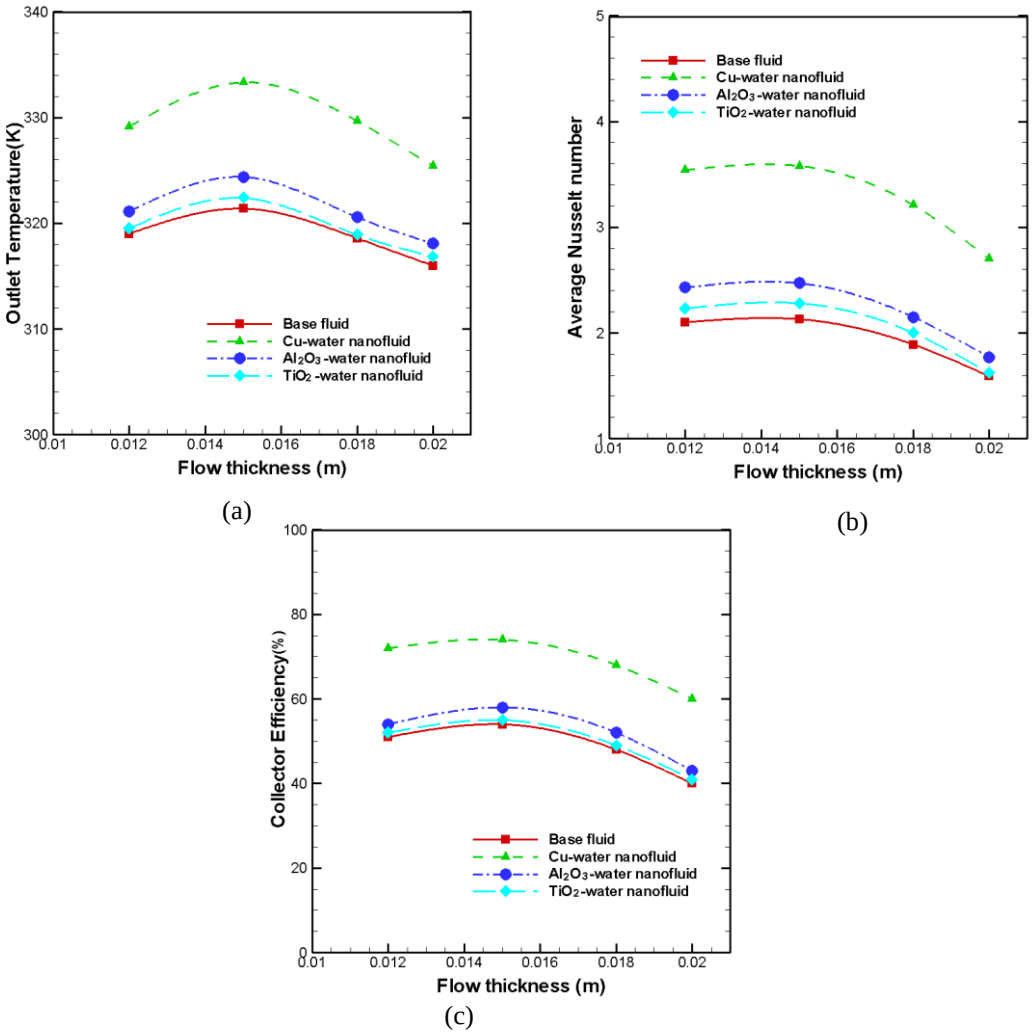

Fig. 9: Effect of flow thickness on (a) average output temperature, (b) Average Nusselt number and (c) collector efficiency with ϕ =

2%, I = 225 (W/m^2) and m = 0.015 (kg/s) for different nanofluid as well as base fluid.

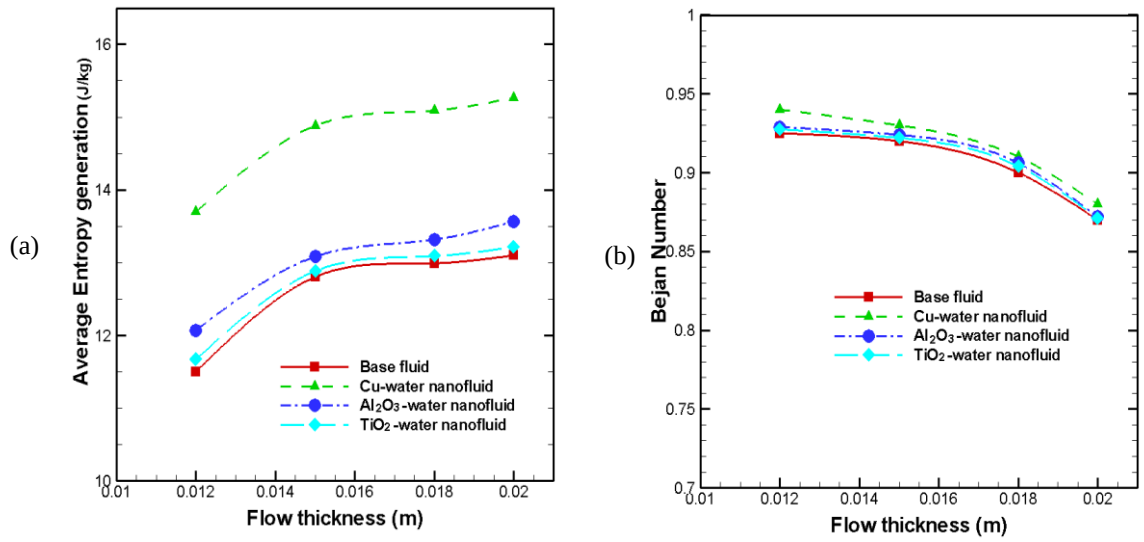

Fig. 10: Effect of flow thickness on (a) average entropy generation and (b) Bejan number with ϕ = 2%, I = 225 (W/m^2) and m = 0.015 (kg/s) for different nanofluidas well as base fluid.

5. Conclusions

In the present article, heat transfer performance of a nanofluid based DASC system has been investigated considering entropy generation under diverse physical orientations and operating conditions. Effect of different combinations of parameters has been examined to observe the output temperature variation. Besides, heat transfer rate, collector efficiency, average entropy generation and Bejan number of the working fluids have been evaluated.
The following inferences are drawn from the present research:

- The isotherms inside the solar collector are remarkably influenced by nanoparticle concentration and depth of flow.
- Rate of heat transfer and efficiency enhances significantly for raising the fluid layer height up to 0.015m. Further increase in fluid layer will lower the average Nusselt number and collector efficiency.
- Higher heat transport and efficiency are observed for nanofluids than the base fluid. Cu- water gives superior efficiency than Al_2O_3- water and TiO_2- water nanofluid.
- Mean entropy generation is obtained higher for rising values of all parameters.
- Bejan number approaches to 1 for the variation of all the parameters. That is the entropy production occurs mainly due to the heat transfer irreversibility though for higher flow thickness, the fluid friction irreversibility tends to rise.

- The nanofluid containing 2% Cu nanoparticles with combination of the solar irradiation 225W/m^2, mass flow rate 0.015 kg/s and flow thickness 0.015m are established to be most effective in enhancing heat transfer rate and collector efficiency.

It is concluded that higher efficiency of the collector can be obtained by making proper combination of parameters in order to minimize the entropy generation and enhance the heat transfer rate simultaneously.

Nomenclature

A	surface area of the collector (m^2)
Be	Bejan number
C_p	specific heat at constant pressure (J kg^{-1} K^{-1})
D	depth of the fluid (m)
h	local heat transfer coefficient (Wm^{-2}K^{-1})
I	intensity of solar radiation (Wm^{-2})
k	thermal conductivity (W m^{-1}K^{-1})
L	length of the collector (m)
m	mass flow rate (kgs^{-1})
Nu	Nusselt number
q	heat flux (Wm^{-2})
q_r	radiative heat flux (Wm^{-2})
T	temperature (K)
u, v	x and y components of velocity (ms^{-1})
U	fluid velocity (ms^{-1})
x, y	dimensional co-ordinates (m)

Greek symbols

α	fluid thermal diffusivity (m^{2}s^{-1})
ϕ	nanoparticles volume fraction
η	collector efficiency (%)
ρ	density (kgm^{-3})
μ	dynamic viscosity (kgm^{-1}s^{-1})

Subscripts

f	fluid
nf	nanofluid
in	input
out	output
s	solid particle

Conflict of Interests

The authors declare no conflict of interest with any person or agency regarding the content of this article.

Acknowledgements

This research has been conducted in the Department of Mathematics, Bangladesh University of Engineering & Technology (BUET), Dhaka and is supported by the Research Support and Publications Division, UGC, 29/1 Agargaon, Dhaka 1207, Bangladesh.

Funding

Research Support and Publications Division, University Grants Commission (UGC), Bangladesh.

References

[1] Garg, H.P, Prakash, J, Solar energy fundamental and applications, Tata McGraw Hill, New Delhi(1997).

[2] Taylor A.R, Phelan E.P, Otanicar P.T, Walker A.C, Nguyen M., Trimble S, Ravi P, Applicability of nanofluids in high flux solar collectors, *International Journal of Renewable and Sustainable Energy*, 3: 023104 (2011).

[3] Taylor, A.R., Phelan, E.P., Otanicar, P.T, Adrian, R., Prasher, R., Nanofluid optical property characterization: towards efficient direct absorption solar collectors, *Nanoscale Research Letters*, 6: 225 (2011).

[4] Verma, V., Kundan, L., Thermal performance evaluation of a Direct Absorption Flat Plate Solar Collector (DASC) using Al_2O_3-H_2O based nanofluids,*IOSR Journal of Mechanical and Civil Engineering*, 6 (2): 29-35, (2013).

[5] Parvin, S., Nasrin, R., Alim, M.A., Heat transfer and entropy generation through nanofluid filled direct absorption solar collector, *International Journal of Heat and Mass Transfer*, 71: 386–395 (2014).

[6] Tyagi, H., Phelan, P., Prasher,R., Predicted efficiency of a low-temperature nanofluid-based direct absorption solar collector, *Journal of Solar Energy Engineering*, 131 (4): 041004-041010(2009).

[7] Otanicar, T.P., Phelan, P.E., Prasher, R.S., Rosengarten, G. and Taylor, R.A., Nanofluid-based direct absorption solar collector, *Journal of Renewable and Sustainable Energy*, 2: 033102 (2010).

[8] Mahian, O., Kianifar, A., Kalogirou, S.A., Pop, I., Wongwises, S., A review of the applications of nanofluids in solar energy, *International Journal of Heat and Mass Transfer*, 57: 582–594 (2013).

[9] Alsabery, A.I.; Parvin, S.; Ghalambaz, M.; Chamkha, A.J.; Hashim, I. Convection Heat Transfer in 3D Wavy Direct Absorber Solar Collector Based on Two-Phase Nanofluid Approach. *Applied Science,10*: 7265 (2020).

[10] Bejan A. A study of entropy generation in fundamental convective heat transfer. *Journal of Heat Transfer-Transactions of the ASME,*101: 718-725 (1979).

[11] Bejan A. Entropy generation minimization: the method of thermodynamic optimization of finite-size systems and finite-time processes. Boca Raton:CRC Press, Florida, USA (1996).

[12] Khorasanizadeh H, Nikfar M, Amani J. Entropy generation of Cu–water nanofluid mixed convection in a cavity. *European Journal Mechanics B-Fluid*, 37: 143–152 (2013).

[13] Mohseni-Languri, E., Taherian, H., Masoodi, R. and Reisel, J.R. An energy and exergy study of a solarthermal air collector, *Thermal Sciences*, 13(1): 205-216 (2009).

[14] Shahi M, Mahmoudi AH, Raouf AH. Entropy generation due to natural convection cooling of a nanofluid. *International Communications in Heat and Mass Transfer*, 38: 972-983 (2011).

[15] Esmaeilpour M, Abdollahzadeh M. Free convection and entropy generation of nanofluid inside an enclosure with different patterns of vertical wavy walls. *International Journal of Thermal Sciences*, 52: 127-136 (2012).

[16] Cho CC, Chen CL, Chen CK. Natural convection heat transfer and entropy generation in wavy-wall enclosure containing water-based nanofluid. *International Journal of Heat and Mass Transfer*, 61: 749-758 (2012).

[17] Karami, M., Akhavan-Bahabadi, M.A.,Delfani, S., Raisee, M., Experimental investigation of CuOnanofluid-based Direct Absorption Solar Collector for residential applications, *Renewable and Sustainable Energy Reviews*, 52: 793–801 (2015).

[18] Tahereh B. Gorji , A.A. Ranjbar, A review on optical properties and application of nanofluids in direct absorption solar collectors (DASCs), *Renewable and Sustainable Energy Reviews*, 72(C):10-32 (2017).

[19] Goel N., Taylor R.A., Otanicar T., A review of nanofluid-based direct absorption solar collectors: Design considerations and experiments with hybrid PV/Thermal and direct steam generation collectors, *Renewable Energy*, 145: 903-913, 2020.

[20] Parvin S., Ahmed M. S., Chowdhury R.,Effect of Solar Irradiation and Mass Flow Rate on Forced Convective Heat Transfer through a Nanofluid-Based Direct Absorption Solar Collector, *AIP Conference Proceedings* 1851: 020067 (2017).doi: 10.1063/1.4984696.

[21] Parvin S., and Alim M.A., Influence of Mass Flow Rate on Forced Convective Heat Transfer through a Nanofluid Filled Direct Absorption Solar Collector, *International Journal of Mechanical and Mechatronics Engineering*, 11(6)(2017).

[22] Kumar, Sanjay & Sharma, Vipin &Samantaray, Manas R. & Chander, Nikhil, Experimental investigation of a direct absorption solar collector using ultra stable gold plasmonic nanofluid under real outdoor conditions, *Renewable Energy*, 162(C): 1958-1969 (2020).

[23] Guo, C., Liu, C., Jiao, S., Wang, R., Rao, Z., Introducing optical fiber as internal light source into direct absorption solar collector for enhancing photo-thermal conversion performance of MWCNT-H_2O nanofluids. *Applied Thermal Engineering*, 173: 115207 (2020).

[24] David Mengen & Firoz Aaron,Solar Irradiance Measuring sites in Bangladesh, SrepGen Projects Report of UNDP (2018).

[25] Ogut, E.B., Natural convection of water-based nanofluids in an inclined enclosure with a heat source, Int. J. of *Thermal Sciences*, 48(11): 2063-2073 (2009).

[26] Pak, B.C., Cho, Y., Hydrodynamic and heat transfer study of dispersed fluids with submicron metallic oxide particle, *Experimental Heat Transfer*, 11: 151-170 (1998).

[27] Maxwell-Garnett, J.C., Colours in metal glasses and in metallic films. Philos. Trans. Roy. Soc. A 203, 385-420, 1904.

[28] Reddy, J.N. and Gartling, D.K., The Finite Element Method in Heat Transfer and Fluid Dynamics, CRC Press, Inc., Boca Raton, Florida, USA (1994).

GANIT

Available online at https://ganitjournal.bdmathsociety.org/

GANIT: Journal of Bangladesh Mathematical Society

GANIT *J. Bangladesh Math. Soc.* 41.2 (2021) 34–40

DOI: https://doi.org/10.3329/ganit.v41i2.57575

Poincare Duality of Morse-Novikov Cohomology on a Riemannian Manifold

Md. Shariful Islam [*a]

[a] *University of Dhaka, Dhaka-1000, Bangladesh*

ABSTRACT

Morse-Novikov or Lichnerowicz cohomology groups of a manifold has been studied by researchers to deduce properties and invariants of manifolds. Morse-Novikov cohomology is defined using the twisted differential $d_\omega = d + \omega\wedge$, where d is the usual differential operator on forms, and ω is a non-exact closed 1-form on the manifold. On a Riemanian manifold each Morse-Novikov cohomolgy class has unique harmonic representative, and has Poincare duality isomorphism. This isomorhism have been proved in many elegant ways in literature. In this article we provide yet another proof using ellepticity of a differential complex, Green's operator, and Hodge star operator which may be useful in other computations related to Morse-Novikov cohomology.

Received: September 02, 2021 **Accepted:** October 21, 2021 **Published Online:** January 07, 2022

Keywords: : Manifold; Cohomology; Harmonic forms; Elliptic Operators; Hodge star operator; Poincare duality.

AMS Subject Classifications 2020: 57R30; 53C12; 58A14.

1 Introduction

Let M be a manifold with differentiable structure of dimension n; denote by $\Omega^k(M)$ the set of all degree k differential forms on M and the de Rham cohomology ring is denoted by $H^k(M)$. Let ω be a closed $1-$form not necessarily exact forming the twisted operator $d_\omega = d + \omega\wedge : \Omega^k(M) \to \Omega^{k+1}(M)$. It can easily be verified that $d_\omega \circ d_\omega = 0$. The cochain complex $(\Omega^*(M), d_\omega)$ of the manifold M is known as the Morse-Novikov complex. The Morse-Novikov or Lichnerowicz cohomology groups of M are the cohomology groups $H^k_\tau(M)$ of this cochain complex. To study poisson geometry, A. Lichnerowicz in [1] studied, the Morse-Novikov cohomology first. The zeros of the form ω has a combinatorial relation with ranks of these cohomologies which has been used to give a generalization of the Morse inequalities in [2] and [3], S. P. Novikov while gave an analytic proof of the real part of the Novikov's inequalities has been studied by Pazhintov [4]. E. Witten exploited exactness of τ to his famous invention of the the Morse-Novikov cohomology for exact τ in his famous discovery *Witten deformation* in [5]. M. Shubin and S. P. Novikov applied the *Witten deformation* to

*Corresponding author. Tel.: +880-1319-071-334 ; fax: +0-000-000-0000 .
E-mail address: mdsharifulislam@du.ac.bd

an rigorous anlysis of limits of eigenvalues of Witten Laplacians for vector field and some more generalized 1-form in [6] and [7]. For 1-forms with non isolated zeros and vector fields, Braverman and Farber [8] generalized them. See [9] for more on this topics. Alexandra Otiman in [10] studied Lichnerowicz cohomology for special classes of closed 1-forms. An important result in this connection due to X. Chen showed in [11], proved that a Riemannian manifold M with almost non-negative sectional curvature and nontrivial first de Rham cohomology ring has trivial Morse-Novikov cohomology ring independent of the closed non-exact 1-form ω. In [12], L. Meng proved the Leray-Hirsch theorem for Morse-Novikov cohomology and for Dolbeault-Morse-Novikov cohomology on complex manifolds, a blow up formula. Locally conformal symplectic manifolds has also been studied using Morse-Novikov cohomology theory (see [13], [14], and [15]). Morse-Novikov cohomology groups using $d+\omega\wedge$ as the differential for a closed 1-form ω, on Riemannian manifold has nice properties like each cohomology class has unique harmonic representative and finite dimensional, and has Poincare duality isomorphism. This isomorhism have been proved in many elegant ways in literature. In this article we provide yet another proof using ellepticity of a differential complex, Green's operator, and Hodge star operator which may be useful in other computations related to Morse-Novikov cohomology. This manuscript is composed from a section of my doctoral thesis [16].

2 Review of known results

For a introduction to Morse-novikov cohomology see [16] [17]. Here we define it with few examples. Let M be a manifold with differentiable structure of dimension n; denote by $\Omega^k(M)$ the set of all degree k differential forms on M and the de Rham cohomology ring is denoted by $H^p(M)$. Let ω be a closed 1-form not necessarily exact forming the twisted operator $d_\omega = d+\omega\wedge : \Omega^k(M) \to \Omega^{k+1}(M)$, where d is the usual exterior derivative. Since $d\circ d = d^2 = 0$, $\omega\wedge\omega = 0$,and $d(\omega\wedge\nu) = d\omega\wedge\nu - \omega\wedge d\nu$ for any k-form ν, it can easily be varified that $d_\omega \circ d_\omega = 0$. The cochain complex $(\Omega^*(M), d_\omega)$ of the manifold M is known as the Morse-Novikov complex. The Morse-Novikov or Lichnerowicz cohomology rings of M are the cohomology rings $H^k_\omega(M)$ of this cochain complex. Let d^ω_k be the restriction of d_ω to $\Omega^k(M)$. The cohomology group is defined as

$$H^k_\omega(M) = \frac{ker(d^\omega_k)}{Im(d^\omega_{k-1})}.$$

This cohomology group is also known as Lichnerowicz cohomology group [1].

Example 1. *[16][17] Morse-Novikov cohomology groups of S^1 are trivial.*

Example 2. *[16][17] Morse-novikov cohomology group of real projective space $H^k_\omega(\mathbb{R}P^n) \cong H^k(\mathbb{R}P^n)$ for all k and any closed 1-form ω. Where $H^k(\mathbb{R}P^n)$ is the de Rham Cohomology group.*

Example 3. *[16][17] Morse-Novikov cohomology groups of $\mathbb{T}^2 = \{(x,y)\in\mathbb{R}^2\}/2\pi\mathbb{Z}^2$ are trivial.*

We now review some well-known facts (see, e.g [18]). Let (M,g) be a closed compact oriented Riemannian manifold of dimension n. At every point $p\in M$, we have an inner product g_p on the tangent space T_pM, and therefore also an inner product on the cotangent space T^*_pM determined by the inverse matrix of the matrix of g_p. This inner product is extended in a natural way to differential forms. So each vector bundle Λ^kT^*M carries a metric that allows us to define an inner product on the space of smooth k-forms on M by the following formula

$$\langle\alpha,\beta\rangle = \int_M g(\alpha,\beta)\text{vol}.$$

Let $\alpha\in\Omega^k(M)$ be a k-form. Define the linear Hodge star operator $*:\Omega^k(M)\to\Omega^{n-k}(M)$ such that for all $\beta\in\Omega^k(M)$

$$\alpha\wedge *\beta = g(\alpha,\beta)\text{vol}.$$

So the inner product defined above can be expressed by the even simpler formula

$$\langle\alpha,\beta\rangle = \int_M \alpha\wedge *\beta.$$

It turns out that $**\alpha = (-1)^{k(n+k)}\alpha$ for $\alpha\in\Omega^k(M)$ and that $\beta\wedge *\alpha = \alpha\wedge *\beta$ for all $\alpha,\beta\in\Omega^k(M)$.

The codifferential $d^*:\Omega^k(M)\to\Omega^{k-1}(M)$ in the exterior algebra may be expressed in terms of the Hodge $*$ operator; for $\beta\in\Omega^k(M)$,

$$d^*\beta=(-1)^{nk+n+1}*(d*\beta).$$

Lemma 1. *(See, for example, [18]) On a closed compact Riemannian manifold, d^* is the formal adjoint of d with respect to the global inner product defined above.*

It follows that $*:\Omega^k(M)\to\Omega^{n-k}(M)$ is an isomorphism. Since $*$ commutes with $\Delta=d^*d+dd^*$, $*$ is the Poincaré duality isomorphism of de Rham cohomology of a compact oriented manifold,

$$H^k(M)\cong H^{n-k}(M) \text{ for every } 0\le k\le n.$$

The interior product in the exterior algebra is defined in terms of the Hodge $*$ operator; for $\beta\in\Omega^k(M)$ and $\omega\in\Omega^1(M)$ is a covector, the interior product $\omega\lrcorner:\Omega^k(M)\to\Omega^{k-1}(M)$ is defined as

$$\omega\lrcorner\beta=(-1)^{nk+n}*(\omega\wedge*\beta).$$

Lemma 2. *The adjoint of $\omega\wedge$ with respect to the inner product defined above is $\omega\lrcorner$.*

Proof. Let $\beta\in\Omega^k(M)$ and $\gamma\in\Omega^{k-1}(M)$, then

$$\begin{aligned}(\gamma,\omega\lrcorner\beta)\,\mathrm{vol}&=(-1)^{nk+n}\,\gamma\wedge**(\omega\wedge*\beta)\\&=(-1)^{nk+n+(n-k+1)(-k+1)}\,\gamma\wedge\omega\wedge*\beta\\&=(-1)^{k+1}(-1)^{k-1}\,\omega\wedge\gamma\wedge*\beta\end{aligned}$$

so that $(\gamma,\omega\lrcorner\beta)\,\mathrm{vol}=(\omega\wedge\gamma,\beta)\,\mathrm{vol}$. □

Laplace and Dirac type operators [18], [19] are examples of elliptic operators. We first define the *principal symbol* of a differential or pseudodifferential operator. If $\pi:E\to M$ and $\pi':F\to M$ are two vector bundles and $P:\Gamma(E)\to\Gamma(F)$ is a differential operator of order k acting on sections, then in local coordinates of a local trivialization of the vector bundles P can be written as

$$P=\sum_{|\alpha|=k}s_\alpha(x)\frac{\partial^k}{\partial x^\alpha}+\text{lower order terms},$$

where the summation is over all possible multi-indices $\alpha=(\alpha_1,\cdots,\alpha_k)$ of length $|\alpha|=k$ and each $s_\alpha(x)\in\mathrm{Hom}(E_x,F_x)$ is a linear transformation. If $\xi=\sum\xi_j dx^j\in T_x^*(M)$ is a non-zero covector at x, we define the *principal symbol* of P to be

$$\sigma(P)(\xi)=i^k\sum_{|\alpha|=k}s_\alpha(x)\xi^\alpha\in Hom(E_x,F_x),$$

where $\xi^\alpha=\xi_{\alpha_1}.\cdots.\xi_{\alpha_n}$. It turns out that the principal symbol is invariant under coordinate transformations. One coordinate-free definition of $\sigma(P)_x:T_x^*M\to\mathrm{Hom}(E_x,F_x)$ can be given as follows. For any $\xi\in T_x^*M$ choose a locally defined function f such that $df_x=\xi$. Then we define the operator

$$\sigma_m(P)(\xi)=\lim_{t\to\infty}\frac{1}{t^m}(e^{-itf}Pe^{itf}),$$

where $(e^{-itf}Pe^{itf})(u)=e^{-itf}(P(e^{itf}u))$. Then the order k of the operator and symbol are defined to be $k=\sup\{m:\sigma_m(P)(\xi)\}<\infty$ and $\sigma(P)(\xi)=\sigma_k(P)(\xi)$. It follows that if P and Q are two differential operators such that the composition PQ is defined, then

$$\sigma(PQ)(\xi)=\sigma(P)(\xi)\sigma(Q)(\xi).$$

Definition 1. *An elliptic differential operator P on M is defined to be an operator such that its principal symbol $\sigma(P)(\xi)$ is invertible for all nonzero covectors $\xi\in T^*M$.*

Example 4. *The symbol of the Dirac operator* $D = \sum c(e_j)\nabla_{e_j}$ *is*

$$\sigma(D)(\xi) = i\sum c(e_j)\xi_j = i\sum c(\xi^j e_j) = ic(\xi^\sharp).$$

The symbol of the Dirac Laplacian D^2 *is*

$$\sigma(D^2)(\xi) = \sigma(D)(\xi)\sigma(D)(\xi) = (ic(\xi^\sharp))^2 = \|\xi^\sharp\|^2,$$

where $\xi^\sharp$ *is the corresponding vector of the covector* ξ *induced by the metric on* M*. The last equality is a consequence of the definition of Clifford multiplication; see [20]. Therefore for non-zero* ξ*, both these symbols are invertible, and hence* D *and* D^2 *are elliptic differential operators.*
An operator P *is strongly elliptic if there exists* $c > 0$ *such that*

$$\sigma(P)(\xi) \geq c|\xi|^2$$

for all non-zero $\xi \in T^*M$*. The Laplacian* Δ *of* $\mathbb{R}^n$ *and* D^2 *on Clifford bundle are strongly elliptic. For more about elliptic differential operators on manifolds see [18], [19], [20].*

3 Main result

Let M be a closed, compact, and oriented Riemannian manifold. We consider the de Rham operator for the differential

$$d_w : \Omega^{e/o}(M) \to \Omega^{o/e}(M),$$

where $\Omega^e(M)$ and $\Omega^o(M)$ denote the bundle of differential forms of even degree and odd degree respectively. We choose a Riemannian metric g on M; this induces a volume form on M and Hermitian inner products on all the spaces $\Omega^k(M)$. Since d_ω is a linear differential operator and the bundle in question carries a Hermitian metric induced from the Hermitian inner product, there exists an unique adjoint of d_ω, denoted by d_ω^*. Combining d_ω and d_ω^* we obtain a deformed differential operator

$$D_\omega = d_\omega + d_\omega^* : \Omega^{e/o}(M) \to \Omega^{o/e}(M).$$

For each k, we define the *Laplace operator* $\Delta_\omega : \Omega^k(M) \to \Omega^k(M)$ by the formula $\Delta_\omega = (d_\omega + d_\omega^*)^2 = d_\omega d_\omega^* + d_\omega^* d_\omega$. A form $\tau \in \Omega^k(M)$ is called ω-harmonic if $\Delta_\omega \tau = 0$. We denote $\mathscr{H}_\omega^k(M) = \ker\Delta_\omega$, the space of all ω-harmonic forms of degree k. Notice that Δ_ω is a second order, formally self adjoint, linear differential operator on $\Omega^k(M)$. Because d_ω and d_ω^* square to zero,

$$(\Delta_\omega\alpha, \beta) = (d_\omega\alpha, d_\omega\beta) + (d_\omega^*\alpha, d_\omega^*\beta) = (\alpha, \Delta_\omega\beta)\,.$$

Theorem 1. $\ker\Delta_\omega$ *is finite dimensional.*

Proof. Since the principal symbols of $d_\omega + d_\omega^*$, and Δ_ω are the same as that of $d + d^*$ and Δ, the operators$d_\omega + d_\omega^*$ and Δ_ω are elliptic operators. The following sequence

$$\Gamma\left(M, \Lambda^0(M)\right) \overset{d_\omega}{\to} \Gamma\left(M, \Lambda^1(M)\right) \overset{d_\omega}{\to} \cdots \overset{d_\omega}{\to} \Gamma\left(M, \Lambda^n(M)\right)$$

is an *elliptic complex*, since the associated symbol sequence

$$0 \to \pi^*\Gamma\left(M, \Lambda^0(M)\right) \overset{\sigma(d_\omega)}{\to} \cdots \overset{\sigma(d_\omega)}{\to} \pi^*\Gamma\left(M, \Lambda^n(M)\right) \to 0$$

is exact, where $\Gamma\left(M, \Lambda^k(M)\right) = \Omega^k(M)$ is the set of smooth sections of the bundle $\pi : \Lambda^k(M) \to M$, and $\sigma(d_\omega)$ is the principal symbol of d_ω. See Chapter IV, Example 2.5 of [19]. We may therefore apply the theorem concerning an elliptic differential complex of vector bundles (see Chapter IV, Theorem 5.2 of [19]) to conclude that $\mathscr{H}_\omega^k(M) = \ker\Delta_\omega$ is finite dimensional, and we have the following orthogonal decomposition of $\Omega^k(M)$:

$$\Omega^k(M) = \mathscr{H}_\omega^k \oplus \mathrm{im}\,(\Delta_\omega G)\,,$$

where $G : \Omega^k(M) \to \Omega^k(M)$ is a Green's operator. □

Now we can state and prove the Hodge theorem for the Morse-Novikov cohomology.

Theorem 2. *Let (M,g) be a closed compact and oriented Riemannian manifold. Then $\mathscr{H}^k_\omega(M) \cong H^k_\omega(M)$. In other words, every Morse-Novikov cohomology class has a unique ω-harmonic representative.*

Proof. Let $\alpha \in \mathscr{H}^k_\omega(M)$, which is smooth by elliptic regularity. Then we have

$$\begin{aligned} (\Delta_\omega \alpha, \alpha) &= 0 \\ \Rightarrow (d_\omega \alpha, d_\omega \alpha) + (d^*_\omega \alpha, d^*_\omega \alpha) &= 0 \\ \Rightarrow \|d_\omega \alpha\|^2 + \|d^*_\omega \alpha\|^2 &= 0. \end{aligned}$$

This implies that α is ω-harmonic if and only if $d_\omega \alpha = 0$ and $d^*_\omega \alpha = 0$. These ω-harmonic forms are closed and therefore define classes in Morse-Novikov cohomology. We have a map $\mathscr{I} : \mathscr{H}^k_\omega(M) \to H^k_\omega(M)$ defined by $\mathscr{I}(\alpha) = [\alpha]$. We show that this map is a bijection.

Suppose $\alpha \in \mathscr{H}^k_\omega$ is d_ω exact, say $\alpha = d_\omega \tau$ for some $\tau \in \Omega^{k-1}(M)$. Then

$$\|\alpha\|^2 = (\alpha, \alpha) = (\alpha, d_\omega \tau) = (d^*_\omega \alpha, \tau) = 0,$$

and therefore $\alpha = 0$. To prove the surjectivity, let $\alpha \in \Omega^k(M)$ such that $d_\omega \alpha = 0$. Then by the decomposition $\Omega^k(M) = \mathscr{H}^k_\omega \oplus \operatorname{im}(\Delta_\omega G)$, for some $\tau \in \mathscr{H}^k_\omega(M)$ and $\beta \in \Omega^k(M)$, we have

$$\alpha = \tau + \Delta_\omega G\beta = \tau + d_\omega d^*_\omega G\beta + d^*_\omega d_\omega G\beta.$$

Applying d_ω on both sides of this equation, it follows that $d_\omega d^*_\omega d_\omega G\beta = 0$, and therefore

$$\|d^*_\omega d_\omega G\beta\|^2 = (d^*_\omega d_\omega G\beta, d^*_\omega d_\omega G\beta) = (d_\omega G\beta, d_\omega d^*_\omega d_\omega G\beta)$$

proving that $d^*_\omega d_\omega G\beta = 0$. Hence we have $\alpha = \tau + d_\omega d^*_\omega G\beta$; therefore $[\alpha] = [\tau]$. □

Now we give a proof of Poincaré duality for Morse-Novikov cohomology, see Proposition 3.5 [21], using the Hodge star operator and the Hodge theorem for Morse-Novikov cohomology.

Theorem 3. *If M is a closed compact oriented manifold of dimension n and ω is a closed 1-form, then the Hodge star operator $* : \Omega^k(M) \to \Omega^{n-k}(M)$ induces the isomorphism*

$$H^k_\omega(M) \cong H^{n-k}_{-\omega}(M).$$

Proof. From $(\omega \lrcorner) = (-1)^{nk+n} * (\omega \wedge) *$, $*^2 = (-1)^{k(n-k)}$, and $d^* = (-1)^{n(k+1)+1} * d *$ on $\Omega^k(M)$, we have the following identities for operators acting on $\Omega^k(M)$. For any $\beta \in \Omega^k(M)$

$$\begin{aligned} (\omega \lrcorner) * \beta &= (-1)^{n(n-k)+n} * (\omega \wedge) *^2 \beta \\ &= (-1)^{n^2+nk+n} (-1)^{k(n-k)} * (\omega \wedge) \beta, \end{aligned}$$

so that $(\omega \lrcorner) * = (-1)^k * (\omega \wedge)$ on $\Omega^k(M)$. Also,

$$\begin{aligned} * (\omega \lrcorner) \beta &= (-1)^{nk+n} *^2 (\omega \wedge) * \beta \\ &= (-1)^{nk+n} (-1)^{(n-k+1)(n-(n-k+1))} (\omega \wedge) * \beta, \end{aligned}$$

so that $* (\omega \lrcorner) = (-1)^{k+1} (\omega \wedge) *$ on $\Omega^k(M)$. Next

$$\begin{aligned} d^* * \beta &= (-1)^{n(n-k+1)+1} * d *^2 \beta \\ &= (-1)^{n(n-k+1)+1} (-1)^{k(n-k)} * d\beta, \end{aligned}$$

so that $d^* * = (-1)^{k+1} * d$ on $\Omega^k(M)$. Finally

$$* d^* \beta = (-1)^{n(k+1)+1} *^2 d * \beta$$

$$= (-1)^{n(k+1)+1}\,(-1)^{(n-k+1)(n-(n-k+1))}\,d*\beta,$$

so that $*d^* = (-1)^k d*$ on $\Omega^k(M)$. From these equations we have

$$(d^* + \omega\lrcorner)* = (-1)^{k+1} * (d - \omega\wedge)$$
$$(d + \omega\wedge)* = (-1)^k * (d^* - \omega\lrcorner)$$

on $\Omega^k(M)$. As before d^* is the L^2 adjoint of d, and $\lrcorner$ represents interior product. It turns out that the L^2 adjoint of $d_\omega = d + \omega\wedge$ is $d^*_\omega = d^* + \omega\lrcorner$ and the Laplacian is $\Delta_\omega = (d_\omega + d^*_\omega)^2 = d_\omega d^*_\omega + d^*_\omega d_\omega = (d + \omega\wedge)(d^* + \omega\lrcorner) + (d^* + \omega\lrcorner)(d + \omega\wedge)$. If $\beta \in \Omega^k(M)$, then by the formulas above we have for all $\beta \in \Omega^k(M)$,

$$\begin{aligned}
*\Delta_\omega\beta &= *(d + \omega\wedge)(d^* + \omega\lrcorner)\beta + *(d^* + \omega\lrcorner)(d + \omega\wedge)\beta \\
&= (-1)^{k-1}(d^* - \omega\lrcorner) * (d^* + \omega\lrcorner)\beta + (-1)^k(d - \omega\wedge) * (d + \omega\wedge)\beta \\
&= (-1)^{k-1}(-1)^k(d^* - \omega\lrcorner)(d - \omega\wedge) * \beta + (-1)^k(-1)^{k+1}(d - \omega\wedge)(d^* - \omega\lrcorner) * \beta \\
&= -((d^* - \omega\lrcorner)(d - \omega\wedge) + (d - \omega\wedge)(d^* - \omega\lrcorner)) * \beta \\
&= -\Delta_{-\omega} * \beta.
\end{aligned}$$

Thus the operator $*$ maps ω-harmonic forms to $(-\omega)$-harmonic forms, so from the Hodge theorem for the Morse-Novikov cohomology $*$ induces the required isomorphism. □

ACKNOWLEDGEMENTS

I convey my deepest gratitude to my Ph.D adviser, Ken Richardson, Professor of Mathematics at Texas Christian University (TCU), for all the support, and encouragement. His inspiration and supports for me have been more than I could imagine.

References

[1] Lichnerowicz A., Les variétés de Poisson et leurs algèbres de Lie associées, *Journal of Differential Geometry*, Vol. 12, Number 2, P. 253-300, 1977.

[2] Novikov P., Multivalued functions and functionals. An analogue of the Morse theory, *Doklady Akademii Nauk SSSR*, Vol. 260, Number 1, P. 31-35, 1981.

[3] Novikov P., The Hamiltonian formalism and a multivalued analogue of Morse theory, *Akademiya Nauk SSSR i Moskovskoe Matematicheskoe Obshchestvo. Uspekhi Matematicheskikh Nauk*, Vol. 37, Number 5(227), P. 3-49,248, 1982.

[4] Pazhitnov A., An analytic proof of the real part of Novikov's inequalities, *Doklady Akademii Nauk SSSR*, Vol. 293, P. 1305–1307, 1983.

[5] Witten E., Supersymmetry and Morse theory, *Journal of Differential Geometry*, 661–692 (1983).

[6] Novikov P., Morse inequalities and von Neumann II_1-factors, *Doklady Akademii Nauk SSSR*, Vol. 289, Number 2, P. 289-292, 1986.

[7] Shubin M., Novikov inequalities for vector fields, *The Gelfand Mathematical Seminars, 1993–1995*, P. 243-274, Birkhäuser Boston, Boston, MA 1996.

[8] Braverman, Maxim and Farber, Michael, Novikov type inequalities for differential forms with non-isolated zeros, *Mathematical Proceedings of the Cambridge Philosophical Society*, Vol. 122, P. 357–375, 1997.

[9] Farber M., Topology of closed one-forms, *Mathematical Surveys and Monographs*, Vol. 108, American Mathematical Society, Providence, RI 2004.

[10] Otiman A., Morse-Novikov cohomology of closed one-forms of rank 1, *arXiv e-prints*, https://ui.adsabs.harvard.edu/abs/2016arXiv160701663O.

[11] X. Chang, Morse-Novikov cohomology of almost nonnegatively curved manifolds, *e-prints*, arXiv:1904.09759.

[12] Lingxu M., Morse-Novikov Cohomology on Complex Manifolds, *J. Geom. Anal.*, https://doi.org/10.1007/s12220-019-00155-w.

[13] Vaisman I., Remarkable operators and commutation formulas on locally conformal Kähler manifolds, *Geometriae Dedicata*, https://doi-org.ezproxy.tcu.edu/10.1007/BF00148231.

[14] Vaisman I., Generalized Hopf manifolds, *Compositio Mathematica*, http://www.numdam.org/item?id=CM-1980-40-3-287-0.

[15] Vaisman I., Locally conformal symplectic manifolds, *International Journal of Mathematics and Mathematical Sciences*, https://doi-org.ezproxy.tcu.edu/10.1155/S0161171285000564.

[16] M. S. Islam, Morse-Novikov cohomological invariants of folliations, *Ph.D thesis*, https://repository.tcu.edu/bitstream/handle/116099117/26769/22592094.pdf?sequence=1

[17] M. S. Islam, Morse-Novikov Cohomology Computations on Low Dimensional Manifolds, *Journal of Bangladesh Mathematical Society*, https://doi.org/10.3329/ganit.v40i2.51313

[18] Roe J., Elliptic operators, topology and asymptotic methods, *Pitman Research Notes in Mathematics Series*, Vol. 395, Longman, Harlow, 1998.

[19] Wells R. Jr., Differential analysis on complex manifolds, third ed., *Graduate Texts in Mathematics*, vol. 65, Springer, New York, 2008, With a new appendix by Oscar Garcia-Prada.

[20] Lawson H. Jr., Michelsohn M., Spin geometry, *Princeton Mathematical Series*, vol. 38, Princeton University Press, Princeton, NJ, 1989.

[21] Otiman A., Morse-Novikov cohomology of locally conformally kahler surfaces, *Math. Z.*, 2018.

GANIT

Available online at https://ganitjournal.bdmathsociety.org/

GANIT: Journal of Bangladesh Mathematical Society

GANIT *J. Bangladesh Math. Soc.* 41.2 (2021) 41–52
DOI: https://doi.org/10.3329/ganit.v41i2.57573

Study on Magnetohydrodynamics Cu-water Nanofluid Flow with Different Shapes of Nanoparticles in a Divergent Channel

Md. Sarwar Alam*, Suraiya Yasmin, and Ashik Chandra Das

Department of Mathematics, Jagannath University, Dhaka-1100, Bangladesh

ABSTRACT

This paper studies the two-dimensional magnetohydrodynamics steady incompressible Cu-water nanofluid flow considering different shapes of nanoparticles in a divergent channel. The continuity equation, momentum equations and energy equation governing the problem are transformed to a set of non-dimensional ordinary differential equations by suitable transformations. The transformed dimensionless equations are solved by using power series approach and then Hermite-Padé approximation method is applied for analyzing the solution. Brick, cylinder and platelet-shaped Cu-nanoparticles are considered to investigate the effect of shape factor. Moreover, impact of physical parameters such as channel angle, flow Reynolds number, Hartmann number, Eckert number, Prandtl number and nanoparticles solid volume fraction on velocity and temperature profiles are also examined. The results show that the different shapes of Cu-nanoparticles have significant effect on the temperature distributions in the channel.

Received: June 17, 2021 **Accepted:** August 05, 2021 **Published Online:** January 07, 2022

Keywords: Magnetohydrodynamics; Cu-water nanofluid; shape factors; divergent channel; Hermite-Padé approximation.

1. Introduction

Jeffery [1] and Hamel [2] discovered two dimensional viscous incompressible fluid flow in a channel with non-parallel walls. This flow is separated by a fixed angle and moved by a source or sink at a peak which is known as the classical Jeffery-Hamel flow. Many researchers [3-8] have investigated this flow considering various effects such as megnetohydrodynamics (MHD) and heat transfer phenomena through convergent-divergent channels. These flows have the similarity solution of Navier-Stokes equation and the dimensionless parameters are depended on the flow Reynolds number and channel angular width [9]. This type of flows has several applications in industrial, aerospace, chemical, civil, environmental, mechanical and biomechanical engineering.

Magnetohydrodynamics (MHD) is related to the mutual interaction of fluid flow and magnetic field. Many natural and man-made flows are influenced by magnetic field. The theory of megnetohydrodynamics (MHD) states that the presence of magnetic field produces a current through a moving conductive fluid. This inclined

* Corresponding author: Md. Sarwar Alam, *E-mail address:* sarwardu75@gmail.com

current results force on ions of the conductive fluid. The investigation of MHD flow through convergent-divergent channels is not only interesting theoretically but also becomes more applications in mathematical modeling of several industries to design cooling system with liquid metals, MHD generators, accelerators, pumps and flow meters

New types of fluids need to develop, which are more effective in terms of heat exchange performance considering the recent demands of modern technology, including chemical production, power station and microelectronics. Presently, it is seen that the thermal conductivity of fluids has been enhanced with nanoparticles by Choi [10]. Nanoparticles have unique chemical and physical properties and have better thermal conductivity and radiative heat transfer compared to the base fluid only. Nanofluids are engineered dilute colloidal dispersions of nanosized (less than 100 nm) particles in a base fluid such as water, oil and ethylene glycol analysed by Das et al. [11]. These nanoparticles are good conductors of heat and enable the basic fluids to enhance their thermal properties.

An extension of the classical Jeffery-Hamel flows to magnetohydrodynamics was studied by Makinde and Mhone [12]. They explained that the effect of external magnetic field works as a parameter in the solution of magnetohydrodynamics flows in convergent-divergent channels. Makinde and Mhone [13] investigated the terrestrial development of small disturbances in magnetohydrodynamics Jeffery-Hamel flows. This concept described at very small magnetic Reynolds number Rm for the stability of hydromagnetic steady flows in convergent-divergent channels using Chebyshev spectral collocation method. Moradi et al. [14] described the effects of heat transfer and viscous dissipation on the Jeffery-Hamel flow of nanofluids. Alam et al. [15-16], Alam and Khan [17] studied MHD Jeffery-Hamel nanofluid flow for different nanoparticles.

Recently, the effect of nanoparticle shapes on irreversibility analysis of nanofluid flow in a microchannel with radiative heat flux and convective heating was investigated by Sindhu and Gireesha [18]. Asifa et al. [19] performed a comparative fractional study of the significance of shape factor in heat transfer performance of molybdenum-disulfide nanofluid in multiple flow. Moreover, the effects of nanoparticle shape and size on the thermohydraulic performance of plate evaporator using hybrid nanofluids was analysed by Bhattad and Sarkar [20]. Furthermore, Das and Alam [21] investigated different shaped Al_2O_3 and TiO_2 nanoparticles on water-based MHD nanofluid flow through convergent-divergent channels.

To the best of Author's knowledge, the shape factors effect of Cu-water nanofluid flow in divergent channel is not available in open literature yet. This study aims to investigate magnetohydrodynamics Cu-water nanofluid flow in a divergent channel with the effects of three different shapes of nanoparticles; brick, cylinder and platelet. The impacts of various physical parameters namely channel angle α, Reynolds number *Re*, Hartmann number *Ha*, Eckert number *Ec*, Prandtl number *Pr* and nanoparticle solid volume fraction ϕ on velocity profiles and temperature distributions are also discussed.

2. Mathematical Formulation

Consider a two-dimensional viscous incompressible Cu-water nanofluid flow from a source or sink between two channel walls intersect at an angle 2α as seen in Fig.2.1. A cylindrical coordinate system (r, φ, z) is used and the velocity is considered to be purely radial such that it depends on r and φ only. Thus there is no variation for the physical parameters along the z direction. The velocity field takes the form $V = [u(r,\varphi), 0, 0]$. An external magnetic field B_0 is operated vertically downward to the top wall. Let α be the semi-angle and the domain of the flow be $-|\alpha| < \varphi < |\alpha|$. The continuity equation, momentum equations and energy equation with viscous dissipation and Joule heating in reduced polar coordinates are

$$\frac{\rho_{nf}}{r}\frac{\partial}{\partial r}\big(ru(r,\varphi)\big) = 0, \tag{2.1}$$

$$u(r,\varphi)\frac{\partial u(r,\varphi)}{\partial r} = -\frac{1}{\rho_{nf}}\frac{\partial p}{\partial r} + v_{nf}\left(\frac{\partial^2 u(r,\varphi)}{\partial r^2} + \frac{1}{r}\frac{\partial u(r,\varphi)}{\partial r} + \frac{1}{r^2}\frac{\partial^2 u(r,\varphi)}{\partial \varphi^2} - \frac{u(r,\varphi)}{r^2}\right) - \frac{\sigma_{nf}B_0^2}{\rho_{nf}r^2}u(r,\varphi) \tag{2.2}$$

$$\frac{1}{\rho_{nf}r}\frac{\partial p}{\partial \varphi} - \frac{2v_{nf}}{r^2}\frac{\partial u(r,\varphi)}{\partial \varphi} = 0, \tag{2.3}$$

$$u(r,\varphi)\frac{\partial \overline{T}(r,\varphi)}{\partial r}=\frac{\kappa_{nf}}{\left(\rho c_p\right)_{nf}}\left(\frac{\partial^2 \overline{T}(r,\varphi)}{\partial r^2}+\frac{1}{r}\frac{\partial \overline{T}(r,\varphi)}{\partial r}+\frac{1}{r^2}\frac{\partial^2 \overline{T}(r,\varphi)}{\partial \varphi^2}\right)+$$

$$\frac{\mu_{nf}}{\left(\rho c_p\right)_{nf}}\left(4\left(\frac{\partial u(r,\varphi)}{\partial r}\right)^2+\frac{1}{r^2}\left(\frac{\partial u(r,\varphi)}{\partial \varphi}\right)^2\right)+\frac{\sigma_{nf}B_0^2}{\left(\rho c_p\right)_{nf}r^2}\left(u(r,\varphi)\right)^2 \tag{2.4}$$

The respective boundary conditions for the problem are as follows

$$\psi=\frac{Q}{2},\ \frac{\partial \psi}{\partial \varphi}=0 \ \text{ at } \varphi=\pm\alpha$$

$$\overline{T}=T_h \ \text{ at } \varphi=\alpha \ \text{ and } \overline{T}=T_c \ \text{ at } \varphi=-\alpha \tag{2.5}$$

where $\psi=\psi(r,\varphi)$ be the stream function and $\frac{\partial \psi}{\partial \varphi}=ur$. The volumetric flow rate through the channel is defined by

$$Q=\int_{-\alpha}^{\alpha} urd\varphi \tag{2.6}$$

Since the flow is symmetrically radial, i.e. $v=0$. Here, B_0 is the electromagnetic induction, u is the velocity along radial direction and p is the fluid pressure. The effective density ρ_{nf}, the effective dynamic viscosity μ_{nf}, the electrical conductivity σ_{nf} and the kinematic viscosity v_{nf} of the nanofluid are given as.

$$\rho_{nf}=\rho_f(1-\phi)+\rho_s\phi, \qquad \mu_{nf}=\frac{\mu_f}{(1-\phi)^{2.5}}, \qquad v_{nf}=\frac{\mu_{nf}}{\rho_{nf}},$$

$$\frac{\sigma_{nf}}{\sigma_f}=1+\left[3\left(\frac{\sigma_s}{\sigma_f}-1\right)\phi\Big/\left(\left(\frac{\sigma_s}{\sigma_f}+2\right)-\left(\frac{\sigma_s}{\sigma_f}-1\right)\phi\right)\right] \tag{2.7}$$

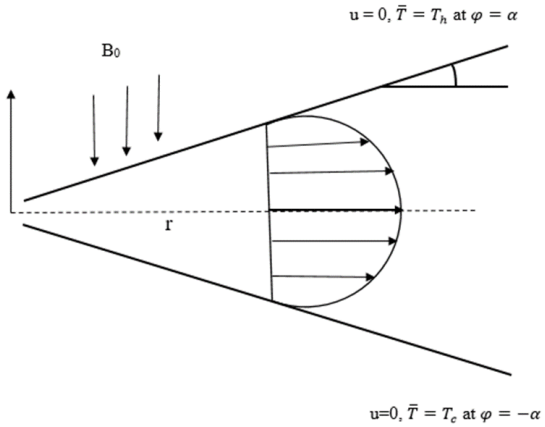

Fig. 2.1: Geometry of the Problem

The corresponding effective thermal conductivity and heat capacity of nanofluid are

$$\kappa_{nf}=\kappa_f\frac{\kappa_s+(m+1)\kappa_f-(m+1)\left(\kappa_f-\kappa_s\right)\phi}{\kappa_s+(m+1)\kappa_f+\left(\kappa_f-\kappa_s\right)\phi},$$

$$(\rho c_p)_{nf} = (1-\phi)(\rho c_p)_f + \phi(\rho c_p)_s \tag{2.8}$$

Here, ϕ is the nanoparticles solid volume fraction and m is the shape factor. The thermophysical properties of water and Cu- nanoparticles as Das et al. [22] are presented in Table 2.1.

Table 2.1: Thermophysical properties of water and Cu-nanoparticles.

Physical properties	Water	Cu
$\rho(kg/m^3)$	997.1	8933
$c_P(J/kgK)$	4179	385
$\kappa(W/mK)$	0.613	401
$\sigma(\Omega m)$	0.05	5.96×10^7

The sphericity and shape factor of Cu-nanoparticles are shown in Table 2.2. As it necessitates $Q \geq 0$, then the flow is diverging from a source at $r = 0$ for $\alpha > 0$.

The dimensionless variable η is introduced as,

$$\eta = \frac{\varphi}{\alpha}$$

Then the dimensionless stream function and temperature are defined by

$$F(\eta) = \frac{2\,\psi(\varphi)}{Q}, \theta(\eta) = \frac{\overline{T} - T_c}{T_h - T_c} \tag{2.9}$$

Table 2.2: Sphericity and shape factor of Cu-nanoparticles [23-25].

Nanoparticle shapes	Aspect ratio	Sphericity	Shape factor
Platelet	1:1/18	0.52	5.7
Cylinder	1:8	0.62	4.9
Brick	1:1:1	0.81	3.7

The pressure term p is eliminated from equations (2.2) and (2.3) by using equation (2.9). The non-dimensional ordinary differential equations of steam function and temperature profile are reduced to the following form

$$F^{(iv)} + 2\alpha\, Re\, A(1-\phi)^{2.5}\, F'\, F'' + (4 - (1-\phi)^{2.5}\, D\, Ha^2)\alpha^2\, F'' = 0, \tag{2.10}$$

$$\theta'' + \frac{B\, Ec\, Pr}{C(1-\phi)^{2.5}}\left[4\alpha^2 F'^2 + (F'')^2 + (1-\phi)^{2.5}\, D\, Ha^2\, \alpha^2\, F'^2\right] = 0, \tag{2.11}$$

Here, prime denotes the differentiation with respect to η. The similarity transforms reduce the boundary conditions as follows:

$$F = 1,\ F' = 0,\ \theta = 1 \quad \text{at } \eta = 1$$
$$F = -1,\ F' = 0,\ \theta = 0 \text{ at } \eta = -1 \tag{2.12}$$

Where, $Re = \frac{Q}{2v_f}$ is Reynolds number, $Pr = \frac{(\mu c_p)_f}{\kappa_f}$ is Prandtl number, $Ec = \frac{U_{max}^2}{(c_p)_f T_h}$ is the Eckert number,

$Ha^2 = \frac{\sigma_f B_0^2}{\rho_f \nu_f}$ is square of Hartmann number and α is the channel angle. Moreover,

$$A = (1-\phi) + \frac{\rho_s}{\rho_f}\phi, \qquad B = (1-\phi) + \frac{(\rho c_p)_s}{(\rho c_p)_f}\phi\,,$$

$$C = \frac{\kappa_s + (m+1)\kappa_f - (m+1)(\kappa_f - \kappa_s)\phi}{\kappa_s + (m+1)\kappa_f + (\kappa_f - \kappa_s)\phi},$$

$D = 1 + \left[3\left(\frac{\sigma_s}{\sigma_f} - 1\right)\phi \Big/ \left(\left(\frac{\sigma_s}{\sigma_f} + 2\right) - \left(\frac{\sigma_s}{\sigma_f} - 1\right)\phi\right)\right]$ are the constants.

3. Series Analysis

The non-linear differential equations (2.10) and (2.11) are solved for stream function and temperature profile. To solve equations (2.10) and (2.11), the power series expansions are assumed in terms of the parameter α as follows:

$$F(\eta) = \sum_{i=0}^{\infty} F_i(\eta)\alpha^i, \;\; \theta(\eta) = \sum_{i=0}^{\infty} \theta_i(\eta)\alpha^i, \quad as \;\; |\alpha| < 1 \tag{3.1}$$

By substituting the equation (3.1) into equations (2.10) and (2.11) along with the boundary conditions (2.12) and then equating the coefficient of power of α.

Order zero(α^0):

$$F_0^{(iv)} = 0, \qquad \theta_0'' + \frac{B\ Ec\ Pr}{C(1-\phi)^{2.5}}(F_0'')^2 = 0 \tag{3.2}$$

$$F_0 = 1, F_0' = 0, \theta_0 = 1 \;\; at\ \eta = 1 \tag{3.3}$$

$$F_0 = -1, F_0' = 0, \theta_0 = 0\ at\ \eta = -1 \tag{3.4}$$

Order one(α^1):

$$F_1^{(iv)} + 2\ Re\ A(1-\phi)^{2.5} F_0' F_0'' = 0, \theta_1'' + \frac{B\ Ec\ Pr}{C(1-\phi)^{2.5}}(2F_0''F_1'') = 0 \tag{3.5}$$

$$F_1 = 0, F_1' = 0, \theta_1 = 0\ at\ \eta = 1 \tag{3.6}$$

$$F_1 = 0, F_1' = 0, \theta_1 = 0\ at\ \eta = -1 \tag{3.7}$$

The first 13 coefficients of the series for stream function $F(\eta)$ and temperature $\theta(\eta)$ have been calculated using algebraic programming language MAPLE. The first few coefficients of the series for $F(\eta)$ and $\theta(\eta)$ in terms of $\alpha, Re, Ha, Ec, Pr, \phi, A, B, C, D$ are as follows:

$$F(\eta;\alpha, Re, Ha, \varphi, A, D) = \tfrac{3}{2}\eta - \tfrac{1}{2}\eta^3 - \tfrac{3}{280}\ Re\ A(1-\phi)^{(5/2)}\eta(\eta^2-5)(\eta-1)^2(\eta+1)^2\alpha + \Big(\tfrac{1}{431200}\eta(\eta-1)^2(\eta+1)^2(43120 + 14375\ Re^2\ A^2\ \phi^4 + 28750\ Re^2\ A^2\ \phi^2 - 2875\ Re^2\ A^2\ \phi^5) - 14375\ Re^2\ A^2\ \phi - 28750\ Re^2\ A^2\ \phi^3 - 98\eta^6\ Re^2\ A^2 - 2472\ \eta^2\ Re^2\ A^2 + 954\ \eta^4\ Re^2\ A^2 - 10780\sqrt{1-\phi}\ D\ Ha^2 - 4795\ \eta^4\ Re^2\ A^2\ \phi + 4795\ \eta^4\ Re^2\ A^2\ \phi^4 + 9590\ \eta^4\ Re^2\ A^2\ \phi^2 - 9590\ \eta^4\ Re^2\ A^2\ \phi^3 + 98\ \eta^6\ Re^2\ A^2\ \phi^5 + 490\ \eta^6\ Re^2\ A^2\ \phi^5 - 980\ \eta^6\ Re^2\ A^2\ \phi^2 + 980\ \eta^6\ Re^2\ A^2\ \phi^3 - 490\ \eta^6\ Re^2\ A^2\ \phi^4 - 959\ \eta^4\ Re^2\ A^2\ \phi^5 + 2472\ \eta^2\ Re^2\ A^2\ \phi^5 - 24720\ \eta^2\ Re^2\ A^2\ \phi^2 + 24720\ \eta^2 Re^2\ A^2\ \phi^3 - 12360\ \eta^2\ Re^2\ A^2\ \phi^4 + 12360\ \eta^2\ Re^2\ A^2\ \phi + 21560\ \sqrt{1-\phi}\ D\ Ha^2\ \phi - 10780\ \sqrt{1-\phi}\ D\ Ha^2\ \phi^2\Big)\alpha^2 +$$

$$O(\alpha^3)+\ldots \tag{3.8}$$

$$\theta(\eta;\ \alpha, Re, Ha, \phi, Ec, Pr, A, B, C, D) = -\frac{1}{4C(1-\phi)^{(5/2)}}(1+\eta)\big(3\ B\ Ec\ \mathrm{Pr}\ \eta^3 - 3\ B\ Ec\ \mathrm{Pr}\ \eta^2 + 3\ B\ Ec\ \mathrm{Pr}\ \eta - 2\ C\ (1-\phi)^{(5/2)} - 3\ B\ Ec\ Pr\big) - \frac{3}{560\ C}\ B\ Ec\ \mathrm{Pr}\ Re\ A(9\eta^4 - 38\eta^2 - 19)\ (\eta-1)^2(\eta+1)^2\alpha + O(\alpha^2)+\ldots \tag{3.9}$$

4. Numerical Procedure: Hermite-Padé Approximants

In this present study, a very effective solution method, known as Hermite-Padé approximants, which was first introduced by Padé [26] and Hermite [27] have been applied. In this method, a function is an approximant for the series

$$S_{N-1}(\alpha) = \sum_{n=0}^{N-1} a_n \alpha^n \qquad as \qquad |\alpha| < 1 \tag{4.1}$$

If it shares with S, the similar first few series coefficients for $|\alpha| < 1$. Therefore, the simple approximants are the partial sums of the series S. As soon as this series converges quickly, such polynomial approximants can provide good approximations of the sum.
Consider the $(d+1)$ tuple of polynomials, where d is a positive integer,

$P_N^{[0]}, P_N^{[1]}, \ldots, P_N^{[d]}$

where, $\deg P_N^{[0]} + \deg P_N^{[1]} + \ldots + \deg P_N^{[d]} + d = N,$ (4.2)
is a Hermite-Padé form of these series if

$$\sum_{i=0}^{d} P_N^{[i]}(\alpha) S_i(\alpha) = O(\alpha^N) \quad as \quad |\alpha| < 1 \tag{4.3}$$

Here, $S_0(\alpha), S_1(\alpha), \ldots, S_d(\alpha)$ may be independent series or different form of a unique series. It requires to find the polynomials $P_N^{[i]}$ that satisfy the equation (4.2-4.3). These polynomials are fully determined by their coefficients. Thus, the total number of unknowns in equation (4.3) is

$$\sum_{i=0}^{d} \deg P_N^{[i]} + d + 1 = N + 1 \tag{4.4}$$

Expanding the left hand side of equation (4.3) in powers of α and equating the first N equations of the system equal to zero, we get a system of linear homogeneous equations. To compute the coefficients of the Hermite-Padé polynomials, it requires the normalization form, such as

$$P_N^{[i]}(0) = 1 \ \text{ for some integer } \ 0 \le i \le d \tag{4.5}$$

It is necessary to emphasize that the only input required for the computation of the Hermite-Padé polynomials are the first N coefficients of the series $S_0(\alpha), S_1(\alpha), \ldots, S_d(\alpha)$. The equation (4.4) simply ensures that the coefficient matrix associated with the system is square. One approach to construct the Hermite-Padé polynomials is to solve the system of linear equations using any standard method such as Gaussian elimination or Gauss-Jordan elimination.
Drazin and Tourigney [28] approximant is a particular kind of algebraic approximants and Khan [29] introduced High-order differential approximant (HODA) as a special type of differential approximants. Drazin-Tourigney differential approximant is applied to both the series solutions (3.8) and (3.9) to analyse the results. Then, the influence of physical parameters namely channel angle α, Reynolds number *Re*, Hartmann number *Ha*, nanoparticles volume fraction ϕ, Eckert number *Ec* on velocity profiles and temperature distributions with the effect of three different shapes of Cu-nanoparticles is presented in section 5.

5. Results and Discussion

Three different shapes' effects of nanoparticles such as: brick, cylinder and platelet are analysed on velocity profiles and temperature distributions for varying values of physical parameters such as; nanoparticles solid volume friction $\boldsymbol{\phi}$, channel angle $\boldsymbol{\alpha}$, Reynolds number $\boldsymbol{Re}$, Hartmann number $\boldsymbol{Ha}$, Eckert number $\boldsymbol{Ec}$ and Prandtl number $\boldsymbol{Pr}$ in the present study.

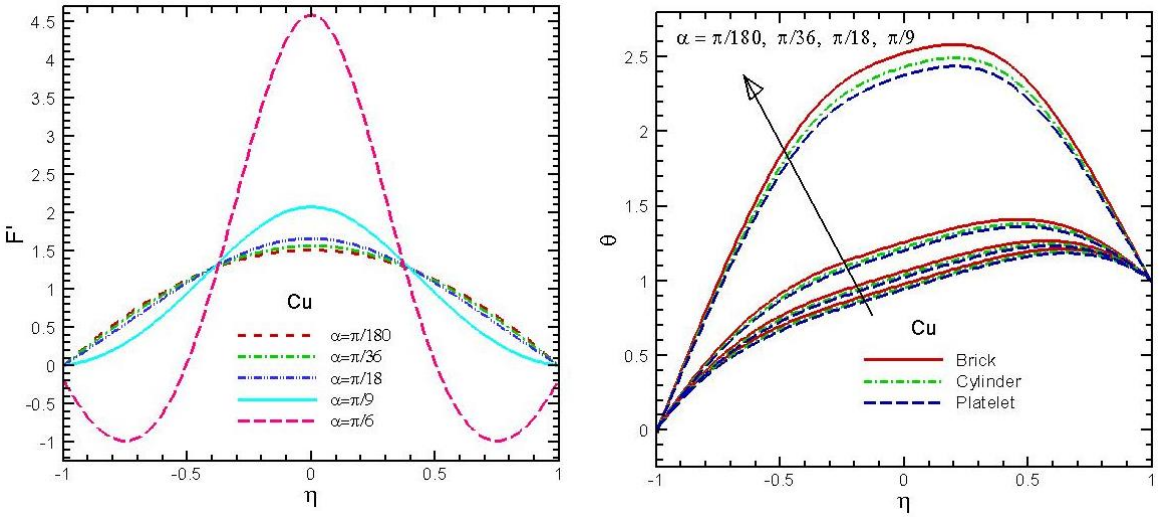

(a) (b)

Fig. 5.1: (a) Velocity Profiles, (b) temperature distributions of Cu –water nanofluid with different values of α at $Re = 10, Ha = 1, \phi = 0.05, Pr = 7.1, Ec = 0.1$.

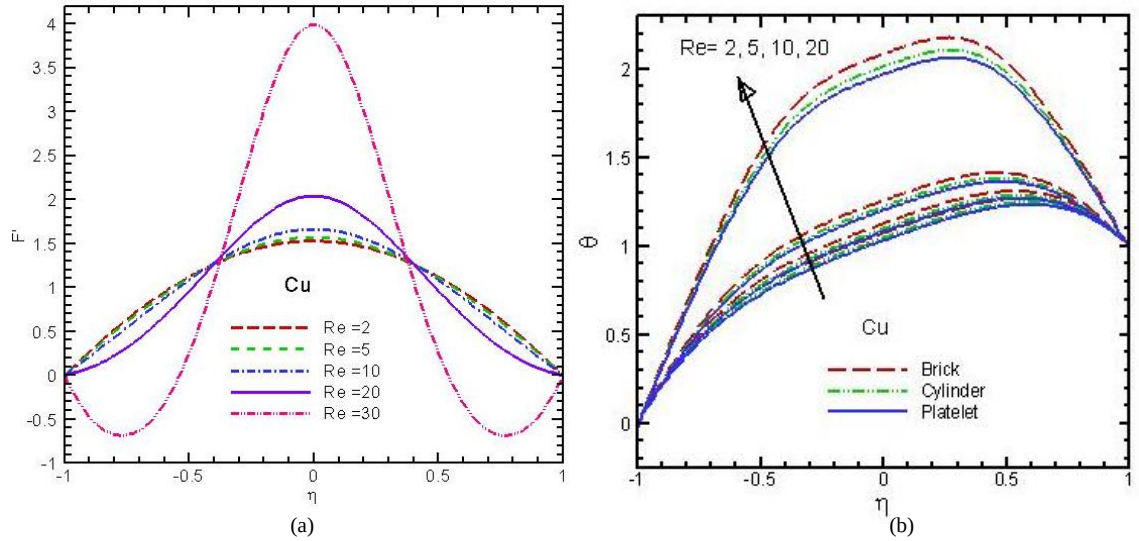

(a) (b)

Fig. 5.2: (a) Velocity Profiles, (b) temperature distributions of Cu–water nanofluid with different values of Re at $\alpha = \pi/18, Ha = 1, \phi = 0.05, Pr = 7.1, Ec = 0.1$.

The channel angle effect on the velocity profiles and temperature distributions for Cu-water nanofluid in the divergent channel is shown in Figs. 5.1(a-b). It is observed in Fig. 5.1 (a) that, the velocity around the centerline increases for the rising values of α. One can also see that the rising values of channel opening α produces backward flow adjacent to the two walls of the channel. Cu –nanoparticle (at $\phi = 0.05$) accelerate the enhancement of centerline velocities more swiftly and there occurs major backward flow near the walls for large value of $\alpha = \pi/6$. It is noticed that if channel opening expands, then exhibited flow generates at the centerline and as a result, a major backward flow raised near the walls for diverging channel. The hypothesis of Fig. 5.1(a) agreed well with those results of Alam et al. [17].

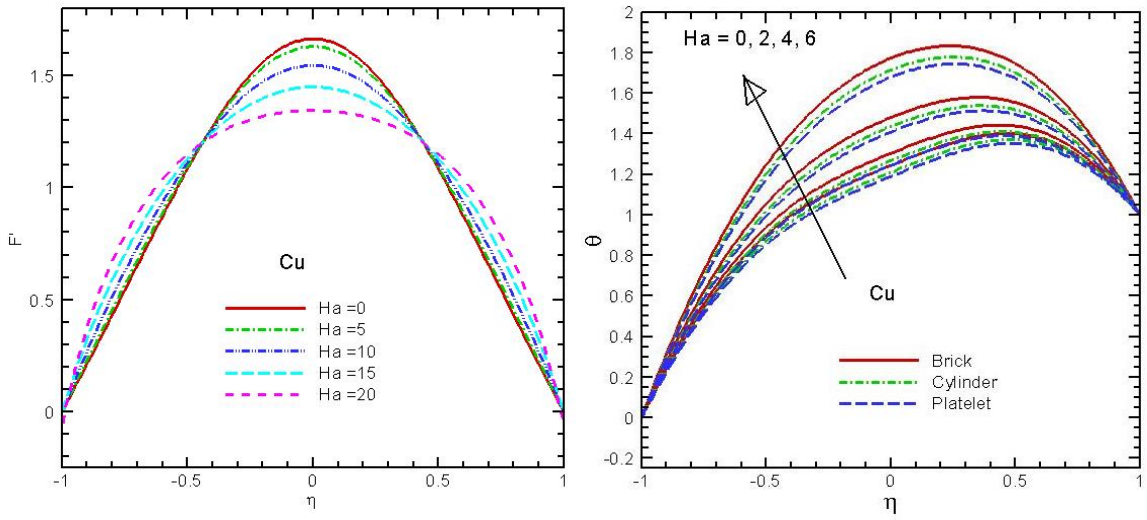

(a) (b)

Fig. 5.3: (a) Velocity Profiles, (b) temperature distributions of Cu–water nanofluid with different values of Ha at $\alpha = \pi/18$, $Re = 10, \phi = 0.05, Pr = 7.1, Ec = 0.1$.

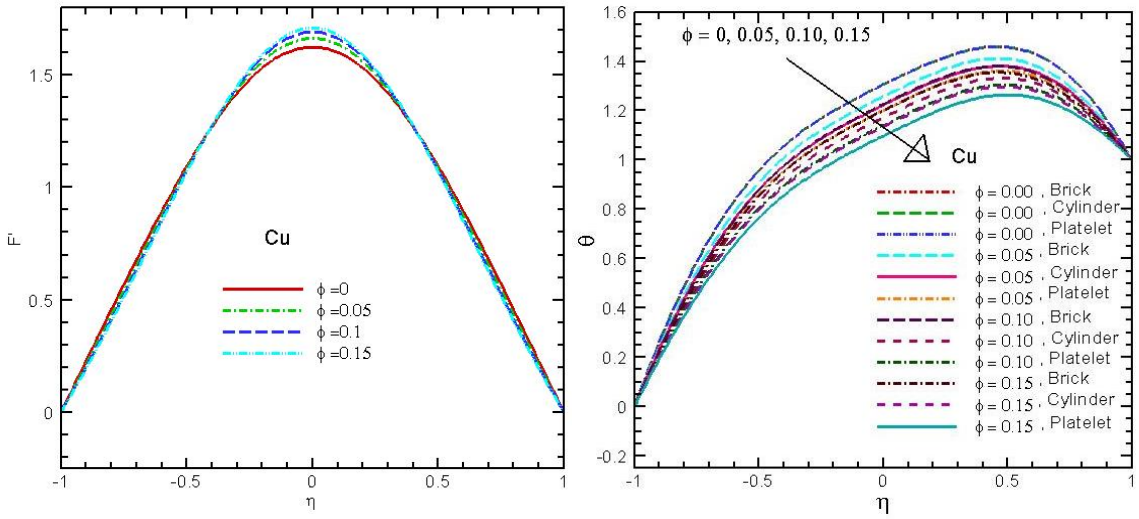

(a) (b)

Fig. 5.4: (a) Velocity Profiles, (b) temperature distributions of Cu–water nanofluid for different values of ϕ at $\alpha = \pi/18,\ Re = 10,\ Ha = 1, Ec = 0.1, Pr = 7.1$.

Figure 5.1(b) represents the effect of channel angle α on temperature profiles. It is noticed that the temperature increases massively around the channel centerline due to the escalating values of channel angle for Cu-nanoparticles. There is almost negligible change in the temperature of the fluid near the walls of the channel. Figures 5.2(a-b) highlight the velocity profiles and temperature distributions of Cu-water nanofluid for the increment of Reynolds number Re. It is interestingly observed in Fig. 5.2(a) that the centerline velocity increases when the value of Re increases, since backward flow arises at the walls. Since Reynolds number is the ratio of momentum forces and the viscous forces. This means that higher values of Re are due to the stronger momentum forces for Cu –water nanofluid. Due to this reason, these forces generate fully developed flow at centerline and an important reverse flow at the channel walls. For increasing values of Re on the variations in temperature are portrayed in Fig. 5.2(b). Since Re is the ratio of momentum forces and viscous forces, it indicates that stronger momentum forces are responsible for rising temperature in divergent channel case. The increasing values of α and Re accelerate the fluid velocity around the channel centerline. These expanded fluid flow produces consistently higher temperature in Figs. 5.1(b) and 5.2(b). It is seen that the brick-shaped nanoparticles have higher temperature followed by cylinder- and platelet- shaped nanoparticles in all incidents.

For a divergent channel, the effects of increasing Hartmann number Ha on the velocity profile and temperature distribution are plotted in Figs. 5.3(a-b). The velocity curves show that the rate of alteration is significantly reduced with increase of Hartmann number. The velocity along the centerline $(-0.5 < \eta < 0.5)$ reduces for the increasing value of Ha. The velocity decreases near the left wall $(-1.0 < \eta < -0.5)$ and right wall $(0.5 < \eta < 1.0)$ uniformly for the decreasing value of Ha. The variation of Ha leads to the variation of the Lorentz force due to magnetic field. This Lorentz force produces more resistance to the alternation phenomena. Figure 5.3(b) demonstrate the effect of Hartmann number on temperature field for Cu–nanoparticles. The higher values of temperature around channel centerline are observed for rising Hartmann number Ha. Near the walls of the channel, there is almost negligible change in the temperature of the fluid. It can be seen that brick –shaped nanoparticles have higher temperature than cylinder – and platelet –shaped nanoparticles.

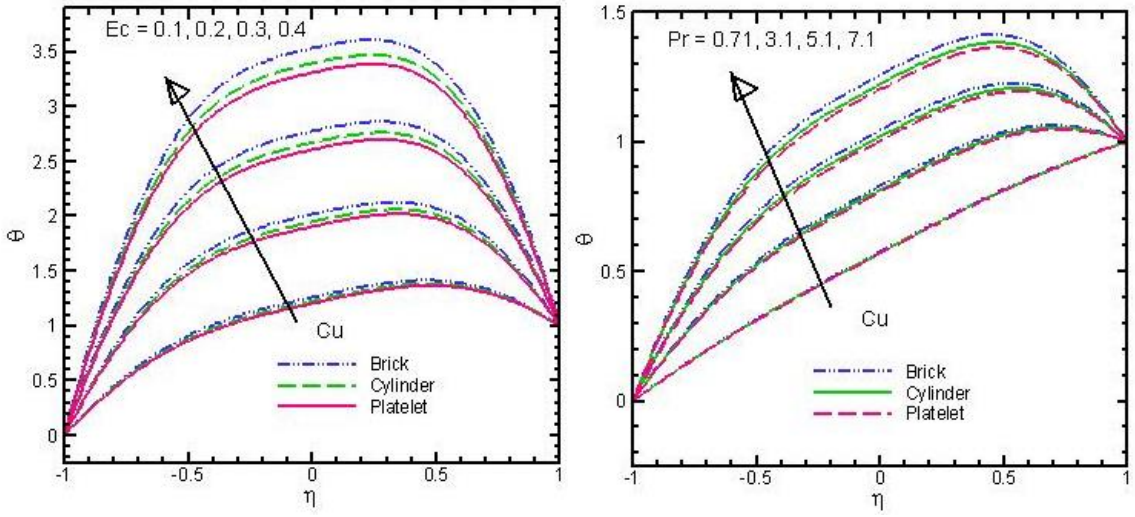

(a) (b)

Fig. 5.5: Temperature profiles of Cu –nanoparticles for different values of (a) Ec and (b) Pr at $\alpha = \pi/18, \phi = 0.05, Re = 10, Ha = 1$.

The effect of solid volume fraction ϕ of Cu -nanoparticles is investigated in the range of $0 \leq \phi \leq 0.15$ with $Ha = 1$ and is displayed in Figs. 5.4(a-b). In Fig. 5.4(a), it is observed that as the solid volume fraction ϕ increases, the velocity increases. The volume fraction ϕ increases when the nanofluids consistency increases and this increasing consistency enhances the fluid flow. For the increasing value of solid volume fraction the velocity expands, but the difference in the velocity is very small. The effects of Cu–nanoparticles solid volume fraction ϕ on temperature distributions with various shape factors are shown in Fig. 5.4(b). It is observed that when the value of ϕ increases, the temperature distribution reduces particularly toward the channel centerline. When $\phi = 0.00$, there is almost negligible change in the temperature of the fluid for three different shaped nanoparticles which is consistent.

Table 5.1: Comparison of the solutions for different number of coefficients of stream function F when $Re = 10, Ha = 1, \alpha = \pi/18, \emptyset = 0.05$

η	$N = 5$	$N = 6$	$N = 7$	$N = 8$	$N = 9$	$N = 10$	$N = 11$	$N = 12$	$N = 13$
-1.0	-1.000000	-1.000000	-1.000000	-1.000000	-1.000000	-1.000000	-1.000000	-1.000000	-1.000000
-0.8	-0.9571418	-0.9571878	-0.9572025	-0.9572074	-0.9572091	-0.9572096	-0.9572098	-0.9572099	-0.9572099
-0.6	-0.8263751	-0.8265170	-0.8265623	-0.8265773	-0.8265824	-0.8265841	-0.8265847	-0.8265850	-0.8265850
-0.4	-0.6105530	-0.6107610	-0.6108278	-0.6108499	-0.6108574	-0.6108600	-0.6108609	-0.6108612	-0.6108614
-0.2	-0.3251298	-0.3252911	-0.3253434	-0.3253608	-0.3253667	-0.3253688	-0.3253695	-0.3253697	-0.3253698
0.0	0.0000000	0.0000000	0.0000000	0.0000000	0.0000000	0.0000000	0.0000000	0.0000000	0.0000000

0.2	0.3251298	0.3252911	0.3253434	0.3253608	0.3253667	0.3253688	0.3253695	0.3253697	0.3253698
0.4	0.6105530	0.6107610	0.6108278	0.6108499	0.6108574	0.6108600	0.6108609	0.6108612	0.6108614
0.6	0.8263751	0.8265170	0.8265623	0.8265773	0.8265824	0.8265841	0.8265847	0.8265850	0.8265850
0.8	0.9571418	0.9571878	0.9572025	0.9572074	0.9572091	0.9572096	0.9572098	0.9572099	0.9572099
1.0	1.0000000	1.0000000	1.0000000	1.0000000	1.0000000	1.0000000	1.0000000	1.0000000	1.0000000

For other values of ϕ, the brick-shaped nanoparticles have highest temperature values compared to cylinder-shaped and platelet-shaped nanoparticles. The effect of Eckert number, Ec on temperature field for Cu – nanoparticles within the channel is discussed in Fig. 5.5(a). We know that Eckert number is the ratio of the square of maximum velocity and specific heat. As a result, it is found from Fig. 5.5(a) that the temperature increases at this region and the fluid flow rate along the centerline becomes faster for increasing values of Eckert number. The effect due to the dissipation term in energy equation is defined by Eckert number. From this figure, it can also be verified that due to the stronger viscous forces, the temperature of the fluid rises in divergent channel. Variations of Prandtl number, Pr on temperature profiles are plotted in Fig. 5.5(b) for Cu-nanoparticles. Rise in temperature for higher values of Prandtl number is observed for Cu–nanoparticles. Prandtl number is the ratio of viscous force and thermal force. Increase of viscosity is responsible for the increasing values of Pr. Thus, the increasing value of temperature distribution of the fluid is seen close to the centerline of the channel. Table 5.1 represents the comparative values of stream function for different numbers of coefficients of the solution (3.8). It is observed that if the number of coefficients in the solution increases from
$N = 5$ to $N = 13$, the values of stream function F increase gradually and uniformly for all values of η.

6. Conclusions

This paper has studied magnetohydrodynamics (MHD) Cu-water nanofluid flow in a divergent channel with the effects of three different shapes of nanoparticles. The influences of different flow parameters on the velocity field and temperature distribution are extensively analysed. The three shapes of nanoparticles are brick, cylinder and platelet –shaped. The major conclusions of this work are as follows:

- The increasing values of α and Re speed up the fluid velocity around the channel centerline and these developd flow produce higher temperature values in this region.
- The fluid velocity lessens while the temperature increases near the channel centerline at greater values of Hartmann number. Besides, fluid flow close the two walls increases as Ha increases.
- The velocity profile rises however the temperature reduces for escalating values of the nanoparticles volume fraction.
- As the values of Eckert number and Prandtl number increased, the temperature distributions around the channel centerline become higher.
- The temperature field inside the channel affected significantly by the nanoparticles shape factors. Brick-shaped nanoparticles have larger temperature values than the cylinder-shaped and platelet-shaped nanoparticles.

Acknowledgements

This work is done within the framework of the Master's program of the second author under Department of Mathematics, Jagannath University, Dhaka.

Funding

Financial support from the National Science and Technology (NST) scholarship is acknowledged.

References

[1] G. B. Jeffery, A viscous fluid of the two dimensional steady motion, *Philosophical Magazine*, 6: 455-465(1915).
[2] G. Hamel, Spiralfo¨rmige Bewgungen Za¨her Flu¨ssigkeiten, *Jahresbericht der Deutschen Math Vereinigung*, 25: 34-60(1916).
[3] Batchelor, K., An introduction to fluid dynamics, Cambridge University Press, Cambridge (1916).
[4] Q. Esmaili, A. Ramiar, E. Alizadeh and D. D. Ganji, An approximation of the analytical solution of the Jeffery-Hamel flow by decomposition method, *Physics Letters A*, 372: 3434-3439 (2008).
[5] R. Sadri, Channel entrance flow. Doctor of Philosophy thesis, Department of Mechanical Engineering, University of Western Ontario (1997).
[6] M. Hamadiche, J. Scott and D. Jeandel, Temporal stability of Jeffery-Hamel flow, *Journal of Fluid Mechanics,* 268: 71 – 88 (1996).
[7] L. Rosenhead, The steady two-dimensional radial flow of viscous fluid between two inclined plane walls, *Proceedings of the Royal Society A*, 175:436 – 467 (1940).
[8] Goldstein, S., Modern developments in fluid mechanics, Clarendon Press: Oxford (1938).
[9] Makinde, O. D., Steady flow in a linearly diverging asymmetrical channel, *Computer Assisted Mechanical and Engineering Sciences*, 4: 157-165 (1997).
[10] S. U. S. Choi, Enhancing thermal conductivity of fluids with nanoparticles, *In proceeding of the 1995 ASME International Mechanical Engineering Congress and Exposition*, 66: 99-105 (1995).
[11] S. K. Das, S. U. S. Choi and W. YU. T. Pradeep, New York: Nanofluids: Science and Technology (2007).
[12] O. D. Makinde and P. Y. Mhone, Hermite-Pade´ Approximation approach to Hydromagnetic flows in convergent-divergent channels, *Applied Mathematics and Computation*, 181: 966-972 (2006).
[13] O. D. Makinde and P. Y. Mhone, Temporal stability of small disturbances in MHD Jeffery-Hamel flows, *Computers and Mathematics with Applications*, 53: 128-136 (2007).
[14] A. Moradi, A. Alsaedi and T. Hayat, Investigation of heat transfer and viscous dissipation effects on the Jeffery-Hamel flow of nanofluids, *Thermal Science*, 19: 563-578 (2015).
[15] Md. S. Alam, M. A. H. Khan and M. A. Alim, Magnetohydrodynamic Stability of Jeffery-Hamel Flow using Different Nanoparticles, *Journal of Applied Fluid Mechanics*, 9: 899-908 (2016).
[16] Md. S. Alam, O. D. Makinde and M. A. H. Khan, Instability of variable thermal conductivity magnetohydrodynamic nanofluid flow in a vertical porous channel of varying width, *Defect and Diffusion Forum*, 378: 85 – 101 (2017).
[17] Md. S. Alam and M. A. H. Khan, Analysis of Magnetohydrodynamic Jeffery- Hamel flow with nanoparticle by Hermite- Padé approximation technique, *International Journal of Engineering Transaction A*, 28: 599 – 607 (2015).
[18] S. Sindhu and B. J. Gireesha, Effect of nanoparticle shapes on irreversibility analysis of nanofluid in a microchannel with individual effects of radiative heat flux, velocity slip and convective heating, *Heat Transfer*, 50: 876-892 (2021).
[19] Asifa, T. Anwar, P. Kumam, Z. Shah and K. Sitthithakerngkiet, Significance of shape factor in heat transfer performance of molybdenum-disulfide nanofluid in multiple flow situations; A comparative fractional study, *Molecules*, 26: 3711 (2021).
[20] A. Bhattad and J. Sarkar, Effects of nanoparticle shape and size on the thermohydraulic performance of plate evaporator using hybrid nanofluids, *Journal of Thermal Analysis and Calorimetry*, 143: 767–779 (2021).
[21] A. C. Das and M. S. Alam, Effect of various shaped Al_2O_3 and TiO_2 nanoparticles on water-based MHD nanofluid flow through convergent-divergent channels, Science & Technology Asia, 26(2): 1-15, (2021).
[22] S. K. Das, S. U. S. Choi and H. E. Patel, Heat transfer in nanofluids- a review, *Heat Transfer Engineering*, 27(10): 3-19 (2006).
[23] R. Ellahi, M. Hassan and A. Zeeshan, Shape effects of nanosize particles in Cu-H_2O nanofluid on entropy generation, *International Journal of Heat Mass Transfer*, 81: 449-456 (2015).
[24] N. Sher Akber and A.W. Butt, Ferromagnetic effects for peristaltic flow of Cu-water nanofluid for different shapes of nanosize particles, *Applied Nanoscience*, Epub Ahead of Print 28 March (2015). DOI: 10.007/s13204-015-0430-x.

[25] R. Ellahi, M. Hasan, A. Zeeshan, The shape effects of nanoparticles suspended in HFE-7100 over wedge with entropy generation and mixed convection, *Applied Nanoscience*, Epub Ahead of print 26 July (2015). DOI: 10.007/s13204-015-0481-z.

[26] H. Padé, Sur Ia repésentation approachée d`une function pour des fractions rationnelles, *Annales Scientifiques del' École Normalle Supérieure,* 9: 1 – 93 (1892).

[27] C. Hermite, Sur Ia générealization des fractions continues algébriques, *Annali di Mathematica Pura e Applicata*, 21: 289-308 (1893).

[28] P.G. Drazin and Y. Tourigny, Numerically study of bifurcation by analytic continuation of a function defined by a power series, *SIAM Journal of Applied Mathematics*, 56: 1 – 18 (1996).

[29] M.A.H. Khan, High-Order Differential Approximants, *Journal of Computational and Applied Mathematics*, 149: 457-468 (2002).